Universal Hamiltonians for quantum simulation and their applications to holography

Tamara Kohler

A dissertation submitted in partial fulfillment
of the requirements for the degree of
Doctor of Philosophy
of
University College London.

Department of Computer Science
University College London

August 18, 2022

I, Tamara Kohler, confirm that the work presented in this thesis is my own. Where information has been derived from other sources, I confirm that this has been indicated in the work.

Abstract

Recent work has demonstrated the existence of universal Hamiltonians – simple spin lattice models that can simulate any other quantum many body system. These universal Hamiltonians have applications for developing quantum simulators, as well as for Hamiltonian complexity, quantum computation, and fundamental physics. In this thesis we extend the theory of universal Hamiltonians. We begin by developing a new method for proving that a given family of Hamiltonians is indeed universal. We then use this method to construct two new universal models – both of which consist of translationally invariant interactions acting on a 1D spin chain.

But the benefit of our method doesn't just lie in the simple universal models it allows us to construct. It also gives deeper insight into the origins of universality – and demonstrates a link between the universality and complexity. We make this insight rigorous, and derive a complexity theoretic classification of universal Hamiltonians which encompasses all known universal models. This classification provides a new, simplified route to checking whether a particular family of Hamiltonians meets the conditions to be a universal simulator.

We also consider the practical use of analogue Hamiltonian simulation. Understanding the effect of noise on Hamiltonian simulation is a key issue in practical implementations. The first step to tackling this issue is characterising the noise processes affecting near term quantum devices. Motivated by this, we develop and numerically benchmark an algorithm which fits noise models to tomographic data from quantum devices to enable this process. This algorithm has applicability beyond analogue simulators, and could be used to investigate the physical noise processes in any quantum computing device.

Finally, we apply the theory of universal Hamiltonians to high energy physics by using them to construct toy models of holographic duality which capture more of the expected features of the AdS/CFT correspondence.

Impact Statement

The development of quantum technologies is expected to have wide ranging applications – from medical devices and sensing, to cryptography and computing. Harnessing the power of quantum physics for technological applications has the potential for a vast array of societal and commercial benefits.

In sensing and cryptography practical applications of quantum technologies are already being realised experimentally. But with quantum computing, perhaps the highest profile arm of quantum technology, practical applications have not yet come to fruition. While there are a number of start ups and established technology companies working on quantum computing, results so far have been limited to small scale proof of principle experiments, or computations which demonstrate quantum speedup but have no clear practical use.

The key challenge in building useful quantum computers is achieving fault-tolerance – quantum computers are far more error prone than their classical counterparts, and the overhead to overcome these errors and build a reliable quantum computer is beyond the reach of current hardware. This leads to interest in models of quantum computation which don't require fault tolerance.

One of the main suggested applications of quantum computers is to simulate quantum many body physics – this could have impact in materials science, fundamental physics, and quantum chemistry. But simulating quantum many body physics doesn't necessarily require a general purpose quantum computer – a specialised device to perform 'analogue' quantum simulation could be effective. It has been suggested that these analogue quantum simulators could be used without requiring full fault tolerance – making them an appealing prospect in the current era of noisy, intermediate scale quantum (NISQ) devices.

These analogue quantum simulators are the focus of this thesis. We investigate the theory of analogue quantum simulators – developing new techniques for determining

what systems can be used as simulators, and demonstrating the existence of new, simple models which could act as 'general-purpose' simulators. Furthermore, we provide a tool for investigating the noise processes in quantum devices, which can help to determine whether the results of a simulation can be considered reliable in the absence of fault tolerance. In addition to these more practical concerns, we use the theory of these analogue quantum simulators to study concepts in high energy physics.

We expect the results in this thesis to be of use to anyone working on developing practical quantum simulators – in particular engineers and researchers looking to build new scalable analogue simulation platforms. Furthermore, the results on investigating noise processes on quantum devices have applicability beyond analogue quantum simulation, and could be used to benchmark general quantum computing devices.

Finally, the results on applying ideas from the theory of analogue quantum simulation to high energy physics are of interest to the academic community of researchers working on holographic theories of quantum gravity.

Acknowledgements

First of all I would like to thank my supervisor, Dr Toby Cubitt, for his support, insight and encouragement over the last few years. I am very grateful for the time he has dedicated to teaching me – whether it was analysing proofs, chatting about how to choose interesting research problems, or working on communicating my research, I always learnt a lot from our discussions.

My thanks also go to my co-authors and other collaborators over my PhD - Emilio Onorati, Harriet Apel, Stephen Piddock, Johannes Bausch and Deniz Stiegemann. I have enjoyed the opportunity to work with and learn from all of you.

The PhD experience wouldn't have been the same without the UCL quantum CDT - and I'm very grateful to my cohort for making my time at UCL so enjoyable (particularly James Watson for also being an entertaining officemate throughout the PhD!) and to Lopa and everyone else who worked on the CDT for their efforts in making the course worthwhile, interesting and fun.

I am very grateful for always having the support of my family - thank you Mum, Dad, Eloise, Bethany, Saskia and Bhaven for everything.

Publications

This thesis is based on the following publications:

1. Tamara Kohler and Toby Cubitt: Toy Models of Holographic Duality between local Hamiltonians. *Journal of High Energy Physics* (2019).
2. Tamara Kohler, Stephen Piddock, Johannes Bausch, and Toby Cubitt.: Translationally-Invariant Universal Quantum Hamiltonians in 1D. *Annales Henri Poincare* (2021).
3. Tamara Kohler, Stephen Piddock, Johannes Bausch and Toby Cubitt: General conditions for universality of Quantum Hamiltonians. *PRX Quantum* (2022).
4. Emilio Onorati, Tamara Kohler and Toby Cubitt: Fitting quantum noise models to tomography data. *arXiv:2103.17243 (quant-ph)* (2021).
5. Harriet Apel, Tamara Kohler and Toby Cubitt: Holographic duality between local Hamiltonians from random tensor networks. *Journal of High Energy Physics* (2022).

The following publications are not included in this thesis:

1. Tamara Kohler and Toby Cubitt: Translationally invariant universal classical Hamiltonians. *Journal of Statistical Physics* (2019).

Contents

Part I

Hamiltonian simulation & universal Hamiltonians

Chapter 1

Introduction

Since Feynman first posited the idea of 'quantum simulators' in 1982 [1], analogue Hamiltonian simulation has become one of the most promising near-term applications of quantum technology [2]. It has been argued that active error correction is not needed in analogue Hamiltonian simulation, since the physical systems of interest are themselves subject to natural noise processes, and any errors in the device are simply simulating these processes. If this argument could be rigorously justified it would imply that the overheads for carrying out useful computations are potentially orders of magnitude lower than for fault tolerant digital quantum computers. Encouraging experimental progress has been made in designing analogue Hamiltonian simulators using a range of implementations, including ultracold gases [3], trapped ions [4] and superconducting circuits [5].

However, until recently the theoretical study of analogue Hamiltonian simulation was less developed. Key questions such as how to characterise the effects of errors on simulators to rigorously justify the lack of error correction were unanswered. Even more fundamentally - there was no precise definition of exactly what it means for one system to simulate another.

Recent work has tackled these problems, by providing a mathematical framework for analogue Hamiltonian simulation [6]. In [6] what it means for one quantum system to simulate another is precisely defined. Moreover, this rigorous definition of simulation is used to begin the task of characterising the effects of errors on simulators. Promisingly, the results in [6] point to the lack of active error correction in analogue Hamiltonian simulation being justifiable.

One possible drawback to the fully rigorous definition of analogue Hamiltonian simulation in [6] is that it is very demanding - it is not immediately obvious that it is

possible to construct any interesting simulations within the framework. However, in [6] it was demonstrated that—not only can interesting examples of rigorous simulations be constructed—there actually exist families of Hamiltonians that are universal, in the sense that they can simulate *all* other quantum Hamiltonians. Moreover, some of the families shown to be universal are very simple - including the Heisenberg and XY-Hamiltonians restricted to a square lattice.

The existence of universal Hamiltonians has a number of implications. It suggests that simpler systems than previously thought might be suitable for use as analogue Hamiltonian simulators, and that time dynamics under simple Hamiltonians is sufficient to perform universal quantum computation. Moreover, universality has been used to demonstrate new Hamiltonian complexity results.

In this thesis the study of universal Hamiltonians is extended. The theory of universal Hamiltonians is developed, with new constructions of universal models and a full characterisation of universal simulators by their complexity classes. An algorithm to characterise noise in near term quantum devices, which could be equally useful for both analogue simulation and digital quantum computation, is developed. And finally, a link between universal Hamiltonians and holography is explored.

1.1 Overview of thesis

We now lay out the structure of the thesis in more detail. The thesis is split into three parts. Part I covers the theory of universal Hamiltonians. The remainder of this chapter introduces all the necessary technical background for the thesis. It begins by outlining key concepts from Hamiltonian complexity theory that are used in the development of the framework of analogue Hamiltonian simulation and universal Hamiltonians. Before going on to cover the framework of analogue Hamiltonian simulation itself, and key results on universal Hamiltonians.

In Chapter 2 the first new result of this thesis is presented. The key results in Chapter 2 are two new universal models - both of which are translationally invariant Hamiltonians acting on a spin chain. However, the impact of this chapter is not only the universal models themselves, but the technique used to demonstrate universality, which is new and significantly more powerful than previous techniques.

The technique developed in Chapter 2 for proving universality gives more insight into the origins of universality, and suggests a link between universality and complexity. In Chapter 3 this link is made rigorous. A full complexity theoretic classification of universal models is derived. The conclusions to Part I are given in Chapter 4.

Part II consists of a single chapter - Chapter 5. In this chapter we present an algorithm for fitting Markovian channels to tomography data, which can be used to analyse noise models in near term quantum devices. The theory behind the algorithm, as well as pseudo-code and numerical simulations are presented (the code itself is publicly available at [7]).

Chapter 6 contains the introduction to Part III. It covers the background of using ideas and techniques from quantum information theory to develop toy models of holographic duality.

In Chapter 7 we present the first application of universal Hamiltonians to holography, with a construction of a toy model of holographic duality between local Hamiltonians. These results are developed in Chapter 8 with a toy model that uses random tensor techniques to capture more aspects expected from holographic dualities. Finally, in Chapter 9 the conclusions of Part III are presented.

1.1.1 Statement of contributions

- *Chapter 1* contains the technical background for this thesis, there are no new results in this chapter. This chapter contains extended versions of the background sections of some of my papers - particularly [8, 9, 10]. Some of the background content was previously covered in a literature review I submitted as part of the first year of the Quantum Technologies CDT.

- *Chapter 2* is based on [8] - this was joint work carried out with Stephen Piddock, Johannes Bausch and Toby Cubitt. The idea for using the new method to construct universal models was Stephen Piddock's. All authors discussed all elements of the paper and proof approaches. The proofs of universality were substantially my work, in discussion with my co-authors who also helped to spot gaps in my reasoning and to fill these in. The no-go for parameterless universality was primarily Stephen Piddock's work, and the complexity theoretic implications were largely Johannes Bausch's work.

- *Chapter 3* is based on [9] - this was again joint work carried out with Stephen Piddock, Johannes Bausch and Toby Cubitt. The proof approach arose from discussions of all four authors when writing [8]. The initial writing of the proofs was done by me, in discussion with my co-authors, who helped to refine my reasoning and make all claims fully rigorous.

- *Chapter 4* contains the general conclusions of [8, 9]. The appendix to Chapter 4 contains an independent, unpublished calculation.

- *Chapter 5* is based on [11] – this was joint work carried out with Emilio Onorati and Toby Cubitt. The idea behind the paper was Toby Cubitt's. Emilio Onorati is first author on the paper. My primary contribution to this chapter was in helping to develop the algorithms (along with Emilio), writing code and running numerics. Since I was not first author on this paper, a number of the proofs and technical theorems regarding matrix perturbation theory which were due to Emilio Onorati have been omitted, and interested readers are referred to [11] instead.

- *Chapter 6* contains the introductory & background material from [10, 12] - joint work with Toby Cubitt and Toby Cubitt & Harriet Apel respectively. The appendices to Chapter 6 contain new results - these were initially published in [10]. The proofs of these were written by me, in discussion with Toby Cubitt.

- *Chapter 7* is largely based on [10] - joint work with Toby Cubitt. The idea of using universal Hamiltonians to construct toy models of holographic dualities between local Hamiltonians was Toby Cubitt's. The idea of using Coxeter groups to analyse these toy models was mine. The proofs were constructed by me, with advice from Toby Cubitt. The 2D/1D construction was not presented in [10], it initially appeared in [8] - but again the proof was written by me in discussion with Toby Cubitt, who in particular encouraged me to consider the case of full rotational invariance and include a discussion of that.

- *Chapter 8* is based on [12] - joint work with Toby Cubitt and Harriet Apel. This work formed Harriet Apel's masters thesis, and she was the first author of the paper. The idea for the project was mine, and I helped Toby Cubitt supervise Harriet Apel's project. The proofs were substantially Harriet Apel's work, my main input was to suggest proof approaches, discuss ideas and help refine the reasoning in the proofs. Since I was not first author on this paper, a number of the proofs of sub-results in this chapter have been omitted, and interested readers are referred to [12] instead.

- *Chapter 9* contains the conclusions to Chapters 7 and 8 - the discussion in this chapter was largely already published in [10, 12], however some of the ideas have been expanded on.

All figures were made by me except Fig. 5.5 which was created by Emilio Onorati and Figs. 6.1 and 8.1 which were created by Harriet Apel.

1.2 Hamiltonian complexity

The focus of this thesis is on Hamiltonian simulation and universality, rather than complexity. However, as we will see in Sections 1.3 and 1.4 previous results in these areas draw heavily on techniques and ideas from Hamiltonian complexity theory. Moreover, in Chapter 3 we demonstrate a deep connection between universality and complexity. So, before diving into the theory of Hamiltonian simulation we will first cover some basic concepts in Hamiltonian complexity, that crop up throughout this thesis.

1.2.1 Complexity theory

The goal of complexity theory is to determine the resources needed to solve computational problems. This is typically done by sorting problems into complexity classes, and analysing relationships between different complexity classes. In classical complexity theory the problems of interest are decision problems - i.e. problems that can be posed as YES or NO questions of the input parameters. The classical complexity classes that we will need in this thesis are:

Definition 1 (P [13, 14, 15])**.** *The class of decision problems solvable in polynomial time by a classical Turing machine.*

Definition 2 (NP: Non-deterministic polynomial time)**.** *The class of decision problems decidable in polynomial time by a non-deterministic classical Turing machine. Equivalently,* NP *is the class of decision problems for which if the answer is* YES *then there is a proof, polynomial in the length of the input, that can be verified in* P*.*

Definition 3 (PSPACE)**.** *The class of decision problems decidable in polynomial space by a classical Turing machine.*

In quantum complexity theory the problems of interest are promise problems. Promise problems are a subset of decision problems, where the inputs are guaranteed to belong to some known subset of all possible inputs. The quantum complexity classes that we will need in this thesis are:

Definition 4 (BQP)**.** *The class of promise problems solvable in polynomial time by a quantum Turing machine with at most* $\frac{1}{3}$ *probability of error.*

Definition 5 (QMA(c,s) [16])**.** *A promise problem* $A = A_{\text{YES}} \cup A_{\text{NO}}$ *is in* QMA(c,s) *if and only if there exists a polynomially-bounded function* p *and a quantum polynomial time verifier* V *such that for all* n *and all* $x \in \{0,1\}^n$*:*

- *If* $x \in A_{\text{YES}}$*, there exists a* $p(n)$*-qubit quantum state* $|\psi\rangle$ *such that* $\Pr[V \text{ accepts } (x, |\psi\rangle)] \geq c$
- *If* $x \in A_{\text{NO}}$ *for all* $p(n)$*-qubit quantum states* $|\psi\rangle$*,* $\Pr[V \text{ accepts } (x, |\psi\rangle)] \leq s$

$\text{QMA}(c, s)$ where c and s are separated by an inverse polynomial in n is the class QMA [16]. $\text{QMA}(c, s)$ where c and s are separated by an exponentially small gap is the class PreciseQMA. PreciseQMA is known to be equal to the class PSPACE [17].

Definition 6 ($\text{QMA}_{\text{EXP}}(c, s)$ [18])**.** *A promise problem* $A = A_{\text{YES}} \cup A_{\text{NO}}$ *is in* $\text{QMA}_{\text{EXP}}(c, s)$ *if and only if there exists a* k *and a quantum exponential time verifier* V *such that for all* n *and all* $x \in \{0, 1\}^n$*:*

- *If* $x \in A_{\text{YES}}$*, there exists a* 2^{n^k}*-qubit quantum state* $|\psi\rangle$ *such that* $\Pr[V \text{ accepts } (x, |\psi\rangle)] \geq c$
- *If* $x \in A_{\text{NO}}$ *for all* 2^{n^k}*-qubit quantum states* $|\psi\rangle$*,* $\Pr[V \text{ accepts } (x, |\psi\rangle)] \leq s$

$\text{QMA}_{\text{EXP}}(c, s)$ where c and s are separated by an inverse exponential in n is the class QMA_{EXP}.

In complexity theory a *reduction* is a procedure for solving a problem by mapping it to a different problem. More precisely:

Definition 7 (Polynomial time reduction)**.** *Problem A reduces to problem B if there exists a map* $A \to B$ *such that b is a YES instance of B if and only if a is a YES instance of A and the map* $A \to B$ *is poly-time computable.*

Finally we will need the concept of "hard" and "complete" problems:

Definition 8. *We say that a problem A is hard for a complexity class C if every problem in C can be reduced to A.*

Definition 9. *We say that a problem A is complete for a complexity class C if A is hard for C and A is in C.*

The set of problems which are *complete* for a given complexity class can be thought of as the hardest problems in that class.

1.2.2 The local Hamiltonian problem

The canonical problem in Hamiltonian complexity is k-LOCAL HAMILTONIAN.

k-LOCAL HAMILTONIAN (g)

Input: Local Hamiltonian $H = \sum_{i=1}^{m} h_i$ on an N-partite Hilbert space of constant local dimension, and $m \leq \text{poly}\, N$. Each $h_i \coloneqq h_{S_i} \otimes \mathbb{1}_{S_i^c}$ acts non-trivially on at most $|S_i| \leq k$ sites, and $\|h_i\| \leq 1$. Two numbers $\alpha, \beta > 0$ with $\beta - \alpha \geq 1/g(N)$.

Promise: The ground state energy $\lambda_{\min}(H)$ either $\geq \beta$, or $\leq \alpha$.

Question: YES if $\lambda_{\min}(H) \leq \alpha$, else NO.

k-LOCAL HAMILTONIAN (poly) is QMA-complete for $k \geq 2$ [16, 19, 20]. k-LOCAL HAMILTONIAN (exp) is PreciseQMA-complete [17].

We can also consider the special case where the set of interaction terms and / or the geometry of the interaction graph is restricted (which can implicitly constrain the family's locality k).

Definition 10 ($\mathcal{M}$-HAMILTONIAN)**.** *The* k-LOCAL HAMILTONIAN (poly) *problem, where the Hamiltonian is restricted to belong to* $\mathcal{M}$*, some (possibly infinite) family of Hamiltonians.*

Definition 11 (PRECISE-$\mathcal{M}$-HAMILTONIAN)**.** *The* k-LOCAL HAMILTONIAN (exp) *problem, where the Hamiltonian is restricted to belong to* $\mathcal{M}$*, some (possibly infinite) family of Hamiltonians.*

An interesting case of a $\mathcal{M}$-HAMILTONIAN is the restriction to translationally invariant Hamiltonians:

TI-LOCAL HAMILTONIAN (g)

Input: Translationally-invariant[1] local Hamiltonian $H = \sum_{i \in \Lambda} h_i$ on an N-partite Hilbert space $(\mathbb{C}^d)^{\otimes \Lambda}$ of constant local dimension d. Each $h_i \coloneqq (h)_{S_i} \otimes \mathbb{1}_{S_i^c}$ for some fixed hermitian operator h acts non-trivially and in a translationally-invariant fashion on at most $|S_i| \leq k$ sites, and $\|h_i\| \leq 1$. Two numbers $\alpha, \beta > 0$.

Promise: $\beta - \alpha \geq 1/g(N)$, and $\lambda_{\min}(H)$ either $\geq \beta$, or $\leq \alpha$.

Question: YES if $\lambda_{\min}(H) \geq \beta$, else NO.

Gottesman and Irani proved in 2009 that TI-LOCAL HAMILTONIAN (poly) is QMA_{EXP}-complete [18], which has since been generalized to systems with lower local dimension [21, 22].

[1] Naturally, translational invariance is defined with respect to the Hilbert space's interaction graph on Λ.

1.2.3 Circuit-to-Hamiltonian Mappings

The key idea behind proofs of QMA-hardness of k-LOCAL HAMILTONIAN is that it is possible to encode arbitrary quantum computation into the ground state of local Hamiltonians [23, 16]. These are often called "circuit-to-Hamiltonian mappings", though the mappings may involve other models of quantum computation than the circuit model. These Hamiltonians are typically constructed in such a way that their ground states are "computational history states". A very general definition of history states was given in [24]; we will only require the simpler "standard" history states here.

Definition 12 (Computational history state)**.** *A computational history state* $|\Phi\rangle_{CQ} \in \mathcal{H}_Q \otimes \mathcal{H}_C$ *is a state of the form*

$$|\Phi\rangle_{CQ} = \frac{1}{\sqrt{T}} \sum_{t=1}^{T} |\psi_t\rangle |t\rangle ,$$

where $\{|t\rangle\}$ *is an orthonormal basis for* $\mathcal{H}_C$ *and* $|\psi_t\rangle = \Pi_{i=1}^{t} U_i |\psi_0\rangle$ *for some initial state* $|\psi_0\rangle \in \mathcal{H}_Q$ *and set of unitaries* $U_i \in \mathcal{B}(\mathcal{H}_Q)$*.*

$\mathcal{H}_C$ *is called the clock register and* $\mathcal{H}_Q$ *is called the computational register. If* U_t *is the unitary transformation corresponding to the* t^{th} *step of a quantum computation, then* $|\psi_t\rangle$ *is the state of the computation after* t *steps. We say that the history state* $|\Phi\rangle_{CQ}$ *encodes the evolution of the quantum computation.*

Note that U_t need not necessarily be a gate in the quantum circuit model. It could also e.g. be one time-step of a quantum Turing machine, or even a time-step in some more exotic model of quantum computation [21], or an isometry [25].

There are many examples of "circuit-to-Hamiltonian" mappings in the literature - in Chapters 2 and 3 we introduce a number of constructions in more detail and outline their relationship to universality.

1.2.4 Perturbation gadgets

The final tool from the Hamiltonian complexity literature that we use in this thesis are perturbation gadgets. "Perturbation gadgets" give a mathematically rigorous version of a concept that is well known in theoretical physics by other names. The quantum many-body models that are studied in condensed matter physics are understood to be effective theories that approximate the correct physics at low energies. For example, the Born-Oppenheimer approximation assumes the motion of atomic nuclei can be treated independently of their electron clouds, allowing effective models of

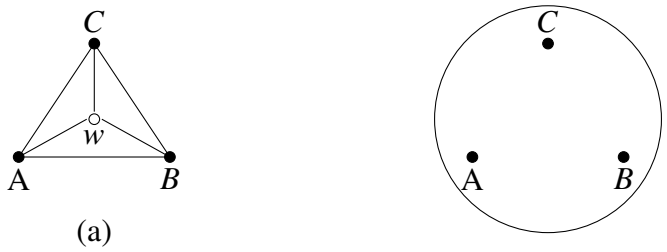

Figure 1.1: (a) The interaction graph of a Hamiltonian, H, consisting only of two body interactions, whose low-energy effective Hamiltonian approximates to high accuracy the 3-body interaction depicted in (b). The white vertex in (a) represents an 'ancilla qubit' - these don't appear in the low-energy effective Hamiltonian as they are projected into a one-dimensional subspace in this regime. Let $H = \Delta^{\frac{1}{3}} \frac{(-A+B)^2}{2} + \frac{(A^2+B^2)\otimes C}{2} - \Delta^{\frac{2}{3}} \left(C \otimes |1\rangle\langle 1|_w + \frac{(-A+B)\otimes X_w}{\sqrt{2}} \right)$ and let $H_{\text{eff}} = A \otimes B \otimes C$. If we restrict to the subspace with energy below Δ, $H_{\text{eff}} \simeq H$ up to errors of order $\frac{1}{\Delta}$. (More precisely: $||H|_\Delta - H_{\text{eff}}|| \leq \frac{1}{\Delta}$.) The perturbation gadgets used to construct this effective Hamiltonian were developed in [28].

just the electronic structure of molecules and materials to be derived by assuming the nuclei locations are fixed. These effective models are accurate at low energies. Similarly, since Wilson's seminal work [26, 27], quantum field theories in high-energy physics are believed to be effective, low-energy theories that emerge from some deeper, underlying model. In atomic and optical physics, one frequently performs perturbation expansions to some finite order to derive effective interaction Hamiltonians.

Perturbation gadgets apply the same general idea to build up Hamiltonians out of one type of interaction, that give rise to low-energy effective Hamiltonians composed of a different type of interaction. The main difference to the standard perturbation theory taught at undergraduate physics is to keep track of rigorous bounds on the approximation errors, rather than to simply truncate a perturbation series at finite order. A typical example of such a gadget is the Hamiltonian depicted in Fig. 1.1, which consists only of two-body interactions, but whose low-energy effective Hamiltonian approximates to high accuracy a many-body interaction.

Perturbation gadgets were first used in Hamiltonian complexity to prove reductions from 3-LOCAL HAMILTONIAN to 2-LOCAL HAMILTONIAN [20]. 3-LOCAL HAMILTONIAN was already known to be QMA-complete (shown using history state methods [19]), so this reduction demonstrated QMA-completeness of 2-LOCAL HAMILTONIAN. Since then, perturbation gadgets have also been used to demonstrate QMA-completeness of Hamiltonians with restricted interaction graphs and types of interactions [28, 29, 30]. We will see in the next section that while perturbation gadgets were designed to

preserve the smallest eigenvalue of a Hamiltonian, they actually achieve something far stronger and can be used to design *perturbative simulations*.

1.3 Hamiltonian simulation

1.3.1 Hamiltonian Encodings

With the key concepts from Hamiltonian complexity under our belt we can turn to consider the complexity-inspired, rigorous mathematical framework of Hamiltonian simulation first outlined in [6]. Clearly, in order for a simulator Hamiltonian, H', to simulate a target Hamiltonian, H, there must exist an encoding map $\mathcal{E} : \text{Herm}_n \to \text{Herm}_m$ which encodes H in H', where n, m are the dimensions of H, H' respectively. This encoding map has to encode all observables on the H system as observables on the $\mathcal{E}(H)$ system. Before deriving the mathematical form of $\mathcal{E}$, the authors of [6] first set out operational requirements that it must satisfy:

I All observables on the target system must correspond to observables on the simulator system, so we require that Hermitian operators are mapped to Hermitian operators, $\mathcal{E}(A) = \mathcal{E}(A)^\dagger$, for all $A \in \text{Herm}_n$.

II The eigenvalues of encoded observables should be equal to the eigenvalues of the original observable, $\sigma(\mathcal{E}(A)) = \sigma(A)$, for all $A \in \text{Herm}_n$, where $\sigma(A)$ denotes the spectrum of A.[2]

III The map should be real linear, $\mathcal{E}(\sum_i \alpha_i h_i) = \sum_i \alpha_i \mathcal{E}(h_i)$ (where h_i is some Hermitian operator), so that individual interactions in the Hamiltonian are encoded separately.

IV A map on states $\mathcal{E}_{state}$ should exist such that $\text{tr}(\mathcal{E}(A)\mathcal{E}_{state}(\rho)) = \text{tr}(A\rho)$, for all $A \in \text{Herm}_n$, so that measurements are correctly simulated.

V The thermodynamic properties of the system should be preserved: $Z_{\mathcal{E}(H)}(\beta) = \text{tr}\left(e^{-\beta\mathcal{E}(H)}\right) = c\,\text{tr}\left(e^{-\beta H}\right) = cZ_H$, where Z_H, $Z_{\mathcal{E}(H)}$ denote the partition function of H, $\mathcal{E}(H)$ respectively, and c is a constant which does not impact the thermodynamic properties of the system.

VI We require $e^{-i\mathcal{E}(H)t}\mathcal{E}_{state}(\rho)e^{i\mathcal{E}(H)t} = \mathcal{E}_{state}(e^{-iHt}\rho e^{iHt})$, so that time evolution according to $\mathcal{E}(H)$ correctly simulates time evolution according to H.

If an encoding map meets these requirements then, in the absence of any errors, H', will exactly replicate the physics of H. It is also desirable for the encoding to be

[2]The spectrum of A is defined as the set of values $\lambda \in \mathbb{C}$ such that $A - \lambda\mathbb{1}$ is not invertible. It is equivalent to the eigenvalues of A, ignoring multiplicities.

local, so that local observables on the target system are mapped to local observables on the simulator system.

In order to determine the mathematical form of encodings the authors of [6] demonstrate that any encoding map which meets conditions I and II along with a convexity condition:[3]

III′ $\mathcal{E}(pA+(1-p)B) = p\mathcal{E}(A)+(1-p)\mathcal{E}(B)$ for all $A, B \in \mathrm{Herm}_n$ and all $p \in [0,1]$

Is necessarily of the form:[4]

$$\mathcal{E}(A) = V\left(A \otimes P + \overline{A} \otimes Q\right)V^\dagger, \tag{1.1}$$

where V is an isometry, $\overline{A}$ denotes complex conjugation, and P and Q are orthogonal projectors.

It should be noted that eq. (1.1) is equivalent to:

$$\mathcal{E}(M) = V(M^{\oplus p} + \overline{M}^{\oplus q})V^\dagger \tag{1.2}$$

for p, q positive integers.

Moreover, encodings of the form given in eqs. (1.1) and (1.2) also satisfy conditions III-VI provided a suitable map on states is also defined.

1.3.2 Map on states

In [6] the authors determine suitable maps on states $\mathcal{E}_{state}(\rho)$ to ensure that conditions IV and VI are met. They find that a natural choice for $\mathcal{E}_{state}(\rho)$ which preserves expectation values of observables is:

$$\mathcal{E}_{state}(\rho) = \begin{cases} V(\rho \otimes \sigma)V^\dagger & \text{for some } \sigma \text{ such that } P\sigma = \sigma, \text{ if } P \neq 0 \\ V(\overline{\rho} \otimes \sigma)V^\dagger & \text{for some } \sigma \text{ such that } Q\sigma = \sigma, \text{ otherwise} \end{cases} \tag{1.3}$$

where P and Q are the projectors from the corresponding encoding (see eq. (1.1)).

[3]The convexity condition III′ is a special case of condition III, however it can also be viewed as a physically motivated requirement in its own right. Consider a situation where we are asked to encode a probabilistic mixture of observables, $pA + (1-p)B$. If the encoded system is to replicate all the physics of the original system then $\mathcal{E}(pA + (1-p)B)$ must have the same expectation value as the corresponding probabilistic mixture of encoded observables $p\mathcal{E}(A) + (1-p)\mathcal{E}(B)$ for all states ρ, which will only hold if condition III′ is met.

[4]The equation quoted here is the form for encoding a Hamiltonian H into a *subspace* of the simulator system. If the encoding is into the full space the isometry V is replaced by a unitary.

Moreover, with this choice time evolution under a map on states $\mathcal{E}_{state}$ is given by:

$$e^{-i\mathcal{E}(H)t}\mathcal{E}_{state}(\rho)e^{i\mathcal{E}(H)t} = \begin{cases} \mathcal{E}_{state}(e^{-iHt}\rho e^{iHt}) & \text{if } p \geq 1 \\ \mathcal{E}_{state}(e^{+iHt}\rho e^{-iHt}) & \text{if } p = 0 \end{cases} \tag{1.4}$$

where p is the number of copies of H in the corresponding encoding, $\mathcal{E}(H)$ (see eq. (1.2)). So if $p \geq 1$, $\mathcal{E}_{state}$ simulates evolution forward in time If $p = 0$, $\mathcal{E}_{state}$ simulates evolution backwards in time. To circumvent the issue of simulating evolution backwards in time, a standard encoding is defined as one for which $p \geq 1$.

Note that the map on states outlined here will not map Gibbs states of the target system to Gibbs states of the simulator system. It may be that in realistic devices, equilibrium states of the simulator are easiest to initialise, and such a map would be preferred. In [6] it is shown that there exists a choice of $\mathcal{E}_{state}$ which fits this criteria, and satisfies conditions IV and VI.

We refer readers to [6, Section 7.1] for full details of the map on states construction.

1.3.3 Local encodings

A *local* encoding is an encoding which maps local observables to local observables, defined as follows:

Definition 13 (Local subspace encoding (Definition 13 from [6]))**.** *Let*

$$\mathcal{E} : \mathcal{B}\left(\otimes_{j=1}^{n}\mathcal{H}_j\right) \to \mathcal{B}\left(\otimes_{j=1}^{n}\mathcal{H}'_j\right)$$

be a subspace encoding. We say that the encoding is local if for any operator $A_j \in \mathrm{Herm}(\mathcal{H}_j)$ *there exists* $A'_j \in \mathrm{Herm}(\mathcal{H}'_j)$ *such that:*

$$\mathcal{E}(A_j \otimes \mathbb{1}) = (A'_j \otimes \mathbb{1})\mathcal{E}(\mathbb{1}).$$

It is shown in [6] that if an encoding $\mathcal{E}(M) = V(M \otimes P + \overline{M} \otimes Q)V^\dagger$ is local, then the isometry V can be decomposed into a tensor product of isometries $V = \otimes_i V_i$, for isometries $V_i : \mathcal{H}_i \otimes E_i \to \mathcal{H}'_i$, for some ancilla system E_i.[5] Moreover, P and

[5]There is a more general definition of simulation which doesn't require the isometries to be tensor product [31]. However, these types of simulations don't preserve the local structure of the Hamiltonian. So while they are interesting from a complexity theoretic perspective, they are not as useful for physical simulation.

Q are orthogonal projectors on $E = \otimes_i E_i$ and are locally distinguishable - for all i there exist projectors P_{E_i} and Q_{E_i} acting on E_i such that $\left(P_{E_i} \otimes \mathbb{1}\right) P = P$ and $\left(Q_{E_i} \otimes \mathbb{1}\right) Q = Q$

1.3.4 From encodings to simulation

Encodings capture the notion of the entire spectrum of a simulator Hamiltonian perfectly replicating the physics of target Hamiltonian. But in practice it is only necessary for the simulator system to replicate the physics of the target system below some energy cut off, Δ, provided Δ is large enough. Due to energy conservation, initial low-energy states will not be affected by states with energy greater than Δ, so as long as Δ is greater than the largest eigenvalue of H, the low energy sector of H' will replicate the physics of H.

[6] therefore says that H' *perfectly* simulates H, if it *exactly* reproduces the physics of H below some energy cutoff Δ, where Δ can be chosen arbitrarily large. For brevity, we abbreviate the low-energy subspace of an operator A via $S_{\leq\Delta(A)} \coloneqq \text{span}\{|\psi\rangle : A|\psi\rangle = \lambda|\psi\rangle \wedge \lambda \leq \Delta\}$.

Definition 14 (Perfect simulation, [6, Def. 20])**.** *We say that H' perfectly simulates H below the cutoff energy Δ if there is a local encoding $\mathcal{E}$ into the subspace $S_{\mathcal{E}}$ such that*

1. $S_{\mathcal{E}} = S_{\leq\Delta(H')}$*, and*
2. $H'|_{\leq\Delta} = \mathcal{E}(H)|_{S_{\mathcal{E}}}$.

No simulation in the real world will ever be perfect, so we need to consider how to modify definition Definition 14 to allow for approximate simulations. If condition (i) from definition Definition 14 only holds approximately then $\mathcal{E}(H)$ and $H'_{\leq\Delta}$ have support on different spaces, so we cannot compare them. However, if $\|\mathcal{E}(\mathbb{1}) - P_{\leq\Delta(H')}\| \leq \eta$, where $\mathcal{E}(M) = V(M \otimes P + \overline{M} \otimes Q)V^\dagger$, then there exists $\tilde{\mathcal{E}} = \tilde{V}(M \otimes P + \overline{M} \otimes Q)\tilde{V}^\dagger$ such that $\|\tilde{V} - V\| \leq \sqrt{2}\eta$ and $\tilde{\mathcal{E}}(\mathbb{1}) = P_{\leq\Delta(H')}$,[6] so an approximate encoding is defined as:

Definition 15 (Approximate simulation, [6, Def. 23])**.** *Let $\Delta, \eta, \epsilon > 0$. A Hamiltonian H' is a (Δ, η, ϵ)-simulation of the Hamiltonian H if there exists a local encoding $\mathcal{E}(M) = V(M \otimes P + \overline{M} \otimes Q)V^\dagger$ such that*

1. *There exists an encoding $\tilde{\mathcal{E}}(M) = \tilde{V}(M \otimes P + \overline{M} \otimes Q)\tilde{V}^\dagger$ into the subspace $S_{\tilde{\mathcal{E}}}$ such that $S_{\tilde{\mathcal{E}}} = S_{\leq\Delta(H')}$ and $\|\tilde{V} - V\| \leq \eta$; and*

[6]The proof that such $\tilde{\mathcal{E}}$ exists is given in [6, Lemma 23].

2. $\|H'_{\leq\Delta} - \tilde{\mathcal{E}}(H)\| \leq \epsilon$.

Note that the role of $\tilde{\mathcal{E}}$ is to provide an *exact* simulation as per Definition 14. However, it might not always be possible to construct this encoding in a local fashion. The local encoding $\mathcal{E}$ in turn approximates $\tilde{\mathcal{E}}$, such that the subspaces mapped to by the two encodings deviate by at most η. ϵ controls how much the eigenvalues are allowed to differ.

If we are interested in whether an infinite family of Hamiltonians can be simulated by another, the notion of overhead becomes interesting: if the system size grows, how large is the overhead necessary for the simulation, in terms of the number of qudits, operator norm or computational resources? We capture this notion in the following definition.

Definition 16 (Simulation, [6, Def. 23])**.** *We say that a family $\mathcal{F}'$ of Hamiltonians can simulate a family $\mathcal{F}$ of Hamiltonians if, for any $H \in \mathcal{F}$ and any $\eta, \epsilon > 0$ and $\Delta \geq \Delta_0$ (for some $\Delta_0 > 0$), there exists $H' \in \mathcal{F}'$ such that H' is a (Δ, η, ϵ)-simulation of H.*

We say that the simulation is efficient if, in addition, for H acting on n qudits and H' acting on m qudits, $\|H'\| = \mathrm{poly}(n, 1/\eta, 1/\epsilon, \Delta)$ and $m = \mathrm{poly}(n, 1/\eta, 1/\epsilon, \Delta)$; H' is efficiently computable given H, Δ, η and ϵ; each local isometry V_i in the decomposition of V is itself a tensor product of isometries which map to $\mathrm{O}(1)$ qudits; and there is an efficiently constructable state $|\psi\rangle$ such that $P|\psi\rangle = |\psi\rangle$.

As already outlined, in [6] it is shown that approximate Hamiltonian simulation preserves important physical properties. We recollect the most important ones in the following.

Lemma 17 ([6, Lem. 27, Prop. 28, Prop. 29])**.** *Let H act on $(\mathbb{C}^d)^{\otimes n}$. Let H' act on $(\mathbb{C}^{d'})^{\otimes m}$, such that H' is a (Δ, η, ϵ)-simulation of H with corresponding local encoding $\mathcal{E}(M) = V(M \otimes P + \overline{M} \otimes Q)V^\dagger$. Let $p = \mathrm{rank}(P)$ and $q = \mathrm{rank}(Q)$. Then the following holds true.*

1. *Denoting with $\lambda_i(H)$ (resp. $\lambda_i(H')$) the i^{th}-smallest eigenvalue of H (resp. H'), then for all $1 \leq i \leq d^n$, and all $(i-1)(p+q) \leq j \leq i(p+q)$, $|\lambda_i(H) - \lambda_j(H')| \leq \epsilon$.*

2. *The relative error in the partition function evaluated at β satisfies*

$$\frac{|\mathcal{Z}_{H'}(\beta) - (p+q)\mathcal{Z}_H(\beta)|}{(p+q)\mathcal{Z}_H(\beta)} \leq \frac{(d')^m \mathrm{e}^{-\beta\Delta}}{(p+q)d^n \mathrm{e}^{-\beta\|H\|}} + (\mathrm{e}^{\epsilon\beta} - 1). \tag{1.5}$$

3. *For any density matrix ρ' in the encoded subspace for which $\mathcal{E}(\mathbb{1})\rho' = \rho'$, we have*

$$\|e^{-iH't}\rho' e^{iH't} - e^{-i\mathcal{E}(H)t}\rho' e^{i\mathcal{E}(H)t}\|_1 \leq 2\epsilon t + 4\eta. \tag{1.6}$$

1.3.5 Perturbative simulations

Even with the relaxation to approximate simulation, the definition of simulation laid out in this section is demanding, and it is not immediately obvious that any interesting examples of simulations exist. We will see in Section 1.4 that not only do interesting simulations exist, but there exist families of Hamiltonians that can simulate all other quantum many body physics. The key technique used to demonstrate these universality results are perturbative simulations.

The following lemmas to construct perturbative simulations were shown in [31, 6]. They allow many perturbation gadget constructions from the Hamiltonian complexity literature to be lifted, and applied to derive simulation results.

Let $\mathcal{H}$ be a Hilbert space decomposed as $\mathcal{H} = \mathcal{H}_- \oplus \mathcal{H}_+$. Let $\Pi_\pm$ be the projectors onto $\mathcal{H}_\pm$. For arbitrary operator M define $M_{++} = \Pi_+ M \Pi_+$, $M_{--} = \Pi_- M \Pi_-$, $M_{+-} = \Pi_+ M \Pi_-$, and $M_{-+} = \Pi_- M \Pi_+$. Consider an unperturbed Hamiltonian $H = \Delta H_0$, where H_0 is block-diagonal with respect to the split $\mathcal{H} = \mathcal{H}_- \oplus \mathcal{H}_+$, $(H_0)_{--} = 0$, $\lambda_{\min}((H_0)_{++}) \geq 1$.

Lemma 18 (First order simulation [31, 6])**.** *Let H_1 be a perturbation acting on the same space as H_0. Suppose there exists a local isometry W such that* $\mathrm{Im}(W) = \mathcal{H}_-$ *and:*

$$||W H_{\text{target}} W^\dagger - (H_1)_{--}||_\infty \leq \frac{\epsilon}{2} \tag{1.7}$$

Then $\tilde{H} = H + H_1$ $(\frac{\Delta}{2}, \eta, \epsilon)$ simulates H_{target}, provided that $\Delta \geq O(\frac{||H_1||^2}{\epsilon} + \frac{||H_1||}{\eta})$.

Lemma 19 (Second order simulation [31, 6])**.** *Let $V = H_1 + \Delta^{\frac{1}{2}} H_2$ be a perturbation acting on the same space as H_0 such that* $\max(||H_1||, ||H_2||) \leq \Lambda$*; H_1 is block diagonal with respect to the split $\mathcal{H} = \mathcal{H}_- \oplus \mathcal{H}_+$ and $(H_2)_{--} = 0$. Suppose there exists a local isometry W such that* $\mathrm{Im}(W) = \mathcal{H}_-$ *and:*

$$||W H_{\text{target}} W^\dagger - (H_1)_{--} + (H_2)_{-+} H_0^{-1} (H_2)_{+-}||_\infty \leq \frac{\epsilon}{2} \tag{1.8}$$

Then $\tilde{H} = H + V$ $(\frac{\Delta}{2}, \eta, \epsilon)$ simulates H_{target}, provided that $\Delta \geq O(\frac{\Lambda^6}{\epsilon^2} + \frac{\Lambda^2}{\eta^2})$.

Lemma 20 (Third order simulation [31, 6])**.** *Let $V = H_1 + \Delta^{\frac{1}{3}} H_1' + \Delta^{\frac{2}{3}} H_2$ be a perturbation acting on the same space as H_0 such that* $\max(||H_1||, ||H_1'||, ||H_2||) \leq \Lambda$*;*

H_1 and H_1' are block diagonal with respect to the split $\mathcal{H} = \mathcal{H}_- \oplus \mathcal{H}_+$ and $(H_2)_{--} = 0$. Suppose there exists a local isometry W such that $\mathrm{Im}(W) = \mathcal{H}_-$ *and:*

$$||WH_{\text{target}}W^\dagger - (H_1)_{--} + (H_2)_{-+}H_0^{-1}(H_2)_{++}H_0^{-1}(H_2)_{+-}||_\infty \leq \frac{\epsilon}{2} \tag{1.9}$$

and also that:

$$(H_1')_{--} = (H_2)_{-+}H_0^{-1}(H_2)_{+-} \tag{1.10}$$

Then $\tilde{H} = H + V$ $(\frac{\Delta}{2}, \eta, \epsilon)$ simulates H_{target}, provided that $\Delta \geq O(\frac{\Lambda^{12}}{\epsilon^3} + \frac{\Lambda^3}{\eta^3})$.

The final lemma, regarding fourth order perturbative simulations, was demonstrated in [32]:

Lemma 21 (Fourth-order simulation - Lemma 12 from [32])**.** *Let H_0, H_1, H_2, H_3, H_4 be Hamiltonians acting on the same space, such that:* $\max\{||H_1||, ||H_2||, ||H_3||, ||H_4||\} \leq \Lambda$*; H_2 and H_3 are block-diagonal with respect to the split $\mathcal{H}_+ \oplus \mathcal{H}_-$; $(H_4)_{--} = 0$. Suppose there exists a local isometry V such that* $\mathrm{Im}(V) = \mathcal{H}_-$ *and*

$$\|VH_{\text{target}}V^\dagger - \Pi_-\left(H_1 + H_4H_0^{-1}H_2H_0^{-1}H_4 - H_4H_0^{-1}H_4H_0^{-1}H_4H_0^{-1}H_4\right)\Pi_-\| \leq \epsilon/2 \tag{1.11}$$

and also that

$$(H_2)_{--} = \Pi_-H_4H_0^{-1}H_4\Pi_- \quad \text{and} \quad (H_3)_{--} = -\Pi_-H_4H_0^{-1}H_4H_0^{-1}H_4\Pi_-. \tag{1.12}$$

Then $H_{\text{sim}} = \Delta H_0 + \Delta^{3/4}H_4 + \Delta^{1/4}H_3 + \Delta^{1/2}H_2 + H_1$ $(\Delta/2, \eta, \epsilon)$-simulates H_{target}, provided that $\Delta \geq O(\Lambda^{20}/\epsilon^4 + \Lambda^4/\eta^4)$.

1.3.6 Errors and noise in Hamiltonian simulation

As set out in the introduction, one of the arguments for why analogue Hamiltonian simulation will be useful in the noisy intermediate scale quantum (NISQ) era is that it doesn't require active error correction. This argument is backed up by claiming that errors in the simulation are modelling the noise experienced by the system being simulated, so form part of the simulation. Analysing how errors on the simulator system map to noise on the system being simulated is crucial in determining the validity of this claim. Any in depth analysis of this point will depend on the physical noise processes occurring on the simulator, but in this section we outline why the notion of simulation defined in [6] begins to justify the lack of error correction in analogue Hamiltonian simulation.

There are three key results regarding errors in [6]. We summarise them here, but refer readers to [6, Section 8.5] for technical details:

1. Any local error $\mathcal{N}'((\mathcal{E}_{state}(\rho)))$ on the simulator system can be mapped to a local error, $\mathcal{N}$, acting on the system being simulated. However, this does not imply that $\mathcal{N}'(\mathcal{E}_{state}(\rho)) = \mathcal{E}_{state}(\mathcal{N}(\rho))$ as the two local errors may have completely different actions on the system of interest.

2. If $\text{rank}(P) = 1$ (which is true for every simulation in [6]) a stronger result can be shown:
$$\mathcal{E}(\mathbb{1})\mathcal{N}'(\mathcal{E}_{state}(\rho))\mathcal{E}(\mathbb{1}) = \mathcal{E}_{state}(\mathcal{N}(\rho)) \tag{1.13}$$
This states that any local error acting on the encoded state is equal to the encoding of a local error on the system being simulated.

3. The second result allows for the possibility that an error on the simulator system may take us out of the low energy subspace. The map $\mathcal{E}(\mathbb{1})\mathcal{N}'(\mathcal{E}_{state}(\rho))\mathcal{E}(\mathbb{1})$ is necessarily in the encoded subspace, but may differ from $\mathcal{N}'$. If we make the physically motivated assumption that the probability of an error that takes us out of the low-energy subspace is low,[7] it is possible to show that the distance between $\mathcal{E}(\mathbb{1})\mathcal{N}'(\mathcal{E}_{state}(\rho))\mathcal{E}(\mathbb{1})$ and $\mathcal{N}'$ is negligible.

Each of these results is stronger than the previous, and they begin to build up evidence for error correction being somewhat less critical for analogue Hamiltonian simulation than in general purpose quantum computation, as noise in the simulator system can be mapped to noise occurring in the system being simulated. However, as already noted, unless the noise on the simulator system maps to natural noise models on the target system this isn't enough to justify the lack of error correction. Evaluating this requires understanding the physical noise processes on the simulator system.

1.4 Universal Hamiltonians

Definition 16 naturally leads to the question of whether there exist families of Hamiltonians that are *so* versatile that they can simulate all other Hamiltonians: in that case, we call such families *universal*.

Definition 22 (Universal Hamiltonians [6, Def. 26])**.** *We say that a family of Hamiltonians is a universal simulator—or simply is universal—if any (finite-dimensional)*

[7] If Δ is large enough this assumption is physically well motivated since such errors would have high energy requirements.

Hamiltonian can be simulated by a Hamiltonian from the family. We say that the universal simulator is efficient if the simulation is efficient for all local Hamiltonians.

In [6] a number of simple families of Hamiltonians - including the Heisenberg and XY-interaction are shown to be universal. Moreover, the authors provide a full classification of universality classes for 2-qubit interactions:

Theorem 23 (Theorem 44 from [6])**.** *Let $\mathcal{S}$ be any fixed set of two-qubit and one-qubit interactions such that $\mathcal{S}$ contains at least one interaction which is not 1-local. Then:*

- *If there exists $U \in SU(2)$ such that U locally diagonalises $\mathcal{S}$, then $\mathcal{S}$-Hamiltonians are universal classical simulators*
- *Otherwise, if there exists $U \in SU(2)$ such that, for each 2-qubit matrix $H_i \in \mathcal{S}$, $U^{\otimes 2} H_i (U^\dagger)^{\otimes 2} = \alpha_i Z^{\otimes 2} + A_i \otimes \mathbb{1} + \mathbb{1} \otimes B_i$, where $\alpha_i \in \mathbb{R}$ and A_i, B_i are arbitrary single-qubit Hamiltonians, then $\mathcal{S}$-Hamiltonians are universal stoquastic Hamiltonian simulators*
- *Otherwise, $\mathcal{S}$-Hamiltonians are universal quantum Hamiltonian simulator*

It should be noted that the class of 2 qubit interactions that are universal quantum simulators coincides precisely with the class of 2 qubit interactions that are QMA-complete [29]. This link will be expanded on in Chapter 3.

In [6] the authors go on to show that the Heisenberg and XY-models remain universal even if the interactions are restricted to lie on a square lattice. Moreover, if the target Hamiltonian is sparse then the simulation on the square lattice remains efficient. In [32] the question of universal qudit Hamiltonians is explored, and it is demonstrated that two natural generalisations of the Heisenberg model to qudits are universal. The authors also classify the k-qudit interactions that are universal when augmented with 1-qubit terms, and demonstrate universality of any interaction which is proportional to the projector onto a pure entangled state.

In a later paper, it has been demonstrated that there exist translationally invariant universal Hamiltonians in 2D [33]. These universal Hamiltonians are not in general efficient in terms of number of qudits in the simulator system, or in terms of the operator norm of the simulator Hamiltonian. However, they are efficient for simulating translationally invariant Hamiltonians.

All previous universality results have made use of perturbation gadgets - universality is demonstrated by stringing together perturbative simulations. For details of these

perturbative proofs of universality we refer readers to [6, 32, 33]. In Chapter 2 we will introduce a new method for proving universality which doesn't rely on perturbation theory.

Chapter 2

Translationally invariant universal Hamiltonians in 1D

2.1 Introduction

Previous universality results have relied heavily on using perturbation gadgets, and constructing complicated 'chains' of simulations to prove that simple models are indeed universal. In this chapter we present a new, simplified method for proving universality. This method makes use of another technique from Hamiltonian complexity theory: history state Hamiltonians [16]. Leveraging the fact that it is possible to encode computation into the ground state of local Hamiltonians, we show that it is possible to prove universality by constructing Hamiltonian models which can compute the energy levels of arbitrary target Hamiltonians.

In order to ensure that the universality constructions preserve the entire physics of the target system (and not just the energy levels), we make use of an idea originally from [34] and used recently in [35, 36, 37]: 'idling to enhance coherence'. Before computing the energy levels of the target system, the computation encoded in the simulator system 'idles' in its initial state for time L. By choosing L to be sufficiently large, we can ensure that with high probability there is a fixed set of spins in the simulator system which map directly to the state of the target system.

As well as providing a route to simplifying previous proofs, this 'history-state simulation method' also offers more insight into the origins of universality, and the relationship between universality and complexity. The classification of two-qubit interactions by their simulation ability in [6], which showed that the universal class was precisely the set of QMA-complete interactions, was suggestive of a connection between simulation and complexity. And a complexity theoretic classification of

universal models already exists in the classical case [38]. But until now it was not clear whether a connection existed for general quantum interactions, or whether it was merely an accident in the two-qubit case. Previous methods for proving universality in the quantum case didn't offer a route to proving a general equivalence between complexity and universality, and the more complicated non-commutative structure of quantum Hamiltonians meant that the techniques from the classical proof couldn't be applied. By demonstrating that it is possible to prove universality by leveraging the ability to encode computation into ground states, we have provided a route to showing that the connection between universality and complexity holds more generally. In Chapter 3 we make this insight rigorous, by deriving a full complexity theoretic classification of universal quantum Hamiltonians.

We also use the 'history-state simulation method' to provide a simple construction of two new universal models. Both of these are translationally invariant systems in 1D, and we show that one of these constructions is efficient in terms of the number of spins in the universal construction (yet not in terms of the simulating system's norm):

Theorem 24. *There exists a two-body interaction $h^{(1)}$ depending on a single parameter $h^{(1)} = h^{(1)}(\phi)$, and a fixed one-body interaction $h^{(2)}$ such that the family of translationally-invariant Hamiltonians on a chain of length N,*

$$H_{\text{univ}}(\phi, \Delta, T) = \Delta \sum_{\langle i,j \rangle} h^{(1)}_{i,j}(\phi) + T \sum_{i=0}^{N} h^{(2)}_i, \tag{2.1}$$

is a universal model, where Δ, T and ϕ are parameters of the Hamiltonian, and the first sum is over adjacent sites along the chain. The universal model is efficient in terms of the number of spins in the simulator system.

By tuning ϕ, T and Δ, this model can replicate (in the precise sense of [6]) all quantum many body physics.

This is the first translationally invariant universal model which is efficient in terms of system size overhead. Its existence implies that, for problems which preserve hardness under simulation, complexity theoretic results for general Hamiltonians can also apply to 1D, translationally invariant Hamiltonians (though care must be taken when applying this, as the construction is not efficient in the norm of the simulating system). This is for instance the case for a reduction from a PreciseQMA-hard local Hamiltonian (LH) problem, for which the reduction to a translationally-invariant

version preserves the correct promise gap scaling. This in turn implies that the local Hamiltonian problem remains PSPACE-hard for a promise gap that closes exponentially quickly, even when enforcing translational invariance for the couplings. This stands in contrast to a promise gap which closes as $1/\text{poly}$ in the system size, in which case the variant is either QMA (for non-translational invariance) or QMA_{EXP} (for translational invariance) complete.

We also construct a universal model which is described by just two free parameters, but where the model is no longer efficient in the system size overhead:

Theorem 25. *There exists a fixed two-body interaction $h^{(3)}$ and a fixed one-body interaction $h^{(2)}$ such that the family of translationally-invariant Hamiltonians on a chain of length N,*

$$H_{\text{univ}}(\Delta, T) = \Delta \sum_{\langle i,j \rangle} h^{(3)}_{i,j} + T \sum_{i=0}^{N} h^{(2)}_i, \tag{2.2}$$

is a universal model, where Δ and T are parameters of the Hamiltonian, and the first sum is over adjacent sites along the chain.

By varying the size of the chain N that this Hamiltonian is acting on, and tuning the Δ and T parameters in the construction, this Hamiltonian can replicate (again in the precise sense of [6]) all quantum many body physics. We are able to demonstrate that constructing a universal model with no free parameters is not possible, but the existence of a universal model with just one free parameter is left as an open question.

The remainder of this chapter is set out as follows. In Section 2.2 we give an overview of the new method for proving universality, and our two new universal constructions. Reading these sections should be enough to gain an intuitive understanding of our approach and our results. The full proofs of our results are given in Section 2.3 - this section may be skipped on an initial reading if you are primarily interested in understanding the general approach, or the applications of the results. The complexity theory implications are discussed in Section 2.4. A discussion of the results in this chapter and Chapter 3 is given in Chapter 4.

2.2 Overview of construction

2.2.1 High-level outline of the construction

As mentioned in subsection 1.2.3, the key technique we make use of in our universality constructions is the ability to encode computations into the ground states of local

Hamiltonians. The model of computation we encode is the quantum Turing machine (QTM) model - standard techniques for encoding QTMs in local Hamiltonians give translationally invariant Hamiltonians [39, 18].

In both the constructions we develop in this work a description of the Hamiltonian to be simulated (the "target" Hamiltonian, H_{target}) is encoded in the binary expansion of some natural number, $x \in \mathbb{N}$. Details of this encoding are given in subsection 2.2.2. The natural number x is then itself encoded in some parameter of the universal Hamiltonian (see subsection 2.2.3 for two methods of encoding natural numbers in parameters of universal Hamiltonians).

The Hamiltonian we use to construct the universal model has as its ground state computational history states (cf Definition 12) which encode two QTMs (M_1 and M_{PE}) which share a work tape. The two computations are 'dovetailed' together - the computation M_1 occurs first, and the result of this computation is used as input for M_{PE}. The first QTM, M_1, extracts the binary expansion of x from the parameter of the Hamiltonian. At the end of M_1's computation, the binary expansion of x is written on the work tape which M_1 shares with M_{PE}. An outline of the methods we use to extract x and write it on the Turing machine tape are given in subsection 2.2.3.

The second QTM, M_{PE} reads in x, which contains a description of H_{target}, from the work tape which it shares with M_1. It also reads in an input state $|\psi\rangle$ - this is unconstrained by the computation (it can be thought of as carrying out the same role as a witness in a QMA verification circuit). It then carries out phase estimation on $|\psi\rangle$ with respect to the unitary generated by H_{target}.

The Hamiltonian which encodes M_1 and M_{PE} has a zero-energy degenerate ground space, spanned by history states with all possible input states $|\psi\rangle$. In order to recreate the spectrum of H_{target} we need to break this degeneracy. We achieve this by adding one body projectors to the universal Hamiltonian which give the correct energy to the output of M_{PE} to reconstruct the spectrum of H_{target}. These break the degeneracy of the zero-energy ground space by giving different energy to the different history states depending on what state the phase estimation was applied to (and therefore what the output of M_{PE} was).

With this construction the energy levels of the universal Hamiltonian recreate the energy levels of H_{target}. To ensure that the eigenstates are also correctly simulated, before M_1 carries out its computation, it 'idles' in its initial state for some time L. This 'idling' ensures that (with high probability) the simulator system is in the (unentangled) state which corresponds to the zeroth time step in the circuit - so

there is a straightforward mapping between the simulator system and the system being simulated. By choosing L large enough, we show that this construction can approximately simulate any target Hamiltonian. A more detailed sketch of how we use idling and phase estimation to achieve simulation is given in subsection 2.2.4, while rigorous proofs are given in Section 2.3.

2.2.2 A Digital Representation of a Local Hamiltonian

As discussed in subsection 2.2.1, we need to encode a description of the target Hamiltonian H_{target} in some parameter of the universal Hamiltonian. In subsection 2.2.3 we outline the two methods we use to encode a natural number in the parameter of a Hamiltonian. But how do we represent $H_{\text{target}} = \sum_{i=1}^{m} h_i$ in the binary expansion of a natural number $x \in \mathbb{N}$, irrespective of its origin?

We will assume that H_{target} is a k-local Hamiltonian, acting on n spins of local dimension d. We emphasize that k can be taken to be n, i.e. the system size—and therefore we can simulate *any* Hamiltonian, not just local ones. However we keep track of the locality parameter k as it is relevant when deriving the overhead of our simulations.

Every value needed to specify the k-local simulated system H_{target} will be represented in Elias-γ' coding, which is a simple self-delimiting binary code which can encode all natural numbers [40, 41]. For the purpose of the encoding, we will label the n spins in the system to be simulated by integers $i = 1, \ldots, n$.

The encoding of H_{target} begins with the three meta-parameters n (spin count), followed by k (locality), and then m (number of k-local terms). Each of the m k-local terms in H is then specified by giving the label of the spins involved in that interaction, followed by a description of each term of the $d^k \times d^k$ Hermitian matrix describing that interaction. Each such matrix entry is specified by giving two integers a and b. The matrix entry can be recovered by calculating $a\sqrt{2} - b$, which is accurate up to a small error.[1]

Specifying H_{target} to accuracy δ requires each such matrix entry to be specified to accuracy $\delta/(md^{2k})$. Therefore the length of the description of H_{target} is

$$md^{2k} \log\left(\|H_{\text{target}}\| md^{2k}/\delta\right) = \text{poly}\left(n, d^k, \log(\|H\|/\delta)\right) \tag{2.3}$$

[1]Note that by Weyl's equidistribution theory $\sqrt{2}a \mod 1$ uniformly covers $[0, 1]$; the set $\mathcal{T} = \{a\sqrt{2} - b \mid a, b \in \mathbb{Z}^+\}$ is dense in $\mathbb{R}$.

Finally, the remaining digits of x specify Ξ—the bit precision to with which the phase estimation algorithm should calculate the energies (i.e. we require QPE to extract Ξ binary digits), and L—the length of time the system should "idle" in its initial state before beginning its computation.

So, the binary expansion $B(x)$ of x has the following form:

$$B(x) \coloneqq \gamma'(n) \cdot \gamma'(k) \cdot \gamma'(m) \cdot \left[\gamma'(i)^{\cdot k} \cdot \left(\gamma'(a_j) \cdot \gamma'(b_j) \right)^{4^k} \right]^{\cdot m} \cdot \gamma'(\Xi) \cdot \gamma'(L). \quad (2.4)$$

Here $\gamma'(n)$ denotes n in Elias-γ' coding, and $\cdot$ denotes concatenation of bit strings.

With regards to the identification of a real number $n = \sqrt{2}a - b$, we observe that it is clearly straightforward to recover n from a and b (by performing basic arithmetic). The other direction works as follows.

Remark 26. *Let $n \in \mathbb{N}$, and let $\Xi \in \mathbb{N}$ denote a precision parameter. Then we can find numbers $a, b \in \mathbb{N}$ such that*

$$\left| n - \sqrt{2}a + b \right| \leq 2^{-\Xi},$$

and the algorithm runs in $\mathrm{O}(\mathrm{poly}(\Xi, \log_2 n))$.

Proof. We solve $2^{\Xi} n = \lfloor 2^{\Xi} \sqrt{2} \rfloor a - 2^{\Xi} b$ as a linear Diophantine equation in the variables a and b, with largest coefficient $\mathrm{O}(2^{\Xi} n)$. This can be done in polynomial time in the bit precision of the largest coefficient, for instance by using the extended Euclidean algorithm [42]. □

In Section 2.3, we describe a construction to $(\Delta', \eta, \epsilon')$-simulate the Hamiltonian described by x, but note that this will only give a $(\Delta', \eta, \epsilon' + \delta)$-simulation of the actual target Hamiltonian H_{target}.

2.2.3 Encoding the target Hamiltonian in parameters of the simulator Hamiltonian

In subsection 2.2.2 we described how we encode the information about the Hamiltonian we want to simulate, H_{target} in a natural number x. Now we require a method to encode x in some parameter of the universal Hamiltonian, and a method to write its binary expansion on the Turing machine tape shared by M_1 and M_{PE}. We develop two constructions, building on the mappings in [39] and [18]. The first construction is efficient in terms of the number of spins in the simulator system, while the second

construction is not efficient, but requires less parameters to specify the universal model. In both cases the computation encoded in the ground state of the Hamiltonian is a QTM, and the mapping from a QTM to the Hamiltonian gives a translationally invariant Hamiltonian.

2.2.3.1 Encoding the target Hamiltonian in a phase of the simulator Hamiltonian

First we consider the construction building on the work in [39]. Here, we encode the natural number $x \in \mathbb{N}$ in a phase $\phi = x/2^{\lceil \log_2 x \rceil}$ of the Hamiltonian.

The Hamiltonian for this construction is given by $H = \sum_{i=1}^{N} h^{(i,i+1)}$ where N is the number of spins in the simulator system, and h is a two-body interaction of the form [43, Theorem 32]:

$$h = A + (e^{i\pi\phi}B + e^{i\pi 2^{-|\phi|}}C + \text{h.c.}) \tag{2.5}$$

where A is a fixed Hermitian matrix and B, C are fixed non-Hermitian matrices. For a detailed construction of the terms in the Hamiltonian we refer the interested reader to [43, Section 4].

The circuit-to-Hamiltonian map encodes two Turing machine computations "dovetailed" together, where the two Turing machines share a work tape. The first computation is a phase estimation algorithm. It extracts the phase ϕ from the Hamiltonian, and writes its binary expansion onto the work tape. The second computation will be outlined in subsection 2.2.4.

In order to extract a digits from a phase $\phi = 0.\phi_1\phi_2\cdots\phi_a\phi_{a+1}\cdots$, we require a runtime of 2^a. In our case, we have $a = |x| = \text{poly}\left(n, d^k, \log(\|H\|/\delta)\right)$, where $|x|$ denotes the number of digits in the binary expansion of x. As our computation is encoded as a computational history state, this in turn means that the spectral gap of the history state Hamiltonian necessarily closes as $\mathrm{O}(2^{-\text{poly}\left(n,d^k,\log(\|H\|/\delta)\right)})$ [44, 15, 24]. This scaling of the spectral gap means that the universal model constructed via this method is not efficient in terms of the norm of the simulator system (see Theorem 31 for full discussion of the scaling).

However, it is important to note that using the construction from [39] it is possible to encode a computation with exponential runtime into a Hamiltonian on polynomially many spins. Details of the construction are given in [43, Section 4.5] (in particular the relevant scaling is discussed on [43, Page 81]). We will not give the details of the construction here, but note that it encodes a Turing machine which runs for $\mathrm{O}(N\exp(N))$ time steps in a Hamiltonian acting on N spins [43, Proposition 45].

Therefore, the universal model constructed via this method is efficient in terms of the number of spins in the simulator system.

2.2.3.2 Encoding the target Hamiltonian in the size of the simulator system

Our second construction builds on the mapping in [18]. Here, we encode the description of the H_{target} into the binary expansion of N - the number of spins the universal Hamiltonian is acting on.

The circuit-to-Hamiltonian map encodes two Turing machine computations "dovetailed" together, where again the two Turing machines share a work tape. The first Turing machine is a binary counter Turing machine. After it has finished running, the binary expansion of N is written on the Turing machine's work tape. In our construction, the binary expansion of N contains the description of H_{target}. We will discuss the second computation in subsection 2.2.4.

The binary counter QTM takes time N to write out the binary expansion of N on its work tape. Since H_{target} is encoded in the binary expansion of N, this run time, as well as the size of the simulator system is exponential in the size of the target system. Moreover, since the runtime is exponential in the size of the target system, the spectral gap of the universal Hamiltonian closes exponentially fast. Therefore, the universal model constructed via this method is not efficient in terms of number of spins or the norm of the simulator system. See Theorem 32 for a full discussion of the scaling of this universal model.

In this case the interactions of the Hamiltonian are entirely fixed - they enforce that the ground state of the Hamiltonian is a history state encoding a QTM computation (for a detailed construction of the terms in the Hamiltonian we refer readers to [18]. There are two additional global parameters in the Hamiltonian which depend on the accuracy of the simulation - we defer discussion of those parameters to the technical proofs of Lemma 29 and Theorem 32. All the information about the target Hamiltonian (the Hamiltonian to be simulated) is entirely encoded in the binary expansion of N - the number of spins in the simulator system.

2.2.4 Dovetailing for simulation

After the computation carried out by M_1 has finished, the binary expansion of x is written out on the work-tape shared by M_1 and M_{PE}. We then construct (using standard techniques from [39, 18]) a Hamiltonian such that the two Turing machines M_1 and M_{PE} share a work tape. At the beginning of its computation, M_{PE} reads in a description of the target Hamiltonian H that we wish to simulate. M_{PE} then carries

out phase estimation on some input state $|\psi\rangle$ (left unconstrained, just like a QMA witness)[2] with respect to the unitary generated by the target Hamiltonian, $U = e^{iH\tau}$ for some τ such that $\|H\tau\| < 2\pi$. It then outputs the eigenphase ϕ in terms of a pair of natural numbers (a, b) such that $\phi = a\sqrt{2} - b$ (which can be done efficiently via Remark 26).

The ground space of the Hamiltonian which encodes the computation of M_1 and M_{PE} has zero energy, and is spanned by history states in a superposition over all possible initial states $|\psi\rangle$. In general the Hamiltonian we want to simulate doesn't have a highly degenerate zero energy ground state, so we need to break this degeneracy and construct the correct spectrum for H_{target}. In order to break the degeneracy and reconstruct the spectrum of H_{target}, we add one body projectors to the universal Hamiltonian, which are tailored such that the QPE output (a, b) identifies the correct energy penalty to inflict.

In order to ensure that the encoding of H_{target} in the universal Hamiltonian is local, we make use of an idea originally from [34] and used recently in [35, 36, 37], which has been called 'idling to enhance coherence'. Before carrying out the phase-estimation computation, the system "idles" in its initial state for time L. By choosing L appropriately large, we can ensure that with high probability the input spins (the spins which form the unconstrained input $|\psi\rangle$ to M_{PE}) are found in their initial states. This means that (with high probability) there are a subset of spins on the simulator system whose state directly maps to the state which is being simulated in the target system. This ensures that the encoding is (approximately) local (see Lemma 29 for detailed analysis of how idling is used to achieve universality).

2.3 Universality

2.3.1 Translationally-Invariant Universal Models in 1D

In this section we prove our main result: there exist translationally invariant, nearest neighbour Hamiltonians acting on a chain of qudits, which are universal quantum simulators.

All the 'circuit-to-Hamiltonian' mappings we make use of in this work are what are known as "Standard form Hamiltonians". Where "Standard form Hamiltonians" are a certain class of circuit-to-Hamiltonian constructions, defined in [45]. We refer interested readers to [45] for the full definition - and simply note that it encompasses

[2] Although quantum phase estimation takes as input an eigenvector of the unitary, we show in the proof that this suffices, as the argument then extends to general input states by linearity.

the Turing-machine based mappings which we make use of in this work [39, 18]. In [45], the following result was shown, which we will make use of in our proofs:

Lemma 27 (Standard form ground states; restatement of [45, Lem. 5.8, Lem. 5.10])**.** *Let H_{SF} be a Standard Form Hamiltonian encoding a computation U, which takes (classical) inputs from a Hilbert space $\mathcal{S}$, and which sets an output flag with certainty if it is given an invalid input. For $\left|\psi_\mu\right\rangle \in \mathcal{S}$ and $\Pi_{t=1}^{T} U_t = U$ we define*

$$\left|\Phi(U,\psi_\mu)\right\rangle := \frac{1}{\sqrt{T}} \sum_{t=1}^{T} U_t \ldots U_1 \left|\psi_\mu\right\rangle |t\rangle .$$

Then $\mathcal{L} = \mathrm{span}\{\left|\Phi(U,\psi_\mu)\right\rangle\}_{\mu=1}^{d^n}$ defines the kernel of H_{SF}, i.e. $H_{\mathrm{SF}}|_{\mathcal{L}} = 0$. The smallest non-zero eigenvalue of H_{SF} scales as $1 - \cos \pi/2T$.

We also require a digital quantum simulation algorithm, summarized in the following lemm:

Lemma 28 (Implementing a Local Hamiltonian Unitary)**.** *For a k-local Hamiltonian $H = \sum_{i=1}^{m} h_i$ on an n-partite Hilbert space of local dimension d, and where $m = \mathrm{poly}\, n$, there exists a QTM that implements a unitary $\tilde{U}$ such that*

$$\tilde{U} = \mathrm{e}^{\mathrm{i}Ht} + \mathrm{O}(\epsilon),$$

and which requires time $\mathrm{poly}(1/\epsilon, d^k, \|H\|t, n)$.

Proof. Follows directly from [46, 47]. □

The polynomial time bound in Lemma 28 suffices for our purposes; a tighter (and more complicated) bound, also for the more general case of sparse Hamiltonians, can be found in [48].

We can now start our main analysis by proving that "dovetailing" quantum computations—rigorously defined and constructed in [39, Lem. 22]—can be used to construct universal simulators.

Lemma 29 (Dovetailing for simulation)**.** *Let M_1 be a QTM which writes out the binary expansion of some $x \in \mathbb{N}$ on its work tape. Assume there exists a standard form Hamiltonian which encodes the Turing machine M_1. Then there also exists a*

Track	Purpose
1	Input track, contains input state $\|\psi\rangle \in \mathbb{C}^2$ followed by string of $\|0\rangle$s
2	Turing machine work tape (shared by M_1 and M_{PE})
3	Tape head and state for M_1
4	Tape head and state for M_{PE}
$5, 6, \ldots$	Clock tracks for standard form clock construction

Table 2.1: Local Hilbert space decomposition for H_{SF}.

standard form Hamiltonian $H_{\mathrm{SF}}(x)$, which encodes the computation M_1 dovetailed with a QTM M_{PE}, such that the family of Hamiltonians

$$H_{\mathrm{univ}}(x) = \Delta H_{\mathrm{SF}}(x) + T \sum_{i=0}^{N-1} \left(\sqrt{2}\Pi_\alpha - \Pi_\beta \right) \tag{2.6}$$

can simulate any quantum Hamiltonian. Here Δ and T are parameters of the model, and Π_α and Π_β are one-body projectors,

Proof of Lemma 29. To prove this we show that the $H_{\mathrm{univ}}(x)$ can satisfy the definition to be an approximate simulation of an arbitrary "target Hamiltonian" H_{target}, to any desired accuracy. We break up the proof into multiple parts. First we construct a history state Hamiltonian $H_{\mathrm{SF}}(x)$, which encodes two Turing machine computations: M_1 which extracts a description of H_{target} from a parameter of H_{SF}, and M_{PE} which carries out phase estimation on the unitary generated by H_{target}. Then we define the one-body projectors Π_α and Π_β which break up the ground space degeneracy of H_{SF}, and inflict just the right amount of penalty to approximately reconstruct the spectrum of H_{target} in its entirety.

Construction of H_{SF}. H_{SF} is a standard form history state Hamiltonian with a ground space laid out in Lemma 27. The local states of the spins on which H_{SF} acts are divided into multiple "tracks". There are a constant number of these, hence a constant local Hilbert space dimension. The exact number will depend on the standard form construction being used. Each track serves its own purpose, as outlined in Table 2.1. See [18, 39] for more detail.

The QTM M_{PE} reads in the description of H_{target}—provided as integer $x \in \mathbb{N}$ output by the Turing machine M_1 whose worktape it shares. M_{PE} further reads in the unconstrained input state $|\psi\rangle$ (see Table 2.1 for details of the local Hilbert space decomposition). But instead of proceeding immediately, M_{PE} idles for L time-steps

(where L is specified in the input string x, as explained in subsection 2.2.2), before proceeding to carry out the quantum phase estimation algorithm.

The quantum phase estimation algorithm is carried out with respect to the unitary $U = \mathrm{e}^{\mathrm{i}H_{\text{target}}\tau}$ for some τ such that $\|H_{\text{target}}\tau\| < 2\pi$. It takes as input an eigenvector $|u\rangle$ of U, and calculates the eigenphase ϕ_u. The output of M_{PE} is then the pair of integers (a_u, b_u) (corresponding to the extracted phase $\phi_u = \sqrt{2}a_u - b_u$ as explained in Remark 26), specified in binary on an output track. To calculate λ_u—the eigenvalue of H_{target}—to accuracy ϵ requires determining ϕ_u to accuracy $\mathrm{O}(\epsilon/\|H_{\text{target}}\|)$ which takes $\mathrm{O}(\|H_{\text{target}}\|/\epsilon)$ uses of $U = \mathrm{e}^{\mathrm{i}H_{\text{target}}\tau}$. The unitary U must thus be implemented to accuracy $\mathrm{O}(\epsilon/\|H_{\text{target}}\|)$, which is done using Lemma 28; the latter introduces an overhead $\mathrm{poly}(n, d^k, \|H_{\text{target}}\|, \tau, 1/\epsilon)$ in the system size n, local dimension d, locality k, and target accuracy ϵ. The error overhead of size $\mathrm{poly}\, 1/\epsilon$ due to the digital simulation of the unitary is thus polynomial in the precision, as are the $\propto 1/\epsilon$ repetitions required for the QPE algorithm. The whole procedure takes time

$$T_{\text{PE}} \coloneqq \mathrm{poly}(d^k, \|H_{\text{target}}\|/\epsilon, n). \tag{2.7}$$

In our construction the input to M_{PE} is not restricted to be an eigenvector of $|u\rangle$, but it can always be decomposed as $|\psi\rangle = \sum_u m_u |u\rangle$. By linearity, for input $|\psi\rangle = \sum_u m_u |u\rangle$ the output of M_{PE} will be a superposition in which the output (a_u, b_u) occurs with amplitude m_u.

After M_{PE} has finished its computation, its head returns to the end of the chain. A dovetailed counter then decrements $a_u, a_u - 1, \ldots, 0$ and $b_u, b_u - 1, \ldots, 0$.[3] For each timestep in the counter $a_u, a_u - 1, \ldots, 0$ the Turing machine head changes one spin to a special flag state $|\Omega_a\rangle$ which does not appear anywhere else in the computation. While for each timestep in the counter $b_u, b_u - 1, \ldots, 0$ the Turing machine head changes one spin to a different flag state $|\Omega_b\rangle$. (See e.g. [49, Lem. 16]) for a construction of a Turing machine with these properties.)

By Lemma 27, the ground space $\mathcal{L}$ of H_{SF} is spanned by computational history states as given in Definition 12, and is degenerate since any input state $|\psi\rangle$ yields a valid computation. Therefore:

$$\ker(H_{\text{SF}}) = \mathcal{L} = \mathrm{span}_{|\psi\rangle}\left(\frac{1}{\sqrt{T}}\sum_{t=1}^{T}\left|\psi^{(t)}\right\rangle|t\rangle\right) \tag{2.8}$$

[3] For general input state $|\psi\rangle = \sum_u m_u |u\rangle$ there will be a superposition where the counter $a_u, a_u - 1, \ldots, 0$ and $b_u, b_u - 1, \ldots, 0$ occurs with amplitude m_u.

where $\left|\psi^{(t)}\right\rangle$ denotes the state of the system at time step t if the input state was $|\psi\rangle$.

A Local Encoding. In order to prove that $H_{\text{univ}}(N)$ can simulate all quantum Hamiltonians, we need to demonstrate that there exists a local encoding $\mathcal{E}(M)$ such that the conditions of Definition 15 are satisfied. To this end, let

$$\left|\Phi_{\text{idling}}(\psi)\right\rangle := \frac{1}{\sqrt{L'}} \sum_{t=1}^{L'} \left|\psi^{(t)}\right\rangle |t\rangle$$

where $L' = T_1 + L$, and where T_1 is the number of time steps in the M_1 computation. This is the history state up until the point that M_{PE} begins its computation (i.e. the point at which the 'idling to enhance coherence' ends). So, throughout the computation encoded by this computation the spins which encode the information about the input state remain in their initial state, and we can write:

$$\left|\Phi_{\text{idling}}(\psi)\right\rangle = |\psi\rangle \otimes \frac{1}{\sqrt{L'}} \sum_{t=1}^{L'} |t\rangle$$

The rest of the history state we capture in

$$\left|\Phi_{\text{comp}}(\psi)\right\rangle := \frac{1}{\sqrt{T - L'}} \sum_{t=L'+1}^{T} \left|\psi^{(t)}\right\rangle |t\rangle ,$$

such that the total history state is

$$|\Phi(\psi)\rangle = \sqrt{\frac{L'}{T}} \left|\Phi_{\text{idling}}(\psi)\right\rangle + \sqrt{\frac{T - L'}{T}} \left|\Phi_{\text{comp}}(\psi)\right\rangle .$$

We now define the encoding $\mathcal{E}(M) = VMV^\dagger$ via the isometry

$$V = \sum_i \left|\Phi_{\text{idling}}(i)\right\rangle \langle i| . \tag{2.9}$$

where $|i\rangle$ are the computational basis states (any complete basis will suffice). $\mathcal{E}$ is a local encoding, which can be verified by a direct calculation:

$$\begin{aligned}
\mathcal{E}(A_j \otimes \mathbb{1}) &= \sum_{ik} \left|\Phi_{\text{idling}}(i)\right\rangle \langle i| \left(A_j \otimes \mathbb{1}\right) |k\rangle \left\langle \Phi_{\text{idling}}(k)\right| \\
&= \sum_{ik} |i\rangle \langle i| \left(A_j \otimes \mathbb{1}\right) |k\rangle \langle k| \otimes \frac{1}{L} \sum_{tt'=1}^{L} |t\rangle \langle t'| \\
&= \left(A_j \otimes \mathbb{1}\right) \sum_{i} |i\rangle \langle i| \otimes \frac{1}{L} \sum_{tt'=1}^{L} |t\rangle \langle t'| \\
&= \left(A_j^{\text{phys}} \otimes \mathbb{1}\right) \sum_{i} \left|\Phi_{\text{idling}}(i)\right\rangle \left\langle \Phi_{\text{idling}}(i)\right| \\
&= \left(A_j^{\text{phys}} \otimes \mathbb{1}\right) \mathcal{E}(\mathbb{1}),
\end{aligned} \tag{2.10}$$

where A_j^{phys} is the operator A acting on the Hilbert space corresponding to the j^{th} qudit.

We now consider the encoding $\mathcal{E}'(M) = V'MV'^{\dagger}$, defined via

$$V' = \sum_{i} |\Phi(i)\rangle \langle i| . \tag{2.11}$$

We have that

$$\begin{aligned}
\|V' - V\|^2 &= \left\| \sum_i \left(|\Phi(i)\rangle \langle i| - \left|\Phi_{\text{idling}}(i)\right\rangle \langle i| \right) \right\|^2 \\
&= \left\| \sum_i \left(\sqrt{\frac{T-L'}{T}} \left|\Phi_{\text{comp}}(i)\right\rangle \langle i| + \left(\sqrt{\frac{L'}{T}} - 1 \right) \left|\Phi_{\text{idling}}(i)\right\rangle \langle i| \right) \right\|^2 \\
&\leq 2\left(1 - \sqrt{\frac{L'}{T}}\right) \leq 2\frac{T-L'}{T} = 2\frac{T_{\text{PE}}}{T}.
\end{aligned} \tag{2.12}$$

By Lemma 27, $S_{\mathcal{E}'}$ is the ground space of H_{SF}.

Splitting the Ground Space Degeneracy of H_{SF}. What is left to show is that there exist one body-projectors Π_α and Π_β which add just the right amount of energy to states in the kernel $\mathcal{L}(H_{\text{SF}})$ to reproduce the target Hamiltonian's spectrum. We

first choose the one body terms in H_{univ} to be projectors onto local subspaces which contain the two states which are outputs of the M_{PE} computation - $|\Omega_a\rangle$ and $|\Omega_b\rangle$:

$$\Pi_a \coloneqq \sum_{i=1}^{N} |\Omega_a\rangle\langle\Omega_a|_i \quad \text{and} \quad \Pi_b \coloneqq \sum_{i=1}^{N} |\Omega_b\rangle\langle\Omega_b|_i \,.$$

We have shown that if the input state is $|u\rangle$, which is an eigenstate of U with eigenphase $\phi_u = a_u\sqrt{2} - b_u$, then the history state will contain a_u terms with one spin in the state $|\Omega_a\rangle$ and b_u terms with one spin in the state $|\Omega_b\rangle$ (each term in the history state will have amplitude $\frac{1}{T}$). If the input is a general state $|\psi\rangle = \sum_u m_u |u\rangle$ then for each u the history state will contain a_u terms with one spin in the state $|\Omega_a\rangle$ and b_u terms with one spin in the state $|\Omega_b\rangle$, where now each of these terms has amplitude m_u/T.

Let $\Pi \coloneqq \sum_i |\Phi(i)\rangle\langle\Phi(i)|$ for some complete basis $|i\rangle$, and we define $H_1 \coloneqq T(\sqrt{2}\Pi_a - \Pi_b)$, where T is the total time in the computation. It thus follows that the energy of $|\Phi(u)\rangle$ with respect to the operator $\Pi H_1 \Pi$ is given by $\phi_u + \mathrm{O}(\epsilon)$.

Finally, we need the following technical lemma from [31].

Lemma 30 (First-order simulation [31])**.** *Let H_0 and H_1 be Hamiltonians acting on the same space and Π be the projector onto the ground space of H_0. Suppose that H_0 has eigenvalue 0 on Π and the next smallest eigenvalue is at least 1. Let V be an isometry such that $VV^\dagger = \Pi$ and*

$$\|VH_{\text{target}}V^\dagger - \Pi H_1 \Pi\| \leq \epsilon/2. \tag{2.13}$$

Let $H_{\text{sim}} = \Delta H_0 + H_1$. Then there exists an isometry $\tilde{V}$ onto the the space spanned by the eigenvectors of H_{sim} with eigenvalue less than $\Delta/2$ such that

1. $\|V - \tilde{V}\| \leq \mathrm{O}(\|H_1\|/\Delta)$
2. $\|\tilde{V}H_{\text{target}}\tilde{V}^\dagger - H_{\text{sim}<\Delta/2}\| \leq \epsilon/2 + \mathrm{O}(\|H_1\|^2/\Delta)$

We will apply Lemma 30 with $H_0 = 2T^2 H_{\text{SF}}$ and $H_1 = T(\sqrt{2}\Pi_a - \Pi_b)$. We have $\lambda_{\min}(H_{\text{SF}}) = 0$ and the next smallest non-zero eigenvalue of H_{SF} is $(1 - \cos(\pi/2T) \geq 1/2T^2)$ by Lemma 27, so $H_0 = 2T^2 H_{\text{SF}}$ has next smallest non-zero eigenvalue at least 1. Moreover, $\|H_1\| = \sqrt{2}T$. Note that V', as defined in eq. (2.11), is an isometry which maps onto the ground state of H_0. By construction we have that the spectrum of H_{target} is approximated to within ϵ by H_1 restricted to the ground space of H_{SF}, thus $\|\Pi H_1 \Pi - \tilde{\mathcal{E}}(H)\| \leq \epsilon$.

Lemma 30 therefore implies that there exists an isometry $\tilde{V}$ that maps exactly onto the low energy space of H_{univ} such that $\|\tilde{V} - V'\| \leq \mathrm{O}(\sqrt{2}T/(\Delta/2T^2)) = \mathrm{O}(T^3/\Delta)$. By the triangle inequality and eq. (3.26), we have:

$$\|V - \tilde{V}\| \leq \|V - V'\| + \|V' - \tilde{V}\| \leq O\left(\frac{T^3}{\Delta} + \frac{T_{\text{PE}}}{T}\right). \tag{2.14}$$

The second part of the lemma implies that

$$\|\tilde{V} H_{\text{target}} \tilde{V}^\dagger - H_{\text{univ}<\Delta'/2}\| \leq \epsilon/2 + \mathrm{O}((\sqrt{2}T)^2/(\Delta/2T^2)) = \epsilon/2 + \mathrm{O}(T^4/\Delta). \tag{2.15}$$

Therefore, the conditions of Definition 15 are satisfied for a $(\Delta', \eta, \epsilon')$-simulation of H_{target}, with $\eta = O\left(T^3/\Delta + T_{\text{PE}}/T\right)$, $\epsilon' = \epsilon + \mathrm{O}(T^4/\Delta)$ and $\Delta' = \Delta/2T^2$. Therefore we must increase L so that $T \geq \mathrm{O}(T_{\text{PE}}/\eta) = \mathrm{poly}(n, d^k, \|H\|, 1/\epsilon, 1/\eta)$ by eq. (2.7), (thereby determining x), and increase Δ so that

$$\Delta \geq \Delta' T^2 + \frac{T^3}{\eta} + \frac{T^4}{\epsilon} \tag{2.16}$$

to obtain a $(\Delta', \eta, \epsilon)$-simulation of the target Hamiltonian. The claim follows. □

We can now prove our main theorem:

Theorem 31. *There exists a two-body interaction depending on a single parameter $h(\phi)$ such that the family of translationally-invariant Hamiltonians on a chain of length N,*

$$H_{\text{univ}}(\phi, \Delta, T) = \Delta \sum_{\langle i,j \rangle} h(\phi)_{i,j} + T \sum_{i=0}^{N-1} \left(\sqrt{2}\Pi_\alpha - \Pi_\beta\right)_i, \tag{2.17}$$

is a universal model, where Δ, T and ϕ are parameters of the Hamiltonian, and the first sum is over adjacent site along the chain. Furthermore, the universal model is efficient in terms of the number of spins in the simulator system.

Proof. The two body interaction $h(\phi)$ makes up a standard form Hamiltonian which encodes a QTM, M_1 dovetailed with the phase-estimation computation from Lemma 29. The QTM M_1 carries out phase estimation on the parameter ϕ in the Hamiltonian, and writes out the binary expansion of ϕ (which contains a description of the Hamiltonian to be simulated) on its work tape. There is a standard form Hamiltonian in [39] which encodes this QTM, so by Lemma 29 we can construct a

standard form Hamiltonian which simulates all quantum Hamiltonians by dovetailing M_1 with M_{PE}.

The space requirement for the computation is $\mathrm{O}(|\phi|)$, where $|\phi|$ denotes the length of the binary expansion of ϕ, and the computation requires time $T_1 = \mathrm{O}(|\phi|2^{|\phi|})$ [43, Theorem 10] As we commented in subsection 2.2.3.1, the standard form clock construction set out in [43, Section 4.5] allows for computation time of $\mathrm{O}(|\phi|2^{|\phi|})$ using a Hamiltonian on $|\phi|$ spins. We therefore find that for a k-local target Hamiltonian H_{target} acting on n spins of local dimension d, the number of spins required in the simulator system for a simulation that is ϵ close to H_{target} is given by $N = \mathrm{O}(|\phi|) = \mathrm{poly}\left(n, d^k, \|H\|, 1/\eta, 1/\epsilon\right)$.

Therefore, the universal model is efficient in terms of the number of spins in the simulator system as defined in Definition 16. □

Note that this universal model is *not* efficient in terms of the norm $\|H_{\mathrm{univ}}\|$. This is immediately obvious, since $\|H_{\mathrm{univ}}\| = \Omega(\Delta)$, and using the relations between Δ', η, ϵ, and T and Δ from Lemma 29 and eq. (2.16),

$$T = T_1 + L + T_{\mathrm{PE}} = O\left(2^x + \mathrm{poly}\left(n, d^k, \|H_{\mathrm{target}}\|, \frac{1}{\epsilon}, \frac{1}{\eta}\right)\right) \quad \text{and} \quad \Delta \geq \Delta' T^2 + \frac{T^3}{\eta} + \frac{T^4}{\epsilon}$$

by eq. (2.7), so T, Δ are both $\mathrm{poly}\left(2^x, \|H_{\mathrm{target}}\|, \Delta', 1/\epsilon, 1/\eta\right)$. For a k-local Hamiltonian H_{target} with description x as presented in subsection 2.2.2, $|x| = \Omega\left(md^{2k}\log\left(\|H_{\mathrm{target}}\|md^{2k}/\delta\right)\right)$.

However if we only wish to simulate a translationally invariant k-local Hamiltonian H_{target}, this can be specified to accuracy δ with just $\log\left(\|H_{\mathrm{target}}\|md^{2k}/\delta\right)$ bits of information. In this case (for $d, k = \mathrm{O}(1)$ and taking $\delta = \epsilon$), the interaction strengths are then $\mathrm{poly}(n, \|H_{\mathrm{target}}\|, \Delta', \frac{1}{\eta}, \frac{1}{\epsilon})$, and the whole simulation is efficient.

Lemma 29 also allows the construction of a universal quantum simulator with two free parameters.

Theorem 32. *There exists a fixed two-body interaction h such that the family of translationally-invariant Hamiltonians on a chain of length N,*

$$H_{\mathrm{univ}}(\Delta, T) = \Delta \sum_{\langle i,j \rangle} h_{i,j} + T \sum_{i=0}^{N-1} \left(\sqrt{2}\Pi_\alpha - \Pi_\beta\right)_i, \tag{2.18}$$

is a universal model, where Δ and T are parameters of the Hamiltonian, and the first sum is over adjacent sites along the chain.

Proof. As in Theorem 31, the two body interaction h makes up a standard form Hamiltonian which encodes a QTM M_1 dovetailed with the phase-estimation computation from Lemma 29. It is based on the construction from [18].

Take M_1 to be a binary counter Turing machine which writes out N—the length of the qudit chain—on its work tape. We will choose N to contain a description of the Hamiltonian to be simulated, as per subsection 2.2.2. There is a standard form Hamiltonian in [18] which encodes this QTM, so by Lemma 29 we can construct a standard form Hamiltonian which simulates all quantum Hamiltonians by dovetailing M_1 with M_{PE}.

Since $B(N)$, as defined in eq. (2.4), contains a description of the Hamiltonian to be simulated, we have that

$$N = \mathrm{poly}\left(2^{\mathrm{poly}(n,\|H_{\mathrm{target}}\|,1/\eta,1/\epsilon)}\right).$$

The standard form clock used in the construction allows for computation time polynomial in the length of the chain, so exp(poly)-time in the size of the target system. As before, by eq. (2.7), we require

$$T = T_1 + L + T_{\mathrm{PE}} = O\left(N + \mathrm{poly}\left(n, d^k, \|H_{\mathrm{target}}\|, \frac{1}{\epsilon}, \frac{1}{\eta}\right)\right) \quad \text{and} \quad \Delta \geq \Delta' T^2 + \frac{T^3}{\eta} + \frac{T^4}{\epsilon}.$$

□

According to the requirements of Definition 15, the universal simulator of the second theorem is not efficient in either the number of spins, nor in the norm. However—as was noted in [33]—this is unavoidable if there is no free parameter in the universal Hamiltonian which encodes the description of the target Hamiltonian: a translationally invariant Hamiltonian on N spins can be described using only $\mathrm{O}(\mathrm{poly}\log(N))$ bits of information, whereas a k-local Hamiltonian which breaks translational invariance in general requires $\mathrm{poly}(N)$ bits of information. So, by a simple counting argument, we can see that it is not possible to encode all the information about a k-local Hamiltonian on n spins in a fixed translationally invariant Hamiltonian acting on $\mathrm{poly}(n)$ spins.

We observe that the parameters Δ and T are qualitatively different to ϕ, in that they do not depend on the Hamiltonian to be simulated, but only the parameters $(\Delta', \epsilon, \eta)$ determining the precision of the simulation.

2.3.2 No-Go for Parameterless Universality

Is an explicit Δ-dependence of a simulator Hamiltonian H_{univ} necessary to construct a universal model? Note that an implicit dependence of H_{univ} on Δ is possible via the chain length $N = N(\Delta)$ in Theorem 31. In the following, we prove that such an implicit dependence is insufficient, by giving a concrete counterexample for which an explicit Δ-dependence is necessary.

To this end, we note that it has previously been shown [35] that a degree-reducing Hamiltonian simulation (in a weaker sense of simulation, namely gap-simulation where only the ground state(s) and spectral gap are to be maintained) is only possible if the norm of the *local* terms is allowed to grow. In order to construct a concrete example in which an explicit Δ-dependence is necessary, we first quote Aharonov and Zhou's result, and then translate the terminology to our setting.

Theorem 33 (Aharonov and Zhou ([35, Thm. 1]))**.** *For sufficiently small constants $\epsilon \geq 0$ and $\tilde{\omega} \geq 0$, there exists a minimum system size N_0 such that for all $N \geq N_0$ there exists no constant-local $[r, M, J] = [\mathrm{O}(1), M, \mathrm{O}(1)]$ gap simulation (where r is the interaction degree, M the number of local terms, and J the local interaction strength of the simulator) of the Hamiltonian*

$$H_A \coloneqq \frac{1}{4} \sum_{i=1}^{N} \sum_{j<i} (1 - \sigma_z^{(i)}) \otimes (1 - \sigma_z^{(j)}) = \sum_{i=1}^{N} \sum_{j<i} |1\rangle\langle 1|^{(i)} \otimes |1\rangle\langle 1|^{(j)}$$

with a localized encoding, ϵ-incoherence, and energy spread $\tilde{\omega}$, for any number of Hamiltonian terms M.

Corollary 34. *Consider a universal family of Hamiltonians with local interactions and bounded-degree interaction graph. Hamiltonians in this family must have an explicit dependence on the energy cut-off (Δ) below which they are valid simulations of particular target Hamiltonians.*

Proof. We first explain the notation used in Theorem 33. As mentioned, the notion of gap simulation is weaker than Definition 15. Only the (quasi-) ground space $\mathcal{L}$ of H_A, rather than the full Hilbert space, needs to be represented ϵ-coherently: $\|H_A|_{\mathcal{L}} - \tilde{H}_A|_{\mathcal{L}}\| < \epsilon$, where $\cdot|_{\mathcal{L}}$ denotes the restriction to $\mathcal{L}$). And only the spectral gap above the ground space, rather than the full spectrum, must be maintained:

$\tilde{\gamma} = \Delta(\tilde{H}_A) \geq \gamma = \Delta(H_A)$. The rest of the spectrum in the simulation can be arbitrary. Energy spread in this context simply means the range of eigenvalues within $\mathcal{L}$ spreads out at most such that $|\lambda_0 - \tilde{\lambda}_0| \leq \tilde{\omega}\gamma$.

A $[\mathrm{O}(1), M, \mathrm{O}(1)]$ simulation with the above parameters then simply means an ϵ-coherent gap simulation, constant degree and local interaction strength, where M—the number of local terms in the simulator—is left unconstrained, and the eigenvalues vary by at most $\tilde{\omega}\gamma$.

It is clear that this notion of simulation falls within our more generic framework of simulation (cf. [35, Sec. 1.1]): a simulation of H_A *also* defines a valid gap simulation of H_A. Since by Definition 16 this simulation can be made arbitrarily precise, with parameters $\epsilon, \tilde{\omega}$ arbitrarily small, and has constant interaction degree by assumption, this contradicts Theorem 33. □

2.4 Applications to Hamiltonian Complexity

In subsection 1.2.2 we discussed the complexity of variants of k-LOCAL HAMILTONIAN. Recall that k-LOCAL HAMILTONIAN is QMA-complete for a polynomial promise gap, but PRECISE-k-LOCAL HAMILTONIAN (k-LOCAL HAMILTONIAN with an exponentially small promise gap) is PSPACE complete, while TI-LOCAL HAMILTONIAN is $\mathrm{QMA}_{\mathrm{EXP}}$ complete. A natural question to ask is thus: how hard is TI-LOCAL HAMILTONIAN (exppoly) - i.e. how hard is PRECISE-TI-LOCAL HAMILTONIAN. Furthermore, is it easier because of the translational invariance, as it was for the poly-promise-gap case? We show that this is *not* the case, and prove the following result.

Theorem 35. TI-LOCAL HAMILTONIAN (exppoly) *is* PSPACE-*complete.*

Proof. The result follows by Theorem 31. A non-translationally invariant Hamiltonian can be simulated by our construction in Theorem 31. The simulation is efficient in number of qubits, so this only incurs a polynomial overhead. Specifying all the local terms in H requires an exponentially long QPE computation to extract $\mathrm{poly}(N)$ many bits from a phase. Because a PreciseQMA-complete local Hamiltonian H already has a $1/\mathrm{exppoly}(N)$-closing promise gap, this does not attenuate the resulting promise gap by more than another exponential factor. Containment in PSPACE follows by [17]. □

For a discussion of the complexity theoretic implications of our results which include analysis of how the matrix bit precision is allowed to scale in k-LOCAL HAMILTONIAN and TI-LOCAL HAMILTONIAN we refer readers to [8, Section 4].

Chapter 3

General conditions for universality of quantum Hamiltonians

3.1 Introduction

The technique derived in Chapter 2 to prove universality of 1d Hamiltonians pointed to a connection between universality and complexity. This connection is not entirely surprising. Indeed, a rigorous complexity theoretic characterisation of universal Hamiltonians has already been demonstrated in the classical case [38]. Essentially, [38] showed that if a family of classical Hamiltonians has a ground state energy problem that is NP-hard, then it is necessarily also capable of simulating the complete physics of any other classical Hamiltonian. The converse implication is immediate.

In the quantum setting, there were hints that a similar result might hold. The classes of two-qubit interactions that are universal for simulating all, stoquastic, and classical Hamiltonians, respectively, were fully characterised in [6], and turned out to coincide precisely with the classes of interactions that have QMA-, StoqMA and NP-complete ground state energy problems. However, the proofs of these two classifications were independent, and it was certainly possible this coincidence only applied in the case of qubits, as the proof techniques relied critically on having only two-qubit interactions. Furthermore, the more complicated non-commutative structure of quantum Hamiltonians made it impossible to replicate the classical approach of [6] to proving a relationship between complexity and simulation.

In this chapter, by extending the simulation technique developed in Chapter 2, we resolve this. We derive necessary and sufficient complexity-theoretic conditions for a

family of Hamiltonians to be an efficient universal model, relating this directly to complexity-theoretic properties of the ground state.

3.2 Main Results

Our main result is a complexity theoretic classification of which families of Hamiltonians are efficient universal models:

Theorem 36 (Universality Classification)**.** *A family of Hamiltonians, $\mathcal{M}$, is an efficient universal model iff $\mathcal{M}$-*HAMILTONIAN *is* QMA*-complete under faithful reductions, and $\mathcal{M}$ is closed.*

The first *faithful reduction* condition for a family of Hamiltonians $\mathcal{M}$ to be an efficient universal model is related to the complexity of $\mathcal{M}$-HAMILTONIAN– the problem of deciding whether or not a Hamiltonian in $\mathcal{M}$ has a low energy ground state. We prove a connection between QMA-completeness of $\mathcal{M}$-HAMILTONIAN, and universality. However, QMA-completeness alone isn't enough for a model to be universal. We demonstrate that in order for $\mathcal{M}$ to be a universal model, $\mathcal{M}$-HAMILTONIAN must be QMA-complete under *faithful* reductions. Where we say that a reduction from a problem in QMA to $\mathcal{M}$-HAMILTONIAN is *faithful* if it maps the subspace picked out by a QMA-verification circuit to the low energy subspace of the Hamiltonian - therefore preserving some of the structure of the verification circuit and the witness. (For a rigorous definition of faithfulness see Section 3.3.)[1]

The second condition, *closure*, relates to combining different Hamiltonians from the same model. We say a model, $\mathcal{M}$, is closed if, given $H_A^{(1)}, H_B^{(2)} \in \mathcal{M}$, acting on (possibly overlapping) sets of qudits A, B respectively, there exists a Hamiltonian $H^{(3)} \in \mathcal{M}$ which can simulate $H_A^{(1)} + H_B^{(2)}$.

Furthermore, in this chapter we provide a recipe for modifying history state Hamiltonians so that the canonical reduction from a QMA-problem to the history state Hamiltonian is faithful. Therefore, all that remains to show that a family of history state Hamiltonians is universal is to demonstrate closure.

We also derive two corollaries, giving complexity-theoretic conditions for families of Hamiltonians to be universal models which aren't efficient in the sense of [6], but

[1]The faithful reduction condition may seem slightly counterintuitive - one way to think of it is that what we require is that it is possible to encode a polynomial time quantum verification circuit into the ground state of the Hamiltonian - but this isn't a mathematically rigorous statement. The concept of a faithful reduction formalises this idea.

are nonetheless interesting. These corollaries, along with the main theorem, give a complete classification of all known universal models.

The remainder of the chapter is set out as follows. The notion of a faithful reduction is outlined in detail in Section 3.3. Our main theorem is proved in Section 3.4. A discussion of the results in this chapter and Chapter 2 is given in Chapter 4.

3.3 Faithfulness condition

3.3.1 Faithful Hamiltonian reductions

The acceptance operator, $Q(U)$, of a QMA-verification circuit, U, is defined as [50, Th. 3.6]:

$$Q(U) = \langle 0|^{\otimes m} U^\dagger \Pi_{\text{out}} U |0\rangle^{\otimes m} \tag{3.1}$$

where U is a unitary acting on $n+m$ qubits (the n qubits forming the witness and m ancillas, initialised in the $|0\rangle$ state), and Π_{out} is the final projective measurement of the circuit.

Definition 37 (Gapped acceptance operators)**.** *Consider a promise problem A which can be verified by a unitary circuit U, with completeness probability c. Let $x \in A$ with $n = |x|$ the size of the instance. We say the acceptance operator is gapped if λ_x, the largest eigenvalue of $Q(U_x)$ which is less than completeness c, it holds that $c - \lambda_x > 1/\text{poly}(n)$.*

In other words, Definition 37 means that any state with acceptance probability below the completeness threshold already lies significantly below it, namely $1/\text{poly}$ bounded away.

Note there is a subtle difference between the promise gap and the question of whether or not the acceptance operator is gapped. For any NO instance of a problem $A \in$ QMA the definition of QMA trivially implies that the acceptance operator is gapped (since the acceptance probability is below the soundness threshold $\lambda_x \leq s$, and $c - s > 1/\text{poly}$ by definition). However, for YES instances it is possible to have an acceptance operator which is not gapped. We will see that for YES instances the question of whether or not the acceptance operator is gapped is related to the *spectral gap* of a Hamiltonian, rather than the promise gap.

The idea of requiring a gap in the spectrum of proof systems has arisen before in the Hamiltonian complexity literature, first in [51] in the definition of the class PGQMA

(Polynomially Gapped QMA).[2] The notion of a gap in the spectrum of the proof system is again seen to be related to the *spectral gap* of a Hamiltonian, as k-LOCAL HAMILTONIAN with the added promise that the spectral gap of the Hamiltonian is inverse polynomial is complete for PGQMA [51].

Definition 38 (Faithful Hamiltonian reduction)**.** *Let $A = A_{\text{YES}} \cup A_{\text{NO}}$ be a promise problem which can be verified by a family of circuits, U, of length T, with completeness probability c. The acceptance operator $Q(U)$ is as defined in eq.* (3.1)*. Consider a reduction from A to the $\mathcal{M}$-HAMILTONIAN problem. For a verification circuit with gapped $Q(U)$, we say the reduction is* faithful *with respect to U if for all instances $x \in A_{\text{YES}}$ there exists a Hamiltonian $H_x \in \mathcal{M}$ acting on* $\text{poly}(n)$ *qudits (where $n = |x|$) such that for the low energy subspace,*

$$\mathcal{S}_0 \coloneqq \text{span}\left\{|\phi\rangle : H_x|\phi\rangle = \tilde{\lambda}|\phi\rangle, \tilde{\lambda} \leq \frac{\kappa(1-c)}{T+1}\right\}$$

for $\kappa = 1/\text{poly}(n)$, the following holds.

1. $\|\Pi_{\mathcal{S}_0} - \Pi_{\mathcal{E}(\mathcal{L})}\| \leq \eta$ *where*
   - $\eta < 1$ *can be made arbitrarily small,*
   - $\Pi_{\mathcal{S}}$ *denotes the projector onto the subspace $\mathcal{S}$,*
   - $\mathcal{E}$ *is some local encoding (independent of the problem being encoded),*
   - $\mathcal{L} \coloneqq \text{span}\{|\psi\rangle : Q(U)|\psi\rangle = \lambda|\psi\rangle, \lambda \geq c\}$.
2. *The spectral gap above the subspace $\mathcal{S}_0$ is $\Omega(1/\text{poly}(T))$.*

For $x \in A_{\text{NO}}$, there are no conditions on H_x. Similarly, if $Q(U)$ is not gapped there are no conditions on the H_x.

Note that the concept of a faithful reduction is a property of a particular verification circuit,[3] not of the problem itself.

Definition 39. *We say that $\mathcal{M}$-HAMILTONIAN is* QMA*-complete under faithful reductions if for all $A \in$ QMA and for any polynomial time* QMA*-verification circuit U which verifies A, there exists a reduction from A to the $\mathcal{M}$-HAMILTONIAN problem which is faithful with respect to U.*

[2] PGQMA is a similar class to QMA with the added condition that the acceptance operator of the verification circuit has an inverse polynomial spectral gap. Note that for PGQMA the gap is required to be between the lowest and second lowest eigenvalue, unlike in our definition.

[3] Although any equivalent model of computation could be substituted into the definition.

3.3.2 The modified Kitaev Hamiltonian

The Hamiltonian we use to prove necessity of the faithfulness condition is a modification of the 5-local Hamiltonian shown to be QMA-complete in [16]. Note that this choice is convenient, but the procedure we set out here to demonstrate faithfulness could be applied to any history-state Hamiltonian in the literature.

The original 5-local Hamiltonian is a "circuit-to-Hamiltonian" mapping, given by

$$H_{\mathrm{K}} = H_{\mathrm{in}} + H_{\mathrm{prop}} + H_{\mathrm{out}} + H_{\mathrm{clock}} \tag{3.2}$$

where the Hamiltonian is acting on the Hilbert space

$$\mathcal{H} := \mathcal{H}_Q \otimes \mathcal{H}_C = (\mathbb{C}^2)^{\otimes n} \otimes (\mathbb{C}^2)^{\otimes T+1} = \mathbb{C}^2 \otimes (\mathbb{C}^2)^{\otimes |W|} \otimes (\mathbb{C}^2)^{\otimes |A|} \otimes (\mathbb{C}^2)^{\otimes T} \tag{3.3}$$

and

$$H_{\mathrm{in}} = \Pi_1^{(1)} \otimes |0\rangle\langle 0|_1^c + \sum_{j \in A} \Pi_j^{(1)} \otimes |0\rangle\langle 0|_1^c \tag{3.4}$$

$$H_{\mathrm{out}} = \Pi_1^{(0)} \otimes |1\rangle\langle 1|_T^c \tag{3.5}$$

$$H_{\mathrm{clock}} = \mathbb{1} \otimes \sum_{t+1}^{T-1} |01\rangle\langle 01|_{t,t+1}^c \tag{3.6}$$

$$H_{\mathrm{prop}} = \frac{1}{2} \sum_{t=1}^{T-1} H_t \tag{3.7}$$

with

$$\begin{aligned} H_t = \mathbb{1} \otimes (&|10\rangle\langle 10|_{t,t+1}^c + |10\rangle\langle 10|_{t+1,t+2}^c) \\ &- U_{t+1} |110\rangle\langle 110|_{t-1,t,t+1}^c - U_{t+1}^\dagger |100\rangle\langle 100|_{t-1,t,t+1}^c \end{aligned} \tag{3.8}$$

where the U_t correspond to the gates applied at time t in the circuit being encoded.

The Hamiltonian without the output penalty,

$$H_0 = H_{\mathrm{in}} + H_{\mathrm{prop}} + H_{\mathrm{clock}}, \tag{3.9}$$

has a degenerate ground space spanned by states of the form

$$\left|\eta^{(0,\alpha)}\right\rangle = \frac{1}{\sqrt{T+1}} \sum_{t=0}^{T} \left|\gamma_t^{(0,\alpha)}\right\rangle \tag{3.10}$$

for arbitrary α where

$$\left|\gamma_t^{(0,\alpha)}\right\rangle = |\alpha_0(t)\rangle \otimes \left|1^t 0^{T-t}\right\rangle^c \tag{3.11}$$

where $|\alpha_0(t)\rangle$ is the state of the quantum circuit at time t if the input state of the ancillas and flag qubit correspond to the binary string $\mathbf{0} = 0^{1+|A|}$, and the input state of the witness is given by $|\alpha\rangle$.

The modified Kitaev Hamiltonian we use is given by

$$H_{\mathrm{MK}} = H_{\mathrm{in}} + H_{\mathrm{prop}} + \kappa H_{\mathrm{out}} + H_{\mathrm{clock}} \tag{3.12}$$

where $\kappa = 1/\mathrm{poly}(T) = \mathrm{o}(1/T^3)$.

3.3.3 The $\mathcal{K}$-Hamiltonian problem is QMA-complete under faithful reductions

Let $\mathcal{K}$ be the family of Hamiltonians of form eq. (3.12). We begin by showing that $\mathcal{K}$-Hamiltonian is QMA-complete, then show that we can always choose the reductions to be faithful.

Lemma 40. $\mathcal{K}$-Hamiltonian *is* QMA*-complete.*

Proof. The proof that $\mathcal{K}$-Hamiltonian is QMA-complete is essentially unchanged from the proof of QMA-completeness in [16]. We sketch the argument here very briefly. Assume the circuit being encoded is a QMA-verification circuit with completeness parameter c and soundness parameter s. First consider the YES instances. By definition, there exists a witness w such that the verification circuit accepts with probability at least c. It follows that the ground state of H_{MK} has energy less than $\frac{\kappa(1-c)}{T+1}$.

For the NO cases we use the following geometrical lemma.

Lemma 41 (Geometrical lemma, Lemma 14.4 [16])**.** *Let H_1, H_2 be two Hamiltonians with ground energies a_1, a_2 respectively. Suppose that for both Hamiltonians the difference between the energy of the (possibly degenerate) ground space and the next highest eigenvalue is larger than Λ, and that the angle between the two ground spaces is θ. Then the ground energy of $H_1 + H_2$ is at least $a_1 + a_2 + 2\Lambda sin^2(\theta/2)$.*

We apply Lemma 41 to H_{MK} with $H_1 = H_{\mathrm{in}} + \kappa H_{\mathrm{out}}$ and $H_2 = H_{\mathrm{prop}} + H_{\mathrm{clock}}$. We have $a_1 = a_2 = 0$. The smallest non-zero eigenvalue of H_1 is κ (since H_{in} and H_{out} are commuting projectors). The smallest non-zero eigenvalue of H_2 scales as $\Omega(1/T^2)$ (see [16] for proof). The angle between the ground spaces satisfies

$$\sin^2(\theta/2) \geq \frac{1-\sqrt{s}}{4(T+1)}. \tag{3.13}$$

Again, the proof of this is unchanged from [16] as the ground space of H_1 is equal to the ground space of $H_{\mathrm{in}} + H_{\mathrm{out}}$.

Therefore in NO instances the ground energy of H_{MK} is lower bounded by $\frac{1-\sqrt{s}}{\mathrm{poly}(T)}$. Setting $c - s = \Omega\left(\frac{1}{\mathrm{poly}(T)}\right)$ we have $\beta - \alpha = \Omega\left(\frac{1}{\mathrm{poly}(T)}\right)$. Therefore we have proven a reduction from QMA to the k-LOCAL HAMILTONIAN of H_{MK}. □

To show that we can always choose the reduction to be faithful, we first prove a lemma about the spectrum and low energy subspace of H_{MK}.

Lemma 42. *Consider a modified Kitaev-Hamiltonian, H_{MK}, encoding the verification circuit of some* QMA *problem. Let $Q(U)$ be the acceptance operator for a verifier circuit U for some $A \in$ QMA. Set*

$$C_0 \coloneqq \mathrm{span}\left\{\left|\eta^{(0,\phi)}\right\rangle : Q(U)\left|\phi\right\rangle = \lambda\left|\phi\right\rangle, \lambda > c\right\}$$

where c is the completeness parameter of the problem, and let $g \coloneqq c - \lambda_x$ where λ_x is the largest eigenvalue of $Q(U)$ which is less than c, as in Definition 37.

If $g > 2T^3(T+1)\kappa$, then there exists a unitary transformation V such that the subspace $\mathcal{S}_0$ defined by $\Pi_{\mathcal{S}_0} \coloneqq V^\dagger \Pi_{C_0} V$ is the low energy subspace of H_{MK}:

$$\mathcal{S}_0 = \mathrm{span}\left\{\left|\psi\right\rangle : H_{\mathrm{MK}}\left|\psi\right\rangle = \lambda\left|\psi\right\rangle, \lambda \leq \frac{\kappa(1-c)}{T+1} + T^3\kappa^2\right\}. \tag{3.14}$$

$$\|\Pi_{\mathcal{S}_0} - \Pi_{C_0}\| = \mathrm{O}(T^3\kappa) \tag{3.15}$$

and the spectral gap above $\mathcal{S}_0$ is given by $\Omega(\frac{g\kappa}{T+1} - T^3\kappa^2)$.

Proof. It is a standard result that the zero-energy ground state subspace $\mathcal{G}$ of H_0 is spanned by history states $\left|\eta^{(0,\alpha)}\right\rangle$ for all α. The spectral gap of H_0 is $\Omega(1/T^3)$ [34].

Since $\|\kappa H_{\text{out}}\| = o\left(\frac{1}{T^3}\right) < \frac{1}{2T^3}$, the Hamiltonian $H_{\text{MK}}|_{\mathcal{G}}$ can be approximated by the Schrieffer-Wolff perturbative expansion (see Appendix A.1). Let $\Pi_{\mathcal{G}}$ be the projector onto $\mathcal{G}$.

The zeroth order term in the expansion is given by $H_0\Pi_{\mathcal{G}} = 0$. The matrix elements of the first order term, $\Pi_{\mathcal{G}}H_{\text{out}}\Pi_{\mathcal{G}}$, are given by [52] [Appendix B]:

$$\left\langle \eta^{(0,\alpha)} \right| \Pi_{\mathcal{G}} H_{\text{out}} \Pi_{\mathcal{G}} \left| \eta^{(0,\beta)} \right\rangle = \frac{\kappa}{T+1} \left(\langle \alpha | \beta \rangle - \langle \alpha | Q | \beta \rangle \right) \tag{3.16}$$

Denote the eigenstates of $Q(U)$ by $|\phi_1\rangle, |\phi_2\rangle, \cdots, |\phi_{2^w}\rangle$ with associated eigenvalues $\lambda_1 \geq \lambda_2 \geq \cdots \geq \lambda_{2^w}$. In the basis spanned by $\left|\eta^{(0,\phi_i)}\right\rangle$, the first order term in the Schrieffer-Wolff expansion is diagonal:

$$\Pi_{\mathcal{G}} H_{\text{out}} \Pi_{\mathcal{G}} = \frac{\kappa}{T+1} \sum_i (1-\lambda_i) \left|\eta^{(0,\phi_i)}\right\rangle \left\langle \eta^{(0,\phi_i)} \right| \tag{3.17}$$

By eq. (A.12) and eq. (3.17) we conclude that in $\mathcal{G}$ the eigenvalues of H_{MK} are given by

$$\tilde{\lambda}_i = \frac{\kappa(1-\lambda_i)}{T+1} \pm T^3\kappa^2 \tag{3.18}$$

Let $\mathcal{R} \coloneqq \text{span}\left\{ |\psi\rangle : H_{\text{MK}} |\psi\rangle = E |\psi\rangle, E \leq \frac{\kappa}{2} \right\}$. By the $\sin(\theta)$ theorem [53]:

$$\|\Pi_{\mathcal{R}} - \Pi_{\mathcal{G}}\| = \|V^\dagger \Pi_{\mathcal{G}} V - \Pi_{\mathcal{G}}\| \leq T^3\kappa \tag{3.19}$$

where $V = e^S$ is the Schrieffer-Wolff transformation. Therefore

$$\|V^\dagger \Pi_{\mathcal{C}_0} V - \Pi_{\mathcal{C}_0}\| = \|\Pi_{\mathcal{S}_0} - \Pi_{\mathcal{C}_0}\| \leq T^3\kappa. \tag{3.20}$$

$\mathcal{C}_0$ is spanned by history states satisfying $H_{\text{eff}}(1)\left|\eta^{(0,\phi)}\right\rangle = \lambda \left|\eta^{(0,\phi)}\right\rangle$ for $\lambda \leq \frac{\kappa(1-c)}{T+1}$. The corresponding eigenvalues of H_{MK} are upper bounded by $\frac{\kappa(1-c)}{T+1} + T^3\kappa^2$. The smallest eigenvalue of H_{MK} which is larger than $\frac{\kappa(1-c)}{T+1} + T^3\kappa^2$ is lower bounded by $\frac{\kappa(1-\lambda_x)}{T+1} - T^3\kappa^2$.

Therefore, since $g > 2T^3(T+1)\kappa$, the subspace

$$\mathcal{S}_0 = \text{span}\left\{ |\psi\rangle : H_{\text{MK}} |\psi\rangle = \lambda |\psi\rangle, \lambda \leq \frac{\kappa(1-c)}{T+1} + T^3\kappa^2 \right\} \tag{3.21}$$

and the spectral gap of H_{MK} above $\mathcal{S}_0$ is given by $\Omega(\frac{g\kappa}{T+1} - T^3\kappa^2)$. □

Lemma 43. *The* $\mathcal{K}$-HAMILTONIAN *problem is* QMA*-complete under faithful reductions.*

Proof. For any verification circuit, U, of any problem in QMA, we can require that the computation 'idles' in its initial state for L time steps before carrying out its verification computation ("idling to enhance coherence" [34]).

The history state of the computation for the first L time steps will be given by

$$\left|\eta_{\text{idling}}^{(0,\alpha)}\right\rangle = |\alpha\rangle \otimes |0\rangle^{|A|+1} \otimes \frac{1}{\sqrt{L}} \sum_{t=1}^{L} \left|1^t 0^{T-t}\right\rangle^c . \tag{3.22}$$

The rest of the history state is captured in

$$\left|\eta_{\text{comp}}^{(0,\alpha)}\right\rangle = \frac{1}{\sqrt{T-L}} \sum_{t=L+1}^{T} \left|\gamma_t^{(0,\alpha)}\right\rangle \tag{3.23}$$

So the total history state is given by

$$\left|\eta^{(0,\alpha)}\right\rangle = \sqrt{\frac{L}{T}} \left|\eta_{\text{idling}}^{(0,\alpha)}\right\rangle + \sqrt{\frac{L-T}{T}} \left|\eta_{\text{comp}}^{(0,\alpha)}\right\rangle \tag{3.24}$$

The encoding $\mathcal{E}(M) = VMV^\dagger$ defined via the isometry

$$V = \sum_i \left|\eta_{\text{idling}}^{(0,i)}\right\rangle \langle i| , \tag{3.25}$$

where the $|i\rangle$ are computational basis states, is local. (This can be verified by direct calculation, see Chapter 2.)

Moreover, we have that

$$\begin{aligned} \|\Pi_{C_0} - \Pi_{\mathcal{E}(\mathcal{L})}\|^2 &= \left\| \sum_{|\phi\rangle \in \mathcal{L}} \left(\left|\eta^{(0,\phi)}\right\rangle \left\langle \eta^{0,\phi}\right| - \left|\eta_{\text{idling}}^{(0,\phi)}\right\rangle \left\langle \eta_{\text{idling}}^{(0,\phi)}\right| \right) \right\|^2 \\ &= \left\| \sum_{|\phi\rangle \in \mathcal{L}} \left(\sqrt{\frac{T-L}{T}} \left|\eta_{\text{comp}}^{(0,\phi)}\right\rangle \left\langle \eta_{\text{comp}}^{(0,\phi)}\right| + \left(\sqrt{\frac{L}{T}} - 1\right) \left|\eta_{\text{idling}}^{(0,\phi)}\right\rangle \left\langle \eta_{\text{idling}}^{(0,\phi)}\right| \right) \right\|^2 \\ &\leq 2\left(1 - \sqrt{\frac{L}{T}}\right) \end{aligned} \tag{3.26}$$

where $\mathcal{L} \coloneqq \{|\phi\rangle : Q|\phi\rangle = \lambda|\phi\rangle, \lambda > c\}$ Therefore $\|\Pi_{C_0} - \Pi_{\mathcal{E}(\mathcal{L})}\|$ can be made arbitrarily small by increasing L.

The result follows immediately from Lemma 42 and the triangle inequality. □

3.4 General Conditions for Universality

In order to state our main theorem we require one more definition.

Definition 44 (Closed Hamiltonian model)**.** *We say that a model $\mathcal{M}$, is closed if for any pair of Hamiltonians $H_A^{(1)}, H_B^{(2)} \in \mathcal{M}$ acting on sets of qudits A, B respectively where in general $A \cap B \neq \{\}$, there exists a Hamiltonian $H^{(3)} \in \mathcal{M}$ which can efficiently simulate $H_A^{(1)} + H_B^{(2)}$.*

We can now prove our main result Theorem 36, which we restate here for clarity:

Theorem 45 (Universality Classification)**.** *A family of Hamiltonians, $\mathcal{M}$, is an efficient universal model iff $\mathcal{M}$-*Hamiltonian *is* QMA*-complete under faithful reductions, and $\mathcal{M}$ is closed.*

Proof. First consider the only if direction. Closure is clearly necessary: if a model $\mathcal{M}$ is universal, all Hamiltonians (including those of the form $H_A^{(1)} + H_B^{(2)}$ for $H_A^{(1)}, H_B^{(2)} \in \mathcal{M}$) can be simulated by a Hamiltonian in the model. In Lemma 43 we proved the $\mathcal{K}$-Hamiltonian problem is QMA-complete under faithful reductions. Any efficient universal model must be able to simulate Hamiltonians in $\mathcal{K}$ with only polynomial overhead, hence $\mathcal{M}$-Hamiltonian must itself be QMA-complete under faithful reductions.

Now consider the if direction. Let $\mathcal{M}$ be a family of Hamiltonians meeting the conditions of the theorem, i.e. such that $\mathcal{M}$-Hamiltonian is QMA-complete under faithful reductions, and $\mathcal{M}$ is closed. We will explicitly construct a universal model, solely based on these conditions.

Consider the following problem:

Yes-Hamiltonian

Input: A k-local Hamiltonian H_{target} acting on n spins with local dimension d.

Question: Output YES

This problem is (clearly) trivial. But we can choose to construct a non-trivial QMA verification circuit for it. We will choose a verification circuit which picks out a

particular subspace that allows us to prove universality. By Definition 39 there must be a faithful reduction with respect to *this* verification circuit from YES-HAMILTONIAN to $\mathcal{M}$-HAMILTONIAN.

The verification circuit we choose, and the subspace it picks out, are captured in the following.

Lemma 46. YES-HAMILTONIAN *can be verified by a circuit U_a with gapped acceptance operator $Q(U_a)$ with ground space*

$$\mathcal{L}_0 \coloneqq \text{span}\{|\phi\rangle : Q(U_a)|\phi\rangle = |\phi\rangle\} \tag{3.27}$$

satisfying

$$\|\Pi_{\mathcal{L}_0} - \Pi_{\mathcal{W}}\| \leq \mathrm{O}\left(a^{-1}\right) \tag{3.28}$$

where

$$\mathcal{W} \coloneqq \text{span}\left\{|w_\mu\rangle = \frac{1}{\sqrt{a^2+1}}|\psi_\mu\rangle\left(a|\#\rangle + |E_\mu\rangle\right) : H_{\text{target}}|\psi_\mu\rangle = E_\mu|\psi_\mu\rangle\right\}. \tag{3.29}$$

Proof. The verifier circuit, C_V, acts on the witness and two ancilla registers, B, B'. It will be helpful to divide the witness into two separate registers: An A register, which is n d-dimensional qudits. And an A' register, which consists of m qutrits with orthonormal basis states $|\#\rangle$, $|0\rangle$ and $|1\rangle$, where $m = \log_2(\epsilon)$. The B register is the same size as the A' register. The B' register consists of a single qubit.

The verifier C_V operates as follows:

1. Apply a unitary rotation $P_a : |0\rangle \to \frac{1}{\sqrt{a^2+1}}(a|\#\rangle + |1\rangle)$ to the B' register.f
2. Carry out controlled-phase-estimation on the A register with respect to the unitary generated by H_{target}, $U = e^{iH_{\text{target}}\tau}$, for some τ such that $\|H_{\text{target}}\tau\| < 2\pi$. The B' register serves as the control qubit. Calculate (an approximation to) the energy E_μ from the eigenphase θ_μ and store the result in the B register (in binary).

   Calculating E_μ to accuracy ϵ requires calculating the eigenphase θ_μ to accuracy $\mathrm{O}(\epsilon/\|H_{\text{target}}\|)$ which takes $\mathrm{O}(\|H_{\text{target}}\|/\epsilon)$ uses of $U = e^{iH_{\text{target}}\tau}$. The unitary U must therefore be implemented to accuracy $O(\epsilon/\|H_{\text{target}}\|)$, which can be done with overhead $\text{poly}(n, d^k, \|H_{\text{target}}\|, \tau, 1/\epsilon)$ where n is system size, d is local dimension and k is locality via Lemma 28. The whole procedure takes time $T_{\text{PE}} = \text{poly}(n, d^k, \|H_{\text{target}}\|/\epsilon)$

3. Carry out a SWAP test between registers A' and B. Accept if outcome 0 is measured, reject otherwise.

The entire procedure takes time $T = \mathrm{O}(\mathrm{poly}(n, d^k, \|H_{\text{target}}\|)/\epsilon)$.

Let

$$\left|\alpha_\mu\right\rangle = \sum_j \left(\frac{1}{2^m} \sum_{k=0}^{2^m-1} e^{2\pi i k (E_\mu - j/2^m)} \right) |j\rangle \tag{3.30}$$

be the result of applying the phase estimation algorithm on $\left|\psi_\mu\right\rangle$ with respect to $U = e^{iH_{\text{target}}\tau}$. Then evidently

$$\left|\phi_\mu\right\rangle = \frac{1}{\sqrt{a^2+1}} \left|\psi_\mu\right\rangle_A \left(a \left|\#\right\rangle_{A'} + \left|\alpha_\mu\right\rangle_{A'}\right) \tag{3.31}$$

is an eigenvector of $Q(U_a)$ with eigenvalue 1, and all eigenvectors of $Q(U_a)$ with eigenvalue 1 are in $\mathrm{span}\{\left|\phi_\mu\right\rangle\}$.

Moreover,

$$\left\langle w_\mu \middle| \phi_\mu \right\rangle \leq \frac{a^2 + \frac{4}{\pi^2}}{a^2+1} \tag{3.32}$$

Therefore

$$\| \left|w_\mu\right\rangle\!\left\langle w_\mu\right| - \left|\phi_\mu\right\rangle\!\left\langle\phi_\mu\right| \| \leq 2\sqrt{1 - \left(\frac{a^2 + \frac{4}{\pi^2}}{a^2+1}\right)^2} \tag{3.33}$$

and

$$\|\Pi_{\mathcal{L}_0} - \Pi_W\| \leq \mathrm{O}\left(a^{-1}\right). \tag{3.34}$$

The next largest eigenvalue of $Q(U_a)$ is $\frac{1}{2}$. □

It follows immediately from eq. (3.34) that

$$\|\mathcal{E}(\Pi_{\mathcal{L}_0}) - \mathcal{E}(\Pi_W)\| \leq \mathrm{O}\left(a^{-1}\right) \tag{3.35}$$

for any encoding $\mathcal{E}$.

It follows from the triangle inequality and Definition 38(1) that for any instance of Yes-Hamiltonian there exists $H_{\text{LS}} \in \mathcal{M}$ with low energy subspace $\mathcal{S}_0 \coloneqq \mathrm{span}\{|\phi\rangle : H_x |\phi\rangle = \lambda_{\min} |\phi\rangle\}$ such that

$$\|\Pi_{\mathcal{S}_0} - \Pi_{\mathcal{E}(W)}\| \leq \eta + \mathrm{O}\left(a^{-1}\right) \tag{3.36}$$

where $\mathcal{E} = V\left(M \otimes P + \overline{M} \otimes Q\right) V^\dagger$ is some local encoding and η can be chosen to be arbitrarily small. The spectral gap above $\mathcal{S}_0$ is $\Omega(1/\text{poly}(T))$.

Another trivial problem (that is therefore also evidently in QMA) is:

FLAG IDENTIFICATION
Input: Classical description of a one-qudit state $|f\rangle$
Question: Output YES.

For this problem we will use a faithful reduction with respect to the non-trivial verification circuit which simply measures a single qudit in the f basis. So, for any single qudit state $|f\rangle$, there exists $H_f \in \mathcal{M}$ such that:

- $H_f |\mathcal{E}_{\text{state}}(\phi)\rangle = \lambda_0^{(f)} |\mathcal{E}_{\text{state}}(\phi)\rangle$ for all $|\phi\rangle$ such that $\langle\phi|f\rangle = 0$
- $H_f |\mathcal{E}_{\text{state}}(f)\rangle = \lambda_1^{(f)} |\mathcal{E}_{\text{state}}(f)\rangle$

for some local encoding $\mathcal{E}_{\text{state}}$, where $\lambda_k^{(f)}$ can be efficiently computed. (Since the problem size is $O(1)$ for a state $|f\rangle$ that can be described in $O(1)$ bits.) Wlog we will take $\lambda_k^{(f)} = k$.

Consider a Hamiltonian acting on N spins:

$$H_{\text{sim}} = \Delta\left(H_{\text{LS}} - \lambda_{\min} \mathbb{1}\right) + a \sum_{i=n'+1}^{N} 2^{i-(n'+1)} H_i^{(1)} \tag{3.37}$$

Where $H_{\text{LS}} \in \mathcal{M}$ is a faithful reduction (with respect to the verifier defined in Lemma 46) from YES-HAMILTONIAN for the Hamiltonian $H_{\text{target}} = \sum_\mu E_\mu \left|\psi_\mu\right\rangle\!\left\langle\psi_\mu\right|$. E_μ in $\left|w_\mu\right\rangle$ is expressed in binary to precision ϵ in qudits $[n'+1, N]$.[4] The $H_i^{(1)} \in \mathcal{M}$ are faithful reductions (with respect to the obvious verification circuit) from FLAG IDENTIFICATION for the flag states $|1\rangle$ acting on the i^{th} qudit. We will require $\Delta > \|H_{\text{target}}\|$.

First we show that H_{sim} can simulate $H' = \sum_\mu E_\mu \left|w_\mu\right\rangle\!\left\langle w_\mu\right|$. The low energy subspace of H_{LS} consists of states in the subspace $\mathcal{S}_0$. On states in $\mathcal{S}_0$, $H_{\text{LS}} - \lambda_{\min}$ has energy zero. While on states in $\mathcal{E}(\mathcal{W})$, $a \sum_{i=n'+1}^{N} 2^{i-(n'+1)} H_i^{(1)}$ has energy in the range $[E_\mu - \epsilon, E_\mu + \epsilon]$.

[4] Here n' is the number of spins in the encoded witness state $\mathcal{E}\left(\left|w_\mu\right\rangle\right)$. Since this is a reduction to QMA we have $n' = \text{O}(\text{poly}(n))$.

It follows from [6, Lemma 24] and eq. (3.36) that there exists an encoding $\mathcal{E}'(M) = V'\left(M \otimes P + \overline{M} \otimes Q\right)V'^{\dagger}$ such that

$$\|V' - V\| \leq \sqrt{2}(\eta + O(a^{-1})) \tag{3.38}$$

and $\mathcal{E}'(\mathbb{1}) = \Pi_{\mathcal{S}_0}$. Moreover,

$$V' = WV \tag{3.39}$$

where W is a unitary satisfying

$$\Pi_{\mathcal{S}_0} = W\Pi_{\mathcal{E}(\mathcal{W})}W^{\dagger} \tag{3.40}$$

and

$$\|W - \mathbb{1}\| \leq \sqrt{2}\|\Pi_{\mathcal{S}_0} - \Pi_{\mathcal{E}(\mathcal{W})}\| \leq \mathrm{O}(\eta + a^{-1}) \tag{3.41}$$

We need the following technical lemma.

Lemma 47 (First-order simulation [31][Lemma 14)**.** *] Let H_0 and H_1 be Hamiltonians acting on the same space and Π be the projector onto the ground space of H_0. Suppose that H_0 is zero on Π and the next smallest eigenvalue is at least 1. Let U be an isometry such that $UU^{\dagger} = \Pi$ and*

$$\|UH_{\text{target}}U^{\dagger} - \Pi H_1 \Pi\| \leq \epsilon/2. \tag{3.42}$$

Let $H_{\text{sim}} = \Delta H_0 + H_1$. Then there exists an isometry $\tilde{V}$ onto the the space spanned by the eigenvectors of H_{sim} with eigenvalue less than $\Delta/2$ such that

1. $\|U - \tilde{V}\| \leq \mathrm{O}\left(\Delta^{-1}\|H_1\|\right)$
2. $\|\tilde{V}H_{\text{target}}\tilde{V}^{\dagger} - H_{\text{sim}<\Delta/2}\| \leq \mathrm{O}\left(\Delta^{-1}\|H_1\|^2\right) + \epsilon/2$

We will apply Lemma 47 with $H_1 = a\sum_{i=n'+1}^{N} 2^{i-(n'+1)}H_i^{(1)}$ and $H_0 = \delta H_{\text{LS}}$ where $\delta = \mathrm{O}(\mathrm{poly}(T))$. We have that in $\Pi_{\mathcal{S}_0}$, H_{LS} has energy zero and by Definition 38(2) the spectral gap above $\mathcal{S}_0$ scales as $\Omega(1/\mathrm{poly}(T))$ so $H_0 = \delta H_{\text{LS}}$ has next smallest eigenvalue at least 1.

Moreover, $\|H_1\| = a\|H_{\text{target}}\|$. Note that V' is an isometry which maps onto the ground state of H_0, $\mathcal{S}_0$. By construction we have that the spectrum of H_{target} is approximated to within ϵ by H_1 restricted to $\mathcal{E}(\mathcal{W})$, so $\|\Pi_{\mathcal{E}(\mathcal{W})}H_1\Pi_{\mathcal{E}(\mathcal{W})} - \mathcal{E}(H_{\text{target}})\| \leq \epsilon$.

Using that the operator norm is unitarily invariant, and that $V' = WV$ gives

$$\|W\Pi_{\mathcal{E}(\mathcal{W})}H_1\Pi_{\mathcal{E}(\mathcal{W})}W^\dagger - \mathcal{E}'(H_{\text{target}})\| \leq \epsilon. \tag{3.43}$$

We also have

$$\begin{aligned}\|\Pi_{\mathcal{S}_0}H_1\Pi_{\mathcal{S}_0} - W\Pi_{\mathcal{E}(\mathcal{W})}H_1\Pi_{\mathcal{E}(\mathcal{W})}W^\dagger\| &= \|\Pi_{\mathcal{S}_0}H_1\Pi_{\mathcal{S}_0} - \Pi_{\mathcal{S}_0}WH_1W^\dagger\Pi_{\mathcal{S}_0}\| \\ &\leq \|H_1 - WH_1W^\dagger\| \\ &\leq 2\|H_1\|\|\mathbb{1} - W\| \\ &\leq \mathrm{O}\left(a\eta\|H_{\text{target}}\|\right)\end{aligned} \tag{3.44}$$

where we have used [6, Lemma 18] in the penultimate step. So

$$\|\Pi_{\mathcal{S}_0}H_1\Pi_{\mathcal{S}_0} - \mathcal{E}'(H_{\text{target}})\| \leq \epsilon + \mathrm{O}\left(a\eta\|H_{\text{target}}\|\right). \tag{3.45}$$

Lemma 47 therefore implies that there exists an isometry $\tilde{V}$ that maps exactly onto the low energy space of H_{sim} such that $\|\tilde{V} - V'\| \leq \mathrm{O}\left(\|H_{\text{target}}\|a/(\Delta/\delta)\right) = \mathrm{O}\left(a\delta\|H_{\text{target}}\|/\Delta\right)$. By the triangle inequality and eq. (3.38), we have

$$\|V - \tilde{V}\| \leq \|V - V'\| + \|V' - \tilde{V}\| \leq \mathrm{O}\left(\frac{a\,\mathrm{poly}(T')\|H_{\text{target}}\|}{\Delta} + \eta + a^{-1}\right). \tag{3.46}$$

The second part of the lemma implies that

$$\|\tilde{V}H'\tilde{V}^\dagger - (H_{\text{sim}})_{<\Delta'/2}\| \leq \epsilon + \mathrm{O}\left(a\eta\|H_{\text{target}}\| + (a|H_{\text{target}}\|)^2/(\Delta/\delta)\right) \tag{3.47}$$

$$= \epsilon + \mathrm{O}\left(a\eta\|H_{\text{target}}\| + \frac{a^2|H_{\text{target}}\|^2\delta}{\Delta}\right). \tag{3.48}$$

Therefore, the conditions of Definition 15 are satisfied for a $(\Delta', \eta', \epsilon')$-simulation of H', with $\eta' = \mathrm{O}\left(\frac{a\,\mathrm{poly}(T')\|H_{\text{target}}\|}{\Delta} + \eta + a^{-1}\right)$, $\epsilon' = \epsilon + \mathrm{O}\left(a\eta\|H_{\text{target}}\| + \frac{a^2\,\mathrm{poly}(T')\|H_{\text{target}}\|^2}{\Delta}\right)$ and $\Delta' = \Delta/\delta = \Delta/\mathrm{poly}(T)$.

By definition we can choose η to be arbitrarily small. We can also make $\mathrm{O}\left(a^{-1}\right)$ arbitrarily small. By increasing T, we can also make ϵ arbitrarily small. Therefore, by choosing Δ such that

$$\Delta \geq \Delta'\,\mathrm{poly}(T') + \frac{a\,\mathrm{poly}(T')\|H_{\text{target}}\|}{\eta'} + \frac{a^2\,\mathrm{poly}(T')\|H_{\text{target}}\|^2}{\epsilon'} \tag{3.49}$$

we can construct H_{sim} which is a $(\Delta', \eta', \epsilon')$-simulation of H' with arbitrarily small ϵ', η'. Since H_{sim} is a sum of Hamiltonians which are all in $\mathcal{M}$, by the closure property there exists $H_{\text{univ}} \in \mathcal{M}$ which can efficiently simulate H_{sim}. Therefore, since simulations compose [6, Lemma 17] H_{univ} can simulate H'.

Finally, we show that $H' = \sum_\mu E_\mu \left|w_\mu\right\rangle\!\left\langle w_\mu\right|$ is itself a simulation of H_{target}. Consider the local encoding

$$\mathcal{E}'(M) = WMW^\dagger, \tag{3.50}$$

where $W = \sum_\mu \left|\psi_\mu\right\rangle |0\rangle \left\langle\psi_\mu\right|$, and the non local encoding

$$\tilde{\mathcal{E}}'(M) = \tilde{W}M\tilde{W}^\dagger \tag{3.51}$$

withk

$$\tilde{W} = \frac{1}{\sqrt{a^2+1}} \sum_\mu \left|\psi_\mu\right\rangle \left(a\,|\#\rangle + \left|E_\mu\right\rangle\right) \left\langle\psi_\mu\right|. \tag{3.52}$$

We have that

$$\|W - \tilde{W}\| = 2\left(1 - \frac{a}{\sqrt{a^2+1}}\right) \tag{3.53}$$

So by increasing a we can make the norm arbitrarily small. We also have that $S_{\tilde{\mathcal{E}}'} = S_{H'}$, so condition 1 from Definition 15 is met. The spectrum of H' is exactly the spectrum of $\tilde{\mathcal{E}}'(H_{\text{target}})$, so condition 2 of Definition 15 is also met. Therefore H' is a simulation of H_{target}.

Using the composition of simulations again, we have that H_{univ} can simulate H_{target}. We have left H_{target} arbitrary, so $\mathcal{M}$ is a universal model.

Finally we consider efficiency. The simulation of H_{target} by H' is clearly efficient. To see that the simulation of H' by H_{sim} is efficient, note that the number of qudits in the simulation, N, must be polynomial in n and $\|H_{\text{target}}\|$ as H_{LS} is in QMA. Furthermore, $\|H_{\text{sim}}\| = \Omega(\Delta) = \text{poly}(T', \|H_{\text{target}}\|, 1/\epsilon', 1/\eta') = \text{poly}(n, \|H_{\text{target}}\|, 1/\epsilon', 1/\eta')$. Thus H_{sim} is an efficient simulation of H'. □

There are two corollaries about universal Hamiltonians which aren't efficient in the sense of [6], but which are nonetheless interesting universal models which are better suited to some applications.

Definition 48. *We say a Hamiltonian can be described succinctly if it can be described by* $\text{O}(\log(n))$ *bits of information when acting on n qudits.*

Corollary 49. *Let $\mathcal{M}$ be a family of succinct Hamiltonians. Then $\mathcal{M}$ is universal and can efficiently simulate any succinct Hamiltonian iff $\mathcal{M}$-*HAMILTONIAN *is* $\mathrm{QMA}_{\mathrm{EXP}}$*-complete under faithful reductions and $\mathcal{M}$ is closed.*

Proof. This proof relies on the same ideas as Theorem 45, so here we sketch the main ideas, highlighting where the proofs differ. First, note the proof that $\mathcal{K}$-HAMILTONIAN is QMA-complete under faithful reductions (Lemma 43) can be repurposed to prove that the $\mathcal{M}$-HAMILTONIAN which was shown to be $\mathrm{QMA}_{\mathrm{EXP}}$-complete in [18] remains $\mathrm{QMA}_{\mathrm{EXP}}$ complete under faithful reductions. The only if direction follows immediately as in Theorem 45 (where now the overhead can be exponential).

To see the if direction, we will assume there exists a family of Hamiltonians, $\mathcal{M}$, such that $\mathcal{M}$-HAMILTONIAN is $\mathrm{QMA}_{\mathrm{EXP}}$-complete under faithful reductions and $\mathcal{M}$ is closed. Consider the following computational problem:

SUCCINCT-YES-HAMILTONIAN

Input: A k-local Hamiltonian H_{target} acting on n spins with local dimension d, which can be described succinctly.

Question: Output YES

SUCCINCT-YES-HAMILTONIAN is clearly a trivial problem. But, as with YES-HAMILTONIAN, we can construct a non-trivial verification circuit, which picks out a particular subspace that allows us to prove universality. By Definition 39 there must be a faithful reduction with respect to *this* verification circuit from SUCCINCT-YES-HAMILTONIAN to $\mathcal{M}$-HAMILTONIAN.

The verification circuit we choose, and the subspace it picks out, are as in Lemma 46. Although the circuit is unchanged, this is now a $\mathrm{QMA}_{\mathrm{EXP}}$-verification circuit, since for Hamiltonians acting on n qudits the circuit length and witness size are of order $\mathrm{poly}(n) = \mathrm{O}(2^{\mathrm{poly}(x)})$, where x is the number of bits of information needed to describe the input to the problem.

It then follows, using the same argument as in Lemma 46, that for any Hamiltonian H_{target} acting on n spins which can be described succinctly, there exists a Hamiltonian in $\mathcal{M}$ which can simulate H_{target} efficiently (where efficiency is defined in terms of number of qudits, not bits of information).

To prove universality, note that in Theorem 32 a construction is given of a universal Hamiltonian, H_{succ}, (with exponential overhead in terms of number of spins and norm of simulating system) which can be described succinctly.

Since there exists a Hamiltonian in $\mathcal{M}$ which can simulate H_{succ} (for any values of the parameters in H_{succ}), and since simulations compose, it follows that $\mathcal{M}$ is a universal model. When simulating general (non-succinct) Hamiltonians, the universal model, $\mathcal{M}$, inherits an exponential overhead in terms of the numbers of qudits and the norm of the simulating system from H_{succ}. □

QMA_{EXP} is a more powerful complexity class than QMA so it may seem odd that it appears to be less efficient as a simulator. However, there are some situations where using a family of Hamiltonians meeting the conditions of Corollary 49 will give a more efficient simulator than using a family of Hamiltonians meeting the conditions of Theorem 45. To see this, note that given a Hamiltonian which can be described succinctly, it can be simulated efficiently (in the sense of [6] i.e. in terms of numbers of qudits, simulating system norm, and ϵ and η parameters) by either a family of Hamiltonians with a QMA-complete $\mathcal{M}$-HAMILTONIAN, or a family of Hamiltonians with a QMA_{EXP}-complete $\mathcal{M}$-HAMILTONIAN. However, the simulation by the QMA-complete family of Hamiltonians will not be efficient in terms of the number of bits needed to describe the simulating Hamiltonian. Whereas the simulation by the QMA_{EXP}-complete family of Hamiltonians would be. So there are situations where simulation using a QMA_{EXP}-complete family of Hamiltonians is more efficient, demonstrating that the question of which family of Hamiltonians is a 'more powerful' simulator doesn't have a straightforward answer.

The obvious example of Hamiltonians that can be succinctly described are translationally invariant Hamiltonians. Examples of translationally invariant universal Hamiltonians are constructed in [33] and Chapter 2, where it is noted that a translationally invariant universal model with fixed interactions must have an exponential overhead in terms of number of spins by a simple counting argument.

By considering the problem PRECISE-$\mathcal{M}$-HAMILTONIAN and introducing the idea of an *exponentially faithful*, reduction we can also derive conditions for universal models which are efficient in terms of the number of qudits in the simulator system, but not in terms of the simulating system's norm. We say a reduction is *exponentially faithful* if it meets the conditions of Definition 38, but where now the gap in the spectrum of the acceptance operator, g, and the corresponding gap in the spectrum of the Hamiltonian is required to satisfy $g > 1/\exp(n)$ for n the size of the input. This is a natural relaxation when considering PRECISE-$\mathcal{M}$-HAMILTONIAN, as it requires the gap in the spectrum of the acceptance operator in YES cases to scale in the same way as the promise gap for the problem.

The natural complexity class when considering PRECISE-$\mathcal{M}$-HAMILTONIAN is PreciseQMA. It is known that every problem in PreciseQMA can be solved by a quantum circuit of length $T = \mathrm{O}(\exp(n))$ acting on $\mathrm{poly}(n)$ qudits, with completeness $c = 1 - 2^{\mathrm{poly}(n)}$ and soundness $s = 2^{\mathrm{poly}(n)}$ (where n is the size of the problem input) [17, Corollary 10]. Therefore, when defining what it means for PRECISE-$\mathcal{M}$-HAMILTONIAN to be PreciseQMA-complete under exponentially faithful reductions there are two classes of circuits we could require faithfulness with respect to - the polynomial sized circuits that give exponentially small completeness-soundness gap, or the exponential sized circuits that give completeness-soundness gap exponentially close to 1. Here we choose the latter, and define:

Definition 50. *We say that* PRECISE-$\mathcal{M}$-HAMILTONIAN *is* PreciseQMA*-complete under exponentially faithful reductions if for all* $A \in$ PreciseQMA *and for any exponential time verification circuit* U *which verifies* A*, there exists a reduction from* A *to the* PRECISE-$\mathcal{M}$-HAMILTONIAN *problem which is exponentially faithful with respect to* U*.*

Corollary 51. *A family of Hamiltonians,* $\mathcal{M}$*, is a universal model which is*

1. *efficient in terms of the numbers of qudits,*
2. *not efficient in terms of the simulating system's norm and*
3. *achieves exponential accuracy in the* ϵ *parameter with polynomial overhead in number of qudits and exponential overhead in simulating system norm*

iff

1. PRECISE-$\mathcal{M}$-HAMILTONIAN *is* PSPACE*-complete under exponentially faithful reductions,*
2. $\mathcal{M}$ *is closed and*
3. $\mathcal{M}$-HAMILTONIAN *is not* QMA*-complete under faithful reductions.*

Proof. Recall that PSPACE = PreciseQMA [17].

First consider the if direction. Assume we have a family of Hamiltonians $\mathcal{M}$ meeting the conditions $i - iii$ of the theorem. Since $\mathcal{M}$-HAMILTONIAN is not QMA-complete under faithful reductions we have to use exponentially faithful reductions to PRECISE-$\mathcal{M}$-HAMILTONIAN, where by Definition 50 we are considering faithfulness with respect to exponential time circuits. The if direction follows immediately since going through the proof of Theorem 45 with an exponentially small gap in the acceptance

operator and exponentially long computation time requires an exponentially large energy penalty Δ, and gives an exponentially small accuracy parameter ϵ.

To see the only if direction, consider a universal model, $\mathcal{M}$ meeting conditions $1-3$ of the theorem. Necessity of closure is trivial. Note, $\mathcal{M}$-HAMILTONIAN cannot be QMA-complete under faithful reductions, because by Theorem 45 if it was the universal model would be efficient in terms of norm.

Consider simulating the family of Hamiltonians $\mathcal{K}$ using the model $\mathcal{M}$ to exponential accuracy in ϵ. This demonstrates that PRECISE-$\mathcal{M}$-HAMILTONIAN is PSPACE-complete (including under exponentially faithful reductions), but it does not contradict the statement that $\mathcal{M}$-HAMILTONIAN is not QMA-complete. This is because the k-LOCAL HAMILTONIAN problem requires that the terms in the Hamiltonian are of order 1, which requires dividing each term in the simulator system by the simulating system norm, which by assumption is exponential in the size of the system. This leads to a Hamiltonian with an exponentially small spectral gap, which attenuates the promise gap too fast to maintain QMA-completeness, but gives PreciseQMA-completeness (and therefore PSPACE-completeness).

□

An example of a universal Hamiltonian meeting the conditions of Corollary 51 is given in Chapter 2. It is a translationally invariant universal model, but includes a phase parameter which encodes information about the target system, so the interactions are not fixed.

Chapter 4

Conclusions on universal Hamiltonians for simulation

In Chapter 2 we presented a new conceptually simple method for proving universality of spin models. This method built on ideas in [35] for proving results about 'gap-simulation', and extended them to derive results about universality. The reliance of this novel method on the ability to encode computation into the low energy subspace of a Hamiltonian suggested that there is a deep connection between universality and complexity. We made this insight rigorous in Chapter 3, where we derived necessary and sufficient conditions for spin systems to be universal simulators (as was done in the classical case [38]).

The "history state" simulation approach was already stronger than previous methods for proving universality, allowing us to prove that the simple setting of translationally invariant interactions on a 1D spin chain is sufficient to give universal quantum models. Furthermore, we used it to provide the first construction of translationally invariant universal model which is efficient in the number of qudits in the simulator system.

Translationally invariant interactions are more prevalent in condensed matter models than interactions which require fine tuning of individual interaction strengths. However, a serious impediment to experimentally engineering either of the universal constructions in Chapter 2 is the local qudit dimension, which is very large—a problem shared by the earlier 2D translationally invariant construction in [33].

The "history state" simulation approach (along with techniques to make phase estimation circuits sparse) has recently been used to demonstrate the existence of what has been termed *strongly* universal Hamiltonian simulators [54]. Where a

strongly universal Hamiltonian is one which can efficiently simulate any k-local Hamiltonian for $k = \mathrm{O}(1)$ (i.e. not just those on a sparse interaction graph). The results in [54] move us closer towards physically realisable universal Hamiltonians, but require precise control over interaction strengths (a problem shared by constructions in [6]) beyond what is feasible with current experimental techniques.

The classification of universal simulators in Chapter 3 gives a still simpler route for proving universality of families of Hamiltonians. All previous universality results [6, 33, 54], including those in Chapter 2, relied on explicit constructions, tailored to particular universal models. These constructions showed that given some arbitrary target Hamiltonian H_{target}, a Hamiltonian from the universal model could be constructed which simulated H_{target}. These constructions drew on techniques from Hamiltonian complexity theory, such as perturbation gadgets and history states, but the proofs of universality required substantial additional work.

That additional work can now in many cases be side-stepped, by using the extensive existing work classifying the complexity of the local Hamiltonian problem [29, 18, 19, 16], along with our main result from Chapter 3 (as well as our recipe for modifying history state Hamiltonians). The remaining step is to demonstrate closure - for some families of Hamiltonians this step is trivial (it follows from the definition of the model), for others it will require some work - however demonstrating closure will always be simpler than demonstrating universality, since closure requires the ability to simulate a limited class of Hamiltonians.

It should be noted that this method of proving universality is not constructive - it doesn't tell you how to simulate a given target Hamiltonian with a Hamiltonian from the a universal model. However, we do not view this as a drawback when compared to previous methods of proving universality. The previous methods for proving universality were theoretically constructive - in the sense that for any target Hamiltonian they provided a mathematical description of a Hamiltonian from the universal model which could simulate it. However, in reality the cost of leaving the target Hamiltonian completely general in the previous proofs was that the simulations constructed had to be very complex - putting them out of reach of current experimental limitations. The benefit of our work is that it gives a simple route to proving universality, so now the work on constructing explicit simulations can focus on simulations which are experimentally feasible.

The problem of constructing universal Hamiltonians where the simulations are experimentally feasible is challenging, but solving it is of fundamental importance.

Current constructions fall down in either requiring precise control of interaction strengths across many orders of magnitude, or in requiring very large local Hilbert space dimension (and in some cases both). The results in Chapter 3 provide an extra tool for tackling this challenge. As we've already mentioned, our results give a new technique for proving universality. This could be applied to, for example, the construction in [22] of a low-dimensional spin chain with $\mathrm{QMA}_{\mathrm{EXP}}$-complete ground state energy problem to check whether the model is universal. The construction in [22] is complex, and checking universality via previous methods would be a difficult technical challenge. With the aid of our results it becomes significantly more straightforward. If it is shown to be universal it would be a universal model which doesn't require tuning of individual interaction strengths, and with local Hilbert state dimension orders of magnitude smaller than any previously known model. This would be an important step towards experimentally feasible universal models - although it should be noted that while the local dimension of this construction (roughly 40) is orders of magnitude smaller than that for current universal models, it would still be an experimental challenge to engineer.

The other direction our results could be used in is investigating the complexity of models which are currently used as analogue simulators, to determine whether there is hope of using them to construct universal models. One platform that is currently used for analogue Hamiltonian simulation is Rydberg atoms [55, 56, 57]. It has been suggested [55] that this might have promise as a universal simulator as in certain regimes the platform naturally encodes the XY-Hamiltonian, which is known to be universal [6]. However, the proof of universality can not be used to construct a universal simulator using Rydberg atoms as it involves complicated chains of perturbative simulations, requiring precise control beyond the reach of current experiments. An alternative approach to investigating the use of Rydberg atoms as universal simulators could be to investigate the complexity of the ground state energy problem of Rydberg interactions where the control over interaction strengths is limited to what is experimentally feasible. As outlined above, demonstrating complexity in this regime is likely to be more straightforward than directly proving universality. If, within the limitations on interaction strength, it is possible to demonstrate hardness of the ground state energy problem, that motivates attempts to look for simple universal constructions. If it is not possible to demonstrate hardness of the ground state energy problem within current experimental limitations, it may be possible to determine how much experimental techniques have to advance in order to overcome the barrier and achieve universality.

It is interesting to note that a proposal for using adiabatic elimination of Rydberg dressed qubits to engineer tunable anisotropic $\{\alpha XX + \beta YY + \gamma ZZ\}$-simulators [58] meets the conditions to be a simulation in the strong sense of [6] - see Appendix B for a proof of this. The proposal in [58] could also be considered in some senses to be a fourth-order perturbative simulation - the process of adiabatically eliminating the 'fast' degrees of freedom to generate an effective Hamiltonian is the same process used in [6] to generate a low energy effective Hamiltonian using perturbation gadgets and the effective Hamiltonian is calculated to fourth order in the detuning. However, the effective Hamiltonian in [58] is not a fourth-order simulation of the form given in Lemma 21. The difference between the two approaches is that perturbative simulations in Lemma 21 are designed to ensure that the fourth order term dominates, so that the final Hamiltonian is dominated by the terms of interest. Whereas in [58] the first order term in the perturbation dominates, and the XX and YY terms in the final Hamiltonian are orders of magnitude smaller than the ZZ terms. An interesting open problem is whether it is possible to use adiabatic elimination of fast degrees of freedom to develop perturbative simulations of the type given in Lemmas 18 to 21 while only using interactions which can be engineered in current experimental platforms.

The example of Rydberg atoms points at an important difference between the idea of universal simulators outlined in this thesis, and the types of simulations currently being engineered in NISQ devices. The Rydberg atom simulation proposal of [58] isn't designed to engineer a totally universal simulator, but instead to achieve the more restricted goal of simulating an interaction where certain parameters are tunable. This is clearly a more modest goal, and is likely to be achievable with far lower experimental overhead. However, understanding the theory of analogue simulation is still crucial for evaluating whether the NISQ simulators are actually replicating the entire physics of the desired interaction. Moreover, as experimental control over quantum system improves, and the proposals for universal simulators become simpler, we can work towards the more ambitious goal of constructing universal simulators.

Another stepping stone on the way to truly universal simulators could be universal 'quasi'-simulators - i.e. systems which can replicate some of the physics of arbitrary Hamiltonians. For example, we might just want to simulate the Hamiltonian up to some energy cut off, or replicate some thermodymical properties of the system, or approximate certain observables (but not necessarily all). This idea of a restricted simulator has been addressed in [35] where the idea of 'gap-simulation' was proposed.

In ‘gap-simulation’ instead of trying to replicate the entire physics of arbitrary Hamiltonians, we are only interested in replicating the ground state and the spectral gap. This sounds like a simpler problem, but still physically interesting. However, the examples of ‘universal gap-simulators’ from [35] can be shown to be universal Hamiltonians in the stronger sense of [6]. It is not known whether this less stringent definition of simulation, or any other, can lead to universal ‘quasi’-simulators which are simpler to engineer experimentally, but it is an interesting avenue for future research.

Aside from designing universal Hamiltonians which are in the reach of current experiments, it would also be interesting to explore what symmetries (other than translational invariance) universal models can exhibit. This is of particular interest for using universal Hamiltonians in holography, where we would like the boundary theory to exhibit (a discrete version of) conformal symmetry. See Part III for further discussion of this.

Finally, the relationship between complexity and universality is interesting from a fundamental physics standpoint. It was already clear that universality implied complexity - since universal models must be able to simulate *all* quantum many body physics. However the reverse direction was not obvious. Our results show that if the problem of deciding whether a Hamiltonian in $\mathcal{M}$ has a low energy ground state is hard for a quantum computer, then $\mathcal{M}$ must be rich enough to capture all quantum many body physics.

Part II

Error mitigation in the NISQ era

Chapter 5

Fitting quantum noise models to tomography data

5.1 Introduction

A key challenge in developing useful applications of quantum devices in the NISQ era is understanding error processes [59]. This is true both for analogue Hamiltonian simulation, where the first step in analysing the effect of noise on a simulation is to characterise what noise is there in the simulator. And for digital computation on pre-fault tolerant devices, where active error mitigation and correction techniques will be needed to prevent the outputs of computations being swamped by errors. In the long term, error correcting codes will be used to suppress noise and achieve fully fault-tolerant computation. But in the NISQ era, the overhead of full fault tolerance is prohibitive, placing it beyond reach of near-term hardware. It is thus important to understand and characterise the underlying noise dynamics in current quantum devices, both in order to inform hardware design, and to prepare error correction and mitigation protocols optimised for the specific noise in the apparatus.

Various methods have been devised to evaluate and analyse noise in quantum dynamics, making different assumptions on, and providing different information about, the noise processes [60]. One way to understand the noise model in a device is to look for compatible Markovian[1] evolutions. Knowing the Lindbladian which best approximates the generator of the physical process can help to understand the physical noise processes occurring in particular hardware.

[1]We call a quantum channel *Markovian* if it is a solution of a master equation with generator in Lindblad form [61, 62]. Equivalently, it is an element of a one-parameter continuous completely positive semigroup.

However, noise in quantum devices may substantially deviate from a memoryless dynamics, so that no compatible Markovian description exists. Therefore, methods to benchmark non-Markovian dynamics are also of considerable interest. A number of approaches for this have been devised; we give a brief overview in subsection 5.1.1. However, there are limitations to these methods - some of these procedures are impractical to compute, others give only a one sided witness of non-Markovianity, and no information about the noise processes in the Markovian case. Thus, finding a theoretically well-defined, but also feasible and low-resource procedure to assess Markovian and non-Markovian noise in quantum devices is desirable.

In this chapter we present two methods, both built on convex optimisation programming, to characterise and quantify noise processes in quantum systems. The first is an efficient algorithm to compute the best-fit Lindblad generator to the measured quantum channel. This can be used to certify Markovian evolution within any desired level of error tolerance, and the form of the resulting Lindbladian gives insight into the noise processes present. Alternatively, if the distance between the memoryless channel generated by the Lindbladian and the experimentally measured channel is significant (in comparison to the error rate of the tomographic reconstruction), this difference constitutes an insightful quantity to evaluate non-Markovian dynamics. The second algorithm calculates a quantitative and operationally meaningful measure of non-Markovianity, first proposed in ref. [63], in terms of the minimal amount of isotropic noise to be added to the generator of an hermiticity- and trace-preserving map, close to the tomographic snapshot, in order to "wash out" memory effects and render the evolution Markovian.[2] A key strength of our approach is that the algorithms we have developed do not require any a priori assumptions on the underlying dynamics, nor any access to or characterisation of the environment, but only a small number of tomographic snapshots – a single one would already suffice.

The algorithms we present here are built on the theoretical work in refs. [63, 64]. We extend their approach in a number of important ways. We change the semi-definite integer programme from [63] into a convex optimisation algorithm that searches for the best-fit Lindbladian generator in a neighbourhood of a given size around the input. This allows us to include an error tolerance parameter that can be tuned at any desired level, making the scheme robust with respect to inaccuracies of the tomographic measurements, and applicable to real-world data with statistical errors.

[2]Directly analogous to robustness of entanglement measures in entanglement theory.

We also fully generalise the set of input operators, lifting the assumption from [63] that the input channel had a non-degenerate spectrum. We lift this limitation in two ways. First, we show that we can perturb any operator with multi-dimensional eigenspaces into an arbitrarily close matrix having non-degenerate spectrum and at the same time retaining the hermiticity-preserving property. This guarantees the uniqueness of the generator while preserving the outcome of the non-Markovianity measure by adjusting the error tolerance parameter accordingly. Second, we consider the more physically relevant case, where we have a non-degenerate quantum channel which arises as a perturbation from a degenerate channel. This is crucial for characterising noise in quantum computing devices, where the channels of interest are typically noisy versions of quantum gates having degenerate eigenvalues. This task is delicate, due to the sensitivity of the Lindblad form to perturbation in the presence of multi-dimensional eigenspaces. To deal with this issue, we develop a mathematical approach to reconstruct these subspaces by leveraging techniques from matrix perturbation theory [65], and implement this as a set of algorithms that serve as a pre-processing phase for the convex optimisation task. Finally, we extend the algorithm to the case where we have a sequence of tomographic snapshots. This offers a significantly more sensitive test of non-Markovianity, or a considerably more precise fit to an underlying Markovian master equation, with only a linear increase in the number of measurement settings required.

We accompany our theoretical analysis with a Python implementation of all the algorithms, which we benchmark numerically on simulated tomographic data in Cirq [66]. The numerical results show that our algorithms successfully identify Markovian-compatible dynamics for a range of 1- and 2-qubit examples, both for noisy quantum gates with degenerate spectrum and non-degenerate quantum channels. The numerics also confirm that our algorithms are able to compute accurate values for the non-Markovianity measure of noisy, non-Markovian quantum channels, which we show to be consistent with a calculation of this measure done by hand.

It should be noted that throughout this chapter we restrict our attention for simplicity to time-independent Markovian noise. This is reasonable for characterising errors in individual gates on current hardware, given the short timescales involved [67] over which noise processes are unlikely to vary significantly. However, it is likely the approach presented in the current work can be extended to encompass the more general case of time-dependent Markovian noise, which would allow assessment of errors in longer quantum circuits, over timescales in which the noise processes may fluctuate. This is an important topic for follow-up work.

The chapter is organised as follows. In the remainder of this section we give an overview of prior work in the field and a high level overview of our approach. In Section 7.3 we introduce our notation and cover preliminaries on convex optimisation and matrix perturbation theory. The precise notion of Markovianity is defined in Section 5.3, where we also present the non-Markovianity measure first defined in [63]. In Section 5.4 we discuss how we extend the approach from [63] to all quantum channels, in particular ones having degenerate spectrum. Our algorithms are presented in Section 5.5, and finally results from numerical simulations are discussed in Section 5.6.

5.1.1 Related work on assessing non-Markovian noise

The nature of non-Markovian noise has been investigated from a variety of perspectives and with a number of different approaches (cfr. review papers [68, 69, 70] and the introduction of [71]). One of the principal ways to quantifying non-Markovianity is based on *divisibility* [72, 73], i.e., the property of a channel encoding evolution from time t_0 to t_1 to be implemented as a concatenation of channels from time t_0 to t and t to t_1 for any $t \in [t_0, t_1]$. Indeed, a channel which is Markovian, in the Lindblad sense, is also divisible. However, the converse is not necessarily true.[3]

The original measure of non-Markovianity [63], on which this work builds, determines whether the observed tomographic data is consistent with a time-independent Markovian master equation. If not, it provides a quantitative measure of how far the observed dynamics is from the closest Markovian trajectory. This task (and also that of determining finite divisibility) was shown to be NP-hard in general [64, 74], but efficiently (classically) computable for any fixed Hilbert space dimension.

Other methods for detecting and measuring non-divisibility and non-Markovianity are based on checking monotonicity of quantities that are known to decrease under completely positive maps such as quantum correlation (see [75], known as the *RHP measure)*, quantum coherence [76], quantum relative entropy [77] or the quantum mutual information [78].

Another approach affirms that a non-Markovian map is one that allows information [79], e.g. the Fisher information [80], to flow from the environment to the system. Non-Markovianity can also be quantified by considering the change in the distinguishability of pairs of input states [81]. The observation of non-monotonic behaviour of channel capacity [82], the geometrical variation of the volume of the

[3]The property of being 'infinitesimal divisible' is known to be equivalent to time-dependent Markovianity, but that is a stronger requirement than divisibility (see [72]).

set of physical states [83], ensembles of Lindblad's trajectories [84] and deep-neural-network and machine learning [85, 86, 87] are among the many alternative strategies to quantify dynamics with memory effects.

A limitation of many of these measures is that they provide one-sided witnesses of non-Markovianity, but cannot show that the dynamics *is* Markovian, or find the master equation consistent with or closest to the observed dynamics.

5.1.2 Our approach

Our main result is a set of algorithms, implemented in Python and benchmarked on simulated data in Cirq, which characterise and quantify the noise processes in a quantum system from one (or a small number of) tomographic snapshot(s). In the case of Markovian or near-Markovian dynamics, we compute a full description of the Lindbladian that best fits the measured data, without requiring any a priori assumptions on the form of the master equation. Conversely, in the case of non-Markovian dynamics we calculate an operationally meaningful measure of non-Markovianity, corresponding to the minimum amount of white noise that has to be added in order to "wash out" the memory effects and render the dynamics Markovian.

More precisely, consider a $d^2 \times d^2$ matrix M resulting from process tomography on the dynamics of a d-dimensional quantum system, together with an error parameter ε which accounts for statistical errors and other sources of uncertainty in the tomographic data, by setting the maximum distance from M to look for a compatible Markovian map. For simplicity, we assume for the moment that M has non-degenerate spectrum, which guarantees that its matrix logarithm $L_0 = \log M$ is unique. However, we highlight that a significant part of this work concerns lifting this assumption, so that the algorithm accepts arbitrary matrices as input. We refer to Section 5.4 and subsection 5.5.1 for full details.

By formulating a convex optimisation programme whose constrains are exactly the necessary and sufficient conditions of a Markovian generator (cfr. Section 5.3 for an in-depth explanation), we retrieve the closest Lindbladian $L'(\vec{m})$ to the complex branch $L_{\vec{m}}$ of the matrix logarithm L_0. Then, by iterating the convex optimisation task over the set of branches $L_{\vec{m}}$ for $\vec{m} \in \{-m_{\max}, -m_{\max}+1, \ldots, 0, \ldots, m_{\max}-1, m_{\max}\}^{\times d^2}$, we keep the Lindbladian $L'(\vec{m})$ whose generated Markovian map $\exp\{L'(\vec{m})\}$ is the closest to M.

If no Lindbladian is found within the ε-ball around M, we compute the non-Markovianity measure of M in the sense of [63], denoted by $\mu_{\min}$. This value

quantifies the minimal amount of isotropic noise to be added to the generator H' of an hermiticity- and trace-preserving map in the ε-neighborhood of M in order to obtain a Markovian evolution; in other words, $\mu_{\min}$ is the smallest scalar μ such that $L' = H' - \mu\,\omega_\perp$ is a valid Lindbladian. This is equivalent to (cfr. Section 5.3)

$$\mu_{\min}(M) \coloneqq \min\left\{\mu : \omega_\perp X \omega_\perp + \frac{\mu}{d}\mathbb{1} \geq 0\right\} \tag{5.1}$$

with the constraint that there exists a branch $L_{\vec{m}}$ such that $\|H' - L_{\vec{m}}\|_{\mathrm{F}} = \|X - L^{\Gamma}_{\vec{m}}\|_{\mathrm{F}} \leq \delta$, where Γ is the involution from the transfer matrix representation in the elementary basis to the Choi representation (more details in subsection 5.2.1), $X = (H')^{\Gamma}$, $\omega_\perp$ is the projection onto the orthogonal complement of the maximally entangled state and δ is the maximal distance for H' from $L_{\vec{m}}$ representing – in some approximation – the radius of the ε-ball around M under the matrix logarithm (more details in subsection 5.5.2).

We have tested our approach on simulated tomographic data from the Cirq platform for the following examples: the Pauli X-gate, a 1-qubit depolarising channel, a 1-qubit unital quantum channel, the 2-qubit ISWAP gate, and a 2-qubit non-unitary Markovian depolarizing CZ-channel. These examples cover 1- and 2-qubit Markovian and 1-qubit non-Markovian channels, as well as operators with degenerate eigenspaces: the algorithm has been successful in analysing all these scenarios. For the Markovian examples, it correctly identified a Markovian evolution within the error tolerance regime suggested by the statistical error in tomographic reconstruction, and extracted the best-fit Lindblad generator. For non-Markovian dynamics, it returned a measure of non-Markovianity - in the case of simple 1 qubit channels we can check this value analytically, and we found that the results of our algorithm were consistent with the analytic value (see subsection 5.6.1.4).

Dealing with channels having degenerate spectrum requires an additional pre-processing phase, where we sample over different basis vectors sets of the multi-dimensional eigenspaces. See Section 5.4 and subsection 5.5.1 for details of how we tackled these complications.

Pseudo-code of all the algorithms is presented in subsection 5.5.2. The code itself is publicly available at [7].

5.2 Notation and preliminaries

We denote elementary basis vectors by $\left|e_j\right\rangle = (0,\ldots,1,0,\ldots,0)^T$ with 1 in the j-th position. The maximally entangled state is $|\omega\rangle = \sum_{j=1}^{d}\left|e_j, e_j\right\rangle/\sqrt{d}$ and $\omega_\perp =$

$\mathbb{1} - |\omega\rangle\langle\omega|$ is the projection onto its orthogonal complement. We write $\mathbb{F}$ to denote the flip operator interchanging the tensor product of elementary basis vectors, i.e. $\mathbb{F}\left|e_j, e_k\right\rangle = \left|e_k, e_j\right\rangle$. We will use the Frobenius norm on matrices, defined by $\|M\|_{\mathrm{F}} = \sqrt{\sum_{j,k}\left|m_{jk}\right|^2}$, and the 1-norm, $\|M\|_1 = \sum_{j,k}\left|m_{jk}\right|$. They are both *submultiplicative*, that is, they satisfy $\|AB\| \leq \|A\|\|B\|$ for all square matrices A and B.

5.2.1 Channel representations and ND^2 matrices

We will consider quantum channels of finite dimension only, i.e. completely positive and trace preserving (CPT) linear operators acting on the space of $d \times d$ matrices. To represent a channel $\mathcal{T}$ as a $d^2 \times d^2$ matrix T, we will adopt the elementary basis representation:

$$T_{(j,k),(\ell,m)} = \left\langle e_j, e_k\right|T\left|e_\ell, e_m\right\rangle \coloneqq \mathrm{Tr}\left[\left|e_k\right\rangle\left\langle e_j\right|\mathcal{T}(|e_\ell\rangle\langle e_m|)\right]. \tag{5.2}$$

This is sometimes called the *transfer matrix* of the channel in the elementary basis. The corresponding representation $|v\rangle \in \mathbb{C}^{d^2}$ of a $d \times d$ matrix V on which the channel acts is then

$$v_{j,k} = \left\langle e_j, e_k\right|\left.v\right\rangle \coloneqq \left\langle e_j\right|V\left|e_k\right\rangle. \tag{5.3}$$

In this representation, the action of the channel on a matrix becomes matrix-vector multiplication, and the composition of channels corresponds to the product of their respective matrix representations.

In order to formulate necessary and sufficient conditions for the generator of a Markovian evolution, we will also make use of another representation, the Choi-matrix (or Choi-representation), defined as

$$\tau(\mathcal{T}) \coloneqq d\big(\mathcal{T} \otimes \mathcal{I}\big)(|\omega\rangle\langle\omega|)\big). \tag{5.4}$$

Conveniently, the two representations are directly related through the Γ-involution [63], acting on the elementary basis as

$$\left|e_j, e_k\right\rangle\left\langle e_\ell, e_m\right|^\Gamma \coloneqq \left|e_j, e_\ell\right\rangle\left\langle e_k, e_m\right|. \tag{5.5}$$

Explicitly, we have

$$\tau = (T)^\Gamma \qquad \text{and} \qquad T = (\tau)^\Gamma. \tag{5.6}$$

The Choi-representation is very useful to investigate the *hermiticity-preserving* property of quantum channels, i.e., quantum maps $\mathcal{T}$ such that $\mathcal{T}(X^\dagger) = \mathcal{T}(X)^\dagger$ for all X. Indeed we have

Lemma 52. *$\mathcal{T}$ is hermiticity-preserving $\iff$ τ is hermitian.*

We will use the terms hermiticity-preserving and Choi-hermitian interchangeably.

Using the terminology from ref. [88], we define the following two properties

Definition 53 (defective matrix)**.** *A matrix is* defective *if the geometric multiplicity of some eigenvalue is strictly less than its algebraic multiplicity. That is, the matrix is not diagonalizable.*

Definition 54 (derogatory matrix)**.** *A matrix is* derogatory *if some eigenvalue has geometric multiplicity strictly larger than one.*

For brevity, we call non-defective, non-derogatory matrices ND^2 *matrices*. These are matrices with non-degenerate spectrum and diagonalisable by a unique choice of normalised eigenvectors. Crucial for our approach is the consequent structure of the complex matrix logarithm of an ND^2 matrix T, given by an infinite number of branches indexed by a vector $\vec{m} = (m_1, \ldots, m_{d^2}) \in \mathbb{Z}^{d^2}$. The 0-branch of the matrix logarithm of a diagonalisable matrix $T = \sum_{j=1}^{d^2} \lambda_j |r_j\rangle\langle\ell_j|$, with $\{\lambda_1, \ldots \lambda_{d^2}\}$ being the eigenvalues of T and ℓ_j, r_j the respective left and right eigenvectors such that $\langle\ell_j|r_k\rangle = \delta_{jk}$, is given by

$$L_0 \coloneqq \log(T) = \sum_{j=1}^{d^2} \log\lambda_j |r_j\rangle\langle\ell_j|; \tag{5.7}$$

the $\vec{m}$-branch is then

$$L_{\vec{m}} \coloneqq L_0 + \sum_{j=1}^{d^2} m_j 2\pi\mathrm{i}\, |r_j\rangle\langle\ell_j|. \tag{5.8}$$

Modified hermitian adjoint The hermitian adjoint operation on a matrix in its vector representation $|v\rangle$ in the elementary basis, is given by $|v^\dagger\rangle \coloneqq \mathbb{F}\,|v^*\rangle$. We call vectors such that $|v\rangle = |v^\dagger\rangle = \mathbb{F}\,|v^*\rangle$ *self-adjoint*, and we say that two vectors v and w are *hermitian-related* if $|w\rangle = |v^\dagger\rangle = \mathbb{F}\,|v^*\rangle$ (and equivalenty $|v\rangle = |w^\dagger\rangle = \mathbb{F}\,|w^*\rangle$). This terminology is unusual with respect to the conventional hermitian conjugation operation on vectors, but the definition adopted here for d^2-dimensional vectors exactly corresponds to the usual hermitian adjoint of their corresponding $d \times d$

matrices on which $\mathcal{T}$ acts. We will conversely denote the standard hermitian conjugation for a matrix A by A^H.

5.2.2 Convex optimisation programmes

At the heart of our algorithms are convex optimisation programmes which either retrieve the closest Lindbladian to the matrix logarithm, or the smallest non-Markovianity parameters (both objects explained into detail in Section 5.3). These convex optimisations over a (scalar or vector) variable x have the general form [89]

standard form

$$\begin{aligned} &\textit{minimize} && f_0(x) && \\ &\textit{subject to} && f_j(x) \leq 0, && j = 1,\dots,n \\ &&& \langle a_k, x\rangle = b_k && k = 1,\dots,m \end{aligned} \tag{5.9}$$

epigraph form

$$\begin{aligned} &\textit{minimize} && \mu && \\ &\textit{subject to} && f_0(x) - \mu \leq 0 && \\ &&& f_j(x) \leq 0, && j = 1,\dots,n \\ &&& \langle a_k, x\rangle = b_k && k = 1,\dots,m \end{aligned} \tag{5.10}$$

where $f_0, f_1, \dots, f_n$ are convex functions. A fundamental property of convex optimisation problems is that any locally optimal point is also globally optimal.

A class of convex optimisation problems, called *second-order cone programmes*, takes the form

$$\begin{aligned} &\textit{minimize} && \langle f, x\rangle && \\ &\textit{subject to} && \left\|A_j x + b_j\right\|_2 \leq \langle c_j, x\rangle + d_j && j = 1,\dots,n \\ &&& Fx = g && \end{aligned} \tag{5.11}$$

where f, g, b_j's and c_j's are vectors (not necessarily of the same dimension), F and A_j's are matrices and d_j's are scalars. The condition $\left\|A_j x + b_j\right\|_2 \leq \langle c_j, x\rangle + d_j$ is called *second-order cone constraint*. Important for our work is the fact that minimization objectives for the Frobenius norm over matrix variables can be converted into a second order cone program via epigraph formulation.

To numerically implement convex optimisation programme, we make use of the Python library CVXPY [90, 91].

5.3 Quantum Markovian channels and embedding problem

Processes which do not retain any memory of their previous evolution are called *Markovian* and satisfy the *Markov property*: given a sequences of points in time $t_1 < t_2 <, \ldots, < t_{n-1} < t_n$, a stochastic process X_t taking values on a countable space has the Markov property if

$$\mathbb{P}(X_{t_n+s} = y \,|\, X_{t_n} = y_n, \ldots, X_{t_2} = y_2, X_{t_1} = y_1,) = \mathbb{P}(X_{t_n+s} = y \,|\, X_{t_n} = y_n) \tag{5.12}$$

for any $s > 0$.

Extending this notion, a *quantum Markov process* is described by a one-parameter semi-group giving rise to a continuous sequence of completely positive and trace preserving (CPT) channels. The generators of this type of semi-group is called *Lindbladian* and must take the well-known *Lindblad form* [61, 62],

$$\mathfrak{L}(\rho) \coloneqq i[\rho, H] + \sum_{\alpha,\beta} g_{\alpha,\beta} \left[F_\alpha \rho F_\beta^\dagger - \frac{1}{2} \left(F_\beta^\dagger F_\alpha \rho + \rho F_\beta^\dagger F_\alpha \right) \right], \tag{5.13}$$

where H is hermitian, $G = (g_{\alpha\beta})$ is positive semi-definite and $\{F_\alpha\}_\alpha$ are orthonormal operators. The first term on the RHS is the Hamiltonian part and describes the unitary evolution of the density operator, while the second term represents the dissipative part of the process. By diagonalising G as $\Gamma \coloneqq U^\dagger G U = \mathrm{diag}(\gamma_\alpha)$ and defining the so-called *jump operators* $J_\alpha \coloneqq \sqrt{\gamma}_\alpha \sum_\beta u_{\beta\alpha} F_\beta$, we can re-write eq. (5.13) in diagonal form,

$$\mathfrak{L}(\rho) \coloneqq i[\rho, H] + \sum_{\alpha} \left[J_\alpha \rho J_\alpha^\dagger - \frac{1}{2} \left(J_\alpha^\dagger J_\alpha \rho + \rho J_\alpha^\dagger J_\alpha \right) \right]. \tag{5.14}$$

The question whether a given quantum map $\mathcal{M}$ is compatible with a Markovian process, in the sense that there exists a memoryless evolution that at a certain time is equal to $\mathcal{M}$, has been investigated from different perspectives, e.g. in the context of complexity [64], channel divisibility [72], regarding spectrum [92] and toward the goal of achieving a quantum advantage [93], and it is sometimes referred to as the *embedding problem*. A method to ascertain whether a given channel is compatible with a Markovian dynamics has been developed in ref. [63], which provides three properties for L' that are necessary and sufficient to satisfy eq. (5.13) (where L' is the elementary basis representation of $\mathfrak{L}$). These are

(i) L' is hermiticity-preserving, that is, $L'\left|v^\dagger\right\rangle = (L'|v\rangle)^\dagger$ for all $|v\rangle$.

(ii) $(L')^{\Gamma}$ is *conditionally completely positive* [94], that is, $\omega_{\perp}\,(L')^{\Gamma}\,\omega_{\perp} \geq 0$, where $\omega_{\perp} = (\mathbb{1} - |\omega\rangle\langle\omega|)$.

(iii) $\langle\omega|\,L' = \langle 0|$, which corresponds to the trace-preserving property.

In this work, we restrict the analysis to time-independent Lindbladian generators, thus their corresponding quantum channel at time t is given by $T(t) = \mathrm{e}^{L't}$. We will call *quantum embeddable* any map whose matrix logarithm admits at least one complex branch satisfying these properties.

Interpreting the above conditions, we observe that they impose a rigid structure on the operator in matrix form, since they involve both eigenvalues and eigenvectors. In particular, from the hermiticity-preserving condition we note that, if λ is an eigenvalue of L' and $|v\rangle$ the corresponding eigenvector, then it follows that:

$$L'\left|v^{\dagger}\right\rangle = (L'\,|v\rangle)^{\dagger} = (\lambda\,|v\rangle)^{\dagger} = \lambda^{*}\left|v^{\dagger}\right\rangle. \tag{5.15}$$

Thus λ^{*} and $\left|v^{\dagger}\right\rangle = \mathbb{F}\,|v^{*}\rangle$ are an eigenvalue and the corresponding eigenvector of L' too.

This implies an important property of Lindbladians in their elementary basis representation L': complex eigenvalues must necessarily come in complex-conjugate pairs λ, λ^{*} and have the same multiplicity. Moreover, the eigenspace of λ must admit a set of basis vectors whose hermitian conjugates span the eigenspace of λ^{*}. If λ is real, then it must necessarily admit a set of vectors spanning its eigenspace which either come in hermitian-related pairs or are self-adjoint. For a Markovian channel $T = e^{L'}$ the conditions for eigenvalues that are either complex or positive and for the vectors spanning their subspaces follow exactly the same rules. On the other hand, negative eigenvalues of T must have even multiplicity (implying that no non-degenerate negative eigenvalue can occur); the eigenspace of a negative eigenvalue must admit a basis of hermitian-related pairs of vectors. This particular structure for Markovian maps and their Lindbladian generators will be exploited in subsection 5.4.2 to reconstruct the eigenspace of an originally degenerate eigenvalue from a set of perturbed eigenvectors.

Conditions (i), (ii) and (iii) will run throughout our analysis, and we will implement them in the algorithms in Section 5.5 as constraints of a convex optimisation problem.

We will also sometimes need to express these conditions in the Choi representation. By expanding condition (iii) as

$$\langle\omega| L' = \frac{1}{\sqrt{d}} \sum_j \langle j,j| \sum_{\substack{a,b\\c,r}} L'^{\,a,b}_{\,c,r} |a,b\rangle\langle c,r| = \frac{1}{\sqrt{d}} \sum_{j,c,r} L'^{\,j,j}_{\,c,r} \langle c,r| \tag{5.16}$$

$$= \frac{1}{\sqrt{d}} \sum_{j,c,r} \left((L')^\Gamma\right)^{j,c}_{\,j,r} \langle c,r| = \langle 0|, \tag{5.17}$$

we can re-formulate it as

$$\mathrm{Tr}_1\left[(L')^\Gamma\right] = \sum_{j,c,r} \left((L')^\Gamma\right)^{j,c}_{\,j,r} |c\rangle\langle r| = 0_{d,d}. \tag{5.18}$$

This is equivalent to $\left\| \mathrm{Tr}_1\left[(L')^\Gamma\right] \right\| = 0$ in any matrix norm.

A measure of non-Markovianity for hermiticity- and trace-preserving ND^2 quantum channels M was introduced in [63] in terms of white noise addition. More precisely, given a set of Choi-hermitian generators $\{L_{\vec{m}}\}_m$ of M with $\langle\omega| L_{\vec{m}} = \langle 0|$, we define

$$\mu_{\min}(M) \coloneqq \min_{\vec{m}} \min\left\{\mu : \omega_\perp (L_{\vec{m}})^\Gamma \omega_\perp + \frac{\mu}{d}\mathbb{1} \geq 0\right\} \tag{5.19}$$

as the *non-Markovianity parameter*. Then $\mu_{\min}$ is the smallest value μ such that $L' = L_{\vec{m}} - \mu\,\omega_\perp$ is a Lindbladian generator for some $L_{\vec{m}}$ and

$$\exp\Big((1-d^2)\mu_{\min}(M)\Big) \in [0,1] \tag{5.20}$$

is a measure of Markovianity for M.

5.4 Multi-dimensional eigenspaces

The analysis in [63] is based on the assumption that all eigenvalues are non-degenerate. Indeed, as pointed out there, the subset of ND^2 matrices is dense in the matrix set with respect to the *Zariski topology*, whose closed sets are the roots of the resultant of the characteristic polynomial and its derivative. Note that the Zariski topology is weaker than the metric topology, and hence any Zariski dense set is also dense in the metric topology [95].

Working with an ND^2 matrix is needed in order to deal with a set of eigenvectors where each of them is unique (up to a scalar factor). This also ensures that the matrix logarithm is unique, up to complex branches. Conversely, if M is not an ND^2 matrix, there is then a continuous freedom in the choice of eigenbasis, and

thus uncountably infinitely many different matrix logarithms (not just the countable infinity of complex branches of the logarithm). This is due to the fact that, in case the matrix is diagonalizable but has an eigenvalue which is not simple, the corresponding degenerate eigenspace allows for infinite number of choices of basis vectors. In the more general case, when M is not diagonalizable, the Jordan canonical form again admits an uncountably infinite number of choices of generalized eigenvectors [96].

5.4.1 Perturbation of hermiticity-preserving matrices

In [11] it is shown that it is always possible, given a defective or derogatory Choi-hermitian matrix, to produce an arbitrarily close ND^2 matrix that preserves the hermiticity-preserving property. Formally:

Theorem 55 (ND^2 matrices are dense in the Choi-hermitian matrix set)**.** *Let M be an hermiticity-preserving matrix, either defective or derogatory (or both). Then for any ϵ there exists an hermiticity-preserving* ND^2 *matrix $\widetilde{M}$ such that $\|\widetilde{M} - M\| < \epsilon$.*

Proof. Interested readers are referred to [11, Theorem 5] for the proof. □

This result allows us to resolve the problem of the freedom of basis choice when given degenerate inputs, and reduce to a unique principle branch of the matrix logarithm. In reality tomographic data, eigenvalues will invariably be non-degenerate. However this case is included for completeness to demonstrate that the algorithm we develop in this work is fully general.

5.4.2 Reconstructing perturbed eigenspaces

The converse situation is when we are given an ND^2 matrix M which may come from the perturbation of a quantum embeddable operator having degenerate subspaces. For instance perturbations of many of the standard unitary gates in quantum computation, such as Pauli gates. This is a delicate situation since in the general case the hermiticity-preserving basis vectors structure characterising Lindblad operators, as discussed in Section 5.3, will be broken under perturbation (even when this is very small) due to the instability of the basis of multi-dimensional eigenspaces. Thus, when looking for the closest Lindbladian, the convex optimisation approach will possibly retrieve a Lindbladian whose matrix exponential is very distant from the original unperturbed operator M.

To illustrate this argument, consider the Pauli X-gate and restrict our attention to the hermiticity-preserving condition (noting that the closest hermiticity-preserving

matrix will always be closer than the closest Lindbladian since the latter imposes more constraints). The operator X has a two-fold degenerate eigenvalue 1 with eigenspace span$\{(1,1,1,1);\,(1,-1,-1,1)\}$ and another two-dimensional eigenspace span$\,\{(1,0,0,-1);(0,1,-1,0)\}$ with respect to eigenvalue -1. We denote these vectors by w_1, w_2, w_3, w_4, respectively; observe that all four vectors are self-adjoint. Write $E = \varepsilon\big(|w_1\rangle\langle w_1| - |w_2\rangle\langle w_2| + |w_3\rangle\langle w_3| - |w_4\rangle\langle w_4|\big)$. Then the ND^2 perturbed operator $X+E$ then has eigenvalues $1+\varepsilon, 1-\varepsilon, -1+\varepsilon, -1-\varepsilon$ with respect to the eigenbasis $\{w_1, w_2, w_3, w_4\}$, and its logarithm $\log(X+E)$ has eigenvalues $\varepsilon, -\varepsilon, \mathrm{i}\pi - \varepsilon, \mathrm{i}\pi + \varepsilon$ (up to first order in ε) with respect to the same eigenbasis. At this point, if we look for the closest hermiticity-preserving operator, since all eigenvectors are self-adjoint we obtain a matrix having again the same eigenbasis and keeping the real part of the eigenvalues of $\log(X+E)$, i.e., $\varepsilon, -\varepsilon, -\varepsilon, \varepsilon$. Clearly, the exponential of this matrix is close to the identity map and not the expected Pauli X-gate, even for very small ε. The same will apply for any complex branch of $\log(X+E)$ where we can add $2\pi\mathrm{i} \bmod k$ to any eigenvalue of $\log(X+E)$.

If we instead consider a perturbation of the same magnitude but along hermitian-related vectors of the eigenspace of -1, say, $E = \varepsilon\big(|w_1\rangle\langle w_1| - |w_2\rangle\langle w_2| + |w_5\rangle\langle w_5| - |w_6\rangle\langle w_6|\big)$ with $w_5 = w_3 + w_4 = (1,1,-1,-1)$ and $w_6 = w_3 - w_4 = (1,-1,1,-1)$ so that $w_5^\dagger = w_6$, then $\log(X+E)$ has again eigenvalues $1+\varepsilon, 1-\varepsilon, -1+\varepsilon, -1-\varepsilon$ but this time with respect to eigenbasis $\{w_1, w_2, w_5, w_6\}$. In this case, the complex branch $\log(X+E) - 2\pi\mathrm{i}\,|w_6\rangle\langle w_6|$ has eigenvalues $\varepsilon, -\varepsilon, \mathrm{i}\pi - \varepsilon, -\mathrm{i}\pi + \varepsilon$ and its closest hermiticity-preserving map has eigenvalues $\varepsilon, -\varepsilon, \mathrm{i}\pi, -\mathrm{i}\pi$. As expected, taking the exponential of this matrix will give a map very close to X. This example highlights both the importance of reconstructing a pair of hermitian-related eigenvectors for the eigenvalue -1 as well as searching over complex branches of the matrix logarithm.

Our strategy to overcome this complication is to reconstruct a compatible hermiticity-preserving structure for the invariant subspaces of those eigenvalues of M that are close to each others and that presumably stem from a perturbation of a unique degenerate eigenvalue. Hence we will look for a new basis of eigenvectors that we will interchange with the actual eigenbasis, creating a new operator R on which to run the convex optimisation problem to retrieve the closest Lindbladian to $\log R$.

We first discuss the single-qubit case and then generalise the approach for multi-qubit quantum channels.

5.4.2.1 One-qubit case

For single-qubit channels we have the following possiblilities: (a) one pair of close eigenvalues, (b) three close eigenvalues, (c) two different pairs, or (d) all four eigenvalues are close.

Consider case (a) with a pair of eigenvalues that is close to the real negative axis and where w_1 and w_2 are the corresponding eigenvectors. Assume that they come from a real negative 2-fold degenerate eigenvalue. We seek a new pair of hermitian-related eigenvectors $\{v, v^\dagger\}$ such that $\text{span}\{v, v^\dagger\} = \text{span}\{w_1, w_2\}$.
Thus we want to find coefficients α, β, μ, ν such that $|v\rangle = \alpha |w_1\rangle + \beta |w_2\rangle$ and $\left|v^\dagger\right\rangle = \alpha^* \left|w_1^\dagger\right\rangle + \beta^* \left|w_2^\dagger\right\rangle = \mu |w_1\rangle + \nu |w_2\rangle$. The solution will parametrise a set of compatible hermitian-related eigenvectors that we will interchange with the vectors w_1 and w_2.

If the two close eigenvalues are near the positive real axis, then if we assume they come from a real eigenvalue we have an additional option: a pair of two self-adjoint eigenvectors $\{v_1, v_2\}$ spanning the eigenspace of w_1 and w_2. In other words, we look for coefficients α, β, μ, ν such that $|v_1\rangle = \alpha |w_1\rangle + \beta |w_2\rangle$ and $|v_2\rangle = \mu |w_1\rangle + \nu |w_2\rangle$ with $|v_1\rangle = \left|v_1^\dagger\right\rangle$ and $|v_2\rangle = \left|v_2^\dagger\right\rangle$. Again, we should implement any possible solution $\{v_1, v_2\}$ as a new basis of eigenvectors related to the pair of eigenvalues.

The third option for case (a) is a pair of complex eigenvalues not close to the real axis. If this was originally a unique, two-fold degenerate complex eigenvalue λ, the hermiticity-preserving condition implies a second two-dimensional eigenspace with respect to eigenvalue λ^*; this will then be case (c).

Now consider case (b), where three eigenvalues of M are all close. In order to represent the perturbation of a quantum embeddable channel, they cannot originate from a 3-fold degenerate complex eigenvalue, since it is not possible to pair three eigenvalues each with a complex partner in a 4-dimensional space. They cannot originate from a real negative eigenvalue either, since the same argument will apply for the logarithm of M, which must also be hermiticity-preserving. M may instead be compatible with a Markovian dynamics if the eigenvalues are close to the real positive axis. Denoting by w_1, w_2 and w_3 the corresponding eigenvectors, we want to substitute them with a set $\{v, v^\dagger, z\}$ with $z = z^\dagger$ and $\text{span}\{v, v^\dagger, z\} = \text{span}\{w_1, w_2, w_3\}$ reconstructing an original unperturbed 3-dimensional eigenspace. Alternatively, we should find a new eigenbasis of three self-adjoint vectors.

In case (c) we say that we have two pairs of different eigenvalues. As we discussed in case (a), if one of this pair stems from a 2-fold degenerate and complex eigenvalue λ, then by the hermiticity-preserving condition the other pair should be close to λ^*. We should thus find a basis v_1, v_2 for the eigenspace of λ and v_3, v_4 for the eigenspace of λ^* such that $v_3 = v_1^\dagger$ and $v_4 = v_2^\dagger$.

Now consider pairs close to the real axis. If both can be associated with a real negative eigenvalue, then the basis of each 2-dimensional subspace corresponding to one pair of eigenvalues should be chosen to be hermitian-related vectors as in case (a). If one pair is close to a real positive number and the other to a negative one, than the eigenspace of the positive eigenvalue can be spanned either by an hermitian-related pair of eigenvectors or two self-adjoint vectors. The last option in case (c) is that both pairs comes from two different 2-fold degenerate real positive eigenvalues. In this case, again each eigenspace can be spanned by a pair of hermitian-related vectors or two self-adjoint vectors.

If all four eigenvalues are close and we presume that they come from a single 4-dimensional eigenspace, then M must necessarily be the (perturbed) identity channel up to a real scalar factor. We check if this is close enough according to the error tolerance parameter.

In Table 5.1 we summarize the above described scenarios for the unperturbed operator.

5.4.2.2 Multi-qubit case

Assume that the multi-qubit channel has a cluster of n eigenvalues that are close to each others, presumably stemming from an n-dimensional eigenspace with respect to an eigenvalue λ. We denote this subspace of M by $\mathcal{S}_\lambda$ and we distinguish three possible cases.

If λ is complex, then as previously discussed the hermiticity-preserving condition implies the existence of a second n-dimensional subspace with respect to the eigenvalue λ^*, $\mathcal{S}_{\lambda^*}$. This remark already tells us that $n \leq d^2/2$; indeed, for the single-qubit case we have ruled out the possibility of a 3-dimensional eigenspace for a complex eigenvalue. If we do not identify a second cluster of n eigenvalues that are close to λ^*, then the channel M is not quantum embeddable. Otherwise, we look for a basis $\{v_1, \ldots, v_n\}$ of $\mathcal{S}_\lambda$ such that $\{v_1^\dagger, \ldots, v_n^\dagger\}$ is a basis for $\mathcal{S}_{\lambda^*}$. Given the eigenvectors $\{w_1, \ldots, w_n\}$ of the cluster of eigenvalues of M related to the perturbed eigenvalues originated from λ, and $\{z_1, \ldots, z_n\}$ related to λ^*, we hence seek n vectors of the form $|v\rangle \coloneqq \alpha_1 |w_1\rangle + \cdots + \alpha_n |w_n\rangle$ such that $v^\dagger \in \mathrm{span}\{z_1, \ldots, z_n\}$. The set of

one single 2-dim degeneracy	(i) positive eigenvalue with either h.r. or s.a. basis vectors	(ii) negative eigenvalue with h.r. basis vectors
one single 3-dim degeneracy	positive eigenvalue with either 1 h.r. and 1 s.a. basis vectors, or 3 s.a. basis vectors	
two distinct 2-dim degeneracies	(i) two positive eigenvalues each with 1 h.r. pair or 2 s.a. basis vectors	(ii) two negative eigenvalues each with h.r. basis eigenvectors
	(iii) a positive eigenvalue with either h.r. or s.a. basis vectors and a negative eigenvalue with h.r. basis vectors	(iv) a pair of complex conjugate eigenvalues λ and λ^* with two h.r. partner vectors in the partner subspaces
one single 4-dim degeneracy	a single 4-degenerate real eigenvalue (identity channel)	

Table 5.1: Structure of a multi-dimensional eigenspace for an hermiticity-preserving operator on one qubit. Here we abbreviate "hermitian related" by h.r. and "self-adjoint" by s.a.

n independent vectors satisfying the condition will be chosen as a new eigenbasis of $\mathcal{S}_\lambda$ and their hermitian counterparts as the eigenbasis of $\mathcal{S}_{\lambda^*}$. The algorithm to retrieve the closest Lindbladian should then run ideally over all feasible solutions of this eigenbasis problem, although in practice this won't be possible since this constitute an infinite set.

If λ is negative, we recall that in this case the relevant constraint is that $\log M$ is Choi-hermitian. The related perturbed subspace of M then needs $n/2$ vectors $v_1, \dots v_n$ such that $\{v_1, v_1^\dagger, \dots, v_{n/2}, v_{n/2}^\dagger\}$ is a basis of $\mathcal{S}_\lambda$. This implies that n must necessarily be even, and indeed in the discussion of the one-qubit case we ruled out the possibility of having 3 eigenvalues stemming from a degenerate negative eigenvalue. Thus, again denoting by $\{w_1, \dots, w_n\}$ the eigenvectors of the perturbed eigenvalues of λ, we seek $n/2$ vectors $|v\rangle \coloneqq \alpha_1 |w_1\rangle + \cdots + \alpha_n |w_n\rangle$ such that $v^\dagger \in \mathcal{S}_\lambda$. The set of vectors given by the $n/2$ pairs $\{v, v^\dagger\}$ will be chosen as the new eigenbasis.

Type of eigenvalue	**constraint on other eigenspaces**	**constraint on dimension n**	**allowed basis vectors**
complex	existence of partner subspace with same dimension	$n \leq d^2/2$	each basis vector has an h.r. vector in partner eigenspace
negative	none	n even	$n/2$ pairs of h.r. basis vectors
positive	none	none	p pairs of h.r. basis vectors and $n-2p$ s.a. basis vectors

Table 5.2: Structure of an n-dim eigenspace of a multi-qubit hermiticity-preserving operator. Here we abbreviate "hermitian related" by h.r. and "self-adjoint" by s.a.

Again, the algorithm for the Lindbladian should run for all feasible sets of hermitian related eigenbasis for the subspace $\mathcal{S}_\lambda$.

The remaining option is a real, positive unperturbed eigenvalue λ generating a cluster of n perturbed eigenvalues of M. Here we have an additional freedom due to the possibility of admitting self-adjoint eigenvectors. More precisely, for each $p = 0, 1, \ldots, n/2$, we seek an eigenbasis of p pairs of hermitian-related vectors and $n-2p$ self-adjoint vectors. Again, in principle all sets of vectors with this structure should be used for the algorithms, for all values of p.

This analysis constitutes the theoretical ground for the pre-processing algorithms given in subsection 5.5.1. We schematically illustrate the argument in Table 5.2.

5.4.2.3 Approximate hermiticity-preserving eigenspace structure

When perturbations "mix" eigenspaces in a way such that it is no longer possible to obtain an exact choice of vectors according to the prescription given above, we should search for vectors that are close to satisfying those conditions. The motivation for this comes from [11, Theorem 9] , which shows that the hermiticity-preserving structure is a stable property with respect to perturbations. The theorem is technical, involving background on matrix perturbation theory which hasn't been covered in this thesis. So we refer interested readers to [11] for a full discussion. It should be noted -

for all the numerical simulations in this chapter we found that the exact prescription in the previous section was sufficient to find a hermiticity-preserving structure when dealing with channels that were perturbations of degenerate inputs.

5.5 Algorithms for retrieval of best-fit Lindbladian and computing non-Markovianity measure $\mu_{\min}$

In this section we present convex optimisation based algorithms to verify whether, given a channel M, there exists a Markovian channel in the ε-neighborhood (ε can be understood as the error-tolerance parameter which captures the error in the tomographic data as well as our maximal tolerance in the amount of approximation error). Alternatively, when such a channel does not exist, we look for the generator of an hermiticity- and trace-preserving channel in the δ-ball of $\log M$ (induced again by the ε-ball of M) with the smallest non-Markovianity parameter μ [63].

Since the M we are interested in arise as tomographic data, and ND^2 matrices form a dense set in the set of matrices, we assume that the input for the algorithms is ND^2. However, following the argument of subsection 5.4.1 it is straightforward to include the possibility of inputs which are not ND^2. This would just require an additional step to check the input, and if it was not ND^2 perturb it to a matrix that is.

Our main algorithm, which provides a recipe for evaluating non-Markovianity, is given in Algorithm 1. It takes as input an estimate of the channel, M, a precision parameter, p, an accuracy parameter ε, and an integer, r, which determines how many random basis choices will be tested in the case of degenerate eigenvalues.

The first step in the algorithm is to determine whether the input matrix has eigenvalues that may originate from a perturbation of degenerate eigenspaces. If the matrix has no such eigenvalues, we run the convex optimisation algorithm directly on the input. Conversely, if the matrix has eigenvalues that may originate from perturbed degenerate eigenspaces, before running the convex optimisation we need to produce a matrix with perturbed degenerate eigenspaces having a suitable hermiticity-preserving structure, as discussed in subsection 5.4.2. The task is performed by Algorithm 2, Algorithm 3 and Algorithm 4, outlined in subsection 5.5.1.

Once these matrices have been constructed we run the convex optimisation **??** on them to determine whether or not there exists a memoryless channel in the ε-neighbourhood of M. If a Markovian map, T, exists within the ε-ball, the algorithm returns the

Lindbladian L' satisfying $T = e^{L'}$. If no Markovian channel is retrieved, the main algorithm calls Algorithm 6 which calculates the non-Markovianity parameter $\mu_{\min}$ (cfr. subsection 5.5.2 for the full description of these two core algorithms).

Finally, in subsection 5.5.3 we present a version of the algorithm extended for the case of a sequence of snapshots from a given quantum process. We look for a Lindbladian whose generated evolution passes ε-close to each snapshot at the appropriate time.

5.5.1 Pre-processing algorithms

The first task in the pre-processing algorithm is to detect sets of eigenvalues which are close together (with closeness parameterised by a precision p, given as input). These are likely to arise from perturbations of degenerate eigenvalues. If the algorithm identifies that all the eigenvalues are real, positive and belong to the same set, then it outputs that the channel is consistent with the identity map.

In all other cases the next step of pre-processing is to construct bases for the degenerate eigenspaces which have a compatible hermiticity-preserving structure, following the analysis in subsection 5.4.2. The algorithm to prepare the basis for an eigenvalue which is either complex or negative real is Algorithm 2. It takes as input the transfer matrix of the channel, M, and two sets of integers. The first set, degenerate_set, contains the indices of the eigenvectors corresponding to the degenerate eigenvalue itself. The second set, conj_degenerate_set, contains the indices of the eigenvectors corresponding to the conjugate eigenvalue.[4]

The idea behind Algorithm 2 is that, for each set of eigenvectors w_1, w_2,...,w_n associated with a degenerate eigenvalue λ and eigenvectors u_1, u_2,...,u_n associated with λ^* we solve the equation

$$\alpha_1{}^* \left|w_1^\dagger\right\rangle + \alpha_2{}^* \left|w_2^\dagger\right\rangle + \cdots + \alpha_n^* \left|w_n^\dagger\right\rangle - \beta_1 \left|u_1\right\rangle - \beta_2 \left|u_2\right\rangle - \cdots - \beta_n \left|u_n\right\rangle = |0\rangle \qquad (5.21)$$

for $\{\alpha_j\}_j$ and $\{\beta_j\}_j$, allowing us to construct a basis with the correct hermiticity preserving structure.

[4]Clearly we require |degenerate_set| = |conj_degenerate_set|. Furthermore in the case of a negative real degenerate eigenvalue we have degenerate_set = conj_degenerate_set.

Algorithm 1: Main algorithm, including pre-processing – Part I

Input : ND^2 matrix M, integer random_samples, positive real numbers p, ε

Result: Lindbladian, L', consistent with M (within error tolerance ε), or if no such L' exists, non-Markovianity parameter μ

$\lambda \leftarrow$ eigenvalues(M)

checklist_positive $\leftarrow$
$\left[(\lambda_i - \lambda_j < p) \cap (\mathrm{Im}(v_i) < p) \cap (\mathrm{Re}(\lambda_i > 0)) \mid i, j \in (0, \dim M), i > j\right]$
checklist_negative $\leftarrow$
$\left[(\lambda_i - \lambda_j < p) \cap (\mathrm{Im}(\lambda_i) < p) \cap (\mathrm{Re}(\lambda_i < 0)) \mid i, j \in (0, \dim M), i > j\right]$
checklist_complex $\leftarrow \left[(\lambda_i - \lambda_j < p) \cap (\mathrm{Im}(\lambda_i) > p) \mid i, j \in (0, \dim M), i > j\right]$
checklist $\leftarrow$ [checklist_positive, checklist_negative, checklist_complex]

if sum(checklist) = 0 **then**
    $L' \leftarrow$ Run **??** on M, M, ε
    if $\|M - \exp(L')\| < \varepsilon$ **then**
    Output L'
    :
    else
        $H, \mu \leftarrow$ Run Algorithm 6 on input M, R, ε
        Output μ
        :
    end
else if sum(checklist_positive) = $\binom{\dim M}{2}$ **then**
    Output The channel is consistent with the identity map
    :
else
    positive_degenerate_sets $\leftarrow$ list of sets of mutually deg. real positive eigenvalues
    negative_degenerate_sets $\leftarrow$ list of sets of mutually deg. real negative eigenvalues
    complex_degenerate_sets $\leftarrow$ list of sets of mutually deg. complex eigenvalues
    conjugate_pairs $\leftarrow$ 2d array indicating pairs of deg. complex sets are conjugate
    positive_bases $\leftarrow$ [], negative_bases $\leftarrow$ [], complex_bases $\leftarrow$ []
    for $i \in$ (0, length(positive_degenerate_sets)) **do**
        $basis \leftarrow$ Run Algorithm 3 on inputs M, positive_degenerate_sets$[i]$, p
        positive_bases.append($basis$)
    end
    (continuing in Part II) ...
end

Algorithm 1 – Part II:

Input : ND^2 matrix M, integer random_samples, positive real numbers p, ε
Result: Lindbladian, L', which is consistent with M (within error tolerance ε), or if no such L' exists, non-Markovianity parameter μ

else
    ... (continuing from Part I)
    for $i \in (0, \text{length(positive\_degenerate\_sets)})$ **do**
        $basis \leftarrow$ Run Algorithm 2 on inputs M, negative_degenerate_sets$[i]$, negative_degenerate_sets$[i]$
        negative_bases.append($basis$)
    end
    for $i \in (0, \text{length(conjugate\_pairs)})$ **do**
        $basis \leftarrow$ Run Algorithm 2 on inputs M, conjugate_pairs$[i, 0]$, conjugate_pairs$[i, 1]$
        complex_bases.append($basis$)
    end
    conj_test $\leftarrow$ list of boolean values indicating if i^{th} eigvect needs to be conjugated
    for $r \in (0, \text{random\_samples})$ **do**
        $S \leftarrow$ Run Algorithm 4 on inputs M, positive_degenerate_sets, negative_degenerate_sets, complex_degenerate_sets, positive_bases, negative_bases, complex_bases, conj_test
        $R_r \leftarrow SMS^{-1}$
        $L_r \leftarrow$ Run **??** on M, R_r, ε
    end
    if $\min(\|\exp(L_r) - M\|) < \varepsilon$ **then**
    $L_{\min} \leftarrow L_r$ that minimises $\|\exp(L_r) - M\|$
    Output $L_{\min}$
    :
    else
        for $r \in (0, \text{random\_samples})$ **do**
            $H_r, \mu_r \leftarrow$ Run Algorithm 6 on input M, R_r, ε
        end
        $\mu_{\min} \leftarrow \min(\mu_r)$
        Output $\mu_{\min}$
        :
    end
end

We solve eq. (5.21) by arranging the vectors into the columns of a matrix

$$A = ({w_1}^\dagger, {w_2}^\dagger, \cdots, {w_n}^\dagger, u_1, u_2, \cdots u_n) \tag{5.22}$$

and finding its kernel. If the variable $\text{Nullity}(A) \coloneqq \dim(\ker(A))$ is equal to the dimension of the degenerate eigenspace then there is a hermiticity-preserving basis which spans the eigenspace (in fact there are uncountably infinitely many choices of hermiticy-preserving bases). The algorithm returns the basis vectors

$$|v_i\rangle = \sum_j \alpha_j^{(i)} \left|w_j\right\rangle \tag{5.23}$$

for $i \in (0, \text{Nullity}(A))$, where $\alpha_j^{(i)}$ is the value of α_j in the i^{th} solution to eq. (5.21).

The pseudo-code for the case of degenerate, positive real eigenvalues is given by Algorithm 3. It follows a similar idea to Algorithm 2, with some additional processing to account for the possibility of self-adjoint eigenvectors. The equation to solve in order to obtain a basis with the correct hermiticity-preserving structure is

$${\alpha_1}^* \left|w_1^\dagger\right\rangle + {\alpha_2}^* \left|w_2^\dagger\right\rangle + \cdots + \alpha_n^* \left|w_n^\dagger\right\rangle - \beta_1 \left|w_1\right\rangle - \beta_2 \left|w_2\right\rangle - \cdots - \beta_n \left|w_n\right\rangle = 0 \tag{5.24}$$

again for $\{\alpha_j\}_j$ and $\{\beta_j\}_j$. As in the previous case, if $\text{Nullity}(A)$ is equal to the dimension of the degenerate eigenspace then there is a hermiticity-preserving basis which spans the eigenspace given by

$$|v_i\rangle = \sum_j \alpha_j^{(i)} \left|w_j\right\rangle. \tag{5.25}$$

However, now the basis may include self-adjoint eigenvectors, as well as hermitian conjugate eigenvectors. These need to be treated separately in the next stage of the pre-processing.

To verify if the i^{th} basis-vector is self-adjoint we check whether $\alpha_j^{(i)} - \beta_j^{(i)} < p$, for all j. If the total number of non-self-adjoint basis vectors is even, the algorithm returns two sets of basis vectors – the self-adjoint set and the non-self-adjoint set. If the total number of non-self-adjoint basis vectors is odd, the algorithm finds the non-self-adjoint basis vector for which $\sum_j \alpha_j^{(i)} - \beta_j^{(i)}$ is minimised, and returns this with the set of self-adjoint basis vectors instead of the non-self-adjoint set.

Note that there is an infinite number of possible basis choices which respect the hermiticity-preserving structure, and which basis is chosen will affect the distance to the closest Lindbladian. To handle this, we use a randomised construction to generate r bases satisfying the hermiticity-preserving property, and we run the convex optimisation algorithm on each one, keeping the optimal result. The number of random bases, r, is an input to Algorithm 1. Running the algorithm with higher r will give a better result (numerical results on degenerate 1- and 2-qubit channels are given in Section 5.6).

The algorithm to prepare a random basis is given in Algorithm 4. It takes as input M, lists indicating the indices of eigenvectors associated to each degenerate eigenvalue $\{sl_\lambda \mid \text{for degenerate } \lambda\}$, and the bases constructed by Algorithm 2 and Algorithm 3. It returns a random choice of basis, S. In order to build S, Algorithm 4 checks whether i is in any of the sl_λ for each $i \in \dim(M)$. If it isn't, we set the i^{th} column of S equal to the i^{th} eigenvector of M. If it is we check whether the i^{th} column needs to be constructed randomly from either self-adjoint basis vectors or non-self-adjoint basis vectors; or whether it needs to be obtained by conjugating another column.

For λ real, which columns are produced randomly (from self-adjoint or non-self-adjoint basis vecors) and which are found via conjugation is arbitrary. For λ complex, either all columns associated to λ are constructed randomly, or all are retrieved by conjugating the basis vectors associated to λ^*. This is determined by which order sl_λ and sl_{λ^*} are given as input to Algorithm 2. If the column needs to be prepared randomly then we generate $|sl_\lambda|$ random seeds κ_j. The i^{th} column of S is then

$$S[:,i] = \sum_j \kappa_j v_j, \tag{5.26}$$

where v_j are the hermiticity-structure preserving basis vectors associated with λ, and the sum is over either all self-adjoint or all non-self-adjoint basis vectors. If the column needs to be obtained by conjugation we find which column it is conjugate to, denoted k, and the i^{th} column of S is then given by

$$S[:,i] = \mathbb{F}S[:,k]^*. \tag{5.27}$$

The final step of preprocessing is to compute $R = SMS^{-1}$ for each random basis. We then run the convex optimisation algorithms (see subsection 5.5.2) on each R, and output the optimal result.

Algorithm 2: Construct conjugate basis for cluster of a complex or real negative eigenvalue

Input : Matrix M, Array of integers degenerate_set, Array of integers conj_degenerate_set
Result: Matrix new_basis
eigvecs $\leftarrow$ eigenvectors(M)
degeneracy_counter $\leftarrow$ length(degenerate_set)
for $i \in (0, \text{degeneracy\_counter})$ **do**
    $j \leftarrow$ degenerate_set[i]
    $k \leftarrow$ conj_degenerate_set[i]
    $|w_i\rangle \leftarrow$ eigvecs[j]
    $|u_i\rangle \leftarrow$ eigvecs[k]
end
$A_1 \leftarrow [\mathbb{F}\left|w_i^*\right\rangle \mid i \in (0, \text{degeneracy\_counter})]$
$A_2 \leftarrow [-|u_i\rangle \mid i \in (0, \text{degeneracy\_counter})]$
$A = (A_1, A_2)^T$ (Kernel of A is solution to
$\alpha_1^*\mathbb{F}\left|w_1^*\right\rangle + \alpha_2^*\mathbb{F}\left|w_2^*\right\rangle + \cdots + \alpha_n^*\mathbb{F}\left|w_n^*\right\rangle - \beta_1|u_1\rangle - \beta_2|u_2\rangle - \cdots - \beta_n|u_n\rangle = |0\rangle$)
nullity = dim (ker(A))
if nullity == degeneracy_counter **then**
    for $i \in (0, \text{degeneracy\_counter})$ **do**
        values_to_sum = $[w_j * \ker(A)^*_{i,j} \mid j \in (0, \text{degeneracy\_counter})]$
        new_basis[:, i] = $\sum_j$(values_to_sum)
    end
    Output True, new_basis
    :
else
    Output False, []
    :
end

Algorithm 3: Construct self-adjoint / conjugate basis for cluster of a real positive eigenvalue

Input : Matrix M, Array of integers degenerate_set, Real number p
Result: Matrices [self_adjoint_basis, conjugate_basis]
eigvecs $\leftarrow$ eigenvectors(M)
degeneracy_counter $\leftarrow$ length(degenerate_set)
for $i \in (0, \text{degeneracy\_counter})$ **do**
    $j \leftarrow$ degenerate_set[i]
    $|w_i\rangle \leftarrow$ eigvecs[j]
end
$A_1 \leftarrow [\mathbb{F}\left|w_i^*\right\rangle \mid i \in (0, \text{degeneracy\_counter})]$
$A_2 \leftarrow [-|w_i\rangle \mid i \in (0, \text{degeneracy\_counter})]$
$A = (A_1, A_2)^T$ (Kernel of A is solution to
$\alpha_1^*\mathbb{F}\left|w_1^*\right\rangle + \alpha_2^*\mathbb{F}\left|w_2^*\right\rangle + \cdots + \alpha_n^*\mathbb{F}\left|w_n^*\right\rangle - \beta_1|w_1\rangle - \beta_2|w_2\rangle - \cdots - \beta_n|w_n\rangle = 0$)
nullity = dim (ker(A))
if nullity == degeneracy_counter **then**
    check_self_adjoint $\leftarrow$
     [True if i^{th} column of ker(A) is self − adjoint within precision $p \mid i \in$
     $(0, \text{degeneracy\_counter})$]
    number_self_adjoint $\leftarrow \sum_i$(check_self_adjoint)
    number_conjugate $\leftarrow$ degeneracy_counter − number_self_adjoint
    if number_conjugate $\mod 2 \neq 0$ **then**
        extra_self_adjoint $\leftarrow$ index of extra dimension which is closest to self adjoint
        check_self_adjoint[extra_self_adjoint] $\leftarrow$ True
        number_self_adjoint = number_self_adjoint + 1
        number_conjugate = number_conjugate − 1
    end
    $k = 0$
    $l = 0$
    for $i \in (0, \text{degeneracy\_counter})$ **do**
        values_to_sum = $[\left|w_j\right\rangle * \ker(A)^*_{i,j} \mid j \in (0, \text{degeneracy\_counter})]$
        if check_self_adjoint[i] **then**
            self_adjoint_basis[:, k] = $\sum_j$(values_to_sum)
            $k = k + 1$
        else
            conjugate_basis[:, l] = $\sum_j$(values_to_sum)
            $l = l + 1$
        end
    end
    Output True, [self_adjoint_basis, conjugate_basis]
    :
else
    Output False, []
    :
end

Algorithm 4: Construct conjugate random choice of basis for quantum channel with cluster(s) of eigenvalues

Input : Matrix M, Three lists of lists positive_degenerate_sets, negative_degenerate_sets, complex_degenerate_sets, Three sets of bases positive_bases, negative_bases, complex_bases, List of boolean values conj_test

Result: Matrix new_basis

```
eigvecs ← eigenvectors(M)
all_degenerate_sets ← [sl | sl ∈
  positive_degenerate_sets ∪ negative_degenerate_sets ∪ complex_degenerate_sets)
for sl ∈ all_degenerate_sets do
    sl.sort()
end
for i ∈ dim(M) do
    if i ∉ sl∀sl ∈ all_degenerate_sets then
        new_basis[:, i] = eigvecs[:, i]
    else
        if i ∈ sl for sl ∈ positive_degenerate_sets then
            sets = positive_degenerate_sets
            bases = positive_bases
        else if i ∈ sl for sl ∈ negative_degenerate_sets then
            sets = negative_degenerate_sets
            bases = negative_bases
        else
            sets = complex_degenerate_sets
            bases = complex_bases
        end
        j ← index of list i is in within list of lists "sets"
        k ← index of i within list j
        n ← length (list j)
        if conj_test[i] then
            random_seeds ← list of n random numbers
            tilde_basis ← ∑ (random_seeds[k] ∗ bases[j][:, k])
            new_basis[:, i] ← tilde_basis/norm (tilde_basis)
        else
            conjugate_value ← index which j is conjugate with
            new_basis[:, i] ← 𝔽(new_basis[:, conjugate_value])*
        end
    end
end
```

Output new_basis

:

5.5.2 Core algorithms

At this stage, we are given the tomographic snapshot M and an ND^2 matrix R from the pre-processing phase (clearly, if M is ND^2 and has no cluster of eigenvalues, then $R = M$).

Algorithm 5 looks for the closest Lindbladian to $\log R$ in the ε-neighborhood of M by formulating a convex optimisation task whose constraints are exactly the necessary and sufficient conditions for a Lindbladian generator, as discussed in Section 5.3. We iterate over different branches of the matrix logarithm and pick the resulting Lindbladian from the convex optimisation programme whose generated channel is the closest to M.

Algorithm 5: Retrieve best-fit Lindbladian

Input : matrix M, ND^2 Matrix R with $\dim R = \dim M$, positive real number ε, positive integer $m_{\max}$

Result: L' closest Lindbladian to $\vec{m}$-branch of $\log R$ such that $\|M - \exp L'\|_{\mathrm{F}} \leq \varepsilon$ is minimal over all $\vec{m} \in \{-m_{\max}, -m_{\max}+1, \ldots, 0, \ldots, m_{\max}-1, m_{\max}\}^{\times d^2}$

$d \leftarrow \sqrt{\dim M}$
$L_0 \leftarrow \log R$
$\xi \leftarrow \varepsilon$
$P_j \leftarrow |r_j\rangle\langle \ell_j|$ *(*$|r_j\rangle$ *and* $\langle \ell_j|$, $j = 1, \ldots, d^2$ *right and left eigenvectors of* M*)*
$|\omega\rangle \leftarrow \sum_{j=1}^{d} |j, j\rangle$, $\omega_\perp \leftarrow \mathbb{1} - |\omega\rangle\langle\omega|$

for $\vec{m} \in \{-m_{\max}, -m_{\max}+1, \ldots, 0, \ldots, m_{\max}-1, m_{\max}\}^{\times d^2}$ **do**
  $L_{\vec{m}} \leftarrow L_0 + 2\pi \mathrm{i} \sum_{j=1}^{d^2} m_j P_j$ *(branches of the matrix logarithm of* L_0*)*
  Run convex optimisation programme on variable X:
    minimise $\left\| X - L_{\vec{m}}^{\Gamma} \right\|_{\mathrm{F}}$
    subject to X hermitian
    $\omega_\perp X \omega_\perp \geq 0$
    $\|\mathrm{Tr}_1[X]\|_1 = 0$
  distance $\leftarrow \left\| M - \exp X^{\Gamma} \right\|_{\mathrm{F}}$
  if distance $< \xi$ **then**
    $\xi \leftarrow$ distance
    $L' \leftarrow X^{\Gamma}$
  end
end

if L' *is not* null **then**
  Output Lindbladian L'
  :
end

The first remark about the algorithm is that we are not searching for the closest Markovian channel, but for the closest Lindbladian to its matrix logarithm. A natural question is then whether the two objects are precisely related, that is, if the closest Lindbladian generates the closest Markovian channel. In the general case, this is not true. A simple counter-example is provided by the perturbed X-gate discussed in subsection 5.4.2, where the closest Lindbladian generates a map close to the identity, although the unperturbed X-gate is a closer Markovian channel. However, consider the upper bound for general matrices A and B (Lemma 11 in [64])

$$\|\exp A - \exp B\| \leq \|A - B\| \exp \|A - B\| \exp \|A\|. \tag{5.28}$$

If we now ask B to be Lindbladian, then the closest Lindbladian L' to A is also the operator minimising this upper bound. This implies that the distance between the Markovian channel $\exp L'$ retrieved by our algorithm and the input matrix $M = \exp L_R$ is upper-bounded by

$$\varepsilon := \|C - L_R\| \exp \|C - L_R\| \exp \|L_R\|, \tag{5.29}$$

where we assume $\exp C$ to be the closest Markovian operator to M. Thus, by appropriately estimating ε and setting it as our tolerance parameter for the algorithms, we are guaranteed to find a compatible Markovian evolution for the input M.

Note that the convex optimisation problem contains a second-order cone constraint (when formulating the Frobenius norm minimisation in epigraph form), a linear matrix inequality (LMI) constraint to ensure the conditionally completely positive condition and a first-order cone constraint representing the trace preserving condition. As in any convex optimisation programme, every minimum will be a global minimum.

Moreover we have $\|A\|_{\mathrm{F}} = \|A^{\Gamma}\|_{\mathrm{F}}$ for A in the elementary basis representation. Thus, $\|L' - L\|_{\mathrm{F}} = \|(L' - L)^{\Gamma}\|_{\mathrm{F}} = \|X - L^{\Gamma}\|_{\mathrm{F}}$. This is useful in order to run the convex optimisation task on the variable X without involutions.

If no Lindbladian generator is found in ε-ball of M, Algorithm 6 will be called to find the channel in the ε-neighborhood with the smallest non-Markovianity parameter according to the definition in eq. (5.19). This can again be retrieved by formulating a convex optimisation programme.

Here the variable δ reflects the neighborhood around $L_{\vec{m}}$ that maps under the exponential into the ε-neighborhood of M; a lower bound is given by Lemma 11

Algorithm 6: Compute non-Markovianity measure $\mu_{\min}$

Input : matrix M, ND^2 Matrix R with $\dim R = \dim M$, positive real number ε, positive integer $m_{\max}$

Result: generator H' of the hermiticity- and trace-preserving channel in the ε-ball of M with the smallest non-Markovianity measure $\mu_{\min}$ over all $\vec{m} \in \{-m_{\max}, -m_{\max}+1, \ldots, 0, \ldots, m_{\max}-1, m_{\max}\}^{\times d^2}$.

$d \leftarrow \sqrt{\dim M}$

$L_0 \leftarrow \log R$

$P_j \leftarrow |r_j\rangle\langle \ell_j|$ *(*$|r_j\rangle$ *and* $\langle \ell_j|$, $j = 1, \ldots, d^2$ *right and left eigenvectors of* M*)*

$|\omega\rangle \leftarrow \sum_{j=1}^{d} |j, j\rangle$, $\omega_\perp \leftarrow \mathbb{1} - |\omega\rangle\langle\omega|$

$\mu_{\min} \in \mathbb{R}^+$ *(initialize it with an high value)*

δ satisfying $\varepsilon = \exp(\delta) \cdot \delta \cdot \|L_0\|_{\mathrm{F}}$, $\delta_{\max} = 10 \cdot \delta$, $\delta_{\mathrm{step}} \in \mathbb{R}^+$

for $\delta < \delta_{\max}$ **do**

  for $\vec{m} \in \{-m_{\max}, -m_{\max}+1, \ldots, 0, \ldots, m_{\max}-1, m_{\max}\}^{\times d^2}$ **do**

    $L_{\vec{m}} \leftarrow L_0 + 2\pi \mathrm{i} \sum_{j=1}^{d^2} m_j P_j$ *(branches of the matrix log* L_0*)*

    Run convex optimisation programme on variables μ and X:

$$\begin{aligned} &\text{minimise} && \mu \\ &\text{subject to} && X \text{ hermitian} \\ &&& \left\| X - L_{\vec{m}}^{\Gamma} \right\|_{\mathrm{F}} \leq \delta \\ &&& \omega_\perp X \omega_\perp + \mu \tfrac{\mathbb{1}}{d} \geq 0 \\ &&& \|\mathrm{Tr}_1[X]\|_1 = 0 \end{aligned}$$

    if $\left\| M - \exp X^{\Gamma} \right\|_{\mathrm{F}} < \varepsilon$ *and* $\mu < \mu_{\min}$ **then**

      $\mu_{\min} \leftarrow \mu$

      $H' \leftarrow X^{\Gamma}$

    end

  end

  $\delta \leftarrow \delta + \delta_{\mathrm{step}}$

end

if H' *is not* null **then**

  Output : hermiticity- and trace-preserving channel generator H', non-Markovianity parameter $\mu_{\min}$

end

in [64], that is, $\varepsilon \leq \exp(\delta) \cdot \delta \cdot \|L_0\|_{\mathrm{F}}$. An upper bound is again provided in Corollary 15 of [64]. However, the boundaries of this region around $L_{\vec{m}}$ related to the ε-ball are not precisely characterised. This can cause problems for the convex optimisation programme, which in some cases can retrieve a Lindbladian for δ in the interval defined by the above bounds whose generated map falls outside the ε-ball. We further discuss this matter with a relevant example in subsection 5.6.1.3 (cfr. also Fig. 5.5). To solve this issue in a practical way, we run over increasing δ values up to 10 times the value determined by the lower bound.

The loop in both algorithms runs a brute-force search over the $\vec{m}$-branches of the matrix logarithm. As previously explained, there are countably infinitely many such branches. However, Khachiyan and Porkolab [97] prove that setting $m_{\max} = \mathrm{O}(2^{2^{\mathrm{poly}(d)}})$ always suffices to find a solution if one exists. In fact, the same authors prove that there is a polynomial-time algorithm for integer semidefinite programming with any fixed number of variables, so for any fixed Hilbert space dimension in our setting, based on the ellipsoid method (which is more efficient that performing brute-force search up to the upper-bound). This polynomial-time algorithm is important theoretically, but not practical. In reality, integer programming solvers use branch-and-cut methods [98].

However, the increased implementation complexity of these more sophisticated techniques is unlikely to be justified here. Instead, we encode a simple, brute-force search over the branches of the logarithm, ordered by increasing $|\vec{m}|$. There are physical reasons why a naive, brute-force search is likely to work well here. Large values of m_j correspond to high-energy / frequency components of the noise. It is unlikely that very high energy underlying physical processes play a significant role, and it is also unlikely that our tomographic data will be sensitive enough to resolve very high-frequency components. Therefore, if there is a Lindblad generator consistent with the tomographic snapshot, it is most likely to occur at low values of $|\vec{m}|$. Numerical studies on synthesised examples of 1-qubit tomography (see Fig. 5.1) confirm that setting a small value of $m_{\max}$ suffices in practice; indeed, even $m_{\max} = 1$ sufficies in all cases we tested. This is also corroborated by the numerics that was carried out in [63].

It would be straightforward to replace the brute-force search by a call to an integer program solver if this ever proved necessary.

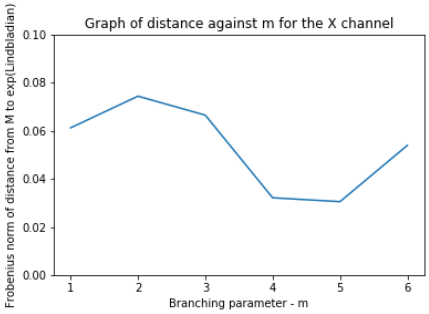

(a) Distance between tomographic results and the Markovian channel output by our algorithm for an X-gate, running Algorithm 1 for 10,000 random samples for each value of m.

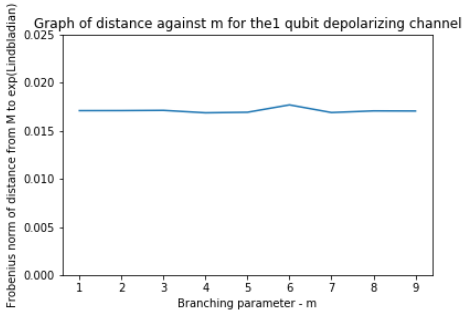

(b) Distance between tomographic results and the Markovian channel output by our algorithm for a depolarizing channel with $p = 0.3$. For each m-value, Algorithm 1 was run for 100 random samples.

Figure 5.1: Investigating how the optimal Lindbladian found by our algorithm varies with the number of branches of the logarithm searched over for the X-gate and depolarizing channel. There is some fluctuation in distance in the case of the X-gate - this is due to the randomised nature of the algorithm (see Section 5.6 for full results on the X-gate).

5.5.3 Multiple snapshots

The approach for single snapshot can be extended to multiple tomographic snapshots taken at a sequence of times. Augmenting the number of measurements is a way to make the conditions for a compatible Markovian evolution, or detection of non-Markovian effects, more stringent, since the requirement is that there exist a single time-independent Lindbladian that generates a dynamical trajectory that passes close to *every* snapshot.

Consider a sequence of tomographic snapshots $M_1, \ldots, M_q$ associated with measurement times $t_1, \ldots, t_q$. In Algorithm 7 we formulate a convex optimisation programme that finds the Lindbladian minimising the sum of the distances from the logarithms of the input matrices (for simplicity, we present the algorithm for the case of ND^2 matrices with no cluster of eigenvalues, and discuss the more general case later in this section). We iterate over different branches and pick the Lindbladian L' for which $\sum_c \|M_c - \exp t_c L'\|_{\mathrm{F}}$ is the smallest. We also require that the distance with respect to any logarithm is not larger than some value δ varying in the same manner as in the single-snapshot case. We certify the evolution as Markovian if the exponential of the retrieved logarithm is within the ε-ball of each input tomographic snapshot.

Once again, dealing with degeneracies requires more work. If the perturbation of an n-degenerate complex eigenvalue is identified, then we should check whether this is consistent with all other snapshots, that is, all measurements show a cluster

Algorithm 7: Retrieve best-fit Lindbladian for multiple snapshots

Input : $(d^2 \times d^2)$-dimensional matrices $M_1 \ldots, M_q$, positive real numbers $t_1, \ldots, t_q$, positive real number ε, positive integer $m_{\max}$

Result: L' Lindbladian minimising $\sum_{c=1}^{q} \|t_c\, L' - \log M_c\|_{\mathrm{F}}$ such that $\|M_c - \exp t_c\, L'\|_{\mathrm{F}} < \varepsilon$ for all c

for $c = 1, \ldots, q$ **do**
  $L_0^c \leftarrow \log M_c$
  $P_j^c \leftarrow |r_j\rangle\langle \ell_j|$ ($|r_j\rangle$ *and* $\langle \ell_j|$, $j = 1, \ldots, d^2$ *right and left eigvecs of* M_c)
end
$\xi \leftarrow q\,\varepsilon$
δ satisfying $\varepsilon = \exp(\delta) \cdot \delta \cdot \|L_0\|_{\mathrm{F}}, \quad \delta_{\max} = 10 \cdot \delta, \quad \delta_{\mathrm{step}} \in \mathbb{R}^+$
for $\delta < \delta_{\max}$ **do**
  for $\vec{m} \in \{-m_{\max}, -m_{\max}+1, \ldots, 0, \ldots, m_{\max}-1, m_{\max}\}^{\times d^2}$, **do**
    $L_{\vec{m}}^c \leftarrow L_0^c + 2\pi \mathrm{i} \sum_{j=1}^{d^2} m_j\, P_j^c$ (*branches of the matrix log of* L_0^c)
    Run convex optimisation programme on variable X:

$$\begin{aligned} &\text{minimise} && \textstyle\sum_c \left\| t_c\, X - (L_{\vec{m}}^c)^{\Gamma} \right\|_{\mathrm{F}} \\ &\text{subject to} && X \text{ hermitian} \\ & && \omega_\perp X \omega_\perp \geq 0 \\ & && \|\mathrm{Tr}_1[X]\|_1 = 0 \\ & && \left\| t_c\, X - (L_{\vec{m}}^c)^{\Gamma} \right\|_{\mathrm{F}} \leq \delta \text{ for } c = 1, \ldots, q \end{aligned}$$

    distance $\leftarrow \sum_c \left\| M_c - \exp t_c\, X^{\Gamma} \right\|_{\mathrm{F}}$
    if $\left\| M_c - \exp t_c\, X^{\Gamma} \right\|_{\mathrm{F}} < \varepsilon$ *for all* $c = 1, \ldots, q$ *and* distance $< \xi$ **then**
      $\xi \leftarrow$ distance
      $L' \leftarrow X^{\Gamma}$
    end
  end
end
if L' *is not* null **then**
  Output Lindbladian L'
  :
end

of n eigenvalues. Because of the hermiticity-preserving condition we also expect a partner cluster of n eigenvalues, corresponding to the complex-conjugate partner subspace. Note that the two clusters will overlap when they approach the negative axis, and conversely that any cluster close to the negative axis is expected to split in two partner clusters representing the perturbation of two eigenvalues related by complex conjugation: this means that when taking successive snapshots, we can avoid the case of perturbed negative eigenvalues by choosing suitable measurement times. Secondly, we should also verify if in all snapshots both the multi-dimensional

subspace of a cluster and its partner subspace are consistent with the same unperturbed pair of hermitian-related eigenspaces, up to some approximation. Indeed, recall that eigenspaces are stable with respect to perturbation. Moreover, since here we are checking for time-*independent* Markovianity from multiple snapshots, we are interested in the case where the Lindbladians for all snapshots are the same.

Given this, and the results of subsection 5.4.2.3, our approach to handling an n-degenerate complex eigenvalue λ is as follows. We select one of the snapshots, c', at random, and apply the pre-processing steps from Algorithm 1 to $M_{c'}$ in order to obtain a random hermitian-related basis of vectors for the λ and λ^* subspaces. Denote these by $\{v_j\}$ and $\{v_j^\dagger\}$ respectively, and denote the projections onto the subspace spanned by these vectors by Π_v and $\Pi_{v^\dagger}$. We then determine whether this choice of basis is compatible with the other snapshots, by checking that

$$\sum_c \left\| \Pi_c(\lambda) - \Pi_v \right\| + \sum_c \left\| \Pi_c(\lambda^\star) - \Pi_{v^\dagger} \right\| \leq \varsigma_1, \tag{5.30}$$

where ς_1 is a tolerance parameter for the perturbation of subspaces (which we set arbitrarily, but that one can derive rigorously using refs. [65] and [99]). A set of basis vectors retrieved with the above approach can then be used as the new eigenvectors of the input matrices $\{M_c\}_c$ for the clusters of eigenvalues, in analogous fashion as for the single-snapshot case, and then run Algorithm 7 on these modified operators. This procedure for constructing a random basis should be repeated a number of times, and the optimal result kept, as in the single snapshot case.

A special case is the perturbation of degenerate real eigenvalues that do not turn into complex ones through the sequence of snapshots, corresponding to real eigenvalues for the Lindbladian generator. In this case, we do not have a partner invariant subspace. As discussed already, an eigenspace of an hermiticity-preserving operator with respect to a real eigenvalue admits self-adjoint eigenvectors in addition to hermitian-related pairs. Consider an n-degenerate real eigenvalue κ. As in the complex case, we pick a snapshot c' at random, and apply the pre-processing steps from Algorithm 1 to $M_{c'}$ to find a basis for the subspace $\Pi_{c'}(\kappa)$. This basis will be composed of a set of vectors $\{v_j\}_{j=1}^p$, a set of hermitian-related vectors $\{v_j^\dagger\}_{j=1}^p$, and a set of self-adjoint vectors $\{s_j\}_{j=1}^{n-2p}$, for some value $p = 1, \ldots, n/2$. Denoting by Π_v,

$\Pi_{v^\dagger}$, Π_s the corresponding projections onto the subspaces spanned by these sets of vectors, the constraint eq. (5.30) turns into:

$$\sum_c \left\| \Pi_c(\kappa) - \Pi_v - \Pi_{v^\dagger} - \Pi_s \right\| \leq \varsigma_2. \tag{5.31}$$

As in the complex case, we run Algorithm 7 on the input matrices resulting by using these vectors as the bases for the degenerate subspace in each M_c, and then repeat the randomised process a number of times.

5.6 Numerical Examples with Cirq

In this section, we present the results of testing our algorithm numerically on noisy dynamics synthesised in Cirq [66]. The numerics serve as a benchmark of both our convex optimisation and pre-processing algorithms. Since we know the 'ideal' channel in each test case, we can compare the outcomes against the true values. The algorithms performed well in all cases. It is worth emphasising that the algorithm itself does not require any information about what the 'ideal' channel is – it merely needs the tomographic data of the channel under consideration. Here the ideal operator is only used to benchmark the results against.

5.6.1 One-qubit numerics

In every one-qubit example each measurement in the simulated process tomography was repeated 10,000 times. Throughout this section we will express distances between matrices using the Frobenius norm.

5.6.1.1 Unitary 1-qubit example: X-gate

In subsection 5.4.2 we demonstrate how the naive algorithm (with no pre-processing) is not guaranteed to find the closest Markovian channel if the input is a 'noisy' X-gate, as the degenerate eigenbases are not stable with respect to perturbations.[5]

We used Cirq's density matrix simulator to simulate process tomography on a 1-qubit X-gate. Denoting the result of the process tomography by M_X, the distance from the ideal operator is

$$\|M_X - X \otimes X\| = 0.025 \tag{5.32}$$

Clearly we expect the closest Markovian channel to be at least as close to M_X as this value.

[5]The transfer matrix for an X-gate has two two-fold degenerate eigenspaces: one with eigenvalue $+1$, and one with eigenvalue -1.

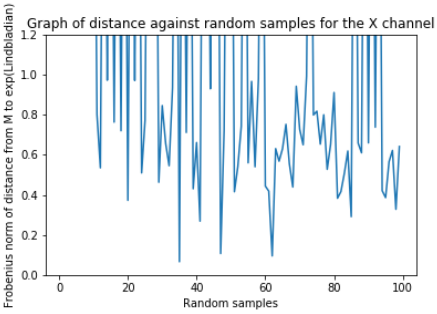

(a) Random samples in the range $(0, 100)$

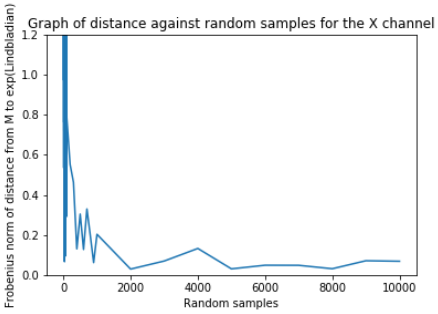

(b) Random samples in the range $(0, 10000)$

Figure 5.2: Results for a simulated 1-qubit X-gate. In both cases the algorithm ran with $\varepsilon = 1$. A y-axis value greater than 1 indicates that no Markovian channel was found in that run.

We applied our convex optimisation algorithm to extract the full description of the best-fit Lindbladian; we denote the generated Markovian channel by T_X. In Fig. 5.2 we show how the distance $\|M_X - T_X\|$ varies with the number of random samples we set the code to run for. As expected, increasing the number of random samples decreases the distance between M_X and T_X, although there is some fluctuation due to the randomised nature of the algorithm. This shows that the 'direction' which the matrix is perturbed in is crucial – as we saw in subsection 5.4.2, perturbations of the same magnitude along different directions can have very different effects on whether a compatible Lindbladian is found.

5.6.1.2 Markovian 1-qubit example: depolarizing channel

The depolarizing channel, implementing the evolution

$$\rho \to (1-p)\rho + \frac{p}{3}\left(X\rho X + Y\rho Y + Z\rho Z\right), \tag{5.33}$$

is an example of a non-unitary, but Markovian, quantum channel.

We simulated process tomography on a depolarizing channel with $p = 0.3$. The transfer matrix for this channel has a non-degenerate +1 eigenvalue, and a three-fold degenerate eigenspace with eigenvalue 0.6. We used our convex optimisation algorithm to construct the closest Markovian channel. Denoting the result of the process tomography by M_{depol} and the transfer matrix of the depolarizing channel by $\mathcal{E}_{\text{depol}}$, we get

$$\|M_{\text{depol}} - \mathcal{E}_{\text{depol}}\| = 0.033 \tag{5.34}$$

In Fig. 5.3 we show how the distance between the tomography result and the closest Markovian channel varies with the number of random samples we allowed the code to run for.

Comparing Fig. 5.3 with Fig. 5.2 (and noticing the different y-axis scales in the two graphs) we see that unlike with the X-gate, Algorithm 1 always finds a good approximation to the tomographic result, even for very few random samples. This suggests that the direction of perturbation is less important for the depolarizing channel than for the X-gate.

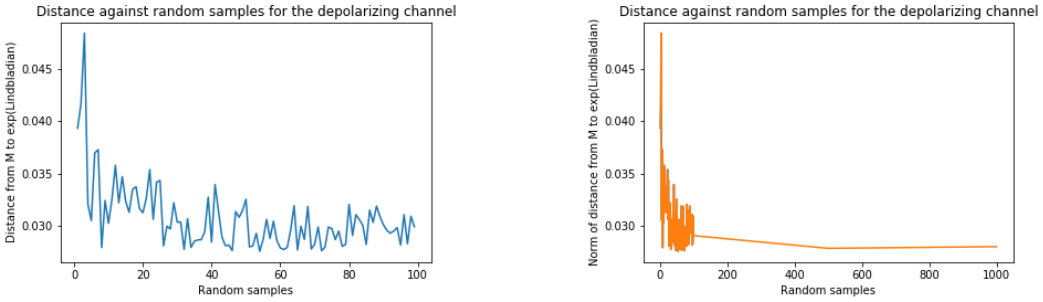

(a) Random samples in the range $(0, 100)$ **(b)** Random samples in the range $(0, 1000)$

Figure 5.3: Results for a simulated 1-qubit depolarizing channel.

5.6.1.3 Non-Markovian and Markovian 1-qubit examples: unital quantum channel

In [100] Kraus operators are constructed for a unital quantum channel, and conditions for the channel to be Markovian have been derived.[6] For a master equation

$$\dot{\rho}(t) = \gamma_1\sigma_1\rho\sigma_1 + \gamma_2\sigma_2\rho\sigma_2 + \gamma_3\sigma_3\rho\sigma_3 - (\gamma_1+\gamma_2+\gamma_3)\rho, \tag{5.35}$$

the Kraus operators for the evolution are:

$$\begin{aligned} A_0 &= \frac{1}{2}(1+\Gamma_1+\Gamma_2+\Gamma_3)^{\frac{1}{2}}\,\mathbb{I} \\ A_1 &= \frac{1}{2}(1+\Gamma_1-\Gamma_2-\Gamma_3)^{\frac{1}{2}}\,\sigma_1 \\ A_2 &= \frac{1}{2}(1-\Gamma_1+\Gamma_2-\Gamma_3)^{\frac{1}{2}}\,\sigma_2 \\ A_3 &= \frac{1}{2}(1-\Gamma_1-\Gamma_2+\Gamma_3)^{\frac{1}{2}}\,\sigma_3, \end{aligned} \tag{5.36}$$

where

$$\Gamma_i := e^{-\int_0^t ds\left(\gamma_j(s)+\gamma_k(s)\right)} \tag{5.37}$$

[6] A channel is said to be unital if the maximally mixed state is a fixed point of the evolution.

and $\{i, j, k\}$ is a permutation of $\{1, 2, 3\}$.

The inequality for the channel to be completely positive is

$$\Gamma_i + \Gamma_j \leq 1 + \Gamma_k, \tag{5.38}$$

where $\{i, j, k\}$ is a permutation of $\{1, 2, 3\}$. The condition for the channel to be Markovian is given by $\gamma_i(t) > 0$, for all t and i.

We simulated process tomography in Cirq on a non-Markovian unital quantum channel with $\gamma_1 = -200$, $\gamma_2 = 201$, $\gamma_3 = 200.5$. The transfer matrix for this channel is non-degenerate. Denoting the tomography result by M_{unital} and the transfer matrix of the unital quantum channel by $\mathcal{E}_{\text{unital}}$, we obtain

$$\|M_{\text{unital}} - \mathcal{E}_{\text{unital}}\| = 0.0335 \tag{5.39}$$

Applying Algorithm 1 with a large error tolerance parameter ($\varepsilon = 1$) found a Markovian channel, T, satisfying $\|T - M_{\text{unital}}\| = 0.609$.

In Fig. 5.4 we show the results of comparing the non-Markovianity parameter μ against the accuracy ε. We first ran Algorithm 1 with varying ε using a step size $\delta_{\text{step}} = 0.5$ in the Algorithm 6 subroutine: the results are shown in Fig. 5.4a. For $\varepsilon \in (0, 0.186)$ no μ-parameter was found by the algorithm. Conversely in Fig. 5.4b, where the same analysis is run with a step size $\delta_{\text{step}} = 0.01$, a non-Markovianity parameter was found for all $\varepsilon \geq 0.025$.

This can be understood by recalling that Algorithm 6 doesn't search for the channel T that minimises μ and is within an ε-ball of M. It searches for the Lindbladian L' that minimises μ and is within a δ-ball of $\log(M)$, then checks whether $\|e^{L'} - M\| \leq \varepsilon$. Since the bounds on δ aren't tight, it repeats this process for $\delta \in \{\delta_i = \delta_{\min} + \delta_{\text{step}} \mid \delta_i < \delta_{\max}\}$, and keeps the best result. If δ_{step} is too large, this can lead to the algorithm failing to select a μ-value within the ε-ball of M, even when one exists: this is what has happened in Fig. 5.4a. An illustration explaining this intricacy is given in Fig. 5.5.

The problem can be eliminated by running Algorithm 6 with a smaller step size. In Figs. 5.4b and 5.4c we show the results of running Algorithm 1 with a varying ε parameter, and where the Algorithm 6 subroutine has a step size $\delta_{\text{step}} = 0.01$. For $\varepsilon = 0$ no μ is found by the convex optimisation algorithm, indicating that there is no compatible Markovian channel in the ε-ball around M, even with white noise

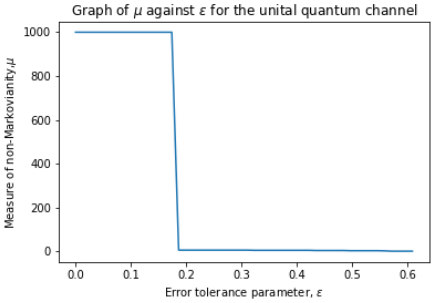

(a) ε in the range $(0, 0.609)$ with step size of 0.5

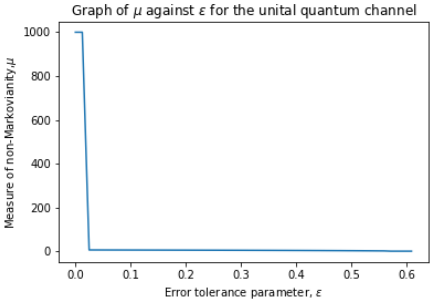

(b) ε in the range $(0, 0.609)$ with step size of 0.01

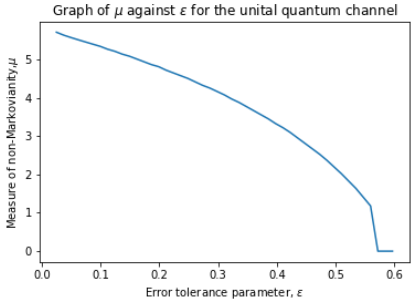

(c) ε in the range $(0.025, 0.609)$

Figure 5.4: Results for a simulated unital quantum channel. A value of $\mu = 1000$ indicates that no μ was found by the algorithm. In Fig. 5.4a the step size is 0.5. In all other figures the step size is 0.01.

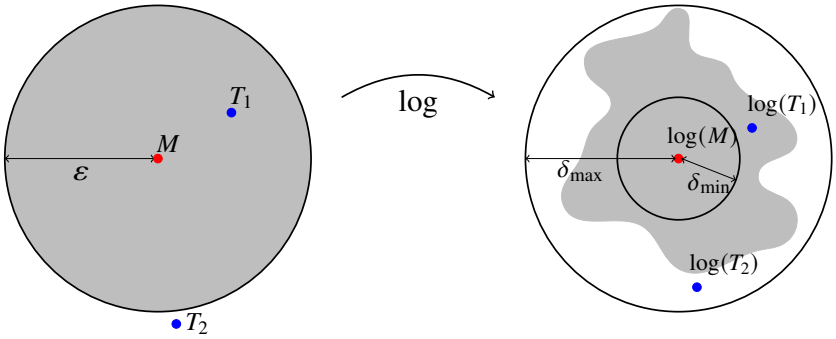

Figure 5.5: A schematic illustration of the distortion of the ε-ball (gray area) under the matrix logarithm, whose boundaries are included between two balls of radius $\delta_{\min}$ and $\delta_{\max}$. Let T_i (for $i = 1, 2$) be quantum channels with non Markovianity-parameter μ_i such that $\|\log(T_i) - \log(M)\| = \delta_i$ and $\|T_i - M\| = \varepsilon_i$ where $\mu_1 > \mu_2$, $\varepsilon_2 > \varepsilon > \varepsilon_1$ and $\delta_2 > \delta_1$. If Algorithm 6 is run on the channel M with $\delta_{\text{step}} > \delta_2 - \delta_1$ the algorithm will not return a non-Markovianity parameter because the convex optimisation finds T_2, but this is rejected by the step which checks if $\|e^{L'} - M\| \leq \varepsilon$. Running Algorithm 6 with a smaller δ_{step} solves this issue.

addition. Above $\varepsilon \approx 0.025$ the convex optimsation algorithm consistently finds an actual value for μ. As ε approaches 0.609 μ decreases to zero, indicating that increasing the size of the ε-ball reduces the amount of white noise required to render the channel Markovian, as expected.

We also simulated process tomography on a Markovian version of the unital channel with $\gamma_1 = 200$. Running Algorithm 1 on the result of the tomography, we found a Markovian channel T satisfying $\|T - M\| = 0.02$.

5.6.1.4 Analytical derivation of the non-Markovianity parameter

In order to benchmark the output of Algorithm 6, we calculate by hand the value of μ for the unital quantum channel numerically investigated in subsection 5.6.1.3. This particular example is convenient because there is no cluster of eigenvalues; indeed, all eigenvalues of the simulated perturbed channel are positive and far apart from each other. This means that all subspaces are 1-dimension and thus we don't have to undergo a search over (infinitely many) feasible basis vectors for the unperturbed channel.

Noting that the white noise addition cannot influence either the hermiticity-preserving or the trace-preserving condition, our strategy will be to construct a matrix from the tomographic data by "filtering" these two properties, and then calculate the minimal value of μ to increase the eigenvalues of its Choi representation in order to satisfy the conditionally complete positivity condition. This approach does not guarantee that we will obtain the closest map compatible with Markovian dynamics through white noise addition, but we can reasonably expect to retrieve an operator that is very close to the optimal one. We will then compare the value for μ from this calculation with the one returned by algorithm when setting ε equal to the distance between the input matrix and the matrix exponential of the map calculated with this analytical method.

Consider the constraints on the eigenvalues and eigenvectors of an hermiticity- and trace-preserving channel having non-degenerate and non-negative spectrum. Hermiticity implies that all eigenvectors must be self-adjoint; the trace-preservaing condition means that one eigenvalue must be equal to 0 with respect to a left eigenvector being proportional to the maximally entangled state $\langle\omega| = \langle(1,0,0,1)|$. By the biorthogonality conditions between left and right eigenvectors, this forces the three right eigenvectors related to the complement of the kernel to have first and fourth components of opposite sign. Hence, we will go through the following steps to turn

the simulated perturbed unital channel $\mathcal{U}$ into an hermiticity- and trace-preserving matrix H' and calculate its non-Markovianity measure by hand:

(1) From the eigenvalues $\lambda_1 > \lambda_2 > \lambda_3 > \lambda_4$, set $\lambda_4 = 0$ and define the matrix $D \coloneqq \mathrm{diag}(\lambda_1, \lambda_2, \lambda_3, 0)$.

(2) From the right eigenvectors $\{w_j\}_j$ build self-adjoint vectors $\left|\tilde{v}_j\right\rangle = 1/2 \cdot (\left|w_j\right\rangle + \left|w_j^\dagger\right\rangle)$, for $j = 1, \ldots, 4$.

(3) Construct three vectors orthogonal to $\langle\omega|$ whose first and fourth components are respectively $v_j^{(1)} = 1/2 \cdot \left(\tilde{v}_j^{(1)} - \tilde{v}_j^{(4)}\right)$ and $v_j^{(4)} = -v_j^{(1)}$, and with $v_j^{(2)} = \tilde{v}_j^{(2)}$ and $v_j^{(3)} = \tilde{v}_j^{(3)}$, for $j = 1, 2, 3$. Define then $S \coloneqq (v_1, v_2, v_3, \tilde{v}_4)$.

(4) Define $H' \coloneqq SDS^{-1}$ and calculate

$$\mu = 2 \cdot |\lambda_{\min}(\omega_\perp (H')^\Gamma \omega_\perp)| \qquad \text{and} \qquad \varepsilon = \|\mathcal{U} - \exp H'\|_{\mathrm{F}}. \tag{5.40}$$

For the simulated channel, under this procedure we obtain a value of $\mu = 5.76983$ and $\varepsilon = 0.01788$. As a comparison, by setting $\varepsilon = 0.01788$ in our algorithm (with $\delta_{\text{step}} = 10^{-5}$) this returns $\mu_{\min} = 5.76539819$; also, as we can see in Fig. 5.4c, $(0.012 - 0.025)$ is indeed the first segment for ε where we retrieve a valid value for $\mu_{\min}$. We refer to the Mathematica notebook supplied as Supplementary Material with [11] for the explicit calculation following this procedure.

5.6.2 Two-qubit examples

In every two-qubit example each measurement in the simulated process tomography was repeated 100,000 times.

5.6.2.1 Unitary 2-qubit example with degenerate eigenvalues: ISWAP gate

The action of the ISWAP gate is to swap two qubits, and introduce a phase of i to the $|01\rangle$ and $|10\rangle$ amplitudes. It has a six-fold degenerate eigenspace with eigenvalue $+1$, a two-fold degenerate eigenspace with eigenvalue -1, and two four-fold degenerate eigenspaces with eigenvalues $\pm i$.

We used Cirq's density matrix simulator to simulate process tomography on the ISWAP-gate. Denoting the result of the process tomography by M_I, we have

$$\|M_I - ISWAP \otimes ISWAP\| = 0.031 \tag{5.41}$$

We then used our convex optimisation algorithm to construct the closest Markovian channel, T_I. We ran Algorithm 1 for 100 random samples, 85 times. The results are shown in Fig. 5.6.

It is clear that a higher number of random samples is required than in the 1-qubit case with the X-gate. This is to be expected, since the degenerate eigenspaces are higher-dimensional, and there are more of them. The probability of randomly choosing a 'good' basis is hence lower.

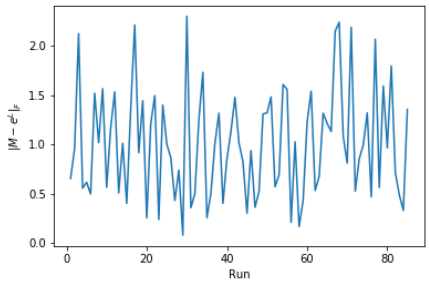

(a) The distance between the tomography result and the Markovian channel constructed by Algorithm 1 in each 100-random sample run.

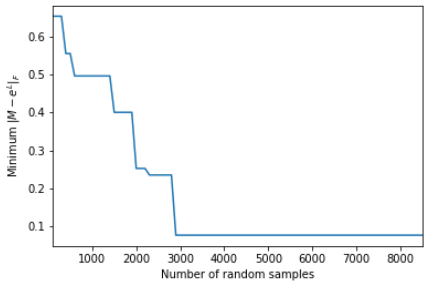

(b) Results from the same simulation as Fig. 5.6a, where now we show *minimum* distance achieved against total number of random samples.

Figure 5.6: Numerics for the simulated ISWAP gate. Algorithm 1 was run for 100 random samples 85 times.

5.6.2.2 Markovian 2-qubit example: depolarizing CZ channel

The CZ is a two-qubit quantum gate. Its action is to apply a Z-gate to the second qubit if the first qubit is in the $|1\rangle$ state. Otherwise it acts as the identity on both qubits.

We simulated process tomography on a depolarizing CZ channel, which applied the CZ-gate with probability 0.1, or an XX / YY / ZZ -gate with probabilities 0.07, 0.08 and 0.09 respectively. This is an example of a non-unitary, but Markovian, quantum channel. The transfer matrix of the channel has six two-fold degenerate eigenspace with eigenvalue +1, 0.7, 0.93, 0.57, 0.67, and 0.47, and non-degenerate eigenvalues of 0.68, 0.66, 0.48 and 0.46.

Denoting the result of the process tomography by M_{CZdepol} and the transfer matrix of the depolarizing channel by $\mathcal{E}_{\text{CZdepol}}$, their distance is

$$\|M_{\text{CZdepol}} - \mathcal{E}_{\text{CZdepol}}\| = 0.033 \tag{5.42}$$

We ran Algorithm 1 on M_{CZdepol} for 100 random samples, 10 times. The results are shown in Fig. 5.7.

Comparing Fig. 5.7 with Fig. 5.6 (and noticing the different y-axis scales in the two graphs) we see that unlike with the ISWAP-gate, Algorithm 1 always finds a good approximation to the tomographic result, even for very few random samples. As in the 1-qubit example, this shows that the direction of the perturbation is less important for the non-unitary channel than it is for the unitary channel.

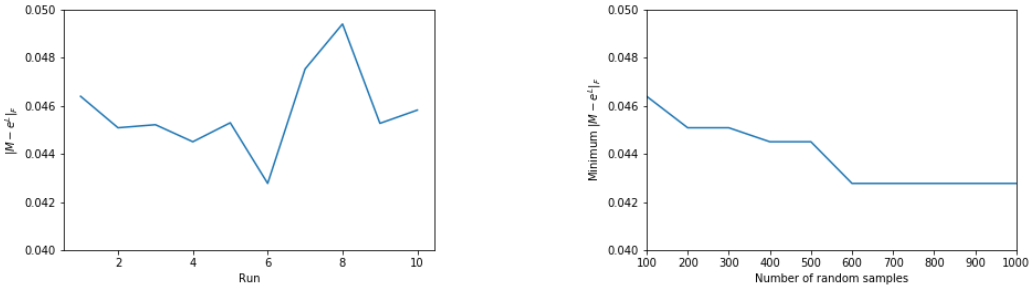

(a) The distance between the tomography result and the Markovian channel constructed by Algorithm 1 in each 100-random sample run.

(b) Results from the same simulation as Fig. 5.7a, where now we show *minimum* distance achieved against total number of random samples.

Figure 5.7: Numerics for the simulated depolarizing CZ channel. Algorithm 1 was run for 100 random samples 10 times.

5.6.3 Time series data

Finally we ran our time series algorithm Algorithm 7 on 10 time steps of the 1-qubit depolarizing channel from subsection 5.6.1.2. The results are shown in Fig. 5.8. For this example the Frobenius norm of the distance between the ideal channel and the tomographic result is different for each snapshot. This makes it more difficult to interpret the Frobenius norm as a distance measure, so we have instead plotted the process fidelity between the tomography result for each snapshot and e^{tL} where L is the time-*independent* Lindbladian which best fits the 10 tomographic snapshots. As can be seen in the figures, there is excellent agreement between the tomography results and the Markovian channel found by Algorithm 7 .

5.7 Conclusions

We have developed novel methods and algorithms, based on previous work [63], to retrieve the best-fit Lindbladian to a quantum channel. We have implemented these algorithms in Python, and benchmarked them on synthetic tomography data generated in Cirq.

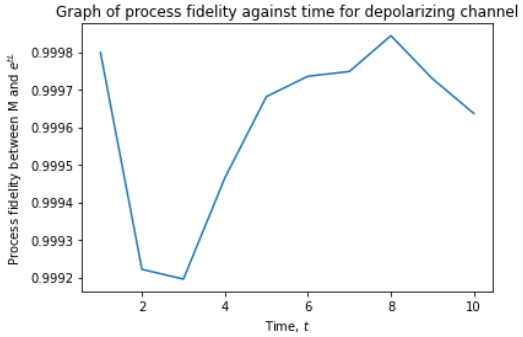

Figure 5.8: The process fidelity between the tomography result and the Markovian channel constructed by Algorithm 7 for 10 time steps of the 1-qubit depolarizing channel.

The key strengths of our method is that it can be applied to a single tomographic snapshot, is completely assumption-free regarding the structure of the analysed operator, and does not rely on any prior knowledge of the environment or the noise model. At the core of the method is a convex optimisation programme which searches for the closest Lindbladian generator within a given distance from the matrix logarithm of the input. This approach is successful in dealing with imprecise tomographic data, extracting Markovian dynamics within any desired regime of tolerance. If no Markovian channel is found, the scheme provides a well-defined quantitative measure of non-Markovianity in terms of the minimal addition of white noise required to "wash-out" memory effects, and render the evolution Markovian.

A significant part of the extension over [63] is focused on the treatment of input matrices that are perturbations of some unknown process with a degenerate spectrum. This situation commonly arises when analysing noisy unitary gates in quantum computation. In order to address the susceptibility of the convex optimisation programme with respect to perturbation of multi-dimensional eigenspaces, we have designed a series of pre-processing algorithms, rigorously rooted in the theory of matrix perturbation, which identify and re-contruct the unperturbed hermiticity-preserving structure of the original channel. To test our theoretical formulation, we have implemented and numerically benchmarked our algorithm on simulated data from the Cirq platform, demonstrating that our algorithms are able both to successfully identify channels consistent with an underlying Markovian dynamics, as well detect and quantitify non-Markovianity.

One drawback of the algorithms developed here is that they require a full tomographic snapshot, thus become infeasible for large numbers of qubits or when a complete tomographic description cannot be attained. Extending these algorithms to the case

where we only have access to measurement data that gives incomplete information about the full dynamics, or incorporating partial prior information, will be explored in future work. Incorporating techniques to account for state preparation and measurement errors in the tomography stages may also be important when applying our algorithms to NISQ hardware. Finally, as stated in the introduction, another key avenue is to further develop the analysis and methods of this chapter to the case of time-dependent noise models, allowing the techniques to be applied to quantum dynamics at longer timescales over which the noise processes are likely to vary.

Code availability

The python code implementing the algorithms presented in this chapter and used to produce the numerical results is available at [7].

The 1-qubit X-gate analysis (with 10,000 random samples) took 2 hours on a standard Intel x86 2.0GHz laptop, and the 2-qubit ISWAP analysis (8,500 random samples) took 2 weeks on a standard Intel x86 3.40Ghz desktop machine. We made no effort to optimise the algorithm implementation. In particular, the most costly part of the algorithms, namely the random sampling in the pre-processing, is trivially parallelisable, but we didn't do this here. The run-time can certainly be reduced significantly if desired.

Part III

Universal Hamiltonians in holography

Chapter 6

Quantum information in holography

6.1 Introduction

The holographic principle states that the description of a gravitational theory in a volume can be mathematically encoded onto its lower dimensional boundary [101, 102]. The most successful realisation of the holographic principle is the AdS/CFT correspondence: a postulated duality between quantum gravity in $(d+1)$-dimensional, asymptotically anti-de-Sitter (AdS) space, and a conformal field theory (CFT) defined on its d-dimensional boundary [103]. It has provided insight into theories of quantum gravity, and has also been used as a tool for studying strongly-interacting quantum field theories. Concepts from quantum information theory have been used to further our understanding of the duality, with a notable example being the relationship between entanglement and geometry captured by the Ryu-Takayanagi formula [104]. Recently it has been shown that important insight into the emergence of bulk locality in AdS/CFT can be gained through the theory of quantum error correcting codes [105].

The relationship between quantum information theory and AdS/CFT has led to interest in using quantum information tools to construct exactly solvable toy models which capture key aspects of the duality. In this thesis we'll be interested in toy models built up from tensor networks. These tensor networks are used to construct holographic quantum error correcting codes (HQECC) [106, 107, 108, 109, 110, 111, 112], which realise many of the interesting structural features of AdS/CFT. There are a number of features of AdS/CFT that a HQECC might want to emulate to be considered a successful toy model:

1. **Entanglement structure.** The relationship between bulk geometry and boundary entanglement in AdS/CFT is one of the key features of the duality. It is captured in the Ryu-Takayanagi formula which states that the entanglement entropy of a boundary region, A, is proportional to the area of a corresponding minimal surface, γ_A, in the bulk geometry[113]:

$$S(A) \approx \frac{|\gamma_A|}{4G_N}, \tag{6.1}$$

where G_N is Newton's constant.

2. **Error correcting properties.** As already outlined, AdS/CFT can be viewed as a quantum error correcting code [105] - bulk information is redundantly encoded in the boundary theory. Consider a fixed time slice of AdS. A boundary region, A, defines a region in the bulk known as its entanglement wedge $\mathcal{E}[A]$ – the bulk region bounded by A and the Ryu-Takayangi surface of A. The AdS-Rindler reconstruction states that a bulk operator acting in $\mathcal{E}[A]$ can be represented as a boundary operator supported on A [105, 114]. A given bulk operator lies in the entanglement wedge of many boundary regions, hence there are multiple representations for each bulk operator with different spatial support on the boundary. Since the bulk operator can be reconstructed on A it is protected against an error where the complementary boundary subregion A^c is erased. Given any partition of the boundary into non-overlapping regions A and A^c, a given bulk operator should always be recoverable on exactly one of the regions (a property known as *complementary recovery*).

3. **Mapping between models.** The AdS/CFT correspondence is a mapping between *models*, not just between states and observables; it relates quantum theories of gravity in the bulk to conformal field theories in one dimension lower on the boundary. For holographic code models, this means realising a mapping between (quasi-)local Hamiltonians in the bulk and local Hamiltonians on the boundary.[1] It should be noted that throughout this section we will use *local* in the computer science sense - i.e. we call a Hamiltonian local if it can be written as a sum of 2-body operators acting on neighbouring spins. In the high energy physics community locality can be used to refer to something stronger - the idea that signals cannot travel instantaneously (or close to instantaneously).

[1]Note the bulk Hamiltonian isn't necessarily strictly local – there may be gravitational Wilson lines which break locality in a restricted way.

In Chapter 9 we discuss how this more physical idea of locality is related to the work in this section.

4. **Symmetries in the boundary theory.** In AdS/CFT the boundary is a conformal field theory - so we'd want to construct a HQECC where the boundary exhibits a (discrete) version of conformal theory.

For more detailed discussion of AdS/CFT readers are referred to [115, 116]

As mentioned previously, the toy models of AdS/CFT we are interested in in this thesis are built up from tensor networks. So before delving into the details of any constructions we cover some technical background on tensors in Section 6.2. Then, in Section 6.3 we go on to present two previously constructed HQECCs which we extend in this thesis. The first, [106], approximately realises the first two desired properties. The second [110], builds on the work in [106] and exactly realises properties 1-2.

In the remaining chapters of the thesis we go on to outline new constructions of HQECC which build on [106, 110]. In Chapter 7 we present a HQECC which applies the theory of universal Hamiltonians to the HQECC in [106] to construct a toy model which approximately realises properties 1-2 and also realises property 3. This is extended in Chapter 8 with a HQECC which uses techniques from [110] and Chapter 7 to exactly realise properties 1-3. Finally, in Chapter 9 we give our conclusions, including a discussion of how these constructions could be extended to realise property 4.

6.2 Technical set-up

A rank n-tensor where each index runs over p values can be viewed as an n-qudit state where each qudit has local dimension p:

$$|\psi\rangle = \sum_{i_1 i_2 \ldots i_t \in \mathbb{Z}_p^t} T_{i_1 i_2 \ldots i_t} |i_1\rangle \otimes |i_2\rangle \otimes \ldots \otimes |i_t\rangle \,. \tag{6.2}$$

If we reshape the tensor to consider t_A "input legs" and t_B "output legs" it represents a linear map, V, between two Hilbert spaces $\mathcal{H}_A \mapsto \mathcal{H}_B$ with dimensions $d_A = p^{t_A}$ and $d_B = p^{t_B}$ respectively:

$$V|a\rangle = \sum_b T_{a,b} |b\rangle \,. \tag{6.3}$$

Larger mappings can be generated by contracting multiple tensors together to form a tensor network (see Fig. 6.1).

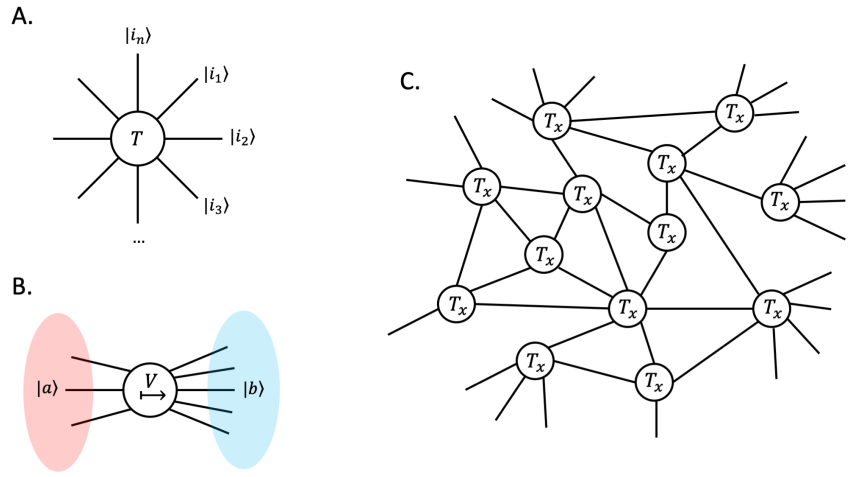

Figure 6.1: A) Graphical representation of tensor from eq. (6.2). B) Graphical representation of reshaping a tensor into a mapping from eq. (6.3). C) Example of contracting tensors together to form a tensor network.

6.2.1 Perfect tensors and pseudo-perfect tensors

Perfect tensors were first introduced in [106], where they were used in the construction of HQECC from a 2D bulk to a 1D boundary.

Definition 56 (Perfect tensors, definition 2 from [106])**.** *A $2m$-index tensor $T_{a_1 a_2 \ldots a_{2m}}$ is a perfect tensor if, for any bipartition of its indices into a set A and a complementary set A^c with $|A| \leq |A^c|$, T is proportional to an isometric tensor from A to A^c.*

This definition is equivalent to requiring that the tensor is a unitary from any set of m legs to the complementary set.

For one of the constructions in Chapter 7 we introduce a generalisation of perfect tensors:

Definition 57 (Pseudo-perfect tensors)**.** *A $2m+1$-index tensor $T_{a_1 a_2 \ldots a_{2m+1}}$ is a pseudo-perfect tensor if, for any bipartition of its indices into a set A and a complementary set A^c with $|A| < |A^c|$, T is proportional to an isometric tensor from A to A^c.*

The states described by (pseudo-)perfect tensors are absolutely maximally entangled (AME) (see Appendix C.1 for details). Furthermore, viewed as an isometry from k indices to n indices, a t-index (pseudo-)perfect tensor is the encoding isometry of a $[n, k, d]$ code, where $t = n + k$ and $d = \left\lfloor \frac{t}{2} \right\rfloor - k + 1$ (see Appendix C.2 for proof).

6.2.1.1 Stabilizer (pseudo-)perfect tensors

The HQECC constructed in [106] uses stabilizer perfect tensors, and in Chapter 7 we'll also restrict our attention to these tensors:

Definition 58 (Stabilizer (pseudo-)perfect tensors)**.** *Stabilizer (pseudo-)perfect tensors describe stabilizer AME states.* [2]

In Appendix C.4 we demonstrate that stabilizer (pseudo-)perfect tensors describe stabilizer QECC. Furthermore, they map Pauli rank one operators to Pauli rank one operators in a consistent basis.

It is possible to construct a t-index (pseudo-)perfect stabilizer tensor for arbitrarily large t by increasing the local Hilbert space dimension. Details of the construction are given in Appendix C.5.

6.2.2 Random tensors

We can construct random states (and hence random tensors) by starting from an arbitrary reference state, $|0\rangle$, and applying a random unitary operation, U. The average over a function of the random state, $f(|\phi\rangle)$, is given by integration over the unitary group, U, with respect to the Haar measure:

$$\langle f(|\phi\rangle)\rangle = \int_{\mathcal{U}(d)} f(|\phi\rangle) dU. \tag{6.4}$$

A random tensor does not generally have any particular properties. However, in the limit of large bond dimension random tensors are approximately perfect with high probability due to the concentration of measure phenomenan [117].

6.2.2.1 Random stabilizer tensors

In Chapter 8 we will be interested in random *stabilizer* tensors. To construct a random stabilizer state we begin with a reference stabilizer state $\left|\tilde{\psi}\right\rangle$, stabilized by S, and apply a random Clifford unitary C to give $|\psi\rangle = C\left|\tilde{\psi}\right\rangle$. Since the Clifford group maps the Pauli group to itself under conjugation this results in a stabilizer state with $S' = CSC^\dagger$.[3]

Uniformly sampling over the Clifford group is not equal to the Haar measure on unitary groups, however the Clifford group does form a 2-design [118, 119, 120]:

Definition 59 (Unitary 2-design, [118])**.** *A set $\mathcal{D} = \{U_k\}_{k=1}^K$ of unitary matrices on $\mathcal{H} = \mathbb{C}^d$ is a unitary 2-design if it fulfils the condition:*

[2] See Appendix C.3 for a definition of stabilizer states and stabilizer codes on qudits of prime dimension.

[3] Here we are not restricting ourselves to qubits - the procedure works for qudits of prime dimension p with the generalised Pauli and Clifford groups.

1. *(Twirling of states) For all* $\rho \in \mathcal{B}(\mathcal{H} \otimes \mathcal{H})$

$$\frac{1}{K} \sum_{U_k \in \mathcal{D}} (U_k \otimes U_k)\, \rho\, (U_k \otimes U_k)^\dagger = \int_{\mathcal{U}(d)} (U \otimes U) \rho (U \otimes U)^\dagger dU. \tag{6.5}$$

This property of the Clifford group will be useful in Chapter 8

6.3 Previous work

6.3.1 HQECC based on perfect tensors

The HaPPY code [106] is a tensor network code, built up by embedding perfect tensors in a tessellation of $\mathbb{H}^2$ by right angled pentagons (see Fig. 6.2). The perfect tensors used to build the code have six legs - five of the legs are contracted through the faces of the pentagons, the remaining uncontracted leg is a bulk degree of freedom. The tessellation is cut off at some finite radius, and uncontracted legs on the edge of the tessellation represent boundary degrees of freedom.

Using the properties of perfect tensors, along with the negative curvature of $\mathbb{H}^2$ it is shown in [106] that the HaPPY code is an isometry from bulk degrees of freedom to boundary degrees of freedom. Moreover, it is an error correcting code, where reconstruction qualitatively mirrors the AdS-Rindler reconstruction (although there do exist pathological choices of boundary regions A and A^c where some bulk operators are not recoverable on either A or A^c, violating complementary recovery). The relationship between entanglement and geometry in the HaPPY code also captures some of the features of AdS/CFT, and for connected boundary regions the Ryu-Takayanagi formula is approximately obeyed.[4]

Local (or quasi-local)[5] bulk Hamiltonians which are pushed through the HaPPY code lead to global Hamiltonians on the boundary theory - these Hamiltonians include terms which act on a $O(1)$ fraction of the boundary manifold.

6.3.2 HQECC based on random tensors

[110] studied toy models of AdS/CFT based on random tensor networks embedded in $\mathbb{H}^d$ for $d \geq 2$ dimensions. In this model a tensor network is constructed out of tensors, picked uniformly at random. In [110] the authors interpret the average over

[4]For holographic *states*, with no bulk degrees of freedom, the Ryu-Takayanagi formula is exactly obeyed for connected boundary regions. With the inclusion of bulk degrees of freedom the authors of [106] are only able to demonstrate entropy bounds, which demonstrate small deviations from the exact formula.

[5]A 'quasi' local Hamiltonian is a generalisation of a local Hamiltonian that allows for the possibility of gravitational Wilson lines - see subsection 7.4.1.6 for a rigorous definition.

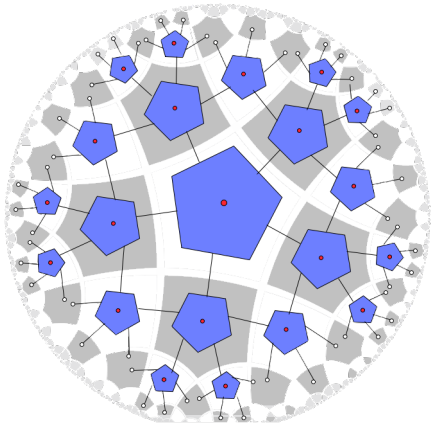

Figure 6.2: The holographic pentagon code from [106]. Each blue pentagon represents a 6 leg perfect tensor (see Definition 56). Five indices of the tensor are contracted through faces of the pentagon, the remaining uncontracted index represents a bulk degree of freedom (shown by the red dot).

random tensors as the partition function of a classical Ising model. In this picture, the Ryu-Takayanagi minimal surfaces appear as domain walls. This mapping allows the authors to demonstrate that for large bond dimension in their construction the Ryu-Takayanagi formula is obeyed exactly for separable bulk states. Moreover, when there is non-trivial entanglement in the bulk the corrections to the Ryu-Takayanagi formula qualitatively mirror what is expected in AdS/CFT.

Furthermore, it is shown that (in the limit of large bond dimension) the random tensor networks constructed in this fashion are approximate isometries from the bulk to the boundary and in the reverse direction, defining a bidirectional holographic code. The bulk-to-boundary mapping also satisfies the error correction properties of the AdS-Rindler reconstruction. However, as in the HaPPY code, (quasi-)local bulk Hamiltonians which are pushed through the tensor network lead to global Hamiltonians on the boundary of the network.

Chapter 7

Toy models of holographic duality between local Hamiltonians

7.1 Introduction

Since holographic quantum codes give a mapping from any bulk operator to the boundary, one can certainly map any local bulk Hamiltonian to the boundary. But this gives a completely non-local boundary Hamiltonian, with global interactions that act on the whole boundary Hilbert space at once. Local *observables* deep in the bulk are expected to map under AdS/CFT duality to non-local boundary observables, so this is fine – indeed, expected – for observables. But a global Hamiltonian acting on the entire boundary Hilbert space has lost all relation to the boundary geometry; there is no meaningful sense in which it acts in one dimension lower. Indeed, for these toy models on finite dimensional spins, any Hamiltonian whatsoever can be realised using a global operator. For the correspondence between bulk and boundary models to be meaningful, the local Hamiltonian describing the bulk physics needs to map to a *local* Hamiltonian on the boundary. For this reason, [106, 109, 110, 111] study the mapping of observables and states in their construction, and do not apply it to Hamiltonians.

By standing on the shoulders of the holographic quantum code results, in particular the HaPPY code [106], and combining stabilizer code techniques with the mathematical theory of Hamiltonian simulation [6] and techniques from Hamiltonian complexity theory, we build on these previous results to construct a holographic duality between quantum many-body models in 3D (2D) hyperbolic space and local models living on

its 2D (1D) boundary.[1] This allows us to extend the toy models of holographic duality in previous HQECC to encompass local Hamiltonians, and in doing so enables us to say something about how energy scales and dynamics in the bulk are reflected in the boundary. It also allows us to explore the duality in the other direction: from boundary to bulk. This gives insight into how the hyperbolic bulk geometry emerges as the geometry of a low-energy effective theory, and how this effective bulk geometry gets distorted at higher energies.

The remainder of this chapter is set out as follows. In Section 7.2 we present our main result, and give an overview of the proof. In Section 7.3 we outline the mathematical background needed to follow the full technical proofs. The proofs themselves are presented in Section 7.4 and Section 7.5 for the 3D/2D and 2D/1D cases respectively. Finally, in Section 7.6 we discuss the implications of our results, including a toy model of black hole formation within these HQECC.

7.2 Main results

In this chapter we construct an explicit duality between quantum systems in hyperbolic space, $\mathbb{H}^d$, and quantum systems on its $d-1$-dimensional boundary, which encompasses states, observables, and local Hamiltonians. The map is a quantum error correcting code, where the logical Hilbert space is a set of 'bulk' qudits, which are embedded in a tessellation of $\mathbb{H}^d$. The physical Hilbert space is a set of 'boundary' qudits, which lie on a $d-1$-dimensional manifold in $\mathbb{H}^d$. Every state and observable in the bulk/logical Hilbert space is mapped to a corresponding state / observable in the boundary/physical Hilbert space. The error correcting properties of the map means that it is possible to recover from erasure of part of the boundary Hilbert space, as in previous HQECC toy models.

Under our mapping, any local Hamiltonian in the bulk is mapped approximately to a 2-local, nearest-neighbour Hamiltonian in the boundary (where a k-local Hamiltonian is a sum over terms which each act non-trivially on at most k-qudits, and nearest-neighbour means the interactions are only between neighbouring qubits). In the language of error correction, this means that the code subspace of our quantum error correcting code is approximately the low-energy subspace of a 2-local

[1]The simulation techniques needed for the 2D/1D and 3D/2D dualities are distinct, and the proofs need to be handled separately. The techniques used for the 3D/2D duality extend to boundary dimensions ≥ 2, however for our explicit construction of these techniques we concentrate on the 3D/2D case as the smallest dimension where these techniques can be applied.

Hamiltonian H_{boundary}, where time evolution in the code subspace is also governed by H_{boundary}.[2]

It is important to emphasise that, as in the case of tensor network constructions of HQECC [106, 109, 110, 111], the duality we construct does not per se have anything to do with quantum gravity. It gives a holographic duality for *any* local quantum Hamiltonian, not specifically Hamiltonians modelling quantum gravity. However, this duality does exhibit some of the structural features of the AdS/CFT correspondence. Notably, entanglement wedge reconstruction and redundant encoding are seen in the construction. The Ryu-Takayanagi formula is also approximately obeyed for connected boundary regions.[3]

Therefore, one natural application of this construction is to toy models of the AdS/CFT correspondence. This requires choosing a bulk Hamiltonian, H_{bulk}, which models semi-classical gravity. Applying our holographic duality to this particular choice of bulk Hamiltonian, the time dynamics and energetic properties of the toy model do then exhibit certain of the features expected of AdS/CFT, in addition to the static features inherited from the underlying HQECC construction (see Section 7.6 for details). However, this toy model certainly does not capture every aspect of AdS/CFT duality. In particular, the boundary model we obtain is not a conformal field theory or Lorentz-invariant. And it is constructed for non-relativistic quantum mechanical systems in Euclidean space, in which time appears as an external parameter, not relativistic quantum systems in Minkowski space. We make no attempt in this work to understand whether AdS space can be embedded in some suitable way into $\mathbb{H}^d$. (Indeed, a more fruitful approach for future research is likely to be to apply the *techniques* we have developed in AdS space, rather than attempting to use the duality on $\mathbb{H}^d$ directly.)

A complete toy model of AdS/CFT duality would have to address these and many other aspects, as well as incorporating gravity more fully. Our holographic duality is one more step towards such a toy model, going beyond previous HQECC constructions, but as yet still a long way short of a full, mathematically rigorous construction of AdS/CFT.

[2]Note that this result does not contradict recent results in [121, 122] regarding the incompatibility of continuous symmetries and quantum error correction, as our H_{boundary} contains high-weight terms.

[3]All these features are inherited from [106], which our construction builds on.

7.2.1 Statement of the results

In this paper we construct a duality between $\mathbb{H}^d$ and its $d-1$-dimensional boundary (for $d = 2, 3$) that encompasses states, observables and Hamiltonians. In particular, we can map any (quasi)-local Hamiltonian in the bulk of $\mathbb{H}^d$ to a local Hamiltonian on its boundary.[4] The key features of our main results are informally captured in the following theorem. For a rigorous statement of the results see Theorem 78 for the 3D/2D duality and Theorem 79 for the 2D/1D duality.

Theorem 60 (Informal statement of holographic constructinos)**.** *Given any (quasi) local bulk Hamiltonian H_{bulk} acting on qudits in $\mathbb{H}^d$ for $d = 2, 3$, we can construct its dual Hamiltonian H_{boundary} on a $d-1$ boundary manifold $\mathcal{M} \in \mathbb{H}^d$ with the following properties:*

1. *All relevant physics of H_{bulk} are arbitrarily well approximated by H_{boundary}, including its eigenvalue spectrum, partition function and time dynamics.*

2. *The boundary Hamiltonian is 2-local, acting on nearest neighbour boundary qubits, realising a mapping between models.*

3. *Any local observable/measurement M in the bulk has a set of corresponding observables/measurements $\{M'\}$ on the boundary with the same outcome. A local bulk operator M can be reconstructed on a boundary region A if M acts within the greedy entanglement wedge of A, denoted $\mathcal{E}[A]$.*[5]

The HQECC we construct also inherits the entanglement properties of [106]. So, while the Ryu-Takayanagi formula is not obeyed exactly, we can derive entropy bounds which demonstrate that in most cases the corrections to the Ryu-Takayanagi formula are small.

This result allows us to extend toy models of holographic duality such as [106, 109, 110, 111] to include a mapping between local Hamiltonians. In doing so we show that the expected relationship between bulk and boundary energy scales can be realised by local boundary models. In particular, in our construction toy models of static black holes (as originally proposed in [106]) correspond to high-energy states of the local boundary model, as would be expected in AdS/CFT.

[4] A 'quasi' local Hamiltonian is a generalisation of a local Hamiltonian that allows for the possibility of gravitational Wilson lines - see subsection 7.4.1.6 for a rigorous definition.

[5] The entanglement wedge, $\mathcal{E}_A$ is a bulk region constructed from the minimal area surface used in the Ryu-Takayanagi formula. It has been suggested that on a given boundary region, A, it should be possible to reconstruct all operators which lie in $\mathcal{E}_A$ [123]. The greedy entanglement wedge is a discretised version defined in [106, Definition 8]

Moreover, in our toy model we can say something about how dynamics in the bulk correspond to dynamics on the boundary. Even without writing down a specific bulk Hamiltonian, we are able to demonstrate that a bulk evolution which is evocative of the formation of a (toy model) static black hole corresponds to the boundary unitarily evolving to a state outside of the code space of the HQECC, as expected in AdS/CFT (see subsection 7.6.3 for details).

Finally, the Hamiltonian simulation construction allows us to derive the mapping in the other direction. Given any local boundary Hamiltonian, one can derive a corresponding bulk Hamiltonian using rigorous formulations of perturbation theory. Constructing boundary-to-bulk mappings is an important goal of full AdS/CFT, where the boundary CFT is better understood, and one of the aims is to understand properties of quantum gravity in the bulk which are less well understood. Our results are a small step in this direction, though as emphasised above they are still a very long way from a full AdS/CFT model.

7.2.2 Proof overview

7.2.2.1 3D/2D duality

To construct the 3D/2D duality between Hilbert spaces, observables and local Hamiltonians described by Theorem 78, we combine new tensor network constructions of HQECC inspired by [106], with the perturbative simulation techniques from [6], outlined in Chapter 1.

We use perturbation gadget methods to show that the highly non-local Hamiltonian that results from mapping a bulk Hamiltonian to the boundary using tensor network constructions, can be approximated to arbitrarily high accuracy as the emergent, low-energy effective Hamiltonian arising from a two-body, nearest-neighbour, local Hamiltonian on the boundary. The Hamiltonian simulation theory developed in [6] allows us to prove that this approximates the entire physics of the bulk.

[106] constructs a HQECC by building a tensor network composed out of perfect tensors, arranged in a tessellation of hyperbolic 2-space by pentagons. This gives a map from 2D bulk to 1D boundary. However, the perturbative Hamiltonian simulation constructions of [6] only work in 2D or higher, which means we require at least a 3D bulk and 2D boundary.[6] We must therefore generalise the holographic tensor network codes to a space with a $\geq$ 2D boundary – so a $\geq$ 3D bulk – as a first step. As it is the smallest dimension in which the perturbative simulations work, we focus

[6]The simulation techniques from [6] cannot be used in 1D as they require a 2D interaction graph. See Appendix D.1 for details of the interaction graphs involved.

on constructing explicit 3D/2D dualities. But the techniques we have developed readily extend to any boundary dimension ≥ 2. When working in $\mathbb{H}^2$ it is possible to use the Poincare disc model to visualise the tessellations and determine their properties. However, in $\mathbb{H}^3$ this is more difficult, and generalising the HQECC to 3D and higher requires a more systematic approach. We use hyperbolic Coxeter groups[7] to analyse honeycombings (higher-dimensional tessellations) of $\mathbb{H}^3$. (These techniques also generalise beyond 3D.) A Coxeter system is a pair (W, S), where W is a group, generated by a set $S \subset W$ of involutions, subject only to relations of the form $(s_i s_j)^{m_{ij}} = 1$ where $m_{ii} = 1$, $m_{ij} \in (\mathbb{N} \setminus 1) \cup \{\infty\}$ for $i \neq j$. Coxeter groups admit a geometric representation as groups generated by reflections. Associated to every hyperbolic Coxeter system is a Coxeter polytope $P \subseteq \mathbb{H}^d$, where P tessellates $\mathbb{H}^d$. All of the properties of the tessellation can be determined directly from the Coxeter system (W, S) using combinatorics of Coxeter groups. For example, we use the Coxeter relations to prove that the boundary of the HQECC is homeomorphic to the Euclidean 2-sphere.

Generalising the method in [106], we construct tensor networks by taking a Coxeter system (W, S) with Coxeter polytope $P \subseteq \mathbb{H}^3$, and placing perfect tensors in each polyhedral cell of (a finite portion of) the tessellation of $\mathbb{H}^3$ by P. Each perfect tensor in the interior of the tessellation has one free index, corresponding to a bulk qudit; the other indices are contracted with neighbouring tensors. Tensors at the outer edge can be shown, again using the Coxeter relations, to have between $\lceil \frac{t}{2} \rceil$ and $t-2$ additional free indices (where the perfect tensor has a total of t indices), which correspond to qudits on the boundary. We can show that if the tessellation of $\mathbb{H}^3$ associated to a Coxeter system (W, S) has the properties required for a HQECC, then the associated Coxeter polytope P has at least 7 faces, which means we require perfect tensors with at least 8 indices. There are no qu*b*it perfect tensors with ≥ 6 indices [124, 125, 126], so we must use qu*d*it perfect tensors.

In order to later generate a local boundary model using perturbation gadgets, we need the tensor network to preserve the Pauli rank of operators. (As we are working with qudits rather than qubits, we mean *generalised* Pauli operators on qu*d*its, rather than qubit Paulis, and we choose prime-dimensional qudits.) We use perfect tensors which describe qudit stabilizer absolutely maximally entangled states (AMES), constructed via the method in [127] from classical Reed-Solomon codes. Using properties of

[7]Coxeter groups were previously used in [111] to describe tensor networks in $\mathbb{H}^2$ for toy models of holographic dualities.

stabilizer groups, we show that tensor networks composed of these qudit stabilizer perfect tensors preserve the generalised Pauli rank of operators.

This Coxeter polytope qudit perfect tensor network gives a HQECC in $\mathbb{H}^3$. The non-local boundary Hamiltonian is given by $H'_{\text{boundary}} = H' + \Delta_S H_S$, where H_S is zero on the code-subspace of the HQECC and at least one on its orthogonal complement, V is the encoding isometry of the HQECC and H' satisfies $VH_{\text{bulk}}V^\dagger = H'\Pi_C = H'VV^\dagger$.[8] Comparing with the classification of Hamiltonian simulations in [6], this mapping is an example of a simulation. (In fact, a perfect simulation in the terminology of [6].)

In order to construct a local boundary Hamiltonian we first determine the distribution of Pauli weights of the terms in H'_{boundary} from the properties of the Coxeter system. We then use perturbation gadgets to reduce the boundary Hamiltonian to a 2-local planar Hamiltonian. This requires introducing a number of ancilla qudits in the boundary system. The techniques we use follow the methods from [28], however the perturbation gadgets derived in [28] can't be used in our construction as the generalised Pauli operators aren't Hermitian. Instead we derive new qudit perturbation gadgets. These gadgets meet the requirements in [6, 31] to be perturbative simulations. Finally we use simulation techniques from [6] to simulate the planar 2-local qudit Hamiltonian with a qubit Hamiltonian on a triangular lattice with full local SU(2) symmetry. (The full technical details and proof are given in subsection 7.4.1.6.)

7.2.2.2 2D/1D duality

For the 2D/1D duality we can re-use the tensor network construction of [106]. As in the 3D/2D case, mapping a (quasi) local bulk Hamiltonian through the tensor network leads to a non-local boundary Hamiltonian of the form $H'_{\text{boundary}} = H' + \Delta_S H_S$, where H_S is zero on the code-subspace of the HQECC and at least one on its orthogonal complement, V is the encoding isometry of the HQECC and H' satisfies $VH_{\text{bulk}}V^\dagger = H'\Pi_C = H'VV^\dagger$.

We can determine the distribution of Pauli weights of the terms in H'_{boundary} from the properties of the tessellation. We then use the "history-state simulation" method outlined in Chapter 2 in order to simulate H'_{boundary} with a 2-local nearest neighbour boundary Hamiltonian. In order to ensure that the scaling of the distance between the bulk qudits and the boundary qudits is reasonable, we use the construction from subsection 2.2.3.1 where the target Hamiltonian is encoded in a phase of the

[8] H'_{boundary} is not unique, as expected in AdS/CFT

simulator Hamiltonian. So, in the language of HQECC, H_{bulk} is encoded in a phase of H_{boundary}.

Unlike in the 3D/2D case there is no way to reduce the dimension of the boundary qudits, so the final H_{boundary} in the 2D/1D case is on high dimensional qudits, and has no local symmetry. (The full technical details and proof are given in Section 7.5.)

7.3 Technical preliminaries

7.3.1 Hyperbolic Coxeter groups

7.3.1.1 Coxeter systems

Two of the HQECC presented in this chapter are tensor networks embedded in tessellations of $\mathbb{H}^3$. We use Coxeter systems to analyse these tessellations.[9]

Definition 61 (Coxeter system [129])**.** *Let $S = \{s_i\}_{i\in I}$, be a finite set. Let $M = \left(m_{i,j}\right)_{i,j\in I}$ be a matrix such that:*

- $m_{ii} = 1$, $\forall i \in I$
- $m_{ij} = m_{ji}$, $\forall i, j \in I, i \neq j$
- $m_{ij} \in (\mathbb{N} \setminus \{1\}) \cup \{\infty\}$, $\forall i, j \in I, i \neq j$

M is called the Coxeter matrix. The associated Coxeter group, W, is defined by the presentation:[10]

$$W = \langle S \mid \left(s_i s_j\right)^{m_{ij}} = 1 \forall i, j \in I \rangle \tag{7.1}$$

The pair (W, S) is called a Coxeter system.

To understand the connection between Coxeter systems and tesselations of hyperbolic space we need to introduce the notion of a Coxeter polytope.

Definition 62. *A convex polytope in $\mathbb{X}^d = \mathbb{S}^d, \mathbb{E}^d$ or $\mathbb{H}^d$ is a convex intersection of a finite number of half spaces. A Coxeter polytope $P \subseteq \mathbb{X}^d$ is a polytope with all dihedral angles integer submultiples of π.*

A Coxeter system can be associated to every Coxeter polytope. Let $(F_i)_{i\in I}$ be the facets of P, and if $F_i \cap F_j \neq \emptyset$ set $m_{ij} = \frac{\pi}{\alpha_{ij}}$, where α_{ij} is the dihedral angle between F_i and F_j. Set $m_{ii} = 1$, and if $F_i \cap F_j = \emptyset$ set $m_{ij} = \infty$. Let s_i be the reflection in F_i. The

[9] An overview of hyperbolic Coxeter groups can be found at [128].

[10] A group presentation $\langle S \mid R \rangle$, where S is a set of generators and R is a set of relations between the generators, defines a group which is (informally) the largest group which is generated by S and in which all the relations in R hold.

Coxeter group with Coxeter matrix $(m_{ij})_{i,j\in I}$ is a discrete subgroup of $Isom(\mathbb{X}^d)$, generated by reflections in the facets of P, and P tiles $\mathbb{X}^d$ [130].

Coxeter systems can be represented by Coxeter diagrams, where a vertex is associated to every s_i (or equivalently to every facet in the corresponding Coxeter polytope). Vertices are connected by edges in the following manner:

- If $m_{ij} = 2$ (i.e. facets F_i and F_j in the Coxeter polytope are orthogonal) there is no edge between the vertices representing s_i and s_j
- If $m_{ij} = 3$ (i.e. the dihedral angle between F_i and F_j is $\frac{\pi}{3}$) there is an unlabelled edge between vertices representing s_i and s_j
- If $m_{ij} \in \mathbb{N} \setminus \{1, 2, 3\}$ (i.e. the dihedral angle between F_i and F_j is $\frac{\pi}{m_{ij}}$) there is an edge labelled with m_{ij} between vertices representing s_i and s_j
- If $m_{ij} = \infty$ (i.e. facets F_i and F_j in the Coxeter polytope diverge) there is a dashed edge between the vertices representing s_i and s_j

A Coxeter group is irreducible if its Coxeter diagram is connected.

Faces of P correspond to subsets of S that generate finite Coxeter groups:[11]

Lemma 63 (From [131]). *$f = \cup_{i\in I} F_i$ is a codimension $|I|$ face of P if and only if $\{s_i \mid i \in I\}$ generates a finite Coxeter group.*

7.3.1.2 Combinatorics of Coxeter groups

In this section we briefly introduce the notions which are used later in the chapter.

Let (W, S) be a Coxeter system. Every element $w \in W$ can be written as a product of generators:

$$w = s_1 s_2 ... s_k \text{ for } s_i \in S \tag{7.2}$$

This description is not unique. We can define a length function with respect to the generating set S such that $l_S(1) = 0$, and:

$$l_S(w) = \min\{l \in \mathbb{N} \mid s_1 s_2 ... s_l = w\} \tag{7.3}$$

An expression for w with the minimum number of generators, $s_1 s_2 ... s_{l_S(w)}$ is called a reduced word for w.

[11] This does not apply to ideal vertices (vertices at the boundary of $\mathbb{X}^d$) however in this work we are only concerned with compact polyhedra, which do not have vertices at infinity.

Coxeter groups satisfy the Deletion Condition:

Definition 64 (Deletion Condition)**.** *Let (W, S) be a pair where W is a group and S is a generating set for W consisting entirely of elements of order two. We say that this pair satisfies the Deletion Condition if for any non reduced word $s_1 \dots s_r$ over S there are two indices i and j such that:*

$$s_1 \dots s_r = s_1 \dots \hat{s}_i \dots \hat{s}_j \dots s_r \tag{7.4}$$

where the carets indicate omission.

The length function on Coxeter groups has a number of important properties:

1. $l_S(ws) = l_S(w) \pm 1$ for all $s \in S$
2. $l_S(sw) = l_S(w) \pm 1$ for all $s \in S$
3. $l_S(w^{-1}) = l_S(w)$ for all $w \in W$
4. $|l_S(u) - l_S(w)| \leq l_S(uw) \leq l_S(u) + l_S(w)$ for all $u, w \in W$
5. $d(u, w) = l_S(u^{-1}w)$ for $u, w \in W$ is a metric on W (referred to as the word metric)

By conditions (i) and (ii), if we define the following sets:

$$\begin{aligned} \mathcal{D}_R(w) &= \{s \in S \mid l_S(ws) = l_S(w) - 1\} \\ \mathcal{A}_R(w) &= \{s \in S \mid l_S(ws) = l_S(w) + 1\} \\ \mathcal{D}_L(w) &= \{s \in S \mid l_S(sw) = l_S(w) - 1\} \\ \mathcal{A}_L(w) &= \{s \in S \mid l_S(sw) = l_S(w) + 1\} \end{aligned} \tag{7.5}$$

then we have $\mathcal{D}_R(w) \cup \mathcal{A}_R(w) = \mathcal{D}_L(w) \cup \mathcal{A}_L(w) = S$ and $\mathcal{D}_R(w) \cap \mathcal{A}_R(w) = \mathcal{D}_L(w) \cap \mathcal{A}_L(w) = \{\}$. We refer to $\mathcal{D}_R(w)$ and $\mathcal{D}_L(w)$ ($\mathcal{A}_R(w), \mathcal{A}_L(w)$) as the right and left descent sets (ascent sets) of w respectively.

Lemma 65 (Corollary 2.18 from [132])**.** *For all $w \in W$, the Coxeter groups generated by $\mathcal{D}_R(w)$ and $\mathcal{D}_L(w)$ are finite.* [12]

The irreducible finite Coxeter groups are classified in Table 7.1. A general Coxeter group is finite if and only if each connected component of the Coxeter graph generates a finite group.

[12] All subsets of S generate a Coxeter group.

Name	Coxeter diagram
A_n $(n \geq 1)$	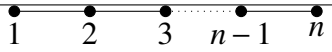
$B_n = C_n$ $(n \geq 3)$	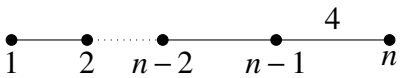
D_n $(n \geq 4)$	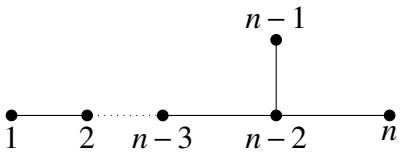
E_6	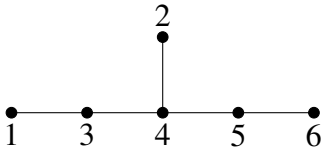
E_7	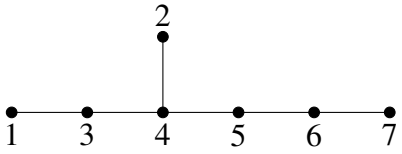
E_8	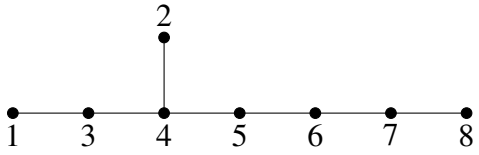
F_4	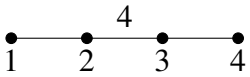
G_2	
H_3	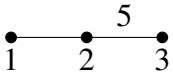
H_4	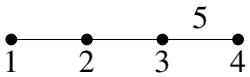
$I_2^{(m)}$ $(m \geq 3)$	

Table 7.1: Diagrams of irreducible finite Coxeter systems. Table reproduced from [133].

Finally, we note that if $s \in \mathcal{D}_R(w)$ ($s \in \mathcal{D}_L(w)$) there is a reduced word for w that ends in s (begins with s).

7.3.1.3 Growth rates of Coxeter groups

The growth series of a Coxeter group with respect to a set of generators S is defined as:

$$f_S(x) = \sum_{w \in W} x^{l_S(w)} = 1 + Sx + \ldots = 1 + \sum_{i \geq 1} a_i x^i \tag{7.6}$$

where a_i is the number of $w \in W$ satisfying $l_S(w) = i$. The growth rate is given by:

$$\tau = \limsup_{n \to \infty} \sqrt[i]{a_i} \tag{7.7}$$

Spherical and Euclidean Coxeter groups have growth rate 0 and 1 respectively. Hyperbolic Coxeter groups have $\tau > 1$.

7.3.2 Perturbative simulations using qudits

We derive a number of qudit perturbation gadgets (based on qubit perturbation gadgets from [28]) for use in our 3D/2D construction. Using the second and third order simulation lemmas from Chapter 1 (Lemmas 19 and 20 respectively) we can show that all of these gadgets are simulations (for appropriate choices of Δ). Details are given in Appendix D.1. The main results are collected here:

Qudit subdivision gadget

The qudit subdivision gadget is used to simulate a k-local interaction by two $\lceil \frac{k}{2} \rceil + 1$-local interactions, by introducing a mediator qudit. The resulting interaction pattern is shown in Fig. 7.1.

Figure 7.1: Subdivision gadget. Let A and B be sets of $\frac{k}{2}$ qudits. The k-local interaction on the left is simulated by the two $\lceil \frac{k}{2} \rceil + 1$-local interactions on the right by introducing a mediator qudit, w. The interactions are given by $M_1 = P_A \otimes P_B + P_A^\dagger \otimes P_B^\dagger$, $M_2 = P_A \otimes X_w + P_A^\dagger \otimes X_w^\dagger$, and $M_3 = P_B \otimes X_w^\dagger + P_B^\dagger \otimes X_w$.

Qudit 3-2 gadget

The 3-2 gadget is used to simulate a 3-local interaction with six 2-local interactions, by introducing a mediator qudit. The resulting interaction pattern is shown in Fig. 7.2.

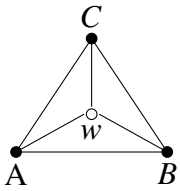

Figure 7.2: 3-2 gadget: A three body interaction between A, B and C $\left(P_A \otimes P_B \otimes P_C + P_A^\dagger \otimes P_B^\dagger \otimes P_C^\dagger\right)$ is simulated by the interaction pattern shown in the figure.

Qudit crossing gadget

The crossing gadget is used to remove crossings in an interaction graph by introducing a mediator qudit. The resulting interaction pattern is shown in Fig. 7.3.

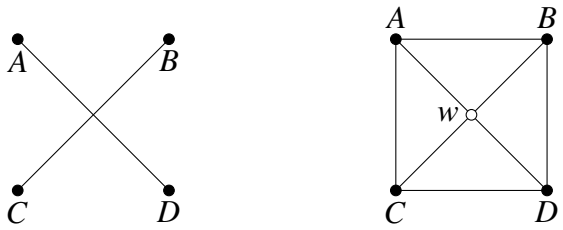

Figure 7.3: Crossing gadget. The interaction pattern on the left is simulated by the interaction pattern on the right.

Qudit fork gadget

The fork gadget is used to reduce the degree of a vertex in the interaction graph by introducing a mediator qudit. The resulting interaction pattern is shown in Fig. 7.4.

Figure 7.4: Fork gadget. The interaction pattern on the left is simulated by the interaction pattern on the right.

Qudit triangle gadget

The qudit triangle gadget is formed by first applying the qudit subdivision gadget, then the qudit fork gadget, in the same way as it is formed for qubits in [28].

Figure 7.5: Triangle gadget. The interaction pattern on the left is simulated by the interaction pattern on the right by first applying the subdivision gadget to edges AB and AC, and then applying the fork gadget to qudit A.

The 3-2 gadget is a third order simulation. The other gadgets are second order simulations.

In [28] it is demonstrated that the qubit perturbation gadgets can be used at many places in an interaction graph in parallel, and that they do not interact with each other. The same arguments follow for the qudit perturbation gadgets introduced here.

7.4 Technical details of the $3D-2D$ construction

7.4.1 General construction

In this section we demonstrate the general procedure for constructing a HQECC using Coxeter groups and (pseudo-)perfect stabilizer tensors with particular properties. In particular in subsection 7.4.1.6 we prove our main result: a holographic duality between quantum many-body models in 3D hyperbolic space and local models living on its 2D boundary. In subsections 7.4.2 and 7.4.3 we construct two examples of sets of Coxeter groups and tensors which have the required properties.

7.4.1.1 Notation

Let (W,S) be a Coxeter system with Coxeter polytope $P \subseteq \mathbb{H}^3$. F_a denotes the face of P corresponding to the generator $s_a \in S$. E_{ab} denotes the edge of P between F_a and F_b.

$P^{(w)}$ denotes the polyhedral cell in the tessellation of $\mathbb{H}^3$ which corresponds to element w of the Coxeter group. Similarly $F_a^{(w)}$ and $E_{ab}^{(w)}$ refer to faces / edges of $P^{(w)}$. F_a^A and E_{ab}^A refer to specific faces / edges in the tessellation of $\mathbb{H}^3$ which are shared by the polyhedral cells associated to the sets of elements $A \subseteq W$.

A bulk qudit which is associated to the polyhedral cell $P^{(w)}$ will be labelled by $q^{(w)}$. A boundary qudit which is associated to the uncontracted tensor index through the face $F_a^{(w)}$ will be labelled by $q_a^{(w)}$.

7.4.1.2 Holographic quantum error correcting codes

The procedure we use to construct the tensor network is based on that in [106], where perfect tensors are embedded in tessellations of $\mathbb{H}^2$. We take a Coxeter system (W,S) with Coxeter polytope, $P \subseteq \mathbb{H}^3$ where $|S| = t-1$, so P has $t-1$ faces. Take the tessellation of $\mathbb{H}^3$ by P, and embed a (pseudo-)perfect tensor, T, with t legs in each polyhedral cell. $t-1$ legs of each tensor are contracted with legs of neighbouring tensors at shared faces of the polyhedra, and a logical, or input, qudit for the tensor network is associated with the uncontracted tensor leg in each polyhedral cell. Cut off the tessellation at some radius R, and the uncontracted tensor legs on the boundary are the physical qudits of the tensor network.

A HQECC is defined as a tensor network composed of (pseudo)-perfect tensors which gives rise to an isometric map from bulk legs to boundary legs [106]. This is equivalent to requiring that the number of output indices from every tensor is greater than or equal to the number of input indices, where the input indices are the indices coming from the previous layer of the tessellation plus the logical index.

We are working in negatively curved geometry, so a majority of the tensors will have more output indices than input indices, but this doesn't guarantee it is true for every tensor. For example, consider the triangulation of $\mathbb{H}^2$ with Schläfli symbol $\{3,8\}$ (Fig. 7.6). This is the tiling which corresponds to the Coxeter diagram shown in Fig. 7.7.

It can be seen that there are triangular cells in the tessellation which share edges with two triangles from the previous layer, and only one in the subsequent layer. If we put a four-index perfect tensor in each cell of this tessellation, then there would be some tensors with three input legs, and only one output leg. These tensors would not be isometries, so it is not obvious that the overall tensor network would be an isometry. In order to ensure that the tensor network is a HQECC we derive a condition to enforce that every tensor has at least as many output indices as input indices. This is a sufficient condition for the tensor network to be a HQECC, but it may not be necessary.

Theorem 66. *Consider a tensor network constructed as above, defined by Coxeter system* (W,S) *and perfect tensor* T *with* t *indices. Define* $\mathcal{F} = \{J \subseteq S \mid W_J \text{ is finite}\}$. *The tensor network will be a HQECC, if* $\forall J \in \mathcal{F} : |J| \leq \left\lfloor \frac{t-2}{2} \right\rfloor$.

Proof. If we order the tensors into layers labelled by the value of the length function $l_S(w)$ at $P^{(w)}$, and include the uncontracted tensor leg in each polyhedral cell as an

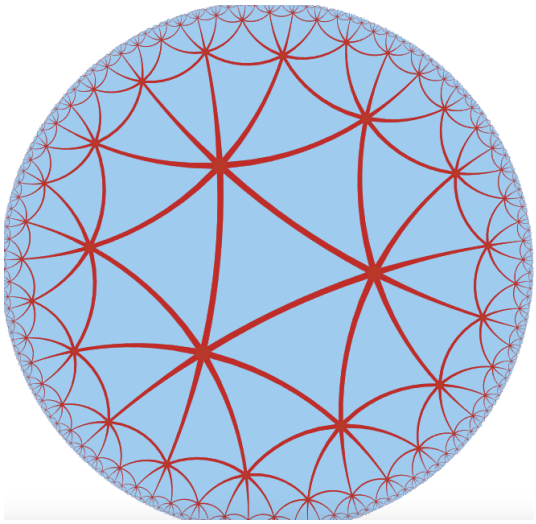

Figure 7.6: The triangulation of $\mathbb{H}^2$ with Schläfli symbol $\{3,8\}$. There are triangular cells in the tessellation which share edges with two triangles from the previous layer, and only one in the subsequent layer. Figure produced via the software [134].

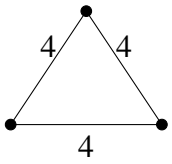

Figure 7.7: The Coxeter diagram for the triangulation of $\mathbb{H}^2$ with Schläfli symbol $\{3,8\}$

input leg, then the number of input legs for a tensor embedded in $P^{(w)}$ is $\mathcal{D}_R(w)+1$. By Lemma 65, $\mathcal{D}_R(w) \in \mathcal{F}$. Therefore the maximum number of input legs to any tensor in the tensor network is $\max(|J| \mid J \in \mathcal{F})+1$. We therefore require $\max(|J| \mid J \in \mathcal{F})+1 \leq \lfloor \frac{t}{2} \rfloor$. □

Theorem 66 gives a sufficient condition for every tensor in the tensor network to have at least as many output indices as input indices.

The requirements of Theorem 66 dictate that we will not be able to use qubit stabilizer tensors to construct HQECC in dimensions greater than two. To see this recall that Lemma 63 stated that $\{s_i \mid i \in I\}$ generates a finite Coxeter group if and only if $f = \cup_{i \in I} F_i$ is a codimension $|I|$ face of P. In dimension d there will exist codimension d faces, so $\max(|J| \mid J \in \mathcal{F}) \geq d$. We therefore require that $\lfloor \frac{t}{2} \rfloor \geq d+1$. For $d \geq 3$ this enforces $t \geq 8$, and there are no qubit perfect tensors with $t > 6$ [124, 125, 126].

HQECC which are constructed in this way inherit all the properties of the 2-dimensional HQECC constructed in [106].

We call HQECC constructed in this way from Coxeter honeycombings and perfect tensors "Coxeter HQECCs".

7.4.1.3 Surface of the HQECC

Define the boundary of the HQECC as the faces in the tessellation which correspond to the uncontracted tensor legs. More precisely:

Definition 67. *The boundary, M, of a Coxeter HQECC of radius R is given by:*

$$M = \bigcup_{F_a^{(w)} \in \mathcal{M}} F_a^{(w)} \tag{7.8}$$

where $\mathcal{M} = \{F_a^{(w)} \mid l_S(w) = R, s_a \in \mathcal{A}_R(w)\}$.

The boundary of hyperbolic n-space is an $n-1$ dimensional sphere. For our HQECC we are cutting off the tessellation of $\mathbb{H}^3$ at some finite radius R, but it is still possible to demonstrate that the boundary is homeomorphic to a 2-sphere.

In order to reason about the boundary we need two lemmas about edges in the tessellation of $\mathbb{H}^3$ by P:

Lemma 68. *Consider an edge, E_{ab}^A, in the tessellation of $\mathbb{H}^3$ by a Coxeter polytope, P. If $l_S(w_1) = l_S(w_2) = L$ for distinct $w_1, w_2 \in A$, then $\mathcal{D}_R(w_1)$ and $\mathcal{D}_R(w_2)$ contain at least one of s_a or s_b.*

Proof. Recall that an edge E_{ab} corresponds to the finite Coxeter subgroup generated by s_a and s_b: $\langle s_a, s_b\rangle = \{\langle s_a, s_b\rangle^x | x \in [0, m_{ab})\}$, where $\langle s_a, s_b\rangle^x$ denotes a string of alternating s_a and s_b of length x. A is set of Coxeter group elements corresponding to the polyhedra that meet at the common edge E_{ab}^A, so $A = \{ws | s \in \langle s_a, s_b\rangle\}$ for any fixed element $w \in A$. Therefore, we have that $w_2 = w_1\langle s_a, s_b\rangle^x$ for some $x \in [1, m_{ab})$; we take x to be the minimum such value. Since $l_S(w_1\langle s_a, s_b\rangle^x) = l_S(w_2) + x > l_S(w_2)$, the deletion condition (Definition 64) implies that there are two generators in the word $w_1\langle s_a, s_b\rangle^x$ which we can delete to get a shorter word for w_2.

By minimality of x, they cannot both be deleted from the $\langle s_a, s_b\rangle^x$ part of this word. If they were both deleted from the w_1 part, so that $w_2 = s_1 \dots \hat{s}_i \dots \hat{s}_j \dots s_L \langle s_a s_b\rangle^x$, we would have $w_1 = w_2(\langle s_a, s_b\rangle^x)^{-1} = w_2\langle s_b, s_a\rangle^x = s_1 \dots \hat{s}_i \dots \hat{s}_j \dots s_L$ which has length $L-2$, contradicting $l_S(w_1) = L$. Therefore, one generator must be deleted from the w_1 part, the other from $\langle s_a, s_b\rangle^x$. Thus $w_2 = s_1 \dots \hat{s}_i \dots s_r \langle s_a, s_b\rangle^{x-1}$.

This word for w_2 has length $L + x - 2$. By the deletion condition, we must be able to delete a further $x-2$ generators to reach a reduced word for w_2. But $\langle s_a, s_b\rangle^{x-1}$

contains $x-1$ generators, so at least one of these must remain. Thus either $w_2 = us_a$ or $w_w = us_b$ for some $u \in A$ of length $l_S(u) = L-1$. Hence at least one of s_a or s_b is in $\mathcal{D}_R(w_2)$.

The w_1 case follows by an analogous argument. □

Lemma 69. *Consider an edge, E^A_{ab}, in the tessellation of $\mathbb{H}^3$ by a Coxeter polytope, P. The set of elements A associated with the polyhedral cells that share the edge E^A_{ab} has the following properties:*

1. *There is a unique minimum length element $w_{\min} \in A$ which has length, $l_S(w_{\min}) = r_{\min}$.*
2. *For $0 \leq x < m_{ab}$, $l_S(w_{\min}\langle s_a, s_b\rangle^{x+1}) = l_S(w_{\min}\langle s_a, s_b\rangle^{x}) + 1$.*
3. *For $m_{ab} \leq x < 2m_{ab}$, $l_S(w_{\min}\langle s_a, s_b\rangle^{x+1}) = l_S(w_{\min}\langle s_a, s_b\rangle^{x}) - 1$.*
4. *There is a unique maximum length element $w_{\max} \in A$ which has length $l_S(w_{\max}) = r_{\min} + m_{ab}$.*
5. *For $r_{\min} < i < r_{\min} + m_{ab}$ there are exactly two elements $w_i, w'_i \in A$ which satisfy $l_S(w_i) = l_S(w'_i) = i$.*

where $\langle s_a, s_b\rangle^x$ denotes a string of alternating s_a and s_b of length x (i.e. $\langle s_a, s_b\rangle^3 = s_a s_b s_a$).

Proof of Lemma 69. 1. Assume there are two minimum length elements in A, $w_{\min}$ and $w'_{\min}$ such that $l_S(w_{\min}) = l_S(w'_{\min}) = r_{\min}$. By Lemma 68 either s_a or s_b is in the descent set of $w_{\min}$ and $w'_{\min}$. This implies that there is at least one element in A with length $r_{\min} - 1$, contradicting our assumption.

2. Assume there is some $x < m_{ab}$ such that $l_S(w_{\min}\langle s_a, s_b\rangle^{x+1}) = l_S(w_{\min}\langle s_a, s_b\rangle^{x}) - 1 = L$. If we let $u = w_{\min}\langle s_a, s_b\rangle^{x+1}$ and assume (wlog) that x is even, it follows that $s_a \in \mathcal{A}_R(u)$. Note that $l_S(w_{\min}) = r_{\min} < L$, $l_S(w_{\min}\langle s_a, s_b\rangle^{x}) = L+1$ and $l_S(w_{\min}\langle s_a, s_b\rangle^{x+1}) = L$. But each generator s_a or s_b that we multiply $w_{\min}$ by can only change the length by ± 1. So u is not the only element of length L in A. By Lemma 68 this implies that at least one of s_a or s_b must be in the descent set of u. Therefore $s_b \in \mathcal{D}_R(u)$.

If we let $v = us_b$ then $s_b \in \mathcal{A}_R(v)$. By a similar argument, $s_a \in \mathcal{D}_R(v)$. If we continue this argument we find that the length of the element $w_{\min}\langle s_a, s_b\rangle^{2x}$ is $r_{\min}$, which is not possible as $w_{\min}$ is the unique element of A with length $r_{\min}$, and by

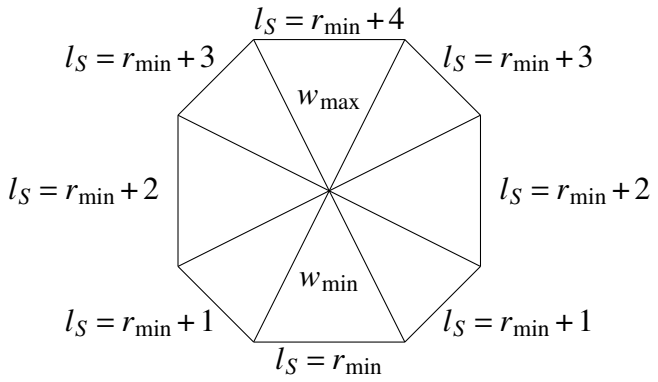

Figure 7.8: A cross section view of the polyhedral cells in the tessellation which meet around a common edge, E_{ab}, for $m_{ab} = 4$.

assumption $x < m_{ab}$ so $\langle s_a, s_b\rangle^{2x} = (s_a s_b)^x \neq I$ by definition of m_{ab}. Therefore there is no $x < m_{ab}$ such that $l_S(w_{\min}\langle s_a, s_b\rangle^{x+1}) = l_S(w_{\min}\langle s_a, s_b\rangle^x) - 1 = L$.

3. From 2 it follows that $l_S(w_{\min}\langle s_a, s_b\rangle^{m_{ab}}) = r_{\min} + m_{ab}$. We have that $\langle s_a, s_b\rangle^{2m_{ab}} = (s_a s_b)^{m_{ab}} = I$, thus $l_S(w_{\min}\langle s_a, s_b\rangle^{2m_{ab}}) = l_S(w_{\min}) = r_{\min}$. As each generator can only change the length of an element by ± 1, for $m_{ab} < x \leq 2m_{ab}$ we must have that $l_S(w_{\min}\langle s_a, s_b\rangle^{x+1}) = l_S(w_{\min}\langle s_a, s_b\rangle^x) - 1$.

4 and 5 follow at once from points 2 and 3. □

An example of the set of polyhedra associated with an edge E_{ab} where $m_{ab} = 4$ is shown in Fig. 7.8. Lemma 69 ensures that the lengths associated to the polyhedra around any edge follow the same pattern.

We can now consider the boundary of the HQECC.

Lemma 70. *The boundary M of a Coxeter HQECC in $\mathbb{H}^3$ is a piecewise linear surface.*

Proof. Within the faces that make up the boundary M is clearly locally Euclidean, and the same will be true at the edges where the faces meet provided no more than two faces meet at an edge. Point (v) from Lemma 69 shows this is indeed the case. □

Lemma 71. *The boundary manifold, M, of a Coxeter HQECC in $\mathbb{H}^3$ is closed - i.e. compact and with no boundary.*

Proof. Assume M has a boundary. This implies that $\exists w \in W$ such that $l_S(w) = R$ where $F_a^{(w)} \in M$ and $E_{a,b}^{(w)} \in \partial M$.

Since $E_{a,b}$ is an edge of P we must have that $\{s_a, s_b\} \in \mathcal{F}$ where $\mathcal{F} = \{J \subseteq S | W_J \text{ is finite}\}$. This implies that $\exists m_{ab} \in \mathbb{N} \setminus \{1\}$ such that $(s_a s_b)^{m_{ab}} = (s_b s_a)^{m_{ab}} = I$.

$E^{(w)}_{a,b} \in \partial M$ implies that $F^{(w)}_b \notin M$, and therefore $s_b \in \mathcal{D}_R(w)$. This gives $w = us_b$ where $u \in W$ and $l_S(u) = R-1$. We also have that $l_S(ws_a) = l_S(us_b s_a) = R+1$ (because by assumption $s_a \in \mathcal{A}_R(w)$).

Putting everything together we find that:

$$l_S(u) = R-1 \tag{7.9}$$

$$l_S(us_b s_a) = R+1 \tag{7.10}$$

$$l\left[u(s_b s_a)^{m_{ab}}\right] = l_S(u) = R-1 \tag{7.11}$$

Therefore, at least one of the following must be true:

1. $\exists x$ such that $1 \leq x < m_{ab}$ where $l[u(s_b s_a)^x] = R+1$ and $l[u(s_b s_a)^x s_b] = R$
2. $\exists x$ such that $1 \leq x < m_{ab}$ where $l[u(s_b s_a)^x s_b] = R+1$ and $l[u(s_b s_a)^{x+1}] = R$

The second case would imply that $l[u(s_b s_a)^x s_b] = R+1 = l_S(us_b s_a)$ but this cannot occur as it is not possible for two elements of the Coxeter group with the same word length to be related by an odd number of generators. If the first case occurs then $F^{(b)}_v \in M$ for $v = u(s_b s_a)^x s_b$ and shares edge E_{ab} with $F^{(a)}_w$, so $E^{(w)}_{ab} \notin \partial M$.

Therefore M does not have a boundary. The boundary of every polyhedron face is included in M so M is compact. □

We now prove that the boundary surface is orientable. A smooth surface is orientable if a continuously varying normal vector can be defined at every point on the surface. This normal vector defines the positive side of the surface (the side the normal vector is pointing to) and a negative side (the side the normal vector points away from). If the surface has a boundary, the normal vector defines an *orientation* on the boundary curve, with the following convention: standing on the positive side of the surface, and walking around the boundary curve in the direction of the orientation, the surface is always on our left.

Lemma 72. *The boundary surface, M, of a Coxeter HQECC in* $\mathbb{H}^3$ *is orientable.*

Proof. A piecewise smooth manifold (such as M) is orientable if, whenever two smooth component surfaces join along a common boundary, they induce *opposite* orientation on the common boundary.

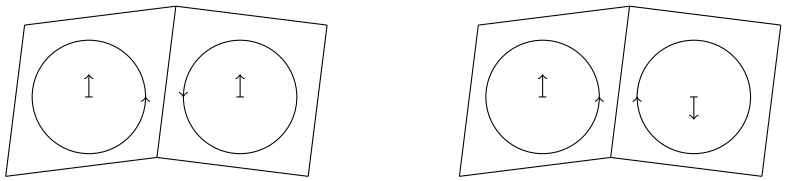

(a) (b)

Figure 7.9: A cross section image of two possibilities for the orientation of faces that meet at a common edge in M. In (a) the two faces will induce opposite orientation on the common edge E, while in (b) the two faces will induce the same orientation on the common edge E.

Define the unit normal vector, $\hat{n}$, to a face $F_a^{(w)} \in M$ to point away from $P^{(w)}$ (i.e. it points into $P^{(v)}$ where $v = ws_A$).

Consider the two possible configurations that could occur when two faces meet at a common edge. If the two faces always induce opposite orientation on the common edge (as in Fig. 7.9 (a)) then M is orientable. If the two faces ever induce the same orientation on the common edge (as in Fig. 7.9 (b)) then M is not orientable.

If two faces which meet at a common edge of M are part of the same polyhedral cell of the tessellation, i.e. they are faces $F_a^{(u)}$ and $F_b^{(u)}$, then it is guaranteed that the orientation of the surfaces will correspond to that shown in Fig. 7.9 (a) as $\hat{n}$ is defined to point away from $P^{(u)}$.

If two faces which meet at a common edge of M are part of different polyhedral cells then parts (ii) and (iii) of Lemma 69 enforce that the orientation of the surfaces will always correspond to that shown in Fig. 7.9 (a).

Therefore M is orientable. □

Lemma 73. *The boundary surface, M, of a Coxeter HQECC in $\mathbb{H}^3$ is connected.*

Proof. Let the boundary surface, M be a sum of connected components, where we denote the i^{th} connected component by $M^{(i)}$. M is closed and orientable so by the classification of surface theorem it is the sum of spheres and connected sums of tori. Both spheres and tori have well defined interiors and exteriors, so we can define the interior and exterior of each $M^{(i)}$.

Define the interior of $M^{(i)}$ to be the region that $\hat{n}^{(i)}$ points away from (i.e. the interior of $M^{(i)}$ contains $P^{(u)}$ for $F_a^{(u)} \in M^{(i)}$, $l_S(u) = R$). The exterior of $M^{(i)}$ is then the

region that $\hat{n}^{(i)}$ points into to (i.e. the exterior of $M^{(i)}$ contains $P^{(v)}$ for $v = us_a$ where $F_a^{(u)} \in M^{(i)}$, $l_S(v) = R+1$).

It follows from this definition that the exterior of each $M^{(i)}$ must be unbounded. To see this, note that for an infinite Coxeter group, W, every $w \in W$ has a non-empty $\mathcal{A}_R(w)$. This means that for arbitrary $w \in W$ there exists $s_a \in S$ such that $l_S(ws_a) = l_S(w)+1$. In terms of the HQECC this implies that the number of polyhedra in the exterior of any $M^{(i)}$ is infinite, so the exterior of $M^{(i)}$ is unbounded.

Assume that $M = \cup_i M^{(i)}$ is composed of more than one connected component $M^{(i)}$. Consider any two components $M^{(1)}$ and $M^{(2)}$. There are three possible configurations:

1. $M^{(1)}$ and $M^{(2)}$ intersect.
2. $M^{(2)}$ is in the interior of $M^{(1)}$ (see Fig. 7.10).
3. $M^{(2)}$ is in the exterior of $M^{(1)}$ (see Fig. 7.11).

However, Case 1 would imply that M is not a surface, contradicting Lemma 70. Thus we only need to consider Cases 2 and 3.

The Coxeter group, and therefore the HQECC, contains a unique identity element of length $l_S(I) = 0$. For any $v \in W$ such that $l_S(v) = R$ we can write a reduced word for v as $v = s_1^{(v)} s_2^{(v)} \ldots s_R^{(v)}$. Using the fact that all the generators are involutions, it follows that $v s_R^{(v)} \ldots s_2^{(v)} s_1^{(v)} = I$. We started with an element of length R, and applied R generators to reach an element of length 0. Since each generator can only change the length of the previous element by ± 1 it follows that each generator must have decreased the length of the element by 1. Therefore in the HQECC there is a path through the tessellation from a polyhedra associated with an element of length R to $P^{(I)}$ which passes through R polyhedra, all associated with elements of length less than R.

From the definition of the interior and exterior of $M^{(i)}$ it is clear that all polyhedra which lie directly on the interior of a given $M^{(i)}$ (i.e. those that are in the interior of $M^{(i)}$ and touching $M^{(i)}$) are associated with Coxeter group elements of length R. While all polyhedra which lie directly on the exterior of a given $M^{(i)}$ (i.e. those that are in the exterior of $M^{(i)}$ and touching $M^{(i)}$) are associated with Coxeter group elements of length $R+1$.

Therefore there must always be a path from polyhedra directly on the interior of a $M^{(i)}$ to $P^{(I)}$ which doesn't cross $M^{(i)}$. In Fig. 7.10 and Fig. 7.11 it is clear that there

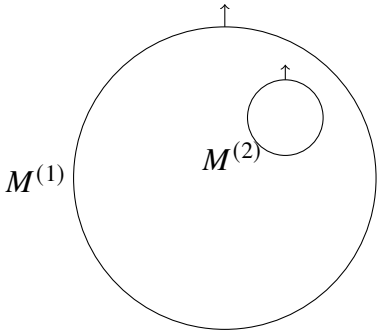

Figure 7.10: The configuration of $M^{(1)}$ and $M^{(2)}$ when $M^{(2)}$ is in the interior of $M^{(1)}$. The arrows are the $\hat{n}^{(i)}$ which point into the exterior of each surface. The polyhedra which lie directly on the interior of a given $M^{(i)}$ are associated with Coxeter group elements of length R, while the polyhedra which lie directly on the exterior of a given $M^{(i)}$ are associated with elements of length $R+1$. Although we have drawn $M^{(1)}$ and $M^{(2)}$ as circles we are not assuming they are spherical, they could be tori, all we are assuming is that they have a well defined interior and exterior.

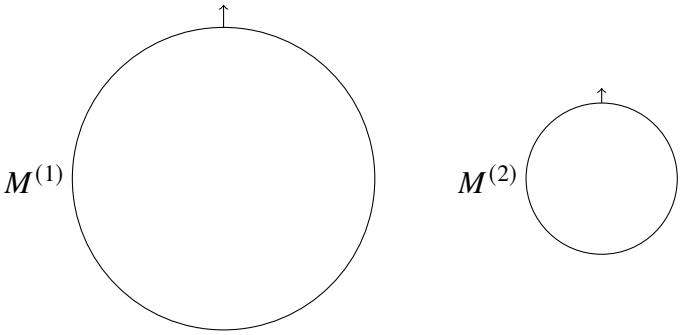

Figure 7.11: The configuration of $M^{(1)}$ and $M^{(2)}$ when $M^{(2)}$ is in the exterior of $M^{(1)}$. The arrows are the $\hat{n}^{(i)}$ which point into the exterior of each surface. The polyhedra which lie directly on the interior of a given $M^{(i)}$ are associated with Coxeter group elements of length R, while the polyhedra which lie directly on the exterior of a given $M^{(i)}$ are associated with Coxeter group elements of length $R+1$. Although we have drawn $M^{(1)}$ and $M^{(2)}$ as circles we are not assuming they are spherical, they could be tori, all we are assuming is that they have a well defined interior and exterior.

is no location for $P^{(I)}$ which meets this condition. Therefore M cannot be made up of more than one connected component. □

Lemma 74. *The boundary surface, M, of a Coxeter HQECC in $\mathbb{H}^3$ is homeomorphic to the 2-sphere.*

Proof. By the classification theorem of closed surfaces, every connected closed surface is homeomorphic to either the sphere, a connected sum of tori, or a connected

sum of real projective planes. Since M is orientable, it is either homeomorphic to a sphere, or a connected sum of tori.

Consider a loop C, on the surface M. This loop is across faces which make up M, which are all associated to polyhedral cells of the tessellation corresponding to Coxeter group elements of length R. Since M is closed (Lemma 71), it cannot pinch down to a single point anywhere. Thus for any polyhedral vertex in M, M must contain at least two faces that meet along one of the edges touching that vertex. Any loop which passes between adjacent faces which only touch via a common vertex can therefore be continuously deformed into a nearby loop which passes through those faces. Thus we can assume wlog neighbouring faces which contain adjacent sections of C share a common edge.

There are four possible ways the polyhedral cells associated to these neighbouring faces could be connected (see Fig. 7.12 for an illustration):

1. The neighbouring faces are associated with the same polyhedral cell.

2. A pair of neighbouring polyhedral cells share a single common edge.

3. A pair of neighbouring polyhedral cells share a common face (and therefore also common edges).

Case 3 is not possible because, if two polyhedra $P^{(u')}$ and $P^{(v')}$ where $l_S(u') = l_S(v') = r$ meet at a face, there would exist $s_a \in S$ such that $l_S(u's_a) = l_S(v') = r = l_S(u')$, contradicting property (i) of the length function of Coxeter groups (see subsection 7.3.1.2). Therefore, for every pair of neighbouring faces containing adjacent sections of the non-contractible loop, either Case 1 or Case 2 must hold.

The surface of the HQECC at radius $R-1$ (which we will denote M') is contained inside M, where "inside" is well-defined as M is orientable by Lemma 72. Consider continuously deforming C so that it lies on M', by the following procedure. Take a section of C which lies on the faces of a single polyhedral cell, $P^{(u)}$, and deform it so that it lies on the faces of $P^{(u)}$ associated with $\mathcal{D}_R(u)$ whilst leaving its endpoints unchanged. To see that this can always be done, note that at the edge where faces $F_a^{(u)}$ and $F_b^{(v)}$ from two polyhedral cells $P^{(u)}$ and $P^{(v)}$ meet (see Fig. 7.12(b)), the faces $F_b^{(u)}$ and $F_a^{(v)}$ are associated with $\mathcal{D}_R(u)$ by Lemma 692 and 3. The faces of $P^{(u)}$ associated with $\mathcal{D}_R(u)$ share common edges, so this deformation can be carried out while leaving the curve intact.

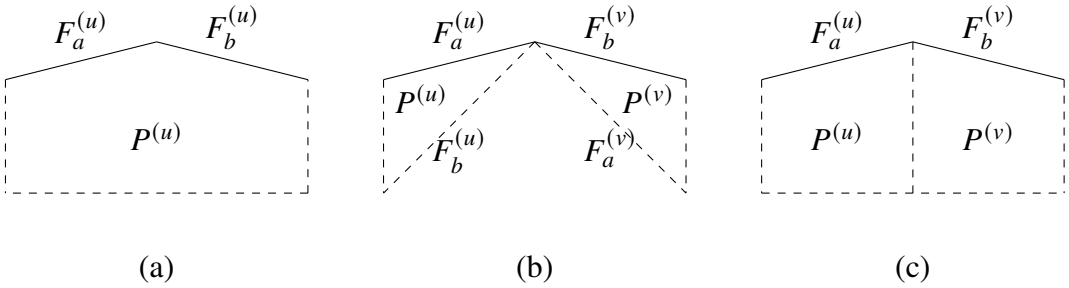

Figure 7.12: A cross section image of the three possible ways which neighbouring faces in a loop C on M could be connected. In (a) the neighbouring faces are associated with a single polyhedral cell. In (b) neighbouring faces are associated with polyhedral cells which share a single common edge. In (c) the neighbouring faces are associated with polyhedral cells which share a common edge. The figures all represent cross-sections of the tessellations, and in all figures dashed edges represent faces of polyhedra which do not form part of M, while solid edges represent faces of polyhedra which form part of M.

We can repeat this contraction procedure until the loop C lies on the faces of $P^{(I)}$. At that point we can continuously contract C through $P^{(I)}$ to a point. Therefore every loop on M can be contracted through the bulk of the tessellation to a point.

Any torus (or connected sum of tori) contains curves which cannot be continuously contracted to a point through the solid torus forming its interior. Therefore M cannot be homeomorphic to the connected sum of tori. Thus M is homeomorphic to a 2-sphere. □

7.4.1.4 The metric on the boundary surface of the HQECC

We can upper-bound the distance between qudits on the boundary surface by the distance according the word metric between the corresponding elements of the Coxeter group. Consider two boundary qudits, $q_a^{(u)}$ and $q_b^{(v)}$. The Coxeter polytopes we use in the HQECC are of size $O(1)$ in every direction, so the distance between $q_a^{(u)}$ and $q_b^{(v)}$ is upper-bounded by $cd(u,v) = cl_S(u^{-1}v)$, for some constant c.

If $q_a^{(u)}$ and $q_b^{(v)}$ are nearest-neighbour qudits on the boundary surface of a HQECC then they are separated by distance $O(1)$. This follows because the boundary surface of the HQECC is connected, so $F_a^{(u)}$ and $F_b^{(v)}$ must share a common edge. The number of Coxeter polyhedra which fit round this edge is upper-bounded by m_{ab}, so $l_S(u^{-1}v) \leq m_{ab} = O(1)$.

7.4.1.5 Operators on the boundary surface of the HQECC

In order to determine the overhead required to simulate the boundary Hamiltonian with a local model, we need to determine the distribution of operator weights that

results from pushing the bulk Hamiltonian through the tensor network. In [106] it is shown that an operator M can be reconstructed on a boundary region A if M lies in the greedy entanglement wedge of A, denoted $\mathcal{E}[A]$, where the greedy entanglement wedge is defined as below:

Definition 75 (Greedy entanglement wedge, definition 8 from [106])**.** *Suppose A is a (not necessarily connected) boundary region. The greedy entanglement wedge of A, denoted $\mathcal{E}[A]$, is the set of bulk points reached by applying the greedy algorithm to all connected components of A simultaneously.*

The greedy algorithm is a simple procedure for finding bulk regions which can be reconstructed on a given boundary region. It considers a sequence of cuts $\{c_\alpha\}$ through the tensor network which are bounded by ∂A and which correspond to a set of isometries $\{P_\alpha\}$ from bulk indices to boundary indices. The algorithm begins with the cut $c_1 = A$, corresponding to $P_1 = \mathbb{1}$. Each cut in the sequence is obtained from the previous one by identifying a (pseudo)-perfect tensor which has at least half of its indices contracted with P_α, and adding that tensor to P_α to construct $P_{\alpha+1}$. In this way $P_{\alpha+1}$ is guaranteed to be an isometry if P_α is. The algorithm terminates when there are no tensors which have at least half their indices contracted with P_α. (See [106] for details). The greedy algorithm only relies on the properties of perfect tensors, so we can apply it to our HQECC in $\mathbb{H}^3$.

A given bulk point will be in the greedy entanglement wedge of many boundary regions. As we are interested in minimising the operator weights of the boundary Hamiltonian we want to calculate the smallest boundary region needed to reconstruct a bulk operator.

Consider a HQECC described by a perfect tensor, T, and a Coxeter system (W, S) with associated Coxeter polyhedra $P \subseteq \mathbb{H}^3$. Let the growth rate of W with respect to S be τ, and let the radius of the HQECC be R.

By the definition of the growth rate, the number of boundary qudits, N, scales as $O(\tau^R)$. Reconstructing an operator which acts on the central bulk qudit requires an $O(1)$ fraction of the boundary, so requires $O(\tau^R)$ boundary qudits.[13]

Consider the number of boundary qudits required to reconstruct on operator which acts on a qudit, $q^{(v)}$, at distance x from the centre. By assumption $\mathcal{A}_R(w) > \mathcal{D}_R(w)$ for all $w \in W$, and hence for all polyhedral cells in our tessellation of $\mathbb{H}^3$. Therefore

[13] In theory it is possible to work out the value of the $O(1)$ constant from the properties of the (pseudo-)perfect tensor and Coxeter system used in a given HQECC, however as we are concerned with asymptotic scaling of weights we don't provide an example of this calculation.

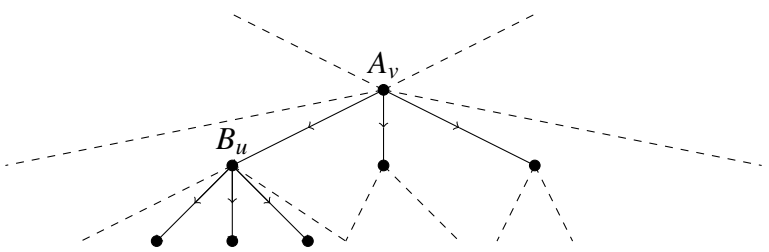

Figure 7.13: If qudit $q^{(v)}$ is at distance x from the centre of the HQECC, and qudit $q^{(u)}$ is a neighbouring qudit at distance $x+1$ from the centre, then an operator A_v acting on $q^{(v)}$ can be pushed through $q^{(u)}$, so pushing an operator $A_v \otimes B_u$ where B_u acts on $q^{(u)}$ through the tensor network will lead to a boundary operator with the same weight as pushing A_v alone through the tensor network.

if we take an operator acting on $q^{(v)}$, we can push it to the boundary while at each step moving outwards in the tensor network - i.e. we are guaranteed to be able to reconstruct the operator on the boundary using only qudits which are a distance $R-x$ from $q^{(v)}$. If we consider shifting the centre of the tensor network to $q^{(v)}$ we can see that there are $O(\tau^{R-x})$ qudits which are at distance $R-x$ from $q^{(v)}$. Not all of these lie on the boundary, but we can upper-bound the number of qudits needed for boundary reconstruction by $O(\tau^{R-x})$.

If we consider a geometrically k-local operator in the bulk, where the deepest qudit the operator acts on is at distance x from the centre,[14] then the number of qudits needed for boundary reconstruction scales as $O(\tau^{R-x})$. To see this consider an operator $A \otimes B$ where A acts on qudit $q^{(v)}$ which is at distance x from the centre, and B acts on a neighbouring qudit $q^{(u)}$ at distance $x+1$, as in Fig. 7.13. We can push A through $q^{(u)}$ to reach the boundary, therefore B can necessarily be reconstructed on a subset of the qudits required to reconstruct A. Hence B makes no difference to the number of qudits required for boundary reconstruction, and we only need to consider the deepest qudit a given operator acts on. In general there may be more than one deepest qudit, however as k is constant this can make at most a constant factor difference to the number of qudits needed for reconstruction.

The number of qudits at distance x from the centre of the tensor network scales as $O(\tau^x)$, so we find that for $x = 0, \ldots, R$ the boundary Hamiltonian has $O(\tau^x)$ operators of weight $O(\tau^{R-x})$. All boundary operators can be chosen to be geometrically $O(\tau^{R-x})$ local (i.e. the $O(\tau^{R-x})$ qudits which an operator act on are spread over an $O(\tau^{-x})$ fraction of the boundary).

[14] Here by deepest operator we mean nearest the centre, so the minimum x.

7.4.1.6 Full holographic duality

In this section we prove our main result: that using a HQECC and simulation techniques from Hamiltonian complexity it is possible to construct a holographic duality between local quantum many-body models in 3D hyperbolic space and local models living on its 2D boundary.

We will require the following Lemma in the proof of the main theorem:

Lemma 76. *Consider a HQECC constructed using Coxeter system* (W, S) *and perfect tensor* T*. Let* $T^{(w)}$ *denote the perfect tensor associated with element* $w \in W$*, and let* $\mathcal{I}^{(w)}$ *be the set of indices of* $T^{(w)}$ *which are contracted through faces* $F_a^{(w)}$ *for* $a \in \mathcal{D}_R(w)$*. Define:*

$$\Pi_{C^{(w)}} = \frac{1}{|\mathcal{S}^{(w)}|} \sum_{M \in \mathcal{S}^{(w)}} \overline{M} \tag{7.12}$$

where $\mathcal{S}^{(w)}$ *is the stabilizer group of the QECC defined by viewing* $T^{(w)}$ *as an isometry from* $\{\mathcal{I}^{(w)} \cup q^{(w)}\}$ *to the complementary set of indices, and* $\overline{M}$ *is the boundary operator associated to the stabilizer* M*.*

Let:

$$H_S = \sum_{w \in W} \left(\mathbb{1} - \Pi_{C^{(w)}}\right) \tag{7.13}$$

Then:

1. *The kernel of* H_S *is the code-subspace of the HQECC,* C*.*
2. *The smallest non-zero eigenvalue of* H_S *is one.*
3. *Energy with respect to* H_S *is equal to the number of logical qudits encoded by the HQECC which have a correctable error.*
4. *Eigenstates of* H_S *with the same energy, but which pick up energy from errors on different logical qudits, are orthogonal.*

Proof. 1. The set $\left\{\cup_{w \in W} \mathcal{S}^{(w)}\right\}$ is a (non-minimal) generating set for the stabilizer group of the HQECC. Therefore, $\Pi_{C^{(w)}} |\psi\rangle = |\psi\rangle$ for all $w \in W$ iff $|\psi\rangle \in C$. So $H_S |\psi\rangle = 0$ iff $|\psi\rangle \in C$.

2. This is immediate as each term in H_S is a projector, so has eigenvalue zero or one.

3. Consider a boundary state $|\phi\rangle$. If there is a correctable error affecting the state of encoded qudit $q^{(w)}$ then $\exists M \in \mathcal{S}^{(w)}$ such that $\overline{M} |\phi\rangle \neq |\phi\rangle$. Therefore $\Pi_{C^{(w)}} |\phi\rangle \neq 1$.

Since $\Pi_{C^{(w)}}$ is a projector, this gives $\Pi_{C^{(w)}}|\phi\rangle = 0$. Therefore, $|\phi\rangle$ picks up energy +1 from the $\left(\mathbb{1} - \Pi_{C^{(w)}}\right)$ term in H_S.

If there is not a correctable error affecting the state of encoded qudit $q^{(w')}$ then $\overline{M}|\phi\rangle = |\phi\rangle$ for all $M \in \mathcal{S}^{(w)}$. So $\Pi_{C^{(w')}}|\phi\rangle = |\phi\rangle$, regardless of any errors affecting other encoded qudits. Therefore $|\phi\rangle$ picks up zero energy from the $\left(\mathbb{1} - \Pi_{C^{(w')}}\right)$ term in H_S.

Therefore the energy with respect to H_S counts the number of bulk qudits which have a correctable error.

4. Consider boundary states, $|\psi\rangle$, $|\phi\rangle$, which have correctable errors affecting the state of encoded qudits $q^{(w)}$ and $q^{(w')}$ respectively. We have:

$$\Pi_{C^{(w)}}|\psi\rangle = 0, \Pi_{C^{(w)}}|\phi\rangle = |\phi\rangle, \Pi_{C^{(w')}}|\psi\rangle = |\psi\rangle, \Pi_{C^{(w')}}|\phi\rangle = 0 \tag{7.14}$$

Therefore $\langle\psi|\phi\rangle = \langle\psi|\Pi_{C^{(w)}}|\phi\rangle = \langle\psi|\Pi_{C^{(w')}}|\phi\rangle = 0$. □

Before proving our main theorem we introduce the concept of a quasi k-local Hamiltonian. These are generalisations of k-local Hamiltonians, where instead of requiring that each term in the Hamiltonian acts on only k-spins, we require that each term in the Hamiltonian has Pauli rank at most k,[15] along with some geometric restrictions on the interaction graph. More precisely:

Definition 77 (Quasi-local hyperbolic Hamiltonians)**.** *Let $\mathbb{H}^d$ denote d-dimensional hyperbolic space, and let $B_r(x) \subset \mathbb{H}^d$ denote a ball of radius r centred at x. Consider an arrangement of n qudits in $\mathbb{H}^d$ such that, for some fixed r, at most k qudits and at least one qudit are contained within any $B_r(x)$. Let Q denote the minimum radius ball $B_Q(0)$ containing all the qudits (which without loss of generality we can take to be centred at the origin). A quasi k-local Hamiltonian acting on these qudits can be written as:*

$$H_{\text{bulk}} = \sum_Z h^{(Z)} \tag{7.15}$$

where the sum is over the n qudits, and each term can be written as:

$$h^{(Z)} = h^{(Z)}_{\text{local}} h^{(Z)}_{\text{Wilson}} \tag{7.16}$$

where:

[15] The Pauli rank of an operator is the number of terms in its Pauli decomposition.

- $h^{(Z)}_{\text{local}}$ *is a term acting non-trivially on at most* k *qudits which are contained within some* $B_r(x)$
- $h^{(Z)}_{\text{Wilson}}$ *is a Pauli operator acting non trivially on at most* $\mathrm{O}(L-x)$ *qudits which form a line between* x *and the boundary of* $B_Q(0)$

The extension to quasi-local bulk Hamiltonians allows us to consider using the HQECC to construct toy models of AdS/CFT with gravitational Wilson lines in the bulk theory.

Theorem 78. *Let* $\mathbb{H}^3$ *denote 3D hyperbolic space, and let* $B_r(x) \subset \mathbb{H}^3$ *denote a ball of radius* r *centred at* x*. Consider any arrangement of* n *qudits in* $\mathbb{H}^3$ *such that, for some fixed* r*, at most* k *qudits and at least one qudit are contained within any* $B_r(x)$*. Let* L *denote the minimum radius ball* $B_L(0)$ *containing all the qudits (which wlog we can take to be centred at the origin). Let* $H_{\text{bulk}} = \sum_Z h_Z = \sum h^{(Z)}_{\text{local}} h^{(Z)}_{\text{Wilson}}$ *be any quasi local Hamiltonian on these qudits, where each* $h^{(Z)}_{\text{local}}$ *acts only on qudits contained within some* $B_r(x)$*.*

Then we can construct a Hamiltonian H_{boundary} *on a 2D boundary manifold* $\mathcal{M} \in \mathbb{H}^3$ *with the following properties:*

1. $\mathcal{M}$ *surrounds all the qudits, has diameter* $O\left(\max(1, \frac{\ln(k)}{r})L + \log\log n\right)$*, and is homeomorphic to the Euclidean 2-sphere.*
2. *The Hilbert space of the boundary consists of a triangulation of* $\mathcal{M}$ *by triangles of* $O(1)$ *area, with a qubit at the centre of each triangle, and a total of* $O\left(n(\log n)^4\right)$ *triangles/qubits.*
3. *Any local observable/measurement* M *in the bulk has a set of corresponding observables/measurements* $\{M'\}$ *on the boundary with the same outcome. A local bulk operator* M *can be reconstructed on a boundary region* A *if* M *acts within the greedy entanglement wedge of* A*, denoted* $\mathcal{E}[A]$*.*
4. H_{boundary} *consists of 2-local, nearest-neighbour interactions between the boundary qubits. Furthermore,* H_{boundary} *can be chosen to have full local* $SU(2)$ *symmetry; i.e. the local interactions can be chosen to all be Heisenberg interactions:* $H_{\text{boundary}} = \sum_{\langle i,j\rangle} \alpha_{ij}(X_iX_j + Y_iY_j + Z_iZ_j)$*.*
5. H_{boundary} *is a* $(\Delta_L, \epsilon, \eta)$*-simulation of* H_{bulk} *in the rigorous sense of [6, Definition 23], with* $\epsilon, \eta = 1/\text{poly}(\Delta_L)$*,* $\Delta_L = \Omega\left(\|H_{\text{bulk}}\|^6\right)$*, and where the maximum interaction strength* $\Lambda = \max_{ij}\left|\alpha_{ij}\right|$ *in* H_{boundary} *scales as* $\Lambda = O\left(\Delta_L^{\text{poly}(n\log(n))}\right)$*.*

Proof. There are four steps to this simulation:

Step 1

Simulate H_{bulk} with a Hamiltonian which acts on the bulk indices of a HQECC in $\mathbb{H}^3$ of radius $R = O\left(\max(1, \frac{\ln(k)}{r})L\right)$.

Note that in a tessellation of $\mathbb{H}^3$ by Coxeter polytopes the number of polyhedral cells in a ball of radius r' scales as $O(\tau^{r'})$, where we are measuring distances using the word metric, $d(u,v) = l_S(u^{-1}v)$. If we want to embed a Hamiltonian H_{bulk} in a tessellation we will need to rescale distances between the qudits in H_{bulk} so that there is at most one qudit per polyhedral cell of the tessellation. If $\tau^{r'} = k$, then $\frac{r'}{r} = \frac{\ln(k)}{\ln(\tau)r} = O\left(\frac{\ln(k)}{r}\right)$. If $\frac{\ln(k)}{r} \geq 1$ then the qudits in H_{bulk} are more tightly packed than the polyhedral cells in the tessellation, and we need to rescale the distances between the qudits by a factor of $O\left(\frac{\ln(k)}{r}\right)$. If $\frac{\ln(k)}{r} < 1$ then the qudits in H_{bulk} are less tightly packed then the cells of the tessellation, and there is no need for rescaling.

The radius, R, of the tessellation needed to contain all the qudits in H_{bulk} is then given by:

$$R = \begin{cases} O\left(\frac{\ln(k)}{r}L\right), & \text{if } \frac{\ln(k)}{r} \geq 1 \\ O(L) & \text{otherwise} \end{cases} \tag{7.17}$$

After rescaling there is at most one qudit per cell of the tessellation. There will be some cells of the tessellation which don't contain any qudits. We can put 'dummy' qudits in these cells which don't participate in any interactions, so their inclusion is just equivalent to tensoring the Hamiltonian with an identity operator. We can upper and lower bound the number of 'real' qudits in the tessellation. If no cells contain dummy qudits then the number of real qudits in the tesselation is given by $n_{\max} = N = O(\tau^R)$, where N is the number of cells in the tessellation. By assumption there is at least one real qudit in a ball of radius r', therefore the minimum number of real qudits in the tessellation scales as $n_{\min} = O\left(\frac{\tau^R}{\tau^{r'}}\right) = O(\tau^R) = O(N)$. Therefore $n = \Theta(\tau^R) = \Theta(N)$.

If the tessellation of $\mathbb{H}^3$ by Coxeter polytopes is going to form a HQECC, the Coxeter polytope must have at least 7 faces. We show in subsection 7.4.2 that this bound is achievable, so we will wlog assume the tessellation we are using is by a Coxeter polytope with 7 faces. The perfect tensor used in the HQECC must therefore have 8 indices. Our method to construct perfect tensors can be used to construct perfect tensors with 8 indices for qudits of prime dimension $p \geq 11$. Qudits of general dimension d can be incorporated by embedding qudits into a d-dimensional subspace

of the smallest prime which satisfies both $p \geq d$ and $p \geq 11$. We then add one-body projectors onto the orthogonal complement of these subspaces, multiplied by some $\Delta'_S \geq |H_{\text{bulk}}|$ to the embedded bulk Hamiltonian. The Hamiltonian, H'_{bulk} on the n p-dimensional qudits is then a perfect simulation of H_{bulk}.

We can therefore simulate any H_{bulk} which meets the requirements stated in the theorem with a Hamiltonian which acts on the bulk indices of a HQECC in $\mathbb{H}^3$.

Now consider simulating H_{bulk} with a Hamiltonian H_B on the boundary surface of the HQECC. Let:

$$H_B = H' + \Delta_S H_S \tag{7.18}$$

where H_S is as defined in Lemma 76, H' satisfies $H'\Pi_C = V(H'_{\text{bulk}} \otimes \mathbb{1}_{dummy})V^\dagger$, V is the encoding isometry of the HQECC, Π_C is the projector onto the code-subspace of the HQECC and $\mathbb{1}_{dummy}$ acts on the dummy qudits.

Provided $\Delta_S \geq \left\|H'_{\text{bulk}}\right\|$, Item 1 and Item 2 from Lemma 76 ensure that H_B meets the conditions in [6] to be a perfect simulation of H'_{bulk} below energy Δ_S, and (as simulations compose) a perfect simulation of H_{bulk}.

There is freedom in this definition as there are many H' which satisfy the condition stated. We will choose an H' where every bulk operator has been pushed directly out to the boundary, so that a 1-local bulk operator at radius x corresponds to a boundary operator of weight $O(\tau^{R-x})$. We will also require that the Pauli rank of every bulk operator has been preserved (see Theorem 98 for proof we can choose H' satisfying this condition).

Step 2 [16]

Having constructed H_B we now want to simulate it with a geometrically 2-local qudit Hamiltonian. To achieve this, we make use of the subdivision and 3-2 gadgets from subsection 7.3.2.

Consider simulating a single k-local interaction which is a tensor product of operators of the form $P_A + P_A^\dagger$ by 2-local interactions using these gadgets. The first step will be to simulate the interaction by two $\lceil \frac{k}{2} \rceil + 1$- local interactions by applying the subdivision gadget. Then apply the subdivision gadget again to give four $O(\frac{k}{4})$-local interactions. Continue until all the interactions are 3-local. Finally use the 3-2 gadget

[16] In steps 2 and 3 we are following the methods developed in [28], replacing the qubit perturbation gadgets with qudit perturbation gadgets, and making use of the structure of the interaction graph on the boundary.

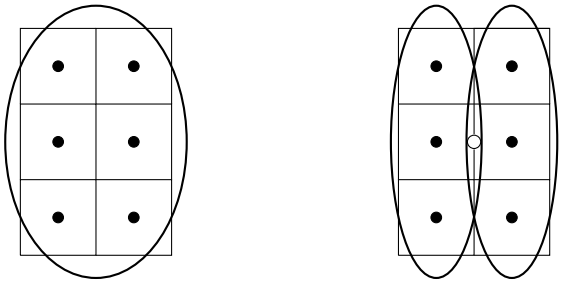

(a) (b)

Figure 7.14: (a) A 6-local interaction in a HQECC where the cells composing the boundary surfaces are square. (b) The 6-local interaction is simulated by two 4-local interactions, by introducing an ancilla qudit (denoted by the white vertex) which is placed on an edge separating the sets of qudits it is interacting with.

to simulate on each 3-local interaction. This process requires $O(k)$ ancillas, and $O(\log(k))$ rounds of perturbation theory.

The original qudits are in the centre of the polygon-cells which form the boundary.[17] Place the ancilla qudits required for this simulation on the edges of the cells separating the sets of qudits they are interacting with (see Fig. 7.14 for an example).

This process can be applied to each of the interactions in H_B independently. H_B contains $O(\tau^x)$ operators of weight $O(\tau^{R-x})$ for $x \in [0, R]$ (see subsection 7.4.1.5). Therefore applying this step to every interaction in H_B will require a total of:

$$N_a = O(\sum_{x=0}^{R} \tau^x \tau^{R-x}) = O(R\tau^R) = O(n\log(n)) \tag{7.19}$$

ancilla qudits. Each edge will therefore contain $O(R) = O(\log(n))$ qudits. When breaking down the interactions to 2-local the ancillas are placed nearest the qudits they are interacting with, so none of the resulting 2-local interactions cross more than two of the cells which make up the boundary.

As there are interactions with Pauli-weights which scale as $O(n)$ this step requires $O(\log(n))$ rounds of perturbation theory. By Lemma 19, the first round of perturbation theory will require interaction strengths of $\Delta_L = \Omega\left(\|H_{\text{bulk}}\|^6\right)$, while r rounds of perturbation theory requires interaction strengths to scale as $\Delta_L^{6^r}$. Therefore, this step requires maximum interaction strengths scaling as $\Lambda = O\left(\Delta_L^{\text{poly}(n)}\right)$.

[17] The polygon cells are the faces of the tensor network which correspond to the uncontracted tensor indices.

Step 3

Each of the ancillas introduced in step 2 has degree at most 6. The degree of the original qudits after step 2 is the same as their degree in the initial hypergraph, which can be calculated as:

$$d = \frac{\sum_{x=0}^{R} \tau^x \tau^{R-x}}{\tau^R} = R \tag{7.20}$$

Therefore there are $O(\tau^R)$ qudits of degree $O(R)$, and $O(R\tau^R)$ qudits of degree $O(1)$.

We reduce the degree of each vertex to at most $3(p-1)$ (where p is the local dimension of each qudit) in the following manner:[18]

1. Use the subdivision gadget to localise each qudit with degree $O(R)$. This requires $O(R)$ ancilla qudits per cell of the boundary, so $O(R\tau^R)$ ancillas in total.

2. Apply the triangle gadget to each qudit to reduce the degree to $3(p-1)$, by pairing edges of the form $P_a + P_a^\dagger$ in parallel. Reducing the degree of one $O(R)$ degree vertex in this manner requires $O(\log(R))$ rounds of perturbation theory, and $O(R)$ ancillas. Therefore applying this step to the entire graph requires $O(R\tau^R)$ ancillas.

Once the degree of each qudit has been reduced there are $O(R)$ qudits in each of the cells of the boundary.

Finally we need to remove all the crossings using crossing gadgets. Each interaction is constrained to 2 of the cells which make up the boundary surface, so we can consider each cell and its adjacent cells separately.[19] There are $O(R)$ qudits, and hence at most $O(R^2)$ interactions in each cell, including contributions from adjacent cells. Therefore there are at most $O(R^4)$ crossings. We use the subdivision gadget to localise each crossing,[20] then apply the crossing gadget in parallel to each localised crossing. This requires $O(R^4)$ ancillas per cell of the boundary, so requires $O(R^4\tau^R) = O(n\log(n)^4)$ ancilla qudits. These ancilla qudits are placed within the corresponding face of the boundary surface.

[18] A recent paper [35] has derived a method to reduce the degree of a Hamiltonian, H, using only polynomial strength interactions. However, this method cannot be used here as it assumes $||H|| = O(\text{poly}(n))$, whereas $||H_B|| = O(\exp(n))$.

[19] This will double-count some crossings as each cell will be included when considering its adjacent cells too, but as we are only interested in the asymptotic scaling this double-counting is not important.

[20] This step can be skipped for edges with only one crossing, where each qudit involved in the crossing interactions has degree at most $3(p-1)$.

This step required $O(\log\log n)$ rounds of perturbation theory, so we require the maximum interaction strength Λ to scale as $\Lambda = O\left(\Delta_L^{\text{poly}(n\log(n))}\right)$

Label the Hamiltonian resulting from this step as H'_B.

Step 4

Finally, if we want the boundary Hamiltonian to have full local $SU(2)$ symmetry, we can simulate H'_B with a qubit $\{XX+YY+ZZ\}$-Hamiltonian on a $2d$ lattice, H_{boundary}.

First use the technique from Lemma 21 in [6] to simulate H'_B with a qubit Hamiltonian by simulating each p-dimensional qudit with $\lceil \log_2 p \rceil$ qubits. The resulting Hamiltonian is given by:

$$H''_B = \mathcal{E}(H'_B) + \Delta \sum_{i=0}^{n'} P_i \tag{7.21}$$

where $\mathcal{E}(M) = VMV^\dagger$, $V = W^{\otimes n'}$,[21] W is an isometry $W : \mathbb{C}^d \to \left(\mathbb{C}^2\right)^{\otimes \lceil \log_2 p \rceil}$, and $P = \mathbb{1} - WW^\dagger$. This requires $n'\lceil \log_2 p \rceil = O(n')$ qubits.

The operators in H''_B are at most $2\lceil \log_2 p \rceil$-local, and the qubits have degree at most $3(p-1)\lceil \log_2 p \rceil$.

Next we use the technique from [6, Lemma 22] to simulate H''_B with a real Hamiltonian. This is a perfect simulation, which requires $2N' = O(n')$ qubits, it increases the locality of the interactions to at most $4\lceil \log_2 p \rceil = O(1)$ and doesn't change the degree of the qubits.

Using the technique from [6, Lemma 39] we then simulate the real Hamiltonian with a Hamiltonian containing no Y operators. This involves adding an ancilla qubit for every interaction in the Hamiltonian. As each qubit is involved in a fixed number of interactions, this only requires $O(n')$ ancilla qubits, so the total number of qubits involved in the Hamiltonian is still $O(n')$. The locality of each interaction in the Hamiltonian is increased by 1. This requires $O(1)$ rounds of perturbation theory.

The qubit subdivision and 3-2 perturbation gadgets from [28] can then be used to reduce the Hamiltonian containing no Ys to a 2-local Pauli interaction with no Ys, leaving a Hamiltonian of the form $\sum_{i>j} \alpha_{ij} A_{ij} + \sum_k (\beta_k X_k + \gamma_k Z_k)$ where A_{ij} is one of X_iX_j, X_iZ_j, Z_iX_j or Z_iZ_j [6, Lemma 39]. This requires $O(1)$ rounds of perturbation theory, and $O(n')$ ancilla qubits.

Next we use the subspace perturbation gadget from [6, Lemma 41] to simulate the Hamiltonian of the form $\sum_{i>j} \alpha_{ij} A_{ij} + \sum_k (\beta_k X_k + \gamma_k Z_k)$ with a $\{XX+YY+ZZ\}$-

[21] n' is the total number of qudits in H'_B.

Hamiltonian. This requires encoding one logical qubit in four physical qubits, so introduces $O(N')$ ancilla qubits, and requires $O(1)$ rounds of perturbation theory.

Finally, we can simulate the general $\{XX+YY+ZZ\}$-Hamiltonian with a $\{XX+YY+ZZ\}$-Hamiltonian on a triangulation of the boundary surface of the HQECC using the perturbation gadgets from [30]. These perturbation gadgets are generalisations of the fork, crossing and subdivision gadgets from [28] which use a pair of mediator qubits, rather than a single ancilla qubit, so that all interactions in the final Hamiltonian are of the form $\{XX+YY+ZZ\}$. Following the method in [30], first reduce the degree of all vertices in the interaction graph to 3 using the subdivision and fork gadgets. This requires $O(1)$ ancillas and $O(1)$ rounds of perturbation theory per qubit, and can be done to all qubits in the Hamiltonian in parallel. Next remove all the crossings. The qudit Hamiltonian H'_B had no crossings, and our simulation of H'_B with a $\{XX+YY+ZZ\}$-Hamiltonian will have introduced $O(1)$ crossings per qudit in H'_B, so $O(n')$ crossings across the entire interaction graph. The crossings are localised using the subdivision gadget, then removed using the crossing gadget. This requires $O(n')$ ancilla qubits.

Step 4 therefore requires a total of $O(n') = O\left(n\log(n)^4\right)$ qubits. The scaling of the interaction strengths in the Hamiltonian is unchanged by this final step as it only required $O(1)$ rounds of perturbation theory.

Each qubit has degree at most 3, so we can construct a triangulation of the boundary surface with a qubit in the centre of each triangle. This is not an $O(1)$ triangulation, but if we increase the diameter of our boundary manifold to $O\left(\max(1,\frac{\ln(k)}{r})L+\log\log n\right)$ then we can construct an $O(1)$ triangulation with a qubit in the centre of each triangle (this follows because we are working in hyperbolic space). This surface will be homeomorphic to a sphere as boundary surface of the HQECC is homeomorphic to a sphere by Lemma 74.

The final Hamiltonian, H_{boundary}, is a (Δ_L,ϵ,η)-simulation of H_{bulk} with full local SU(2) symmetry. The total number of qubits required scales as $O\left(n\log(n)^4\right)$, and the interaction strengths in the Hamiltonian scale as $\max_{ij}|\alpha_{ij}| = O\left(\Delta_L^{\text{poly}(n\log(n))}\right)$ where $\Delta_L = \Omega\left(\|H_{\text{bulk}}\|^6\right)$. The perturbation gadget techniques require that $\epsilon,\eta = 1/\text{poly}(\Delta_L)$.[22]

[22]In steps 2 and 3 we assume that all operators are Pauli rank 2 operators of the form $P_A+P_A^\dagger$. We have shown that the HQECC preserves the Pauli rank of operators (Theorem 98), so accounting for operators of general form will only increase the overheads calculated by a constant factor.

It is immediate from the definition of the greedy entanglement wedge [106, Definition 8] that bulk local operators in $\mathcal{E}(A)$ can be reconstructed on A. The boundary observables / measurements $\{M'\}$ corresponding to a bulk observable / measurement M have the same outcome because simulations preserve the outcome of all measurements.

□

Note that the fact that H_{boundary} is a $(\Delta_L, \epsilon, \eta)$-simulation of H_{bulk} immediately implies, by Lemma 17, that the partition function, time dynamics, and all measurement outcomes of the boundary are the same as that of the bulk, up to $O(1/\text{poly}(\epsilon, \eta))$ errors which can be made as small as desired by increasing Δ_L.

7.4.2 HQECC constructed from pentagonal prisms

The proof of Theorem 78 does not require any particular HQECC – all it requires is that one exists. Here and in subsection 7.4.3 we provide examples of two pairs of Coxeter group and tensor which can be used to construct a HQECC. There are many more which could be constructed.

First we construct a HQECC using a perfect tensor, and a non-uniform Coxeter polytope. The Coxeter polytope, P_1, we use is a pentagonal prism. It is described by the Coxeter diagram, $\Sigma(P_1)$, shown in Fig. 7.15. The elliptic subdiagrams of $\Sigma(P_1)$ are shown in Table 7.2.[23]

The maximum $|J|$ such that W_J is finite is three, so $|\mathcal{D}_R(w)| \leq 3 \; \forall w \in W$. Clearly if we construct a perfect tensor with 8 legs, and place one tensor in each polyhedral-cell in a tessellation of $\mathbb{H}^3$ by pentagonal prisms then the tensor network will be a HQECC. Details of the tensor are given in subsection 7.4.2.1.

The growth rate of the Coxeter group is 3.13.[24]

7.4.2.1 Perfect tensor

We use the procedure set out in Appendix C.5 to construct a perfect tensor with the required properties.

[23] Elliptic subdiagrams are subdiagrams containing $J \subseteq S$ such that W_J is finite.

[24] The growth rate was calculated using CoxIterWeb [135], a web applet which computes invariants of Coxiter groups.

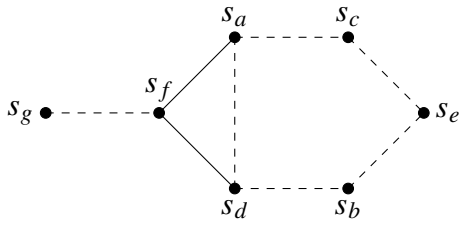

Figure 7.15: Coxeter diagram, $\Sigma(P_1)$, for the the Coxeter group associated with the pentagonal prism. The vertices of the graph are labelled with the corresponding generator of the Coxeter group. The faces F_f and F_g of the Coxeter polyhedra (corresponding to the generators s_f and s_g) are the pentagonal faces of the prism, the faces $F_a - F_e$ are the quadrilateral faces.

Name	Diagram	Generating sets
A_1	•	$\{s_a\},\{s_b\},\{s_c\},\{s_d\},\{s_e\},\{s_f\},\{s_g\}$
$A_1 \times A_1$	• •	$\{s_a,s_b\},\{s_a,s_e\},\{s_a,s_g\},\{s_b,s_c\},$ $\{s_b,s_f\},\{s_b,s_g\},\{s_c,s_d\},$ $\{s_c,s_f\},\{s_c,s_g\},\{s_d,s_e\},$ $\{s_d,s_g\},\{s_e,s_f\},\{s_e,s_g\}$
A_2 (equivalently $I_2^{(3)}$)	•—•	$\{s_a,s_f\},\{s_d,s_f\}$
$A_1 \times A_1 \times A_1$	• • •	$\{s_a,s_e,s_g\},\{s_a,s_b,s_g\},\{s_c,s_d,s_g\},$ $\{s_d,s_e,s_g\},\{s_b,s_c,s_f\},\{s_b,s_c,s_g\}$
$A_2 \times A_1$	•—• •	$\{s_a,s_b,s_f\},\{s_a,s_e,s_f\},\{s_c,s_d,s_f\},\{s_d,s_e,s_f\}$

Table 7.2: Elliptic subdiagrams of $\Sigma(P_1)$.

Construct a AME(8, 11) stabilizer state via a classical Reed Solomon code with $n = 8, k = 4$ over $\mathbb{Z}_{11}$ defined by the set $S = \{1,2,3,4,5,6,7,8\} \in \mathbb{Z}_{11}$. The generator matrix is given by:

$$G = \begin{pmatrix} 1 & 1 & 1 & 1 & 1 & 1 & 1 & 1 \\ 1 & 2 & 3 & 4 & 5 & 6 & 7 & 8 \\ 1 & 4 & 9 & 5 & 3 & 3 & 5 & 9 \\ 1 & 8 & 5 & 9 & 4 & 7 & 2 & 6 \end{pmatrix} \tag{7.22}$$

In standard form this becomes:

$$G = \begin{pmatrix} 1 & 0 & 0 & 0 & 10 & 7 & 1 & 2 \\ 0 & 1 & 0 & 0 & 4 & 4 & 3 & 4 \\ 0 & 0 & 1 & 0 & 5 & 2 & 10 & 4 \\ 0 & 0 & 0 & 1 & 4 & 10 & 9 & 2 \end{pmatrix} \tag{7.23}$$

Giving a parity check matrix:

$$H = \begin{pmatrix} 1 & 7 & 6 & 7 & 1 & 0 & 0 & 0 \\ 4 & 7 & 9 & 1 & 0 & 1 & 0 & 0 \\ 10 & 8 & 1 & 2 & 0 & 0 & 1 & 0 \\ 9 & 7 & 7 & 9 & 0 & 0 & 0 & 1 \end{pmatrix} \tag{7.24}$$

The stabilizer generators of the AME$(8,11)$ stabilizer state are then given by:

$$M = \left(\begin{array}{cccccccc|cccccccc} 1 & 0 & 0 & 0 & 10 & 7 & 1 & 2 & 0 & 0 & 0 & 0 & 0 & 0 & 0 & 0 \\ 0 & 1 & 0 & 0 & 4 & 4 & 3 & 4 & 0 & 0 & 0 & 0 & 0 & 0 & 0 & 0 \\ 0 & 0 & 1 & 0 & 5 & 2 & 10 & 4 & 0 & 0 & 0 & 0 & 0 & 0 & 0 & 0 \\ 0 & 0 & 0 & 1 & 4 & 10 & 9 & 2 & 0 & 0 & 0 & 0 & 0 & 0 & 0 & 0 \\ 0 & 0 & 0 & 0 & 0 & 0 & 0 & 0 & 1 & 7 & 6 & 7 & 1 & 0 & 0 & 0 \\ 0 & 0 & 0 & 0 & 0 & 0 & 0 & 0 & 4 & 7 & 9 & 1 & 0 & 1 & 0 & 0 \\ 0 & 0 & 0 & 0 & 0 & 0 & 0 & 0 & 10 & 8 & 1 & 2 & 0 & 0 & 1 & 0 \\ 0 & 0 & 0 & 0 & 0 & 0 & 0 & 0 & 9 & 7 & 7 & 9 & 0 & 0 & 0 & 1 \end{array}\right) \tag{7.25}$$

The tensor which describes the stabilizer state is a perfect tensor.

7.4.3 HQECC based on the order-4 dodecahedral honeycomb

There are only four compact, regular honeycombings of $\mathbb{H}^3$, and all the honeycombings are by polyhedra with even number of faces, so to use any of them in a HQECC would require a pseudo-perfect tensor. Here we use the order-4 dodecahedral honeycomb.

The Coxeter polytope, P_2, we use is right angled dodecahedron. It is described by the Coxeter diagram, $\Sigma(P_2)$, shown in Fig. 7.16. The elliptic subdiagrams of $\Sigma(P_2)$ are shown in Table 7.3.

The maximum $|J|$ such that W_J is finite is three, so $|\mathcal{D}_R(w)| \leq 3\ \forall w \in W$. Clearly if we construct a pseudo-perfect tensor with 13 legs, and place one tensor in each polyhedral-cell in a tessellation of $\mathbb{H}^3$ by right-angled dodecahedra then the tensor network will be a HQECC. Details of the tensor are given in subsection 7.4.3.1.

The growth rate of the Coxeter group is 7.87.[25]

[25]The growth rate was calculated using CoxIterWeb [135], a web applet which computes invariants of Coxiter groups.

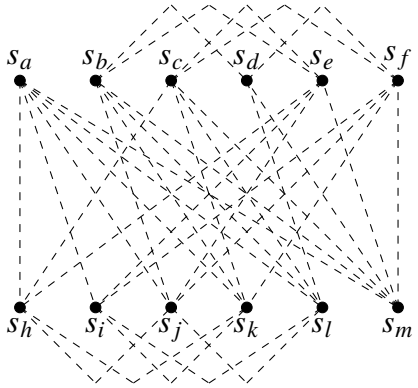

Figure 7.16: Coxeter diagram, $\Sigma(P_2)$, for the the Coxeter group associated with order-4 dodecahedral honeycomb. Each pentagonal face of a dodecahedral cell has a dihedral angle of $\frac{\pi}{2}$ with the five faces it intersects, and diverges from the other six faces of the dodecahedron.

Name	Diagram	Generating sets
A_1	•	$\{s_a\},\{s_b\},\{s_c\},\{s_d\},\{s_e\},\{s_f\},$ $\{s_g\},\{s_h\},\{s_i\},\{s_j\},\{s_k\},\{s_l\}$
$A_1 \times A_1$	• •	$\{s_a,s_b\},\{s_a,s_c\},\{s_a,s_d\},\{s_a,s_e\},$ $\{s_a,s_f\},\{s_b,s_c\},\{s_b,s_f\},\{s_b,s_g\}$ $\{s_b,s_h\},\{s_c,s_d\},\{s_c,s_h\},\{s_c,s_i\},$ $\{s_d,s_e\},\{s_d,s_i\},\{s_d,s_j\},\{s_e,s_f\},$ $\{s_e,s_j\},\{s_e,s_k\},\{s_f,s_k\},\{s_f,s_g\},$ $\{s_g,s_l\},\{s_g,s_h\},\{s_g,s_k\},\{s_h,s_l\}$ $\{s_h,s_i\},\{s_i,s_j\},\{s_i,s_l\},\{s_j,s_l\},$ $\{s_j,s_k\},\{s_k,s_l\}$
$A_1 \times A_1 \times A_1$	• • •	$\{s_a,s_b,s_c\},\{s_a,s_c,s_d\},\{s_a,s_d,s_e\},\{s_a,s_e,s_f\}$ $\{s_a,s_f,s_b\},\{s_b,s_f,s_g\},\{s_b,s_c,s_h\},\{s_b,s_g,s_h\}$ $\{s_c,s_h,s_i\},\{s_c,s_d,s_i\},\{s_d,s_e,s_j\},\{s_d,s_i,s_j\},$ $\{s_e,s_f,s_k\},\{s_e,s_j,s_k\},\{s_f,s_g,s_k\},\{s_g,s_k,s_l\}$ $\{s_g,s_h,s_l\},\{s_h,s_i,s_l\},\{s_i,s_j,s_l\},\{s_j,s_k,s_l\}$

Table 7.3: Elliptic subdiagrams of $\Sigma(P_2)$.

7.4.3.1 Pseudo-perfect tensor

We use the procedure set out in Appendix C.5 to construct a pseudo-perfect tensor with the required properties.

Construct a AME(13, 13) stabilizer state via a classical Reed Solomon code with $n = 13, k = 6$ over $\mathbb{Z}_{13}$ defined by the set $S = \{0, 1, 2, 3, 4, 5, 6, 7, 8, 9, 10, 11, 12\} \in \mathbb{Z}_{13}$. The generator matrix is given by:

$$G = \begin{pmatrix} 1 & 1 & 1 & 1 & 1 & 1 & 1 & 1 & 1 & 1 & 1 & 1 & 1 \\ 0 & 1 & 2 & 3 & 4 & 5 & 6 & 7 & 8 & 9 & 10 & 11 & 12 \\ 0 & 1 & 4 & 9 & 3 & 12 & 10 & 10 & 12 & 3 & 9 & 4 & 1 \\ 0 & 1 & 8 & 1 & 12 & 8 & 8 & 5 & 5 & 1 & 12 & 5 & 12 \\ 0 & 1 & 3 & 3 & 9 & 1 & 9 & 9 & 1 & 9 & 3 & 3 & 1 \\ 0 & 1 & 6 & 9 & 10 & 5 & 2 & 11 & 8 & 3 & 4 & 7 & 12 \end{pmatrix} \tag{7.26}$$

In standard form this becomes:

$$G = \begin{pmatrix} 1 & 0 & 0 & 0 & 0 & 0 & 12 & 7 & 5 & 9 & 4 & 8 & 6 \\ 0 & 1 & 0 & 0 & 0 & 0 & 6 & 9 & 3 & 3 & 11 & 8 & 11 \\ 0 & 0 & 1 & 0 & 0 & 0 & 11 & 7 & 6 & 8 & 11 & 1 & 7 \\ 0 & 0 & 0 & 1 & 0 & 0 & 7 & 1 & 11 & 8 & 6 & 7 & 11 \\ 0 & 0 & 0 & 0 & 1 & 0 & 11 & 8 & 11 & 3 & 3 & 9 & 6 \\ 0 & 0 & 0 & 0 & 0 & 1 & 6 & 8 & 4 & 9 & 5 & 7 & 12 \end{pmatrix} \tag{7.27}$$

Giving a parity check matrix:

$$H = \begin{pmatrix} 1 & 7 & 2 & 6 & 2 & 7 & 1 & 0 & 0 & 0 & 0 & 0 & 0 \\ 6 & 4 & 6 & 12 & 5 & 5 & 0 & 1 & 0 & 0 & 0 & 0 & 0 \\ 8 & 10 & 7 & 2 & 2 & 9 & 0 & 0 & 1 & 0 & 0 & 0 & 0 \\ 4 & 10 & 5 & 5 & 10 & 4 & 0 & 0 & 0 & 1 & 0 & 0 & 0 \\ 9 & 2 & 2 & 7 & 10 & 8 & 0 & 0 & 0 & 0 & 1 & 0 & 0 \\ 5 & 5 & 12 & 6 & 4 & 6 & 0 & 0 & 0 & 0 & 0 & 1 & 0 \\ 7 & 2 & 6 & 2 & 7 & 1 & 0 & 0 & 0 & 0 & 0 & 0 & 1 \end{pmatrix} \tag{7.28}$$

The stabilizer generators of the AME(13, 13) state are given by:

$$M = \left(\begin{array}{c|c} G & 0 \\ 0 & H \end{array}\right) \tag{7.29}$$

The tensor which describes the AME(13, 13) stabilizer state is a pseudo-perfect tensor.

7.5 Technical details of the $2D-1D$ construction

We can use the universal Hamiltonian constructions from Chapter 2 to construct a 2D-to-1D holographic quantum error correcting code (HQECC) with a local boundary Hamiltonian.

Theorem 79. *Consider any arrangement of n qudits in* $\mathbb{H}^2$*, such that for some fixed r at most k qudits and at least one qudit are contained within any* $B_r(x)$*. Let Q denote the minimum radius ball* $B_Q(0)$ *containing all the qudits. Let* $H_{\text{bulk}} = \sum_Z h_Z$ *be any (quasi) k-local Hamiltonian on these qudits.*

Then we can construct a Hamiltonian H_{boundary} *on a 1D boundary manifold* $\mathcal{M}$ *with the following properties:*

1. $\mathcal{M}$ *surrounds all the qudits and has diameter* $\mathrm{O}\left(\max\left(1, \log(k)/r\right) Q + \log\log n\right)$.
2. *The Hilbert space of the boundary consists of a chain of qudits of length* $\mathrm{O}\left(n \log n\right)$.
3. *Any local observable/measurement M in the bulk has a set of corresponding observables/measurements* $\{M'\}$ *on the boundary with the same outcome. A local bulk operator M can be reconstructed on a boundary region A if M acts within the greedy entanglement wedge of A, denoted* $\mathcal{E}[A]$.[26]
4. H_{boundary} *consists of 2-local, nearest-neighbour interactions between the boundary qudits.*
5. H_{boundary} *is a* $(\Delta_L, \epsilon, \eta)$*-simulation of* H_{bulk} *in the sense of Definition 15, with* $\epsilon, \eta = 1/\text{poly}(\Delta_L)$*,* $\Delta_L = \Omega\left(\|H_{\text{bulk}}\|\right)$*, and where the interaction strengths in* H_{boundary} *scale as* $\max_{ij} |\alpha_{ij}| = \mathrm{O}\left((\Delta_L + 1/\eta + 1/\epsilon)\,\text{poly}(e^R 2^{e^R})\right)$.

Proof. There are two steps to this simulation. The first step follow exactly the same procedure as Step 1 in Theorem 78 (but using tessellations of $\mathbb{H}^2$ rather than $\mathbb{H}^3$ so we just recap it very briefly here.

[26] The entanglement wedge, $\mathcal{E}_A$ is a bulk region constructed from the minimal area surface used in the Ryu-Takayanagi formula. It has been suggested that on a given boundary region, A, it should be possible to reconstruct all operators which lie in $\mathcal{E}_A$ [123]. The greedy entanglement wedge is a discretised version defined in [106, Definition 8]

Step 1. First simulate H_{bulk} with a Hamiltonian which acts on the bulk indices of a HQECC in $\mathbb{H}^2$ of radius $R = \mathrm{O}(\max(1, \log(k)/r)\, L)$. Then use composition of simulations and the isometry defined by the tensor network to simulate H_{bulk} with a Hamiltonian H_B on the boundary surface of the HQECC (see Theorem 78 for details).

Step 2. Simulate H_B with a local, nearest neighbour Hamiltonian using the technique from Theorem 31.

In order to achieve the scaling quoted we make use of the structure of H_B due to the HQECC. As in Theorem 78, H_B will contain $\mathrm{O}(\tau^x)$ Pauli rank-1 operators of weight τ^{R-x} for $0 \leq x \leq R$. A Pauli rank-1 operator of weight w can be specified using $\mathrm{O}(w)$ bits of information. So, if we encode H_B in the binary expansion of ϕ as

$$B(\phi) = \gamma'(R) \cdot_{x=0}^{R} \left[\gamma'(i)^{\cdot \tau^{R-x}} \cdot (P_1 \cdot \ldots \cdot P_{\tau^{R-x}}) \right]^{\cdot \tau^x} \cdot \gamma'(L),$$

we have $|\phi| = \mathrm{O}(R\tau^R) = \mathrm{O}(n \log n)$. The number of boundary spins in the final Hamiltonian therefore scales as $\mathrm{O}(n \log n)$. The final boundary Hamiltonian is a (Δ, ϵ, η)-simulation of H_{bulk}.

In order to preserve entanglement wedge reconstruction [106], the location of the spins containing the input state on the Turing machine work tape has to match the location of the original boundary spins. So, instead of the input tape at the beginning of the M_{PE} computation containing the input state, followed by a string of $|0\rangle$s, the two are interspersed. Information about which points on the input tape contain the input state can be included in the description of the Hamiltonian to be simulated.

It is immediate from the definition of the greedy entanglement wedge [106, Definition 8] that bulk local operators in $\mathcal{E}(A)$ can be reconstructed on A. The boundary observables/measurements $\{M'\}$ corresponding to bulk observables/measurements $\{M\}$ which have the same outcome, because by definition simulations preserve the outcome of all measurements. The claim follows. □

It should be noted that the boundary model of the resulting HQECC does not have full rotational invariance. In order to use the universal Hamiltonian construction the spin chain must have a beginning and end, and the point in the boundary chosen to "break" the chain also breaks the rotational invariance. However, it is possible to construct a HQECC with full rotational symmetry by using a history state Hamiltonian construction with periodic boundary conditions, as in [18, Section 5.8.2].

In [18, Section 5.8.2] a Turing machine is encoded into a local Hamiltonian acting on a spin chain of length N with periodic boundary conditions. The ground space of the resulting Hamiltonian is $2N$ fold degenerate. It consists of history states, where any two adjacent sites along the spin chain can act as boundary spins for the purpose of the Turing machine construction - giving rise to $2N$ distinct ground states.[27]

We can apply this same idea to construct a rotationally invariant HQECC, which maps a (quasi-)local bulk Hamiltonian, H_{bulk} in $\mathbb{H}^2$ to a local Hamiltonian H_{boundary} acting on a chain of N qudits. The code-space of the HQECC is $2N$-fold degnerate, and below the energy cut-off H_{boundary} has a direct sum structure:

$$H_{\text{bulk}} \rightarrow H_{\text{boundary}}\big|_{\leq \frac{\Delta}{2}} = \begin{pmatrix} \overline{H}_{\text{bulk}} & 0 & \dots & 0 \\ 0 & \overline{H}_{\text{bulk}} & \dots & 0 \\ \vdots & \vdots & \ddots & 0 \\ 0 & 0 & \dots & \overline{H}_{\text{bulk}} \end{pmatrix} \tag{7.30}$$

where each factor in the direct sum acts on one of the possible rotations of the boundary Hilbert space.

Observables are mapped in the same way as the Hamiltonian. In order to preserve expectation values, we choose the map on states to be of the form:[28]

$$\rho_{\text{boundary}} = \mathcal{E}_{\text{state}}\left(\rho_{\text{bulk}}\right) = \begin{pmatrix} \overline{\rho}_{\text{bulk}} & 0 & \dots & 0 \\ 0 & 0 & \dots & 0 \\ \vdots & \vdots & \ddots & 0 \\ 0 & 0 & \dots & 0 \end{pmatrix} \tag{7.31}$$

We can choose that the bulk state maps into the 'unrotated' boundary Hilbert space, so that the geometric relationship between bulk and boundary spins is preserved.[29]

[27] The factor of two arises because there is freedom about which of the two adjacent sites is assigned to be the 'left' boundary, and which is the 'right' boundary.

[28] See [6, Section 7.1] for a discussion of maps on states in simulations.

[29] Although the bulk states maps into one factor of the direct sum structure, every state in the low-energy portion of the boundary does have a bulk interpretation. But most of these states are rotated with respect to the bulk geometry.

7.6 Discussion

7.6.1 Main result

In our bulk/boundary mapping, local Hamiltonians in hyperbolic space, $\mathbb{H}^d$, are mapped to local Hamiltonians on its boundary. At first glance this may appear to be at odds with the bulk reconstruction expected in AdS/CFT, where observables deep in the bulk are expected to map to non-local observables on the boundary CFT. However, while the local simulation in our construction ensures that the boundary *Hamiltonian* is local, it does not affect the locality of *observables*. As in the HaPPY code, observables deep in the bulk in our construction map to observables which require a large fraction of the boundary to be reconstructed, while observables near the boundary of the HQECC can be reconstructed on smaller fractions of the boundary (see point 3 from Theorems 78 and 79 for details). This includes local Hamiltonian terms in the bulk when viewed as energy *observables*. For a local Hamiltonian term deep in the bulk, the corresponding energy observable on the boundary is not a single local term in the boundary Hamiltonian, but is made up a sum over many local terms acting across a large area of the boundary.

Point 1 from Theorems 78 and 79 demonstrates that the boundary surface in our construction really is a boundary geometrically. The radius of the boundary surface is at a distance $\log\log n$ from the n bulk qudits. In subsection 7.6.4 we compare this with the spherical and Euclidean case.

Point 4 from Theorem 78, which follows immediately from work in [6], says that we can always choose that the boundary Hamiltonian in our holographic duality has full local SU(2) symmetry. This hints at the possiblity of systematically incorporate local symmetries into the construction, such as gauge symmetries. Doing so would involve tailoring our general construction to specific bulk models of interest, which is an intriguing possibility that we leave to future work.

Finally it is worth commenting on the energy scales in the construction. There are two large energy scales in the boundary theory. The first, Δ_S, is the energy penalty applied to boundary states which violate stabilizers of the HQECC. Above this energy scale, the geometry of the corresponding tensor network in the bulk is modified in a way that corresponds to toy models of black holes proposed previously [106]. We discuss this more fully in subsection 7.6.3. The second, Δ_L, is the energy scale at which the local simulation of point 5 from Theorems 78 and 79 breaks down. At energies above Δ_L there is no longer any meaningful duality between bulk and boundary. Δ_L has no meaning in the bulk picture.

7.6.2 Boundary to bulk mapping

So far throughout this chapter we have considered the tensor network as a map from bulk to boundary. But one of the holy grails of AdS/CFT is to construct a mapping in the opposite direction: from boundary to bulk, as that opens up the possibility of studying bulk quantum gravity via the better-understood boundary CFT. Our construction allows us to construct a toy model of such a boundary-to-bulk mapping.

Consider the boundary Hamiltonian H_{boundary} dual to some k-local bulk Hamiltonian H_{bulk} on n_{bulk} qudits, from Theorems 78 and 79. Whatever the form of H_{bulk}, H_{boundary} can always be decomposed in the form:

$$H_{\text{boundary}} = \Delta_L H_L + \Delta_S \tilde{H}_S + \tilde{H}_{\text{bulk}} \tag{7.32}$$

where $H_L = \sum_{i \in \mathcal{A}} H_{i0}$ contains strong terms which penalise states outside of the simulator subspace (these arise from the perturbation gadget techniques in the 3D/2D case, and the history state techniques in the 2D/1D case); $\tilde{H}_S$ contains all the terms arising from the simulation of the stabilizer Hamiltonian H_S (apart from the terms already included in H_L); and $\tilde{H}_{\text{bulk}}$ contains all the remaining terms arising from the simulation of H_{bulk} (again, apart from the terms included in H_L).

Let:

$$H_{\text{generic}} = \Delta_L H_L + \Delta_S \tilde{H}_S, \tag{7.33}$$

which is the boundary Hamiltonian dual to the zero Hamiltonian in the bulk. We can recover a geometric interpretation of the bulk from eq. (7.33). Consider decomposing $H_{\text{generic}}|_{\frac{\Delta_L}{2}}$ into subspaces $\mathcal{H}_n$ of energy $(n-1/2)\Delta_S \leq E \leq (n+1/2)\Delta_S$ for $n \in \mathbb{N}$ such that $E \leq \frac{\Delta_L}{2}$. Note that Lemma 76 and the fact that $\tilde{H}_S$ is a simulation (Definition 15 from Chapter 1) of H_S, $H_{\text{generic}}|_{\frac{\Delta_L}{2}}$ is block-diagonal with respect to the Hilbert space decomposition $\mathcal{H}_{\text{boundary}} = \bigoplus_n \mathcal{H}_n$.

A boundary state $|\psi\rangle_{\text{boundary}}$ with support only on the subspace $\mathcal{H}_0$ corresponds to the bulk geometry of an unperturbed tensor network. This subspace $\mathcal{H}_0$ is precisely the image of the isometry defined by the full tensor network. Thus the bulk state $|\psi\rangle_{\text{bulk}}$ dual to $|\psi\rangle_{\text{boundary}}$ can be recovered by applying the inverse of the encoding isometry V_0 for the unbroken tensor network: $|\psi\rangle_{\text{bulk}} = V_0^\dagger |\psi\rangle_{\text{boundary}}$.

A boundary state $|\psi\rangle_{\text{boundary}} \in \mathcal{H}_n$ with $n \geq 1$ corresponds to a bulk geometry where one or more of the tensors in the network has been removed (see Fig. 7.17 for details). To see this, note that a state on the boundary is in $\mathcal{H}_{n\geq 1}$ iff it has violated one of the

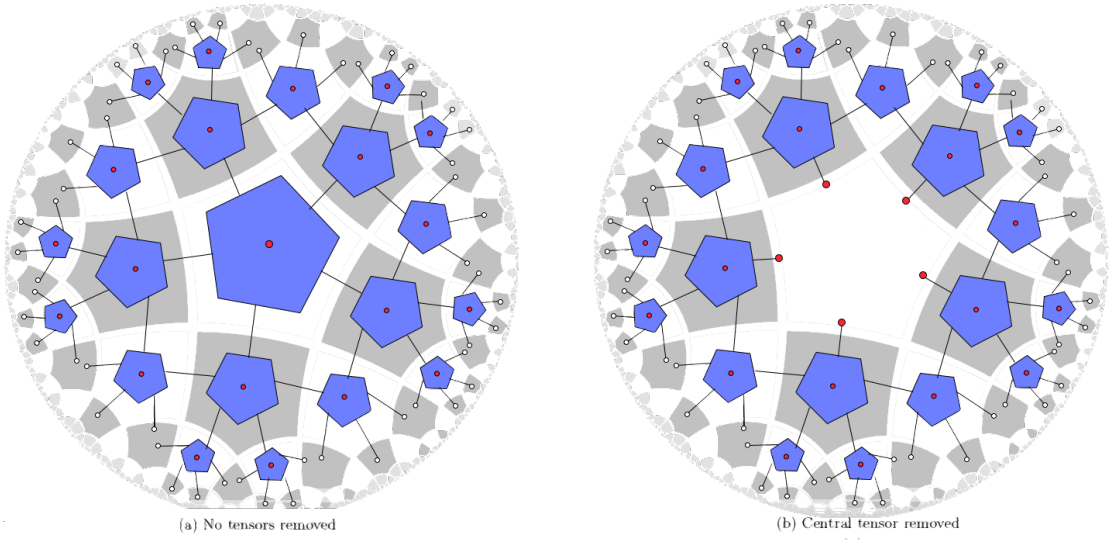

(a) No tensors removed (b) Central tensor removed

Figure 7.17: (a) The pentagon code from [106]. Red dots indicate bulk (logical) indices, white dots indicate boundary (physical) indices. (b) The pentagon code from [106] with the central tensor removed. The indices from neighbouring tensors which were contracted with the central tensor are now logical indices.

stabilizer terms of the HQECC (see Lemma 76). In the bulk it isn't meaningful to talk about states violating stabilizer terms, as the stabilizers don't act on the same Hilbert space as the bulk indices. However, if a tensor is removed from the network, the stabilizer terms associated with that tensor *do* act on the bulk indices of this modified tensor network. Therefore, for any boundary state $|\psi\rangle_{\text{boundary}} \in \mathcal{H}_n$, it is possible to determine whether it is associated with a bulk geometry which contains holes in the tensor network ($n > 0$), and how many (n), by considering just H_{generic}. Moreover, if the bulk geometry does contain holes, the location of holes can be inferred from which stabilizer terms in H_{generic} are violated by $|\psi\rangle_{\text{boundary}}$. Since (see Lemma 76) states violating different stabilizer terms are orthogonal, the subspace $\mathcal{H}_n$ corresponding to n holes in the bulk further decomposes into $\mathcal{H}_n = \bigoplus_c \mathcal{H}_{n,c}$, where the sum is over all configurations c of n holes in the tensor network. The dual bulk state can be recovered by applying the inverse of the encoding isometry $V_{n,c}$ of the tensor network with holes in the appropriate locations: $|\psi\rangle_{\text{bulk}} = V_{n,c}^\dagger |\psi\rangle_{\text{boundary}}$.

By linearity, states $|\psi\rangle_{\text{boundary}}$ with support across multiple subspaces $\bigoplus_n \bigoplus_i \mathcal{H}_{n,c}$ correspond to coherent superpositions of states with different bulk geometries, and the dual state in the bulk can be recovered via: $|\psi\rangle_{\text{bulk}} = \bigoplus_n \bigoplus_c V_{n,c}^\dagger |\psi\rangle_{\text{boundary}}$. All of this also extends to observables and operators on $\mathcal{H}_{\text{boundary}}$ in the obvious way.

A very similar analysis applies to general boundary Hamiltonians of the form eq. (7.32). H_{generic} determines the subspace decomposition $\mathcal{H}_{\text{physical}} = \bigoplus_n \bigoplus_c \mathcal{H}_{n,c}$ as before, which is independent of $\tilde{H}_{\text{bulk}}$, giving exactly the same bulk geometric interpretation of states in (and operators on) $\mathcal{H}|_{\frac{\Delta_L}{2}} = \mathcal{H}_{\text{physical}} = \bigoplus_n \bigoplus_c \mathcal{H}_{n,c}$. The only new aspect is how to recover the bulk Hamiltonian H_{bulk} dual to $\tilde{H}_{\text{bulk}}$.

If we consider $\tilde{H}_{\text{bulk}}|_{\frac{\Delta_L}{2}}$, all ancilla qudits are projected onto a one-dimensional subspace by $\Delta_L H_L$, so do not appear. Thus the resulting Hamiltonian only acts on the 'physical' qudits in the boundary theory, $\mathcal{H}_{\text{physical}}$. (I.e. the same Hilbert space as the non-local boundary Hamiltonian $H'_{\text{boundary}} = H' + \Delta_S H_S$ obtained by pushing bulk interactions and stabilizers through the tensor network, see subsection 7.2.2 for discussion, or Step 1 of Theorems 78 and 79 for full details.)

We can make the relationship between this Hamiltonian and the bulk geometry explicit, by considering how it looks with respect to the Hilbert space decomposition $\mathcal{H}_{\text{physical}} = \bigoplus_n \bigoplus_c \mathcal{H}_{n,c}$. For example, its action on the Hilbert space of the unbroken tensor network is given by:

$$H_{\text{bulk},0} = V_0 \tilde{H}_{\text{bulk}}|_{\mathcal{H}_0} V_0^\dagger \tag{7.34}$$

For general $\tilde{H}_{\text{bulk}}$, the resulting $H_{\text{bulk},0}$ will not be have any particular local structure. However, there do exist $\tilde{H}_{\text{bulk}}$ that give rise to every k-local $H_{\text{bulk},0}$. Indeed, we know exactly what form the $\tilde{H}_{\text{bulk}}$ corresponding to k-local $H_{\text{bulk},0}$ take, because these are precisely the Hamiltonians we constructed in Theorems 78 and 79 going in the other direction! Moreover, if we start with a $\tilde{H}_{\text{bulk}}$ which is dual to a k-local $H_{\text{bulk},0}$, and add weak terms coupling e.g. $\mathcal{H}_0$ and $\mathcal{H}_1$, then the resulting H_{bulk} will have a $H_{\text{bulk},0}$ as a low-energy effective theory for energies $< \Delta_S$. But it will now be possible for a state $|\psi\rangle \in \mathcal{H}_0$ to evolve to a state $|\varphi\rangle \in \mathcal{H}_1$ under the action of H_{bulk}.

7.6.3 Black hole formation in HQECC

In [106] it was suggested that black holes can be incorporated into HQECC models of AdS/CFT by removing tensors from the tensor network. Recall, if a tensor is removed from the bulk then its one logical index is replaced by $t-1$ logical indices, corresponding to the indices that were previously contracted with the missing tensor (see Fig. 7.18).

This increases the code subspace of the boundary Hilbert space, and [106] suggested that this can be interpreted as describing bulk configurations which contain a black hole. It is noted in [106] that this model ensures that every boundary state is dual

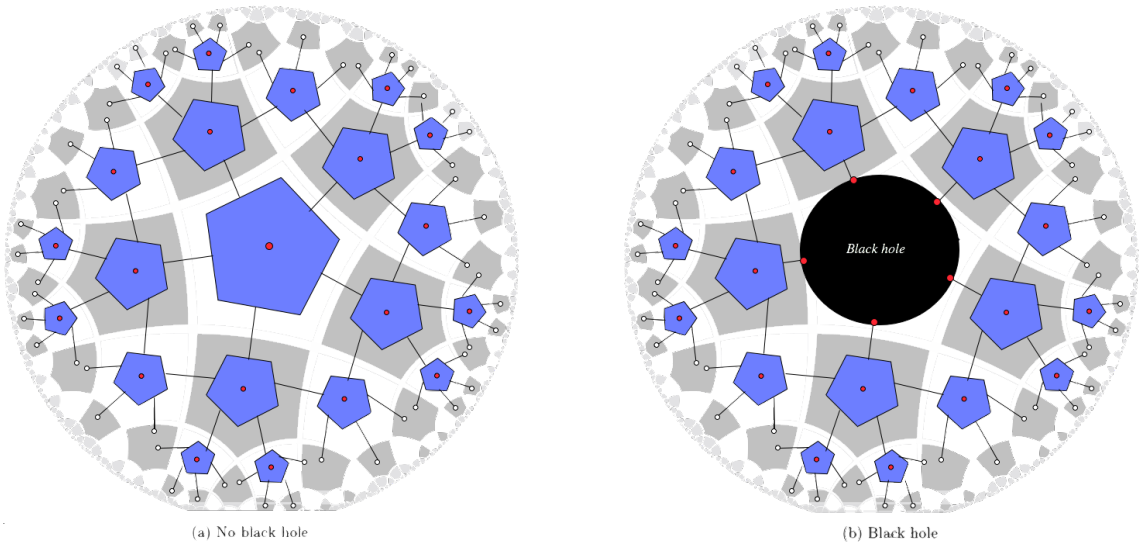

Figure 7.18: (a) The pentagon code from [106]. Red dots indicate bulk (logical) indices, white dots indicate boundary (physical) indices. (b) The pentagon code from [106] with a central black hole. The central tensor has been removed, and the indices from neighbouring tensors which were contracted with the central tensor are now logical indices.

to a bulk state, and that black hole entropy scales with area, as expected from the Beckenstein-Hawking bound [136, 137].

This method of incorporating black holes into HQECC toy models of holography may at first appear ad hoc and artificial. However, by extending the toy models of holographic duality to encompass Hamiltonians, it emerges more naturally, and can also be extended to toy models of black hole *formation*. Indeed, by considering the boundary dynamics dual to black hole formation in the bulk, we will see that removing a tensor from the network is the only way to preserve energy under unitary dynamics.

Consider a HQECC, with boundary Hamiltonian:

$$H_{\text{boundary}} = H_{\text{generic}} + \tilde{H}_{\text{bulk}} \tag{7.35}$$

where H_{generic} is as defined in the previous section. We will choose $\tilde{H}_{\text{bulk}}$ to ensure that $H_{\text{bulk},0}$ is some local Hamiltonian which models semi-classical gravity, given by:

$$H_{\text{bulk},0} = \sum_{Z} h_Z \tag{7.36}$$

where the parameter Δ_S in H_{generic} satisfies: $\Delta_S \gg ||h_Z||$, but $\Delta_S < \sum_Z ||h_Z||$. To see that it is always possible to choose $\tilde{H}_{\text{bulk}}$ which gives $H_{\text{bulk},0}$ of this form, note that we could push $H_{\text{bulk},0}$ through the tensor network and construct such a $\tilde{H}_{\text{bulk}}$. Here we are allowing ourselves the freedom to add some additional perturbation to $\tilde{H}_{\text{bulk}}$.

Consider the boundary state:

$$|\psi_1\rangle = \otimes_x \overline{A}_x |\psi_0\rangle \tag{7.37}$$

where ψ_0 is the vacuum state (the ground state), $\overline{A}_x = W^\dagger A_x W$ is the boundary operator dual to some local bulk operator A_x, and the tensor product is over $O(n)$ boundary operators, which correspond to bulk local operators acting on a shell of $O(n)$ qudits near the boundary.[30] This boundary state corresponds to a shell of matter in the bulk near the boundary.

Each bulk local excitation will pick up energy, δ_E, from only a few of the local h_Z terms, but the overall state will have large energy from summing over all these contributions. The energy on the boundary is equal to the energy in the bulk theory, so we must have:

$$\langle\psi_1| H_{\text{boundary}} |\psi_1\rangle = \sum_{x=0}^{O(n)} \delta_E = O(n\delta_E). \tag{7.38}$$

For suitably chosen Δ_S, the total energy of this configuration $E(|\psi_1\rangle) = O(n\delta_E) > \Delta_S$. However, the local operators $\overline{A}_x$ are encoded versions of bulk operators, so acting on $|\psi_0\rangle$ with $\overline{A}_x$ will not take the state outside of the code subspace. Therefore, $|\psi_1\rangle$ is in the code subspace of the HQECC.

The boundary will evolve under H_{boundary}. The bulk time dynamics can be approximated by $H_{\text{bulk},0}$. This will lead to an error ϵt that increases only linearly in t [6, Proposition 29]. So this approximation will be valid for sufficiently long times.

If we assume that under the action of $H_{\text{bulk},0}$ this shell of matter collapses inwards towards the centre of the HQECC (as would be expected from a Hamiltonian that models gravity), then the bulk will unitarily evolve to a configuration where most regions are in a low energy state (with respect to the Hamiltonians that act there), and most of the energy comes from a few ($O(1)$) terms near the centre of the HQECC. Denote the boundary state dual to this bulk configuration by $|\psi_2\rangle$.

[30] The hyperbolic geometry ensures that there are $O(n)$ qudits in a shell near the boundary.

The evolution is unitary, so we must have that:

$$\langle\psi_2|\, H_{\text{boundary}}\, |\psi_2\rangle = \langle\psi_1|\, H_{\text{boundary}}\, |\psi_1\rangle \tag{7.39}$$

where $\langle\psi_1|\, H_{\text{boundary}}\, |\psi_1\rangle = O(n\delta_E) > \Delta_S$. The bulk must have the same energy as the boundary. But the maximum energy the bulk could have picked up from $O(1)$ h_Z terms is given by:

$$\sum_{x=0}^{O(1)} ||h_Z|| = O\left(||h_Z||\right). \tag{7.40}$$

By assumption $\Delta_S \gg ||h_Z||$, so it is not possible for the bulk to pick up energy greater than Δ_S from $O(1)$ h_Z terms.

If we consider the boundary system, it is possible for the boundary to pick up energy greater than Δ_S either from (the encoded version) of many h_Z terms, or by violating one of the stabilizers of the HQECC. Since the bulk state dual to $|\psi_2\rangle$ cannot pick up energy from many h_Z terms, the only way for $|\psi_2\rangle$ to pick up energy greater than Δ_S is to violate a stabilizer term.

Violating a stabilizer corresponds to picking up energy from the $\tilde{H}_S$ term in the boundary Hamiltonian. On the boundary it is clear that if we begin in a state inside the code space with energy greater than Δ_S it is possible to unitarily evolve to a state which is outside the code space and violates a stabilizer (provided that $\tilde{H}_{\text{bulk}}$ does not commute with $\tilde{H}_S$ – see discussion below).

In the undisturbed bulk geometry it is not meaningful to talk about violating a stabilizer, as the stabilizers do not act on the same Hilbert space as the bulk logical indices. If, however, one of the bulk tensors has been removed, as in the models of black holes from [106], then the stabilizers corresponding to the removed tensor *do* act on the Hilbert space of the $t-1$ new logical indices, and it is meaningful to talk about these stabilizers being violated.

Therefore, the only way for the system to conserve energy under these dynamics is for the tensor network corresponding to the boundary state to be 'broken', and for at least one of the stabilizers corresponding to the missing tensor to be violated. This process therefore predicts the dynamical formation of a toy model black hole as proposed in [106].

In order for this process to occur we must have:

$$[\tilde{H}_S, \tilde{H}_{\text{bulk}}] \neq 0 \tag{7.41}$$

(If we had some $\tilde{H}'_{\text{bulk}}$ which commuted with $\tilde{H}_S$ then there would be no coupling between the code-space, $C \in \mathcal{H}_{\text{boundary}}$, and the rest of the boundary, $\overline{C} \in \mathcal{H}_{\text{boundary}}$. So it would not be possible for $|\psi_1\rangle \in C$ to unitarily evolve to $|\psi_2\rangle \in \overline{C}$.)

In the bulk, eq. (7.41) implies that $H_{\text{bulk},0}$ is a low energy effective theory. The full bulk Hamiltonian includes some coupling between $\mathcal{H}_0$ and $\mathcal{H}_{\geq 1}$ (where $\mathcal{H}_n$ is as defined in the previous section). It therefore doesn't act only on the logical indices of the unbroken tensor network, and so the tensor network is always an approximation to the actual bulk theory. Another recent paper which examined bulk geometries containing black holes also showed that the bulk reconstruction in AdS/CFT is necessarily only approximate [138].

eq. (7.41) also implies that the toy model black hole degrees of freedom will (in general) be entangled with the rest of the tensor network. We can write the boundary Hamiltonian as:

$$H_{\text{boundary}}|_{\frac{\Delta_L}{2}} = H_C \otimes \mathbb{1} + \mathbb{1} \otimes H_{\overline{C}} + \text{coupling terms} \tag{7.42}$$

where eq. (7.41) ensures that the coupling terms are non-zero. Since the coupling terms are non-zero, any boundary state which is separable across the C / $\overline{C}$ partition (equivalently, any bulk state which is separable across the black hole boundary) is not a stationary state of H_{boundary}, so separable states will always evolve to entangled states. Therefore, the black hole degrees of freedom (if we trace out the rest of the tensor network) will always evolve to a mixed state. Similarly, on the boundary tracing out part of the system will lead to a mixed state. In this sense the black hole (and the equivalent state on the boundary) has thermalized.

It also follows from this discussion that the toy models of black holes correspond to high energy states on the boundary, which pick up their energy from a small number of high energy terms in the Hamiltonian.

Therefore, with an appropriately chosen $\tilde{H}_{\text{bulk}}$, we can model black hole formation in our HQECC. No information is lost in this process (as the dynamics are unitary we can always reverse them). But the isometry which takes bulk states to boundary states will have changed, so the 'dictionary' for reconstructing the bulk state from the boundary state will be different. In particular, the fraction of the boundary needed to reconstruct an operator acting on the central bulk region will increase in the presence of a toy-model black hole.

To see this consider a central black hole where one tensor is removed from the HQECC. An operator which acts on the degrees of freedom representing the black hole acts on all $t-1$ of the logical indices, so will need to be pushed through all of the $t-1$ tensors at radius 1 in the HQECC. In the absence of any black hole an operator acting on the central bulk index could be reconstructed via pushing through just $\lceil \frac{t}{2} \rceil$ of the tensors at radius 1 in the HQECC. Thus the fraction of the boundary needed for bulk reconstruction of the centre has increased.

Throughout this discussion we have concentrated on a black hole in the centre of the bulk for clarity, but these qualitative conclusions apply equally well to black holes situated at any point in the bulk.

7.6.4 Other geometries

We have constructed a duality between quantum many-body models in $\mathbb{H}^d$ and models living on its $d-1$-dimensional boundary, as a toy model for a duality between Anti-de Sitter space and its boundary. From a cosmological perspective it would also be interesting to consider toy models of dualities between positively curved / flat geometries, and their boundaries.

There is no reason to suspect that the error correcting properties of AdS/CFT should be recreated in such dualities, so it is not clear that the error correcting code constructions of HQECC will be relevant. However, the analogue Hamiltonian simulation theory from [6] can be applied in any geometry. It follows immediately from the results in [6] that it is possible to construct a duality between Euclidean or spherical geometry in dimension 3, and a 2D 'boundary' surface. However, it is not clear whether such a 'boundary' surface can be considered a geometric boundary in any meaningful sense.

In Euclidean geometry, results from [6] imply that in order to simulate n bulk qudits in $\mathbb{E}^3$ with a local boundary model requires $O(\text{poly}(n))$ boundary qudits. If we maintain the density of qudits from the bulk on the boundary, this implies that if the bulk qudits were contained in a ball of radius R, then the boundary surface would be at a radius $R' = O(R + \text{poly}(n))$. So the distance between the bulk qudits and the boundary surface would increase polynomially with n.

The situation in the positively curved case is worse. $\mathbb{S}^3$ is finite, so the boundary surface required to simulate n qudits which lie in $\mathbb{S}^3$ might not itself lie in $\mathbb{S}^3$. Therefore, while it is possible to construct a duality between $\mathbb{E}^3$ or $\mathbb{S}^3$ and a 2D

surface, it is not clear whether such a duality could be considered a bulk / boundary mapping.

7.6.5 Limitations to our constructions

The constructions presented in this chapter inherit some of the drawbacks of the HaPPY code. In particular, the Ryu-Takayanagi formula is not obeyed exactly for arbitrary bulk regions; there exist certain pathological choices of boundary region, A, for which there are bulk operators that are not recoverable on A nor on A^c (violating complementary recovery). Like the HaPPY code, the tensor network cannot describe sub-AdS geometry as it is only defined at scales larger than the AdS radius. A number of holographic codes have been constructed which build on the HaPPY code and do not have these drawbacks. Notable examples include bidirectional holographic codes (BHC) composed of pluperfect tensors [109], and random tensor network constructions [110].

In Chapter 8 we present two further constructions of HQECC, which build on the techniques in [110] and overcome some of these drawbacks.

Chapter 8

Holographic duality between local Hamiltonians from random tensor networks

8.1 Introduction

In this chapter we demonstrate that the holographic toy model mapping between local Hamiltonians described in Chapter 7 can be constructed from networks of random tensors rather than tensors chosen with particular properties. This is motivated by the construction of a toy model of holographic duality that simultaneously maps between local Hamiltonians and recovers the expected Ryu-Takayangi entropy formula for general cases. These properties have previously been demonstrated independently using Hamiltonian simulation theory Chapter 7 and random tensor networks [110] respectively. By showing that both these properties can be realised simultaneously, this work advances a further step along the path of mathematically rigorous constructions of holographic codes that capture more features of the AdS/CFT correspondence. Perhaps the most important consequence is to push the boundary further out between those features of holography that can already be realised without incorporating gravity into the model, and those that could be inherently gravitational.

The following section of this chapter informally presents our main results with an overview of the proofs. The full mathematical proofs of our main results are given in Section 8.2 going via results concerning the concentration of random stabilizer tensors about perfect tensors and the agreement with the Ryu-Takayanagi entropy formula, before finally presenting a description of our holographic toy model. The

conclusions of the current chapter and the previous chapter are presented together in Chapter 9.

8.1.1 Our results

We set up a duality between states, observables and local Hamiltonians in d-dimensional hyperbolic space and its $(d-1)$-dimensional boundary, for $d = 2, 3$. In the model a general local Hamiltonian acting in the bulk has an approximate dual 2-local nearest-neighbour Hamiltonian on the boundary. The mapping has redundant encoding leading to error correcting properties where the reconstruction of any bulk operator acting in the entanglement wedge of a boundary region is protected against erasure of the rest of the boundary Hilbert space. This implies complementary recovery for all partitions of the boundary and all local bulk operators. The entanglement entropy of general boundary regions obeys the Ryu-Takayanagi formula exactly where there is no bulk entanglement. Furthermore the effect of introducing bulk entanglement qualitatively agrees with the entropic corrections expected in real AdS/CFT.

The explicit encoding is a chain of simulations, the first of which is described by a tensor network HQECC. The geometry of our network is inherited from Chapter 7 where hyperbolic bulk space is tessellated by space-filling Coxeter polytopes. In our set-up a random stabilizer tensor is placed in each polytope with one tensor index identified as the bulk index and the rest contracted through the faces of the polytopes. With a suitably high tensor bond dimension we are able to achieve several features of AdS/CFT simultaneously with high probability. Therefore, by choosing a model of semi-classical gravity in the bulk this construction is an explicit toy model of holography, providing a mathematically rigorous tool for exploring the physics of this setting. The notable features of our construction are summarised in the following statement of our main result, these are then made precise in Theorem 79 for the 2D to 1D duality and in Theorem 90 for 3D to 2D.

Theorem 80 (Informal statement of holographic constructions)**.** *Given any (quasi) local bulk Hamiltonian acting on qudits in $(d = 2, 3)$-dimensional AdS space, we can construct its dual Hamiltonian acting on the $(d-1)$-dimensional boundary surface such that:*

1. *All relevant physics of the bulk Hamiltonian are arbitrarily well approximated by the boundary Hamiltonian, including its eigenvalue spectrum, partition function and time dynamics.*

2. *The boundary Hamiltonian is 2-local acting on nearest neighbour boundary qudits, realising a mapping between models.*

3. *The entanglement structure mirrors AdS/CFT as the Ryu-Takayanagi formula is obeyed exactly for any boundary subregion in the absence of bulk entanglement.*

4. *Any local observable/measurement in the bulk has a set of corresponding observables/measurements acting on portions of boundary as described by the AdS Rindler reconstruction giving complementary recovery.*

This result could be extended to higher dimensions. In particular, all the techniques in Theorem 90 generalise to higher dimensions, all that is needed to generalise the result is to find examples of tessellations meeting the requirements of the construction. While the formal theorems set out the details of the boundary, intuitively the geometry is what we expect from the concept of a boundary of a finite bulk space and the number of boundary qudits scales almost linearly with the number of bulk qudits.

The proof combines many of the techniques from previous works: perturbation gadgets and the structure of the Coxeter group Chapter 7; the theory of Hamiltonian simulation [6], history state simulation techniques Chapter 2 and drawing comparison to a classical Ising model [110]. The main function of the results in this chapter are to demonstrate that these techniques can be successfully employed together with no arising contradictions, generating a more complete toy model of holography. Full proof of the result and the relation between the bond dimension and the probability of obtaining the encoding described are given in Section 8.2.

8.2 Results with technical details

We construct tensor network HQECCs by embedding random stabilizer tensors with t legs into each cell of space-filling tessellations of hyperbolic 2-space and hyperbolic 3-space. The tessellations are defined by Coxeter systems chosen such that the Coxeter polytope has an odd number of faces[1]. Each tensor has one uncontracted leg associated as the logical bulk index, the remaining legs are contracted with the tensors that occupy the neighbouring polyhedral cells. The tessellation is finite such that at the cut-off the uncontracted tensor legs become the physical boundary indices.

In this section we demonstrate particular properties of this construction. First we present a mathematically rigorous characterisation of the concentration of random stabilizer tensors about perfect tensors with increasing bond dimension, using the

[1] An odd number of faces is essential for complementary recovery see Lemma 88

algebraic structure of the stabilizer group to arrive at a probability bound on having an exact perfect tensor. Then we demonstrate via an Ising model mapping that the entanglement structure of general boundary subregions obeys the Ryu-Takayanagi formula exactly when there is no entanglement in the bulk input state. Here we also show that the construction exhibits complementary recovery for all choices of boundary bipartition and all local bulk operators, an advance on previous models where exceptions could be found. Finally we use simulation techniques to break down global interactions at the boundary to demonstrate that at the same time as achieving exact Ryu-Takayanagi we can describe a duality between models that encompasses local Hamiltonians.

8.2.1 Random stabilizer tensor networks describe an isometry

In contrast to the perfect tensor case, it is not immediately clear that random stabilizer tensor networks with large dimension correspond to an *exact* isometric mapping or maximum distance stabilizer codes. Since the product of isometries is still an isometry, we can focus on proving a result for an individual random stabilizer tensor. Our first result is that random stabilizer tensors with large bond dimension are perfect stabilizer tensors with high probability. This implies that simultaneously exhibiting the advantageous properties of perfect stabilizer and random tensors is realisable. This was previously shown to be true for random tensors in HQECCs where the dimensions of the bulk indices and boundary indices were chosen appropriately [110]. In the following we explicitly work out the relation between the probability and bond dimension, and our result is applicable to tensors with uniform bond dimension.

The key ingredient in this proof is that random states in high dimensional bipartite systems are subject to the "concentration of measure" phenomenon. This means that with high probability a function of the random state will concentrate about its expectation value [117]. We will show that for a random stabilizer state on n qudits, the von Neumann entropy of every subset of the tensor's indices with $|A| = \lfloor t/2 \rfloor$ is maximal with high probability. This is a necessary and sufficient condition for the state to be AME and therefore for the tensor to be perfect. To ensure the tensor is exactly perfect as opposed to close to perfect – which would not guarantee that the tensor described MDS stabilizer codes – we will use the particular algebraic structure of stabilizer states to constrain the values that the entropy can take.

8.2.1.1 Concentration bounds

Measure concentration is the surprising observation that a uniform measure on a hypersphere will strongly concentrate about the equator as the dimension of the hypersphere grows. This implies that a smoothly varying function of the hypersphere will also concentrate about its expectation. Levy's lemma formalises the concentration of measure in the rigorous sense of an exponential probability bound on a finite deviation from the expectation value:

Lemma 81 (Levy's lemma; see [139])**.** *Given a function $f : \mathbb{S}^d \mapsto R$ defined on the d-dimensional hypersphere $\mathbb{S}^d$, and a point $\phi \in \mathbb{S}^d$ chosen uniformly at random,*

$$\text{Prob}_H \left[|f(\phi) - \langle f \rangle| \geq \epsilon \right] \leq 2 \exp\left(\frac{-2C_1(d+1)\epsilon^2}{\eta^2} \right), \tag{8.1}$$

where η is the Lipschitz constant of f, given by $\eta = \sup |\nabla f|$, and C_1 is a positive constant (which can be taken to be $C_1 = (18\pi^3)^{-1}$).

Pure d_{AB}-dimensional quantum states can be represented by points on the surface of a hypersphere in $(2d_{AB} - 1)$ dimensions due to normalisation. Therefore by setting $d = 2d_{AB} - 1$, the above can be applied to functions of states $|\phi\rangle_{AB}$ chosen randomly with respect to the Haar measure. However for this construction it is important that we use random stabiliser states, $|\psi\rangle_{AB}$, so we must take an exact 2-design. Low showed in [140] that in general t-designs give large deviations, particularly for low t. However, by leveraging intermediate results of [140] alongside a quantisation condition on entropy for stabiliser states we will show that $S(\text{tr}_B(|\psi\rangle\langle\psi|)) = \log d_A$ with high probability. In order to arrive at this more general concentration result for entropy we will need the following bound on moments.

Lemma 82 (Bound on moments; see [140] Lemma 3.3)**.** *Let X be any random variable with probability concentration*

$$\text{Prob}\left(|X - \mu| \geq \epsilon \right) \leq C_2 e^{-a\epsilon^2}. \tag{8.2}$$

(Normally μ will be the expectation of X, although the bound does not assume this.) Then,

$$\langle |X - \mu|^m \rangle \leq C_2 \Gamma(m/2+1) a^{-m/2} \leq C_2 \left(\frac{m}{2a} \right)^{m/2} \tag{8.3}$$

for any $m > 0$.

In particular, if the function f is a polynomial of degree 2 then the expectation value with respect to the Haar measure or an exact 2-design are equal. While the von

Neumann entropy is not such a function, the flat eigenspectra of stabiliser states demonstrated in subsection 8.2.1.3 allows us to equivalently consider the Rényi-2 entropy which is the logarithm of a degree 2 polynomial, $S_2(\rho_A) = -\log\big(\mathrm{tr}(\rho_A^2)\big)$. We first use Levy's lemma to bound the probability concentration of the purity of Haar random states, then using Lemma 82 link this concentration to entropy of pseudo random states.

8.2.1.2 Expectation of $\mathrm{tr}(\rho_A^2)$

The average reduced density matrix of any bipartite Haar random state is the maximally mixed state, $\mathbb{1}/d_A$, following from the invariance of the Haar measure. This is the premise for expecting that the average entropy of high dimensional random stabilizer states is close to maximal with some small fluctuation. However, we will need the expectation of the purity of random stabilizer states, $\mathrm{tr}(\rho_A^2)$, in order to translate Levy's lemma applied to a Haar random degree-2 polynomial into a concentration statement concerning the entropy of stabilizer states.

Lemma 83 (Average of the purity)**.** *Given a stabilizer state $|\psi\rangle_{AB}$ on t qudits of prime dimension p, bipartitioned into subsets A and B of t_A and t_B qudits respectively where $t_A \leq t_B$. The average purity of the reduced density matrix is given by,*

$$\left\langle \mathrm{tr}_A(\rho_A^2) \right\rangle = \frac{d_A + d_B}{d_{AB} + 1} \tag{8.4}$$

where $d_A = p^{t_A}$, $d_B = p^{t_B}$, $d_AB = p^{t_A + t_B}$ are the dimensions of the respective (sub)spaces.

Proof. See the proofs of [12, Lemmas 3.4 & 3.5]. □

8.2.1.3 Quantised entropy of stabilizer states

Applying Levy's lemma to the purity of Haar random states, along with the bounds on moments from Lemma 82, is already sufficient to conclude that high dimensional random stabilizer tensors are *close* to perfect with high probability [2]. Some properties of perfect tensors will follow approximately from this statement. For example, the tensor is an approximate isometry across any bipartition where the departure can be suppressed by scaling the bond dimension. One could individually investigate the behaviours of this approximate perfect tensor to see if the deviation can be suppressed in all relevant cases. Instead we look to exploit the algebraic structure of the stabilizer group to demonstrate a strengthened result: high dimensional random stabilizer tensors are *exactly* perfect still with high probability.

[2] $S(\rho_A)$ is always lower bounded by $S_2(\rho_A)$

Theorem 84 (Quantisation of entropy)**.** *Given a stabilizer state $|\psi\rangle_{AB}$ on t qudits of prime dimension p, bipartitioned into subsets A and B of t_A and t_B qudits respectively where $t_A \leq t_B$. The reduced density matrix, ρ_A, has a flat spectrum and its entropy, $S(\rho_A)$, is quantised in units of* $\log p$.

Proof. See [12, Theorem 3.6] □

8.2.1.4 Random stabilizer tensors are perfect tensors with high probability

Our first key result is that a random stabilizer tensor is exactly perfect with probability that can be pushed arbitrarily close to 1 by scaling the bond dimension, p. Formally,

Theorem 85 (Random stabilizer tensors are perfect)**.** *Let the tensor T, with t legs, describe a stabilizer state $|\psi\rangle$ chosen uniformly at random where each leg corresponds to a prime p-dimensional qudit. The tensor T is perfect in the sense of Definition 56 with probability*

$$P \geq \max\left\{0, 1 - \frac{1}{2p^b}\binom{t}{\lfloor t/2 \rfloor}\right\} \tag{8.5}$$

in the limit where p is large, Where $0 < b \leq 1$.

Proof. A sufficient condition for a tensor to be perfect is that the reduced density matrix of every subset of legs $|A| = \lfloor t/2 \rfloor$ is maximally mixed, using condition (ii) from Definition 93 of an AME state. We first use concentration results to find the probability of being maximally entangled across a given bipartition with $d_A = p^{\lfloor t/2 \rfloor}$ and $d_B = p^{\lceil t/2 \rceil}$.

Applying Levy's lemma to the purity (using the bound on the Lipschitz constant found in e.g. [140, Lemma 4.2].) gives a bound on the probability tails for Haar random states, $|\phi\rangle_{AB}$,

$$\begin{aligned}
\text{Prob}_H\left(|\operatorname{tr}(\sigma_A^2) - \mu| \geq \epsilon\right) &\leq 2\exp\left(\frac{-4C_1 p^t \epsilon^2}{\eta^2}\right) && (8.6)\\
&\leq 2\exp\left(\frac{-4C_1 p^t \epsilon^2}{4}\right) && (8.7)\\
&\leq 2\exp\left(-C_1 p^t \epsilon^2\right), && (8.8)
\end{aligned}$$

where $\sigma_A = \operatorname{tr}_B(|\phi\rangle\langle\phi|)$ and μ is the mean of purity. Since purity is a degree-2 polynomial, and stabililizer states form a 2-design, the expectation value over random stabilizer states and Haar random states coincide (see subsection 8.2.1.2).

This can be combined with Lemma 82 where $m = 1$, $C_2 = 2$ and $a = C_1 p^t$ to give

$$\langle |\operatorname{tr}(\sigma_A^2) - \mu| \rangle_H \leq C_2 \left(\frac{m}{2a}\right)^{m/2} \tag{8.9}$$

$$= 2\left(\frac{1}{2C_1 p^t}\right)^{1/2}. \tag{8.10}$$

Starting with Markov's inequality, eq. (8.10) is used to upper bound the probability that the purity of stabilizer states is higher than the mean:

$$\operatorname{Prob}_{k=2}\left(\operatorname{tr}(\rho_A^2) \geq \mu + \delta\right) \leq \frac{\langle \operatorname{tr}(\rho_A^2) \rangle_{k=2}}{\mu + \delta} \tag{8.11}$$

$$= \frac{\langle \operatorname{tr}(\sigma_A^2) \rangle_H}{\delta + \mu} \tag{8.12}$$

$$= \frac{\langle \operatorname{tr}(\sigma_A^2) - \mu \rangle_H + \mu}{\delta + \mu} \tag{8.13}$$

$$\leq \frac{\langle |\operatorname{tr}(\sigma_A^2) - \mu| \rangle_H + \mu}{\delta + \mu} \tag{8.14}$$

$$\leq \frac{2\sqrt{\frac{1}{2C_1 p^t}} + \mu}{\delta + \mu}, \tag{8.15}$$

where $\rho_A = \operatorname{tr}_B(|\psi\rangle\langle\psi|)$. We have considered the $\operatorname{tr}(\rho_A^2) > \mu$ case since it is the lower tail of $S(\rho_A)$ we are interested in bounding. In eq. (8.12) we have replaced the expectation over random stabilizer states ρ_A with the expectation over Haar random states σ_A, since $\operatorname{tr}(\rho_A^2)$ is a degree-2 polynomial and stabilizer states form a 2-design.

Theorem 84 demonstrated that the eigenspectrum is flat and therefore all Rényi entropies are equal. Therefore we can relate the above probability statement to the von Neumann entropy via the Rényi-2 entropy using $S(\rho_A) = S_2(\rho_A) = -\log\left(\operatorname{tr}(\rho_A^2)\right)$,

$$\operatorname{Prob}_{k=2}\left(\operatorname{tr}(\rho_A^2) \geq \mu + \delta\right) = \operatorname{Prob}_{k=2}\left(\log \operatorname{tr}(\rho_A^2) \geq \log(\mu + \delta)\right) \tag{8.16}$$

$$= \operatorname{Prob}_{k=2}\left(-\log \operatorname{tr}(\rho_A^2) \leq -\log(\mu + \delta)\right) \tag{8.17}$$

$$= \operatorname{Prob}_{k=2}\left(S(\rho_A) \leq -\log(\mu + \delta)\right). \tag{8.18}$$

Using Lemma 83 to substitute the average purity $\left(\mu = \frac{d_A+d_B}{d_A d_B+1}\right)$ further manipulation gives this probability in terms of deviation from the maximum entropy:

$$\begin{aligned}&\text{Prob}_{k=2}\left(\text{tr}(\rho_A^2) \geq \mu+\delta\right)\\ &\quad= \text{Prob}_{k=2}\left(S(\rho_A) \leq \log d_A - \underbrace{\log\left(\frac{d_A+d_B}{d_B+1/d_A}+\delta d_A\right)}_{\Delta}\right).\end{aligned} \tag{8.19}$$

Combining eq. (8.15) and eq. (8.19) gives

$$\text{Prob}_{k=2}\left(S(\rho_A) \leq \log d_A - \Delta\right) \leq \frac{2\sqrt{\frac{1}{2C_1 p^t}}+\mu}{\delta+\mu}. \tag{8.20}$$

In the limit of large p this bound scales as:

$$\frac{2\sqrt{\frac{1}{2C_1 p^t}}+\mu}{\delta+\mu} = O\left(\frac{p^{-t/2}+p^{-\lfloor t/2\rfloor}}{\delta+p^{-\lfloor t/2\rfloor}}\right) = O\left(\frac{1}{\delta p^{\lfloor t/2\rfloor}}\right). \tag{8.21}$$

We know that the entropy is quantised in units of $\log(p)$ (see Theorem 84). Therefore if the deviation from the mean, Δ, is less than $\log(p)$, then eq. (8.20) describes the probability of the entropy being less than its maximum value. The quantisation is less than the quantisation unit if:

$$\Delta \leq \log p \tag{8.22}$$

$$\frac{d_A+d_B}{d_B+1/d_A}+\delta d_A \leq p \tag{8.23}$$

$$\frac{p^{\lfloor t/2\rfloor}+p^{\lceil t/2\rceil}}{p^{\lceil t/2\rceil}+p^{-\lfloor t/2\rfloor}}+\delta p^{\lfloor t/2\rfloor} \leq p. \tag{8.24}$$

For any t, the following marginally stronger condition on δ will also ensure that eq. (8.22) is satisfied

$$2+\delta p^{\lfloor t/2\rfloor} \leq p \tag{8.25}$$

$$\delta \leq p^{-\lfloor t/2\rfloor}(p-2), \tag{8.26}$$

which is satisfied by $\delta = O(p^{b-\lfloor t/2 \rfloor})$ with $0 \leq b < 1$. Combining this and the bound from eq. (8.21), we find that in the limit of large p, eq. (8.20) becomes,

$$\text{Prob}_{k=2}\left(S(\rho_A) \neq \log d_A\right) \leq \frac{1}{\delta p^{\lfloor t/2 \rfloor}} \tag{8.27}$$

$$\leq \frac{1}{p^b} \tag{8.28}$$

and the state is maximally entangled across a *given* equal bipartition with probability,

$$P' \geq 1 - \frac{1}{p^b}. \tag{8.29}$$

Maximal entropy across *every* bipartition is required for the state to be AME and hence the tensor to be perfect. The number of distinct ways to equally bipartition a tensor of t legs is $\binom{t}{\lfloor t/2 \rfloor}/2$. Making no assumption about the dependence of the events A_i, Fréchet inequalities [141, 142] bound the conjunction probability of N events by:

$$\begin{aligned} \max\{0, P(A_1) + P(A_2) + \ldots + P(A_N) - (N-1)\} &\leq P(A_1 \cap A_2 \cap \ldots \cap A_N) \\ &\leq \min\{P(A_1), P(A_2), \ldots P(A_N)\}. \end{aligned} \tag{8.30}$$

Hence the joint probability of all $\binom{t}{\lfloor t/2 \rfloor}/2$ bipartitions satisfying $S(\rho_A) = \log d_A$ is lower bounded by

$$P \geq \max\left\{0, \binom{t}{\lfloor t/2 \rfloor}\frac{P'}{2} - \left[\binom{t}{\lfloor t/2 \rfloor}/2 - 1\right]\right\} \tag{8.31}$$

$$\geq \max\left\{0, 1 - \frac{1}{2p^b}\binom{t}{\lfloor t/2 \rfloor}\right\}. \tag{8.32}$$

□

Consequently by making p arbitrarily large, P' and subsequently P can be pushed close to 1 independent of t. Therefore by scaling the bond dimension we can ensure that, with high probability, the random stabilizer tensor is exactly a perfect tensor describing a qudit stabilizer AME state.

It follows from this result that an individual random stabilizer tensor inherits all the properties of perfect stabilizer tensors with probability that can be made arbitrarily close to 1 by increasing the bond dimension p. That is, they are an isometry across

any bipartition and describe a family of stabilizer MDS codes, where there exists a consistent choice of basis that preserves the Pauli rank of the operator.

8.2.2 Entanglement structure

We now investigate the entanglement structure of our proposed holographic code, since the principal motivation for choosing random tensors was to demonstrate a construction that exactly obeys Ryu-Takayanagi while simultaneously mapping between local Hamiltonians. In this section we show that with high probability, when the bond dimension is large, our HQECC construction obeys the Ryu-Takayanagi entropy formula exactly for all boundary regions. We demonstrate this rigorously for arbitrary unentangled bulk states. We lean heavily on the work of [110], where by mapping to a classical spin system they were able to say something about the entropies in a random network.

First using their lower bound on the average entanglement entropy we make an exact statement of Ryu-Takayanagi for stabilizer product bulk states, while the general product state case is only approximate. Reusing their mapping Hayden et al. also present near complementary recovery via an entropic argument. We follow their proof structure but taking care and refining our network set-up to ensure any local operator acting on a bulk index can be recovered on either subregion for all bipartitions of the boundary. Finally we use this complementary recovery result to elevate the exact statement of Ryu-Takayanagi to apply to arbitrary product bulk states.

8.2.2.1 Approximate Ryu-Takayanagi

Hayden et al. investigated properties of general random tensor networks in [110], particularly their entanglement structure. Their methods involve interpreting functions of the tensor network as partition functions of the classical Ising model, which leads to Ryu-Takayanagi minimal surfaces manifesting as domain walls between spin regions. For further details of the construction we refer to [110]. In particular, for the case of random tensor networks constructed via 2-designs, they derive the following bounds on entropy:

Lemma 86 (Lower bound on the entanglement entropy; discussion in appendix F of [110])**.** *The average entanglement entropy of a general boundary region A of a random stabilizer tensor network is lower bounded by*

$$S_{RT}(\rho_A) - [\ln k + o(1)] \leq \langle S_2(\rho_A)\rangle_{\neq 0} \leq \langle S(\rho_A)\rangle_{\neq 0}, \tag{8.33}$$

where $\langle\rangle_{\neq 0}$ *is the average over all choices of network excluding the cases resulting in* $\rho_{\mathcal{B}} = 0$ *where the entropy is not well-defined.*

Using the above results we come to our first statement about the entanglement entropy of general boundary subregions that can be applied to our construction.

Lemma 87 (Approximate Ryu-Takayanagi)**.** *For a random stabilizer tensor network with bond dimension p, let* $S(\rho_A)$ *be the entanglement entropy of A, any (disconnected or connected) subregion of the boundary. Given*

1. *an arbitrary tensor-product bulk input state:*

$$\text{Prob}\left[S_{RT}(\rho_A) - S(\rho_A) \geq a \cdot (\ln k + o(1))\right] \leq \frac{1}{a}. \tag{8.34}$$

   Hence the entanglement entropy can be made to be $(a \cdot \ln k)$*-close to the Ryu-Takayanagi entropy with probability* $\left(1 - \frac{1}{a}\right)$ *by scaling the bond dimension p.*

2. *a stabilizer tensor-product bulk input state, conditional on* $\log p > a \cdot (\ln k + o(1))$*:*

$$\text{Prob}\left[S_{RT}(\rho_A) = S(\rho_A)\right] \geq 1 - \frac{1}{a}. \tag{8.35}$$

   Therefore by scaling p, a can be made arbitrarily large so that the probability of having ***exactly*** *the Ryu-Takayanagi entropy is pushed to 1.*

$S_{RT}(\rho_A) = |\gamma_A| \ln(p)$ *is the Ryu-Takayanagi entropy for an unentangled bulk state.* $\rho_{\mathcal{B}}$ *is the density operator of the resulting boundary state after the bulk state has been encoded by the tensor network such that* $\rho_A = \text{tr}_{A^c}(\rho_{\mathcal{B}})$*.* k *is the number of minimal geodesics through the graph and* $a > 0$*.*

Proof. The proof follows by applying Markov's inequality to the bounds in Lemma 86 for the case of general product states. And using quantisation of entropy for stabilizer states. See [12, Lemma 3.10]. □

The proof of Lemma 87 does not require that A is a single connected boundary region since minimal domain walls ground states apply for disconnected boundary regions, depicted in Fig. 8.1. This is a key advantage over the techniques used in the HaPPY paper [106] which do require a connected boundary region. Furthermore, the above result accounts for the possibility of multiple geodesics which may occur for our network's geometry.

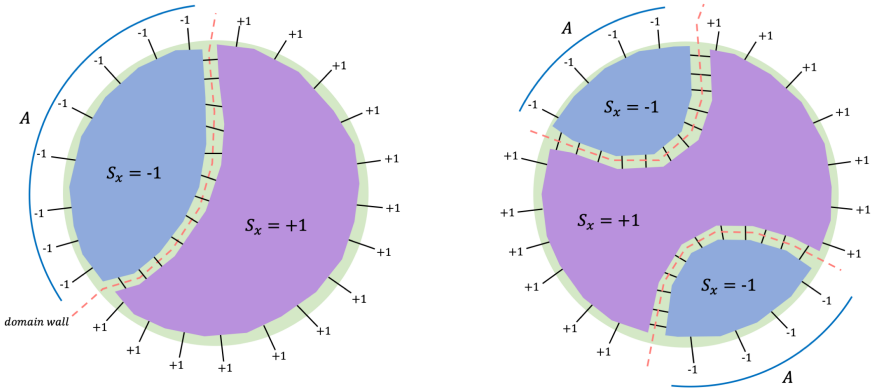

Figure 8.1: Example of spin configurations used to calculate the entanglement entropy for connected boundary region (left) and disconnected region (right).

8.2.2.2 Full complementary recovery

Both the HaPPY code [106] and the extension in Chapter 7 achieve approximate complementary recovery through the greedy entanglement wedge. However there exists certain "pathological" choices of boundary bipartitions where some local bulk operators cannot be recovered on either subregion. General random holographic codes in [110] also realise approximate complementary recovery, where all bulk indices except those in contact with the Ryu-Takayanagi surface can be recovered. In the following lemma, by careful choice of tessellation and random tensor construction, we lift complementary recovery to all bulk indices.

Lemma 88 (Complementary recovery)**.** *For a tensor network compromised of random stabilizer tensors, with arbitrarily high probability we have full complementary recovery in the sense that any logical operator acting on any single bulk tensor index, C, can be recovered on either the boundary subregion (A) or its complement (A^c) conditional on:*

1. *the hyperbolic bulk tessellation describing the network's geometry consisting of polytopes with an odd number of faces;*

2. *the dimension of a bulk dangling index, D_b, being less than that of internal connections in the network, D;*

3. *the bond dimension of the tensors being sufficiently large.*

Proof. Appendix B of [110] shows that complementary recovery is equivalent to the following entropic equation:

$$S(\rho_C) + S(\rho_{A^c\bar{C}}) = S(\rho_{A^cC\bar{C}}). \tag{8.36}$$

We use the Ising model mapping from [110, Section 4] (summarised in Appendix E.1) to approximate these entropies, where again the errors can suppressed by scaling the tensor bond dimension. Each term is calculated by considering the energy penalties from the bulk and boundary pinning fields as well as domain walls of the ground state. The above equation is satisfied only if the spin domain walls described by the ground state corresponding to $S(\rho_{A^c\bar{C}})$ and $S(\rho_{A^cC\bar{C}})$ coincide. The only difference between the two set-ups is that the bulk pinning field on the vertex labelled C switches sign. This section of the proof follows immediately from [110, Section 4].

Therefore for general bulk indices we do have complementary recovery. However there is a potential problem if C describes a bulk tensor that is adjacent to the minimal domain wall associated with the boundary subregion A i.e. the tensor has legs that cross the domain wall. In some cases the domain wall will move when the bulk pinning field is flipped, so that operators acting on that bulk tensor are not recoverable either on A or A^c.

This problematic scenario can be avoided by careful choice of tensor network. To see that the conditions listed above are sufficient to avoid these situations we consider the limiting case. Let l be the number of tensor nearest-neighbours in the bulk, i.e. the number of faces of the bulk tessellation. Choose C to be a bulk dangling index where the connected tensor is in the spin down domain when calculating $S(\rho_{A^c\bar{C}})$. The bulk pinning field is spin-down, so at most $\lfloor l/2 \rfloor$ of C's legs can cross the domain wall, otherwise the lowest energy configuration would have C in the spin-up domain. Considering the energy penalty trade off:

$$\text{energy penalty if } s_x = -1 \text{ for } x \in C\text{: } \beta E_{-1} = \lfloor l/2 \rfloor \log D \tag{8.37}$$

$$\text{energy penalty if } s_x = +1 \text{ for } x \in C\text{: } \beta E_{+1} = \lceil l/2 \rceil \log D + \log D_b, \tag{8.38}$$

and

$$E_{+1} > E_{-1}. \tag{8.39}$$

Then consider the case where the bulk pinning field for S is flipped, $S(\rho_{A^cC\bar{C}})$.

$$\text{energy penalty if } s_x = -1 \text{ for } x \in C\text{: } \beta E_{-1} = \lfloor l/2 \rfloor \log D + \log D_b, \tag{8.40}$$

$$\text{energy penalty if } s_x = +1 \text{ for } x \in C\text{: } \beta E_{+1} = \lceil l/2 \rceil \log D \tag{8.41}$$

Given $D_b < D$ and l is odd ($\lfloor l/2 \rfloor + 1 = \lceil l/2 \rceil$) the inequality in eq. (8.39) is still true and the domain wall does not move. □

There exist space-filling tessellations of hyperbolic space in 2 and 3 dimensions. In 2-dimensions one example is the tessellation composed of pentagons from [106]. In 3-dimensions one example is based on a non-uniform Coxeter polytope with 7 faces and described in subsection 7.4.2 of Chapter 7. We can meet the second condition without considering tensors with different dimensional indices by taking a tensor with $fs+1$ p-dimensional indices, where f is the number of faces of each cell in the tessellation. Then s tensor indices will be contracted through each of the f polytope faces, and one index will be the bulk degree of freedom. So, in the Ising action $D_b = p$ and $D = p^s$ so that $D_b < D$. We are free to choose p arbitrarily large to satisfy the final condition of Lemma 88 and ensure that the entropies in eq. (8.36) are arbitrarily well approximated by the free energy of the ground state of an appropriate Ising model. Indeed, large bond dimension is also a requirement to achieve isometric tensors with high probability (Theorem 85) so this condition is already required.

8.2.2.3 Exact Ryu-Takayanagi

Exact Ryu-Takayanagi for any bulk state in tensor product form can be demonstrated by combining the two previous results.

Lemma 89 (Exact Ryu-Takayanagi)**.** *We can construct a random stabilizer tensor network existing in 2 and 3-dimensional hyperbolic space such that the entanglement entropy of any (disconnected or connected) boundary subregion agrees exactly with the Ryu-Takayanagi entropy formula when there is no bulk entanglement. This occurs with probability:*

$$\text{Prob}\left[S_{RT}(\rho_A) = S(\rho_A)\right] \geq 1 - \frac{1}{a}, \tag{8.42}$$

conditional on $\log p > a \cdot (\ln k + o(1))$*. All quantities carry their definitions from Lemma 87.*

Proof. For the $\bigotimes |0\rangle$ bulk stabilizer state we have exact Ryu-Takayanagi for any boundary subregion from Lemma 87. From this stabilizer state we can get to an

arbitrary tensor product state by applying local operators to bulk tensors in turn. If we have full complementary recovery as described in Lemma 88, the action of such a logical operator on the boundary cannot change the entropy of the two boundary subregions.

See [12, Lemma 3.12] for more detailed discussion. □

The above theorem implies that the entanglement structure expected from AdS/CFT is achieved in our construction with high probability since by scaling the bond dimension, a can be made arbitrarily large so that the probability of having exactly the Ryu-Takayanagi entropy can be made arbitrarily close to 1. Therefore the entanglement structure of a network compromised of random stabilizer tensors is closer to AdS/CFT than one built from perfect tensors where Ryu-Takayanagi does not generally apply.

[110] also explores the entanglement structure for entangled bulk states in Haar random tensor networks, examining qualitatively how introducing entanglement in the bulk leads to displacement of the minimal surface and increased entropy of the boundary region. The minimal surface will never enter bulk regions of sufficiently high entanglement leading to discontinuous jumps as the boundary region varies. This transition is speculatively linked to the Hawking-Page transition where upon increasing temperature a black hole emerges from the perturbed AdS bulk geometry [143]. The same techniques are used to study boundary two-point correlation functions which decay as a power law when the bulk has hyperbolic geometry, defining the spectrum of scaling dimension. They find a separation in scaling dimensions that is expected in AdS/CFT where there is a known scaling dimension gap [144, 145]. This analysis could be recycled to further investigate the entanglement structure of stabilizer random tensors and we expect these proof techniques to be more fruitful than those of the HaPPY paper.

8.2.3 HQECC between local Hamiltonians with random stabilizer tensors

In previous sections we have demonstrated the desirable entanglement and error correcting properties of a holographic code where we inherit the geometry from the constructions in Chapter 7 but replace each perfect tensor with a random stabilizer tensor. Furthermore, Theorem 85 stated that individually a random stabilizer tensor is highly likely to be a perfect stabilizer tensor so all the successes from the constructions in Chapter 7 can also be retained. Now we put everything together to demonstrate that

our construction will, with high probability, describe a bulk to boundary encoding that exhibits several key features of the AdS/CFT correspondence.

Theorem 90 (Main result: 3D to 2D holographic mapping)**.** *Let $\mathbb{H}^3$ denote 3D hyperbolic space, and let $B_r(x) \subset \mathbb{H}^3$ denote a ball of radius r centred at x. Consider any arrangement of n qudits in $\mathbb{H}^3$ such that, for some fixed r, at most k qudits and at least one qudit are contained within any $B_r(x)$. Let L denote the minimum radius ball $B_L(0)$ containing all the qudits (which wlog we can take to be centred at the origin). Let $H_{\text{bulk}} = \sum_Z h_Z$ be any (quasi)-local Hamiltonian on these qudits.*

Then we can construct a Hamiltonian H_{boundary} on a 2D boundary manifold $\mathcal{M} \in \mathbb{H}^3$ with the following properties:

1. *$\mathcal{M}$ surrounds all the qudits, has diameter $O\left(\max(1, \frac{\ln(k)}{r})L + \log\log n\right)$, and is homomorphic to the Euclidean 2-sphere.*

2. *The Hilbert space of the boundary consists of a tesselation of $\mathcal{M}$ by polygons of $O(1)$ area, with a qudit at the centre of each polygon, and a total of $O\left(n(\log n)^4\right)$ polygons/qudits.*

3. *Any local observable/measurement M in the bulk has a set of corresponding observables/measurements $\{M'\}$ on the boundary with the same outcome. Any local bulk operator M can be reconstructed on a boundary region A if M acts within the entanglement wedge[3] of A, denoted $\mathcal{E}[A]$. This implies complementary recovery.*

4. *H_{boundary} consists of 2-local, nearest-neighbour interactions between the boundary qudits.*

5. *H_{boundary} is a $(\Delta_L, \epsilon, \eta)$-simulation of H_{bulk} in the rigorous sense of [6], Definition 23, with $\epsilon, \eta = 1/\text{poly}(\Delta_L)$, $\Delta L = \Omega\left(||H_{\text{bulk}}||^6\right)$, and where the maximum interaction strength $\Lambda = \max_{ij} |\alpha_{ij}|$ in H_{boundary} scales as $\Lambda = O\left(\Delta_L^{\text{poly}(n\log(n))}\right)$.*

6. *The entanglement entropy of any subregion of the boundary agrees exactly with the Ryu-Takayanagi formula when there is no entanglement in the bulk.*

Proof. In this proof we use a tensor network construction where the network's underlying graph is a tessellation of 3-d hyperbolic space generated from Coxeter polytopes. We place a random stabilizer tensor in each polyhedral cell of the finite

[3]The entanglement wedge as defined by the spin domain wall in the corresponding spin picture.

bulk tessellation. Each tensor has one index identified as the bulk qudit while the rest are contracted with tensors in neighbouring polyhedral cells.

In order to demonstrate that properties 1,2,4,5 and 6 hold we need that with high probability every tensor in our tensor network is simultaneously perfect, and that the network exactly obeys the Ryu-Takayanagi formula. From Theorem 85 and Lemma 89 we have probability bounds on both these events occurring individually. To get a bound the joint probability of these related events we again use Fréchet inequalities:

$$\begin{aligned}\text{Prob}\left[S(A) = S_{RT}(A) \cap \text{ perfect network}\right] \\ \geq \max\left\{0, \left[1 - \frac{1}{2p^b}\binom{t}{\lfloor t/2 \rfloor}\right]^n - \frac{1}{a}\right\}. \quad (8.43)\end{aligned}$$

This probability can be pushed arbitrarily close to 1 by increasing the bond dimension of the tensors.

For larger tensor networks, the bond dimension must be chosen larger in order to maintain high probability of having all perfect tensors. The bond dimension must scale as $p = O(n^q)$ for $q > 1/b$ in order for the probability of having an exact isometry tensor network to go to 1 as the size of the network increases. However for any given n, p can be chosen to be some large finite constant such that all properties resulting from tensor network being perfect will follow automatically for our modified HQECC. So, with high probability we can construct a tensor network that is composed of perfect tensors which exactly obeys the Ryu-Takayanagi formula.

The local boundary Hamiltonian is built up by composing simulations using results from [6]. The series of simulations are exactly the simulations used in Steps 1-3 in the proof of Theorem 78 in Chapter 7 - we recap them here for completeness, but refer readers to the original for further details.

Step 1: First we simulate the bulk Hamiltonian with a Hamiltonian that acts on the bulk indices of a HQECC in $\mathbb{H}^3$ of radius $R = O\left(\max(1, \frac{\ln(k)}{r})L\right)$.[4] This is a perfect simulation. The new bulk Hamiltonian act on $O(n)$ qudits of dimension p, and the HQECC will contain $O(n)$ random stabilizer tensors. Since the network is composed of perfect tensors with high probability, we can then define a non-local boundary Hamiltonian which is a perfect simulation of the original bulk Hamiltonian using the

[4]This scaling occurs since we may need to rescale the distances between qudits to embed them in a tessellation - see Theorem 78 in Chapter 7 for details.

isometry defined by the HQECC. This non-local boundary Hamiltonian also acts on $O(n)$ qudits.

Step 2: Next we simulate the non-local boundary Hamiltonian by a geometrically 2-local qudit Hamiltonian using the peturbative simulations outlined in Theorem 78 in Chapter 7.

Step 3: Finally we use the perturbative simulations from Step 3 in Theorem 78 in Chapter 7 to reduce the degree of each vertex to $3(p-1)$ so that the interaction graph can be embedded in a tessellation of the boundary surface. The perturbative simulations used in Steps 2 and 3 are approximate, but the errors they introduce are tracked in Theorem 78 in Chapter 7 and can be made arbitrarily small by tuning the gadget parameters in the Hamiltonian. Practically, perturbation gadgets involve introducing ancillary qudits with neighbouring interactions into the Hamiltonian interaction graph. These "gadgets" modify the graph to obtain a new operator that reproduces the same low energy spectrum with different interactions.

In order to demonstrate the scaling claimed in the theorem we need to upper bound the number of ancillary qudits introduced by the perturbative simulations. This requires us to determine the distribution of Pauli weights of terms in the boundary Hamiltonian after Step 1 of the simulation. As long as the tensor network preserves Pauli rank of operators, this distribution will be unchanged from that calculated in Theorem 78 in Chapter 7. For the geometry in Chapter 7 Pauli rank is preserved through the network since there exists a basis for the family of codes described by the perfect stabilizer tensor that maps logical Pauli operators to physical Pauli operators (Theorem 98).

Any individual high-dimensional random stabilizer tensor is perfect with high probability and so a consistent basis exists for the family of codes described by any *individual* tensor in our network. This is necessary since when considering a single tensor as an error correcting code from 1 to $t-1$ legs, or as a code from 2 to $t-2$ legs, some of the output legs are the same. Therefore for both codes to preserve Pauli rank there must be consistent basis for those legs. However unlike the construction from Chapter 7, the basis that preserves Pauli rank will not be consistent across different tensors since every random stabilizer tensor will not be concentrated on the same perfect tensor. We can convince ourselves that this is acceptable by examining the hyperbolic geometry in Fig. 6.2 and seeing that the output legs of separate tensors' codes are always disjoint i.e. there's never a leg in the tensor network which is an

output for two different tensors. The two sets of output legs are independent so the basis for the different tensors can be chosen independently.

Therefore the number of ancillary qudits introduced by our simulations will be unchanged from Theorem 78 in Chapter 7, where it is shown that the final boundary Hamiltonian acts on $O(n\,\mathrm{poly}(\log(n)))$ qudits. Since we enforce that the polygon cells of the boundary tessellation have area $O(1)$, the final boundary surface must have radius $R' = O\left(\max(1, \frac{\ln(k)}{r})L + \log\log n\right)$.

Properties 1,2,4, 5 and 6 follow immediately from the argument above and the results in Theorem 78 in Chapter 7. The complementary recovery described in point 3 follows from Lemma 88, since our construction can satisfy the conditions of the lemma, as described in subsection 8.2.2.2. □

It should be noted that in Theorem 78 in Chapter 7 the perturbative simulations are taken one step further, and the final boundary Hamiltonian is a qubit Hamiltonian with full local $SU(2)$ symmetry. In Chapter 7 this can be achieved without changing the scaling of the final boundary radius since in the perfect tensor case the local Hilbert dimension p of the tensors is independent of the size of the tensor network. This means that going from a Hamiltonian as outlined in Theorem 90 to a qubit Hamiltonian with full $SU(2)$ local symmetry requires $O(1)$ rounds of perturbation theory, and $O(n)$ additional ancilla qubits, which does not affect the final scaling.

However, in the case of random tensors we need the ability to increase the local dimension of the tensors as the size of the tensor network increases, to ensure that *every* tensor in the network is perfect with high probability. The bond dimension must scale as $p = O(n^q)$ for $q > 1/b$ in order for the probability of having an exact isometry tensor network to go to 1 as the size of the network increases (where $b < 1$ as defined in Theorem 85). This dependence of p on n means that reducing the boundary Hamiltonian to act on qubits and have $SU(2)$ symmetry requires $O(n^{1+2q}\,\mathrm{poly}(\log(n))$ ancilla qudits. Therefore maintaining the density of qubits on the boundary surface would require a boundary radius of $R' = O((1+2q)L') > 3L'$, where $L' = \max(1, \frac{\ln(k)}{r})L$ and L is the radius that contains all the bulk qudits. At this point the boundary can no longer be considered a geometric boundary of the bulk geometry, which is why we omit the final simulation step from our construction.

It may be possible to construct a boundary Hamiltonian on qudits with $SU(2)$ or $SU(p)$ local symmetry while maintaining the scaling outlined here by using qudit perturbation gadgets. It is known that the qudit generalisations of the Heisenberg Hamiltonian

with either symmetries remain universal for all local dimension greater than 2 (see [32]), but the scaling of the ancillas required would need to be investigated.

Theorem 91 (Main result: 2D to 1D holographic mapping)**.** *Consider any arrangement of n qudits in $\mathbb{H}^2$, such that for some fixed r at most k qudits and at least one qudit are contained within any $B_r(x)$. Let Q denote the minimum radius ball $B_Q(0)$ containing all the qudits. Let $H_{\text{bulk}} = \sum_Z h_Z$ be any (quasi) k-local Hamiltonian on these qudits.*

Then we can construct a Hamiltonian H_{boundary} on a 1D boundary manifold $\mathcal{M}$ with the following properties:

1. *$\mathcal{M}$ surrounds all the qudits and has diameter $\mathrm{O}\left(\max\left(1, \log(k)/r\right) Q + \log\log n\right)$.*
2. *The Hilbert space of the boundary consists of a chain of qudits of length $\mathrm{O}\left(n \log n\right)$.*
3. *Any local observable/measurement M in the bulk has a set of corresponding observables/measurements $\{M'\}$ on the boundary with the same outcome. Any local bulk operator M can be reconstructed on a boundary region A if M acts within the entanglement wedgeFootnote 3 of A, denoted $\mathcal{E}[A]$. This implies complementary recovery.*
4. *H_{boundary} consists of 2-local, nearest-neighbour interactions between the boundary qudits.*
5. *H_{boundary} is a $(\Delta_L, \epsilon, \eta)$-simulation of H_{bulk} in the rigorous sense of [6], with $\epsilon, \eta = 1/\mathrm{poly}(\Delta_L)$, $\Delta_L = \Omega\left(\|H_{bulk}\|\right)$, and where the interaction strengths in H_{boundary} scale as $\max_{ij} |\alpha_{ij}| = \mathrm{O}\left(\Delta_L\right)$.*
6. *The entanglement entropy of any subregion of the boundary agrees exactly with the Ryu-Takayanagi formula when there is no entanglement in the bulk.*

Proof. In this proof we use a tensor network construction where the network's underlying graph is a tessellation of 2-d hyperbolic space generated from Coxeter polytopes. We place a random stabilizer tensor in each polyhedral cell of the finite bulk tessellation. Each tensor has one index identified as the bulk qudit while the rest are contracted with tensors in neighbouring polyhedral cells. The proof that with high probability every tensor in the network is perfect, and that the network obeys the Ryu-Takayanagi formula follows exactly as in Theorem 90.

The first step in the simulation is unchanged from Theorem 90. Then, instead of using perturbative simulations to construct the local boundary Hamiltonian, we use the history-state simulation method, as in Theorem 79 in Chapter 7. The history state simulation method is again approximate, but it is non-perturbative. The overhead it incurs both in terms of ancillary qudits and errors is calculated in Theorem 79 in Chapter 7 - as in Theorem 90 we can use the fact that our random tensor networks preserve the Pauli rank of operators to argue that the scaling of weights of boundary operators is unchanged from the perfect tensor case. Again, we have to take care since the dimension of the qudits now scales as $p = \mathrm{O}(n^q)$. This means that describing a Pauli rank-1 operator of weight w requires $\mathrm{O}(w \log(n))$ bits of information, as opposed to $\mathrm{O}(w)$ in the perfect tensor case. So the number of spins on the boundary manifold scales as $\mathrm{O}(n \log(n)^2)$. Due to the hyperbolic geometry this doesn't change the asymptotic scaling of the distance from the new boundary to the old boundary.

Properties 1,2,4, 5 and 6 follow immediately. As in Theorem 90 the complementary recovery described in point 3 follows from Lemma 88.

□

It also follows from the above that all the work in Chapter 7: exploring the map between models, the dynamics of the bulk and boundary and their relative energy scales, also applies to our modified holographic code construction with high probability. Our construction illustrates that a mapping between models is possible without having to chose carefully selected tensors, which allows us to simultaneously achieve a mapping between models, perfect Ryu-Takayanagi and perfect complementary recovery.

Chapter 9

Conclusions on universal Hamiltonians for holography

Even in the absence of a duality at the level of Hamiltonians, holographic quantum codes such as [106, 110] already provide a simple, tractable toy model of many of the interesting static features expected of the real AdS/CFT "dictionary", such as redundant encoding and complementary recovery of information on the boundary [105, 146], entropic relations such as the Ryu-Takayanagi formula [147, 104], and even toy models of (static) black holes satisfying the Beckenstein-Hawking bound [136, 137]. However, without a holographic mapping between local Hamiltonians, these toy models give more limited insight into the relationship between bulk and boundary energy scales – a key aspect of AdS/CFT, where non-classical bulk spacetime geometries are believed to correspond to high-energy boundary state. More importantly, HQECC alone gave no insight into how dynamics in the bulk is reflected in the boundary.

By extending the toy models of holographic duality to encompass Hamiltonians, we show one way to complete this "dictionary". For example, it follows almost immediately from our constructions that the toy models of static black holes proposed in [106] do indeed correspond to high-energy states of the local boundary model, which moreover pick up their energy from a small number of high-energy terms in the boundary Hamiltonian.

More intriguingly, our constructions allows these toy models to say something about how dynamics in the bulk is reflected in the boundary. Even without writing down any specific local bulk Hamiltonian, the structure of the bulk/boundary mapping we construct implies that dynamics in the bulk is dual to boundary dynamics with

some of the qualitative features of AdS/CFT duality. In particular we show that the formation of a (toy model) black hole in the bulk dynamics is dual to a boundary dynamics in which local excitations unitarily evolve to a non-local excitation that lives outside the code space.

On the other hand, our construction shows that *any* local Hamiltonian in the bulk has a corresponding local boundary model. This implies that, at least in these toy models, the holographic duality has little to do with quantum gravity per se, but is entirely a consequence of the hyperbolic geometry. In order to investigate which parts of holography are inherently gravitational these toy models need to be pushed further, to understand what aspects of the duality cannot be incorporated for arbitrary, non-gravitational bulk physics.

Another way to complete the holographic 'dictionary' was suggested in [112], where it is argued that the dynamics for a particular holographic state should be the unitary representation of Thompson's group (a discrete analogue of the conformal group).[1] While [112] concentrates on a particular holographic state, they discuss how to generalise their results. The key advantage of the method in [112] is that it gives a boundary system which is conformally invariant, as would be expected in AdS/CFT. However, the results in [112] apply to holographic states, not holographic codes. A subspace of the boundary Hilbert space is identified as the bulk Hilbert space in [112], but it is not clear that this is redundantly encoded in the boundary, as would be expected in AdS/CFT. Even if one identified a good boundary Hilbert space and a symmetry subgroup to identify with time dynamics, there is no reason to expect the generators of this time dynamics will be local. In our construction we have not attempted to include conformal invariance in the boundary theory.

It should be noted that the discrete version of conformal symmetry on the boundary of the HQECC [112] is only known to exist for tessellations of $\mathbb{H}^2$ by ideal triangles. An area for future work is to extend the concepts to more general tessellations of $\mathbb{H}^2$, as well as higher dimensions. This would involve finding generalisations of what's known as Thompson's group T, and demonstrating that these generalisations are isomorphic to groups which generate tessellations of $\mathbb{H}^d$.

Another key avenue of further research would be to look into combining the work done in Chapters 7 and 8 with the methods in [112] to construct a bulk-boundary correspondence between local Hamiltonians which has the error-correction properties of holographic codes, the entanglement structure of AdS/CFT, as well as a conformally

[1] A holographic state is a holographic code with no bulk logical indices.

invariant boundary. The first step in this research avenue is to extend the work in [112] to holographic codes - this will require determining whether there exist tensors with the necessary symmetry properties to map a general bulk Hamiltonian to a boundary theory which exhibits a discrete version of conformal theory. If tensors with these symmetries do exist it implies that it is possible to construct toy models of AdS/CFT which simultaneously meet all the desiderata laid out in Chapter 6 - with the qualification that some properties will only hold approximately, unless a randomised version of the construction exists. Perhaps a more interesting outcome would be if this can't be done for general bulk Hamiltonians, but can for bulk Hamiltonians of certain types - in this case pushing these toy models to their limits may begin to give some insight into what sort of bulk Hamiltonians are appropriate as toy models of gravitational bulk theories.

Finally, investigating the issue of 'locality' in the more 'physical' sense highlighted in Chapter 6 is another interesting avenue of future research. As previously noted, the toy models outlined here are local in the sense that the boundary Hamiltonian is geometrically local. However due to the heavy weight interactions of the terms in the Hamiltonian the Lieb-Robinson velocities in the boundary system are far higher than in the bulk system, and lead to almost-instantaneous interactions between well separated parts of the bulk. It seems naively that this is a necessary feature of any such model, since in AdS/CFT operators deep in the bulk are mapped to operators which require large portions of the boundary for reconstruction. Investigating how this feature can be compatible with a constant speed of light on the boundary will lead to a deeper understanding of the correspondence.

Appendix A

Appendices for Chapter 3

A.1 The Schrieffer-Wolff expansion

Consider a finite dimensional Hilbert space decomposed into a direct sum:

$$\mathcal{H} = \mathcal{H}_+ \oplus \mathcal{H}_- \tag{A.1}$$

Let Π_- be the projector onto $\mathcal{H}_-$ and Π_+ be the projector onto $\mathcal{H}_+$. Let H_0 and H_1 be Hermitian operators acting on $\mathcal{H}$ such that H_0 is block diagonal with respect to the direct sum. Assume all the eigenvalues of H_0 on $\mathcal{H}_-$ are in the range $[0, \lambda_0]$ for $\lambda_0 < 1$.

Consider the perturbed Hamiltonian $\tilde{H} = \Delta H_0 + H_1$ where $\Delta \gg 1$ and $\|V\| < \frac{\Delta}{2}$. The Schrieffer-Wolf transformation is a unitary rotation e^S which is used to perturbatively diagonalise $\tilde{H}$. It satisfies the following properties:

$$\Pi_- \left(e^S \tilde{H} e^{-S}\right) \Pi_+ = \Pi_+ \left(e^S \tilde{H} e^{-S}\right) \Pi_- = 0 \tag{A.2}$$

$$\Pi_- S \Pi_- = \Pi_+ S \Pi_+ = 0 \ , \ \|S\| < \frac{\pi}{2} \tag{A.3}$$

The effective low-energy Hamiltonian H_{eff} acting on $\mathcal{H}_-$ is given by

$$H_{\text{eff}} = \Pi_- \left(e^S \tilde{H} e^{-S}\right) \Pi_- \tag{A.4}$$

Define $\mathcal{R} \coloneqq \left\{|\psi\rangle : \langle\psi|\,\tilde{H}\,|\psi\rangle \in \left[\lambda_0 - \frac{\Delta}{2}, \lambda_0 + \frac{\Delta}{2}\right]\right\}$, and let $\Pi_{\mathcal{R}}$ be the projector onto $\mathcal{R}$. Then

$$e^{S}\Pi_{\mathcal{R}}e^{-S} = \Pi_{-} \tag{A.5}$$

The operators S and H_{eff} can be expressed as Taylor series:

$$S = \sum_{j=1}^{\infty} S_j \tag{A.6}$$

$$H_{\text{eff}} = \sum_{j=1}^{\infty} H_{\text{eff}}^{(j)}. \tag{A.7}$$

A systematic method for calculating the Taylor coefficients is given in [148, Section 3.2]. We will only need the first two coefficients:

$$H_{\text{eff}}^{(0)} = H_0\Pi_{-} \quad \text{and} \quad H_{\text{eff}}^{(1)} = \Pi_{-}H_1\Pi_{-} \tag{A.8}$$

The size of the operators in the Taylor expansion can be bounded (see [148, Lemma 3.4]):

$$\|S_j\| \leq \mathrm{O}\left(\left(1 + \frac{\lambda_0}{\pi\Delta}\right)\left(\frac{\|H_1\|}{\Delta}\right)^{j}\right) \tag{A.9}$$

$$\|H_{\text{eff}}^{(j)}\| \leq \mathrm{O}\left(\Delta\left(1 + \frac{\lambda_0}{\pi\Delta}\right)\left(\frac{\|H_1\|}{\Delta}\right)^{j}\right) \tag{A.10}$$

This implies [31]

$$\|S\| \leq \mathrm{O}\left(\Delta^{-1}\|H_1\|\left(1 + \frac{\lambda_0}{\pi\Delta}\right)\right) \tag{A.11}$$

$$\|H_{\text{eff}} - H_{\text{eff}}(k)\| \leq \mathrm{O}\left(\Delta^{-k}\|H_1\|^{k+1}\left(1 + \frac{\lambda_0}{\pi\Delta}\right)\right) \tag{A.12}$$

where $H_{\text{eff}}(k) = \sum_{j=1}^{k} H_{\text{eff}}^{(j)}$.

Appendix B

Appendices for Chapter 4

B.1 Perturbative simulations using adiabatic elimination of Rydberg-dressed qubits

In this appendix we prove that the proposal for simulation using adiabatic elimination of Rydberg dressed qubits from [58] is a simulation in the rigorous sense of [6]. First we require a general lemma about simulations using fourth order perturbative expansions - the proof of this lemma builds heavily on the proof of [32, Lemma 12], but has different conditions on the perturbation terms.

Lemma 92. *Let H_0 and A, be Hamiltonians acting on the same space, such that: $\|A\| \leq \Lambda$; H_0 is block-diagonal with respect to the split $\mathcal{H}_+ \oplus \mathcal{H}_-$; $(H_0)_{--} = A_{--} = 0$. Suppose there exists a local isometry V such that $\mathrm{Im}(V) = \mathcal{H}_-$ and*

$$\begin{aligned} &\|VH_{\text{target}}V^\dagger - \Pi_-\left(-\frac{1}{\Delta}AH_0^{-1}A + \frac{1}{\Delta^2}A_{-+}H_0^{-1}A_{++}H_0^{-1}A_{+-}\right)\Pi_- \\ &+\frac{1}{2\Delta^3}\Pi_-\left(AH_0^{-2}A\Pi_-AH_0^{-1}A - AH_0^{-1}AH_0^{-1}AH_0^{-1}A\right)\Pi_-\| \leq \epsilon/2 \end{aligned} \tag{B.1}$$

Then $H_{\text{sim}} = \Delta H_0 + A$ $(\Delta/2, \eta, \epsilon)$-simulates H_{target}, provided that $\Delta \geq O(\Lambda^{5/4}/\epsilon^{1/4} + \Lambda/\eta)$.

Proof. This proof follows the structure of [32, Lemma 12]. As set out in Appendix A.1, the Schreiffer-Wolff transformation is a unitary operator e^S which maps the low-energy space of H_{sim} onto $\mathcal{H}_-$, the ground space of H_0. Define $\widetilde{V} = e^{-S}V$, which therefore maps exactly onto the low energy space of H_{sim}. And, using equation (22) of [31], we have $\|V - \widetilde{V}\| = \|I - e^{-S}\| = O(\|S\|) = O(\|A\|/\Delta) = O(\Lambda/\Delta) \leq \eta$, so $\widetilde{V}$ satisfies condition 1 of Definition 15.

To check condition 2 of Definition 15, we have to bound:

$$\|H_{\text{sim}}|_{\leq\Delta} - \widetilde{V}H_{\text{target}}\widetilde{V}^\dagger\| = \|V\widetilde{V}^\dagger H_{\text{sim}}\widetilde{V}V^\dagger - VH_{\text{target}}V^\dagger\| = \|H_{\text{eff}} - VH_{\text{target}}V^\dagger\|$$

where $H_{\text{eff}} = (e^S H_{\text{sim}} e^{-S})_{--}$. We can expand H_{eff} as a Taylor series in $1/\Delta$. The first three terms are given in [31] as:

$$H_{\text{eff}}^{(1)} = A_{--} \quad \text{and} \quad H_{\text{eff}}^{(2)} = -\frac{1}{\Delta}A_{-+}H_0^{-1}A_{+-}$$

$$H_{\text{eff}}^{(3)} = \frac{1}{\Delta^2}A_{-+}H_0^{-1}A_{++}H_0^{-1}A_{+-} - \frac{1}{2\Delta^2}(A_{-+}H_0^{-2}A_{+-}A_{--} + \text{h.c})$$

The fourth-order term is given in [32] as:

$$\begin{aligned} H_{\text{eff}}^{(4)} = \frac{1}{2\Delta^3}\Pi_-\left(AH_0^{-2}A\Pi_-AH_0^{-1}A - AH_0^{-1}AH_0^{-1}AH_0^{-1}A + AH_0^{-2}AH_0^{-1}A\Pi_-A\right)\Pi_- \\ + \frac{1}{2\Delta^3}\Pi_-\left(AH_0^{-1}AH_0^{-2}A\Pi_-A - AH_0^{-3}A\Pi_-A\Pi_-A + \text{h.c}\right)\Pi_- \end{aligned} \tag{B.2}$$

Substituting in $A_{--} = 0$ gives:

$$\begin{aligned} H_{\text{eff}}^{(1)} &= 0 \\ H_{\text{eff}}^{(2)} &= -\frac{1}{\Delta}A_{-+}H_0^{-1}A_{+-} \\ H_{\text{eff}}^{(3)} &= \frac{1}{\Delta^2}A_{-+}H_0^{-1}A_{++}H_0^{-1}A_{+-} \\ H_{\text{eff}}^{(4)} &= \frac{1}{2\Delta^3}\Pi_-\left(AH_0^{-2}A\Pi_-AH_0^{-1}A - AH_0^{-1}AH_0^{-1}AH_0^{-1}A\right)\Pi_- \end{aligned} \tag{B.3}$$

Putting these expressions together with eq. (B.1) gives:

$$\|H_{\text{eff}} - VH_{\text{target}}V^\dagger\| = \|H_{\text{eff}} - H_{\text{eff}}(4)\| + \frac{\epsilon}{2} \leq \text{O}\left(\Delta^{-4}\|H_1\|^5\right) + \frac{\epsilon}{2} \tag{B.4}$$

where we have used eq. (A.12) in the final step. Since $\text{O}\left(\Delta^{-4}\Lambda^5\right) \leq \frac{\epsilon}{2}$ this proves the result. □

The set up in [58] is a pair of Rydberg atoms with ground states $|g_-\rangle$, $|g_+\rangle$ off resonantly coupled by circularly polarised lasers to two Rydberg Zeeman levels, $|r_-\rangle$ and $|r_+\rangle$. The authors propose to use the system to simulate an anisotropic $\alpha XX + \beta YY + \gamma ZZ$-Hamiltonian with tunable coupling strengths by adiabatically eliminate the fast Rydberg degrees of freedom, and varying the detuning parameter.

The effective Hamiltonian in [58] is found using Brillouin-Wigner perturbation theory, and it is not clear whether the proposed set up meets the rigorous criteria to be a simulation, as defined in [6]. In the following we use Lemma 92 to demonstrate that it is.

In the rotating wave frame the Hamiltonian of the system is given by:

$$H = \sum_{i=1}^{2} \left(H_A^{(i)} + H_L^{(i)} \right) + H_{\text{vdW}} \tag{B.5}$$

where:

$$H_A = -\Delta_+ |r_+\rangle \langle r_+| - \Delta_- |r_-\rangle \langle r_-| \tag{B.6}$$

$$H_L = \frac{1}{2}\Omega_+ |g_-\rangle \langle r_+| + \frac{1}{2}\Omega_- |g_+\rangle \langle r_-| + \text{h.c.} \tag{B.7}$$

$$H_{\text{vdW}} = \begin{pmatrix} V_{++}(\rho) & 0 & 0 & W_{++}(\rho) \\ 0 & V_{+-}(\rho) & -3W_{++}(\rho) & 0 \\ 0 & -3W_{++}(\rho) & V_{+-}(\rho) & 0 \\ W_{++}(\rho) & 0 & 0 & V_{++}(\rho) \end{pmatrix} \tag{B.8}$$

where Δ_σ denotes the laser detunings, Ω_σ the Rabi frequencies, and wlog we have set the local laser phases to zero. The $V_{\sigma\sigma'}(r)$ are the diagonal vdW interactions between the pair states $|r_\sigma r_{\sigma'}\rangle$. The $W_{\sigma\sigma'}(r)$ are the "flip-flip", "flop-flop" and "flip-flop" interactions between Rydberg pair sttes. We refer readers to [58] for a detailed discussion of the physical interactions giving rise to this Hamiltonian.

Setting:

$$\Delta H_0 = \sum_{i=1}^{2} H_A^{(i)} + H_{\text{vdW}} \tag{B.9}$$

and

$$A = H_L^{(i)} \tag{B.10}$$

where to keep the algebra as simple as possible we have let $\Delta_+ = \Delta_- = \Delta$ (this condition could easily be lifted, it just makes the algebra slightly more tedious).

We find that, as required by Lemma 92, $(H_0)_{--} = A_{--} = 0$. Moreover:

$$\begin{aligned} \Pi_- A H_0^{-1} A \Pi_- = &\frac{|\Omega_+|^2}{16}(2|g_-g_-\rangle\langle g_-g_-| + |g_-g_+\rangle\langle g_-g_+| + |g_+g_-\rangle\langle g_+g_-|) \\ &+ \frac{|\Omega_-|^2}{16}(|g_+g_-\rangle\langle g_+g_-| + 2|g_+g_+\rangle\langle g_+g_+| + |g_-g_-+\rangle\langle g_-g_+|) \end{aligned} \tag{B.11}$$

$$\Pi_- A H_0^{-1} A H_0^{-1} A \Pi_- = 0 \tag{B.12}$$

$$\begin{aligned}\Pi_- A H_0^{-2} A \Pi_- A H_0^{-1} A \Pi_- = &\frac{|\Omega_+|^4}{256}(2|g_-g_-\rangle\langle g_-g_-| + |g_-g_+\rangle\langle g_-g_+| + |g_+g_-\rangle\langle g_+g_-|) \\ &+ \frac{|\Omega_-|^4}{256}(|g_+g_-\rangle\langle g_+g_-| + 2|g_+g_+\rangle\langle g_+g_+| + |g_-g_+\rangle\langle g_-g_+|) \\ &+ \frac{|\Omega_+|^2|\Omega_-|^2}{256}(|g_+g_-\rangle\langle g_+g_-| + |g_-g_+\rangle\langle g_-g_+|)\end{aligned} \tag{B.13}$$

$$\Pi_- A H_0^{-1} A H_0^{-1} A H_0^{-1} A \Pi_- = \begin{pmatrix} \tilde{V}_{++}(\rho) & 0 & 0 & \tilde{W}_{++}(\rho) \\ 0 & \tilde{V}_{+-}(\rho) & \tilde{W}_{+-}(\rho) & 0 \\ 0 & \tilde{W}^*_{+-}(\rho) & \tilde{V}_{+-}(\rho) & 0 \\ \tilde{W}^*_{++}(\rho) & 0 & 0 & \tilde{V}_{--}(\rho) \end{pmatrix} \tag{B.14}$$

where:

$$\tilde{V}_{++} = \frac{|\Omega_+|^4}{256}\left(\frac{\Delta}{E_{++}} + \frac{\Delta}{E_{--}}\right) \tag{B.15}$$

$$\tilde{V}_{+-} = \frac{|\Omega_+|^2|\Omega_-|^2}{256}\left(\frac{\Delta}{E_{+-}} + \frac{\Delta}{E_{-+}}\right) \tag{B.16}$$

$$\tilde{V}_{--} = \frac{|\Omega_-|^4}{256}\left(\frac{\Delta}{E_{++}} + \frac{\Delta}{E_{--}}\right) \tag{B.17}$$

$$\tilde{W}_{++} = \frac{\Omega_+^2(\Omega_-^*)^2}{256}\left(\frac{\Delta}{E_{++}} + \frac{\Delta}{E_{--}}\right) \tag{B.18}$$

$$\tilde{W}_{+-} = \frac{|\Omega_+|^2|\Omega_-|^2}{256}\left(\frac{\Delta}{E_{+-}} + \frac{\Delta}{E_{-+}}\right) \tag{B.19}$$

where:

$$E_{\sigma\sigma}(\rho) = V_{++}(\rho) - 2\Delta + \sigma W_{++}(\rho) \tag{B.20}$$

$$E_{\sigma\bar{\sigma}}(\rho) = V_{+-}(\rho) - 2\Delta + \sigma W_{+-}(\rho) \tag{B.21}$$

Putting these equations together with Lemma 92 demonstrates that the simulation set up proposed in [58] for using dressed Rydberg qubits to simulate an anisotropic $\{\alpha XX + \beta YY + \gamma ZZ\}$-Hamiltonian is a simulation in the rigorous sense of [6].

However, as discussed in Chapter 4 its usefulness is limited by the different orders of magnitude of the $XX+YY$ interactions compared to the ZZ interactions.

Appendix C

Appendices for Chapter 6

C.1 (Pseudo-)perfect tensors and absolutely maximally entangled states

Perfect and pseudo-perfect tensors are closely related to the concept of absolutely maximally entangled (AME) states, which are maximally entangled across all bipartitions. More formally:

Definition 93 (Absolutely maximally entangled states, definition 1 from [149])**.** *An AME state is a pure state, shared among n parties $P = \{1, ..., n\}$, each having a system of dimension q. Hence, $|\Phi\rangle \in \mathcal{H}_1 \otimes ... \otimes \mathcal{H}_n$, with the following equivalent properties:*

1. *$|\Phi\rangle$ is maximally entangled for any possible bipartition. This means that for any bipartition of P into disjoint sets A and B with $A \cup B = P$, and without loss of generality $m = |B| \leq |A| = n - m$, the state $|\Phi\rangle$ can be written in the form:*

$$|\Phi\rangle = \frac{1}{\sqrt{d^m}} \sum_{\boldsymbol{k} \in \mathbb{Z}_q^m} |k_1\rangle_{B_1} |k_2\rangle_{B_2} ... |k_m\rangle_{B_m} |\phi(\boldsymbol{k})\rangle_A \tag{C.1}$$

   with $\langle \phi(k) | \phi(k') \rangle = \delta_{kk'}$

2. *The reduced density matrix of every subset of parties $A \subset P$ with $|A| = \lfloor \frac{n}{2} \rfloor$ is maximally mixed, $\rho_A = q^{-\lfloor \frac{n}{2} \rfloor} \mathbb{1}_{q^{\lfloor \frac{n}{2} \rfloor}}$.*

3. *The reduced density matrix of every subset of parties $A \subset P$ with $|A| \leq \frac{n}{2}$ is maximally mixed.*

4. *The von Neumann entropy of every subset of parties $A \subset P$ with $|A| = \lfloor \frac{n}{2} \rfloor$ is maximal, $S(A) = \lfloor \frac{n}{2} \rfloor \log q$.*

5. *The von Neumann entropy of every subset of parties $A \subset P$ with $|A| \leq \frac{n}{2}$ is maximal, $S(A) = |A| \log q$.*

These are all necessary and sufficient conditions for a state to be absolutely maximally entangled. We denote such state as an AME(n,q) state.

The connection between perfect tensors and AME states was noted in [106], and separately in [150] (where perfect tensors are referred to as multi-unitary matrices). Here we generalise the arguments from [150] to encompass the case of pseudo-perfect tensors.

A t-index tensor, where each index ranges over q values, describes a pure quantum state of t q-dimensional qudits:

$$|\psi\rangle = \sum_{a_1 a_2 \ldots a_t \in \mathbb{Z}_q^t} T_{a_1 a_2 \ldots a_t} |a_1 a_2 \ldots a_t\rangle \tag{C.2}$$

A necessary and sufficient condition for $|\psi\rangle$ to be an AME state is that the reduced density matrix of any set of particles A such that $|A| \leq \lfloor \frac{t}{2} \rfloor$ is maximally mixed. The reduced density matrix ρ_A can be calculated as $\rho_A = MM^\dagger$, where M is a $|A| \times |A^c|$ matrix formed by reshaping T. Therefore, the state $|\psi\rangle$ is an AME state if and only if the tensor T is an isometry from any set of indices A to the complementary set of indices A^c with $|A| \leq |A^c|$.

If t is even (odd) this implies that T is a perfect (pseudo-perfect) tensor. Therefore an AME state containing an even (odd) number of qudits can be described by a perfect (pseudo-perfect) tensor, and every perfect (pseudo-perfect) tensor describes an AME state on an even (odd) number of qudits.

C.2 (Pseudo-)perfect tensors and quantum error correcting codes

An $[n, k, d]_q$ quantum error correcting code (QECC) encodes k q-dimensional qudits into n q-dimensional qudits, such that $d-1$ located errors (or $\frac{d-1}{2}$ unlocated errors) can be corrected. The quantum Singleton bound states that $n - k \geq 2(d-1)$. A QECC that saturates the quantum Singleton bound is known as a quantum maximum distance separable (MDS) code.

Previous work has established that every AME$(2m, q)$ state is the purification of a quantum MDS code [149, 151].[1] Furthermore, viewing the perfect tensor which describes an AME$(2m, q)$ state as a linear map from 1 leg to $2m-1$ legs, it is the encoding isometry of the quantum MDS code encoding one logical qudit [106].

We can generalise the proof in [151] to further characterise the connection between (pseudo-)perfect tensors and QECC:

Theorem 94. *Every AME(t, q) state is the purification of a $[t-k, k, \lfloor \frac{t}{2} \rfloor - k + 1]_q$ QECC for $1 \leq k \leq \lfloor \frac{t}{2} \rfloor$*[2].

Proof. Let $|\Phi\rangle$ be an AME(t, q) state, and let $m = \lfloor \frac{t}{2} \rfloor$. For any partition of the state into disjoint sets L, A and B such that $|L| = k \leq m$, $|A| = m-k$ and $|B| = \lceil \frac{t}{2} \rceil$ we can write:

$$|\Phi\rangle = \sqrt{\frac{1}{q^m}} \sum_{\boldsymbol{i} \in \mathbb{Z}_q^k, \boldsymbol{j} \in \mathbb{Z}_q^{m-k}} |i_1 \ldots i_k\rangle_L \, |j_1 \ldots j_{m-k}\rangle_A \, |\phi(\boldsymbol{i}, \boldsymbol{j})\rangle_B \tag{C.3}$$

The set $A \cup B$ are the physical qudits. Define the basis states of a QECC as:

$$\begin{aligned} |\Phi_{\boldsymbol{i}}\rangle &= \sqrt{q^k}_L \langle i_1 \ldots i_k | \Phi \rangle \\ &= \sum_{\boldsymbol{j} \in \mathbb{Z}_q^{m-k}} \sqrt{\frac{1}{q^{m-k}}} \, |j_1 \ldots j_{m-k}\rangle_A \, |\phi(\boldsymbol{i}, \boldsymbol{j})\rangle_B \end{aligned} \tag{C.4}$$

Encode a logical state in the physical qudits as:

$$|a\rangle = \sum_{\boldsymbol{i} \in \mathbb{Z}_q^k} a_{\boldsymbol{i}} \, |\boldsymbol{i}\rangle \rightarrow \sum_{\boldsymbol{i} \in \mathbb{Z}_q^k} a_{\boldsymbol{i}} \, |\Phi_{\boldsymbol{i}}\rangle \tag{C.5}$$

Now consider tracing out $m-k$ of the physical qudits. Since the sets A and B in eq. (C.3) are arbitrary, we can always choose that the qudits we trace out are in the set A. The qudits we are left with are then in the state:

$$\rho_B = \frac{1}{q^{m-k}} \sum_{\boldsymbol{i}, \boldsymbol{i'}, \boldsymbol{j}} a_{\boldsymbol{i}} a^*_{\boldsymbol{i'}} \, |\phi(\boldsymbol{i}, \boldsymbol{j})\rangle \left\langle \phi(\boldsymbol{i'}, \boldsymbol{j}) \right| \tag{C.6}$$

[1] The original proof actually demonstrates that AME$(2m, q)$ states are the purification of a threshold quantum secret sharing (QSS) scheme, however every pure QSS scheme is equivalent to a quantum MDS code [152] so the result follows immediately.

[2] The proof of this theorem is a straightforward generalisation of [151, Theorem 2]

We can recover the logical state by performing the unitary operation:

$$U_B \left|\phi(\boldsymbol{i},\boldsymbol{j})\right\rangle_B = \begin{cases} \left|i_1\right\rangle_{B_1} \ldots \left|i_k\right\rangle_{B_k} \left|j_1\right\rangle_{B_{k+1}} \ldots \left|j_{m-k}\right\rangle_{B_m} & \text{for } t \text{ even} \\ \left|i_1\right\rangle_{B_1} \ldots \left|i_k\right\rangle_{B_k} \left|j_1\right\rangle_{B_{k+1}} \ldots \left|j_{m-k}\right\rangle_{B_m} \left|0\right\rangle_{B_{m+1}} & \text{for } t \text{ odd} \end{cases} \tag{C.7}$$

which will give:

$$U_B \rho_B U_b^\dagger = \left|a\right\rangle \left\langle a\right| \otimes \frac{1}{q^{m-k}} \sum_{\boldsymbol{j}} \left|\boldsymbol{j}\right\rangle \left\langle \boldsymbol{j}\right| \tag{C.8}$$

Therefore, any set of $t-m$ qudits contains all the information about the logical state. By the no-cloning theorem, any set of m qudits contains no information about the logical state, so the QECC can correct exactly $m-k = \left\lfloor \frac{t}{2} \right\rfloor - k$ erasure errors. This gives $d = \left\lfloor \frac{t}{2} \right\rfloor - k + 1$. □

Therefore, an AME$(2m,q)$ state is the purification of a quantum MDS code with parameters $[2m-k, k, m-k+1]_q$; while an AME$(2m+1,q)$ state is the purification of a QECC with parameters $[2m+1-k, k, m-k+1]_q$. The parameters in the AME$(2m+1,q)$ case do not saturate the Singleton bound, so it is not an MDS code, but it is an optimal QECC.[3]

If we consider the (pseudo-)perfect tensor, T, which describes an AME(t,q) state $\left|\Phi\right\rangle$ we have:

$$\left|\Phi\right\rangle = \sum_{\boldsymbol{i}\in\mathbb{Z}_q^k, \boldsymbol{j}\in\mathbb{Z}_q^{t-k}} T_{\boldsymbol{i},\boldsymbol{j}} \left|\boldsymbol{i}\right\rangle_L \left|\boldsymbol{j}\right\rangle_P \tag{C.9}$$

where L and P are the sets of logical and physical qudits in the corresponding QECC, $|L| = k$, $|P| = t-k$. The basis states for the QECC are then:

$$\left|\Phi_{\boldsymbol{i}}\right\rangle = \sum_{\boldsymbol{j}\in\mathbb{Z}_q^{t-k}} T_{\boldsymbol{i},\boldsymbol{j}} \left|\boldsymbol{j}\right\rangle_P \tag{C.10}$$

and the encoding isometry is:

$$V = \sum_{\boldsymbol{i}\in\mathbb{Z}_q^k, \boldsymbol{j}\in\mathbb{Z}_q^{t-k}} T_{\boldsymbol{i},\boldsymbol{j}} \left|\boldsymbol{j}\right\rangle \left\langle \boldsymbol{i}\right| \tag{C.11}$$

[3]The terms MDS quantum code and optimal quantum code are sometimes used interchangeably. Here, by an optimal quantum code we mean either an MDS code, or a code for which $n-k$ is odd so which cannot saturate the Singleton bound, but for which the distance d is maximal given this constraint.

So, viewed as an isometry from k legs to $t-k$ legs a (pseudo-)perfect tensor is the encoding isometry of a $[t-k, k, \lfloor \frac{t}{2} \rfloor - k + 1]_q$ QECC.

C.3 Qudit stabilizer codes and states

We restrict our attention to qudits of dimension p where p is an odd prime.

C.3.1 Generalised Pauli group

The generalised Pauli operators on p dimensional qudits are defined as:

$$X = \sum_{j=0}^{p-1} |j+1\rangle \langle j| \tag{C.12}$$

$$Z = \sum_{j=0}^{p-1} \omega^j |j\rangle \langle j| \tag{C.13}$$

where $\omega = e^{\frac{2\pi i}{p}}$. The generalised Pauli operators obey the relations $X^p = Z^p = \mathbb{1}$ and $XZ = \omega ZX$.

The Pauli group on n qudits is given by $\mathcal{G}_{n,p} = \langle \omega^a X^{\boldsymbol{b}} Z^{\boldsymbol{c}} \rangle$ where $a \in \mathbb{Z}_p$, $\boldsymbol{b}, \boldsymbol{c} \in \mathbb{Z}_p^n$. Two elements $\omega^a X^{\boldsymbol{b}} Z^{\boldsymbol{c}}$ and $\omega^{a'} X^{\boldsymbol{b'}} Z^{\boldsymbol{c'}}$ commute if and only if $\boldsymbol{b'} \cdot \boldsymbol{c} = \boldsymbol{b} \cdot \boldsymbol{c'}$, where all addition is mod p.

C.3.2 Qudit stabilizer codes

A stabilizer code C on n qudits is a p^k-dimensional subspace of the Hilbert space given by:

$$C = \{|\psi\rangle \mid M|\psi\rangle = |\psi\rangle \, \forall M \in S\} \tag{C.14}$$

where S is an Abelian subgroup of $\mathcal{G}_{n,p}$ that does not contain $\omega\mathbb{1}$.

The projector onto C is given by [153]:

$$\Pi = \frac{1}{|S|} \sum_{M \in S} M \tag{C.15}$$

where $|S| = p^{n-k}$. S is an elementary Abelian p-group, so this implies that a minimal generating set for S contains $n-k$ elements [154].

The minimum weight of a logical operator in an $[n, k, d]$ stabilizer code is d. This is also the minimum weight of any operator that is not in the stabilizer, but which commutes with every element of the stabilizer.

A stabilizer code with $k = 0$ is a stabilizer state.

C.4 Stabilizer (pseudo-)perfect tensors

A stabilizer (pseudo-)perfect tensor describes stabilizer AME states. This implies, using the method in [155] for generating short qubit stabilizer codes from longer ones, that the QECCs described by the tensors are stabilizer codes:

Theorem 95. *If a (pseudo-)perfect tensor, T, with t legs describes a stabilizer AME(t,p) state, then the $[t-k, k, \lfloor \frac{t}{2} \rfloor - k + 1]_p$ QECCs (for $1 \leq k \leq \lfloor \frac{t}{2} \rfloor$) described by the tensor are stabilizer codes. The stabilizers of the code are given by the stabilizers of the AME state which start with $I^{\otimes k}$, restricted to the last $t-k$ qudits.*

Proof. Consider an AME(t,p) stabilizer state with stabilizer S:

$$|\Phi\rangle = \sqrt{\frac{1}{p^m}} \sum_{\boldsymbol{i} \in \mathbb{Z}_p^m} |i_1 ... i_m\rangle_A \, |\phi(\boldsymbol{i})\rangle_B \tag{C.16}$$

where $|A| = m = \lfloor \frac{t}{2} \rfloor$, $|B| = \lceil \frac{t}{2} \rceil$.

We have that $M|\Phi\rangle = |\Phi\rangle$ for all $M \in S$, where $|S| = p^t$ so a minimal generating set for S contains t elements. We can always pick a generating set for S so that M_1 and M_2 begin with X and Z respectively, and M_3 to M_t begin with $\mathbb{1}$ [155]. Define M'_j to be M_j restricted to the last $t-1$ qudits, where $j = 1, \ldots, t$.

Consider the codespace, C, for a $[t-1, 1, \lfloor \frac{t}{2} \rfloor]_p$ error correcting code described by T:

$$|\psi\rangle = \sum_{i_1 \in \mathbb{Z}} a_{i_1} \left|\Phi_{i_1}\right\rangle \tag{C.17}$$

where $\sum_i a_i^2 = 1$ and $\left|\Phi_{i_1}\right\rangle = \sqrt{p}\,\langle i_1|\Phi\rangle$. If we act on $|\psi\rangle \in C$ with M'_j we find $M'_j|\psi\rangle = |\psi\rangle$ for $j = 3, \ldots, t$, $M'_j|\psi\rangle = |\psi'\rangle \in C$ where $|\psi'\rangle \neq |\psi\rangle$ for $j = 1, \ldots, 2$.

The group S' generated by M'_j for $j = 3, \ldots, t$ contains $|S'| = p^{t-2}$ elements, and it stabilizes the $[t-1, 1, \lfloor \frac{t}{2} \rfloor]_p$ code described by T with codespace C.

This procedure for discarding two stabilizer generators from a $[n,k,d]$ code to obtain an $[n-1, k+1, d-1]$ code is always possible provided $d > 1$ [155]. So we can repeat the procedure $\lfloor \frac{t}{2} \rfloor - 1$ times, demonstrating that the $[t-k, k, \lfloor \frac{t}{2} \rfloor - k + 1]_p$ QECCs for $1 \leq k \leq \lfloor \frac{t}{2} \rfloor$ described by the perfect tensor are stabilizer codes. □

We also require that all the QECC used in our construction map logical Pauli operators to physical Pauli operators. It is known that for qubit stabilizer codes a basis can always be chosen so that this is true [155], and the same group-theoretic proof applies

to qudit stabilizer codes.[4] The physical Pauli operators we obtain using this method are not given by acting on the logical Pauli operators with the encoding isometry, but they have the same action in the code subspace. So, we have that for qudit stabilizer codes it is always possible to pick a basis where $VPV^\dagger = P'VV^\dagger$ where P is a k-qudit Pauli operator, P' is an n-qudit Pauli operator, and V is the encoding isometry of the QECC.

In our holographic QECC we do not have complete freedom to pick a basis, so we also need to show that we can pick this basis consistently. In order to show this we will require two lemmas about qudit stabilizer codes.

Lemma 96. *The smallest subgroup, G, of the Pauli group $\mathcal{G}_{n,p}$ such that $\forall P \in \mathcal{G}_{n,p}$, $P \neq \mathbb{1}^{\otimes n}$, $\exists M \in G$ where $MP \neq PM$ is the entire Pauli group.*

Proof. Consider the following process for constructing a set A element by element such that $\forall P \in \mathcal{G}_{n,p}$, $P \neq \mathbb{1}^{\otimes n}$, $\exists M \in A$ where $MP \neq PM$:

1. Select an arbitrary element of $\mathcal{G}_{n,p}$, $P^{(1)} = \omega^{a^{(1)}} X^{\boldsymbol{b}^{(1)}} Z^{\boldsymbol{c}^{(1)}}$.
2. Pick an element $P^{(1')} = \omega^{a^{(1')}} X^{\boldsymbol{b}^{(1')}} Z^{\boldsymbol{c}^{(1')}}$ such that $\boldsymbol{b}^{(1')} \cdot \boldsymbol{c}^{(1)} \neq \boldsymbol{b}^{(1)} \cdot \boldsymbol{c}^{(1')}$. This ensures that $P^{(1')}$ does not commute with $P^{(1)}$, and $P^{(1')}$ is our first element of A.
3. Pick an arbitrary element, $P^{(i)}$ of $\mathcal{G}_{n,p}$ which commutes with every element of A and is not the identity.
4. Choose any element, $P^{(i')}$ of $\mathcal{G}_{n,p}$ which does not commute with $P^{(i)}$, and add it to A.
5. Repeat steps (3) and (4) until $\forall P \in \mathcal{G}_{n,p}$, $P \neq \mathbb{1}^{\otimes n}$, $\exists M \in A$ such that $MP \neq PM$.

When we construct A, every element $P^{(i')} = \omega^{a^{(i')}} X^{\boldsymbol{b}^{(i')}} Z^{\boldsymbol{c}^{(i')}}$ which we add to A is independent from every element already in A. To see this note that by assumption there is some $P^{(i)}$ which commutes with every element in A, but does not commute with $P^{(i')}$. If $P^{(i')}$ was not independent from the other elements of A, and $\boldsymbol{b}^{(i')} = \sum_k \boldsymbol{b}^{(k)}$ and $\boldsymbol{c}^{(i')} = \sum_k \boldsymbol{c}^{(k)}$ where $P^{(k)} \in A$ for all k, then $\boldsymbol{b}^{(i')} \cdot \boldsymbol{c}^{(i)} = \sum_k \boldsymbol{b}^{(k)} \cdot \boldsymbol{c}^{(i)} = \sum_k \boldsymbol{b}^{(i)} \cdot \boldsymbol{c}^{(k)}$ and $\boldsymbol{b}^{(i)} \cdot \boldsymbol{c}^{(i')} = \sum_k \boldsymbol{b}^{(i)} \cdot \boldsymbol{c}^{(k)}$ so $\boldsymbol{b}^{(i')} \cdot \boldsymbol{c}^{(i)} = \boldsymbol{b}^{(i)} \cdot \boldsymbol{c}^{(i')}$, and $P^{(i')}$ would commute with $P^{(i)}$, contradicting our initial assumption.

[4] The discussion in [155] actually shows that there is an automorphism between $\mathcal{G}_{k,2}$ and $N(S)/S$, where $N(S)$ is the normalizer of S in $\mathcal{G}_{n,2}$. As $N(S) \in \mathcal{G}_{n,2}$ this is sufficient. The discussion in [155] can be extended to qudits of prime dimension by replacing phase factors of 4 with factors of p, and dimension factors of 2 with factors of p.

We need to determine the minimum number of elements in A when this process terminates.

Suppose we have repeated steps (3) and (4) m times, so that $|A| = m$. If there is an element $P^{(k)} = \omega^{a^{(k)}} X^{\boldsymbol{b}^{(k)}} Z^{\boldsymbol{c}^{(k)}}$ of $\mathcal{G}_{n,p}$ which commutes with every element of A then $\boldsymbol{b}^{(i')} \cdot \boldsymbol{c}^{(k)} = \boldsymbol{b}^{(k)} \cdot \boldsymbol{c}^{(i')}$ for all $P^{(i')} \in A$. $P^{(k)}$ is described by $2n$ degrees of freedom: $b_1^{(k)}, \ldots b_n^{(k)}$ and $c_1^{(k)}, \ldots c_n^{(k)}$, and there are m homogeneous equations which $P^{(k)}$ needs to satisfy.[5] Provided $m < 2n$, the set of equations is underdetermined, and we can always choose a $P^{(k)}$ which commutes with every element of A and is not the identity. If $m = 2n$ then the solution to the equations is uniquely determined, and is the identity. At this point we cannot continue with the process, so it terminates with $|A| = 2n$.

Therefore, the smallest set A of elements of $\mathcal{G}_{n,p}$ such that $\forall P \in \mathcal{G}_{n,p}$, $P \neq \mathbb{1}^{\otimes n}$, $\exists M \in A$ where $MP \neq PM$ contains $2n$ elements. At this stage A is not a group because all the elements of A are independent so the set isn't closed. Any $2n$ independent elements of $\mathcal{G}_{n,p}$ generate the entire group, so the smallest group G which contains every element of A is $\mathcal{G}_{n,p}$ itself. □

Lemma 97. *In an $[n, k, d]_p$ stabilizer code, the action of an encoded Pauli operator $\overline{P}$ on any $d-1$ physical qudits can be chosen to be any element of $\mathcal{G}_{d-1,p}$.*

Proof. The encoded Pauli operator $\overline{P}$ is not unique, and the different possible physical operators are related by elements of the stabilizer. We therefore need to show that the stabilizer S restricted to any set of $d-1$ qudits is the entire Pauli group $\mathcal{G}_{d-1,p}$.

An $[n, k, d]_p$ stabilizer code can correct all Pauli errors of weight $d-1$ and less. A correctable error doesn't commute with some element of the stabilizer, so for any Pauli operator of weight $d-1$ there $\exists M \in S$ such that $[M, P] \neq 0$. The result follows immediately from Lemma 96. □

Theorem 98. *If there exists a basis such that the QECC described by a (pseudo-)perfect tensor, T, from qudit l to $t-1$ qudits maps Pauli operators to Pauli operators, then all other QECC described by T which include qudit l in the logical set also map Pauli operators to Pauli operators in that basis.*

[5] The equations are homogeneous as all constant terms are equal to zero. Homogeneity of the equations ensures that the equations are not inconsistent.

Proof. Let the AME state described by T be given by:

$$|\Phi\rangle = \sum_{a\in\mathbb{Z}_p} \sum_{\boldsymbol{b}\in\mathbb{Z}_p^{k-1}} \sum_{\boldsymbol{c}\in\mathbb{Z}_p^{m-k}} |a\rangle_l |b_1...b_{k-1}\rangle_L |c_1...c_{m-k}\rangle_A |\phi(a,\boldsymbol{b},\boldsymbol{c})\rangle_B \tag{C.18}$$

where $m = \left\lfloor \frac{t}{2} \right\rfloor$, and $|B| = \left\lceil \frac{t}{2} \right\rceil$.

The basis states of the $[t-1, 1, \left\lfloor \frac{t}{2} \right\rfloor]_p$ QECC from qudit l to other $t-1$ qudits are given by:

$$|\Phi_a\rangle = \sum_{\boldsymbol{b}\in\mathbb{Z}_p^{k-1}} \sum_{\boldsymbol{c}\in\mathbb{Z}_p^{m-k}} |b_1...b_{k-1}\rangle_L |c_1...c_{m-k}\rangle_A |\phi(a,\boldsymbol{b},\boldsymbol{c})\rangle_B \tag{C.19}$$

and the encoding isometry is given by:

$$V = \sum_a |\Phi_a\rangle \langle a| \tag{C.20}$$

The basis states of a $[t-k, k, \left\lfloor \frac{t}{2} \right\rfloor - k + 1]_p$ QECC from a set L qudits (where $l \in L$, $|L| = k$) to $t-k$ qudits is given by:

$$\left|\Phi_{a,\boldsymbol{b}}\right\rangle = \sum_{\boldsymbol{c}\in\mathbb{Z}_p^{m-k}} |c_1...c_{m-k}\rangle_A |\phi(a,\boldsymbol{b},\boldsymbol{c})\rangle_B \tag{C.21}$$

and the encoding isometry is given by:

$$V' = \sum_a \left|\Phi_{a,\boldsymbol{b}}\right\rangle \langle a,\boldsymbol{b}| \tag{C.22}$$

By assumption we have:

$$VP_1V^\dagger = QVV^\dagger \tag{C.23}$$

where $P_1 \in \mathcal{G}_{1,p}$ and $Q \in \mathcal{G}_{n,p}$, $n = t-1$.

Therefore:

$$\sum_{aa'} |\Phi_a\rangle \langle a| P_1 |a'\rangle \langle \Phi_{a'}| = Q \sum_a |\Phi_a\rangle \langle \Phi_a| \tag{C.24}$$

Consider the action of V' on $P_1 \otimes P_2 \in \mathcal{G}_{k,p}$:

$$
\begin{aligned}
V'(P_1 \otimes P_2)V'^{\dagger} &= \sum_{a,a',\boldsymbol{b},\boldsymbol{b'}} \left|\Phi_{a,\boldsymbol{b}}\right\rangle \langle a,\boldsymbol{b}| (P_1 \otimes P_2) |a,\boldsymbol{b}\rangle \left\langle\Phi_{a,\boldsymbol{b}}\right| \\
&= \sum_{a,a',\boldsymbol{b},\boldsymbol{b'}} \langle \boldsymbol{b}|\Phi_a\rangle \langle a| P_1 |a'\rangle \langle \boldsymbol{b}| P_2 \left|\boldsymbol{b'}\right\rangle \left\langle\Phi_{a'}\right|\boldsymbol{b'}\rangle \\
&= \sum_{a,a',\boldsymbol{b},\boldsymbol{b'}} \langle \boldsymbol{b}| P_2 \left|\boldsymbol{b'}\right\rangle \langle \boldsymbol{b}| (|\Phi_a\rangle \langle a| P_1 |a'\rangle \langle \Phi_{a'}|) \left|\boldsymbol{b'}\right\rangle \\
&= \sum_{a,\boldsymbol{b},\boldsymbol{b'}} \langle \boldsymbol{b}| P_2 \left|\boldsymbol{b'}\right\rangle \langle \boldsymbol{b}| (Q |\Phi_a\rangle \langle \Phi_a|) \left|\boldsymbol{b'}\right\rangle \qquad \text{(C.25)} \\
&= \sum_{a,\boldsymbol{b},\boldsymbol{b'},\boldsymbol{b''}} \langle \boldsymbol{b}| P_2 \left|\boldsymbol{b'}\right\rangle \langle \boldsymbol{b}| Q'_2 \left|\boldsymbol{b''}\right\rangle Q' \left|\Phi_{a,\boldsymbol{b''}}\right\rangle \left\langle\Phi_{a,\boldsymbol{b'}}\right| \\
&= \sum_{a,\boldsymbol{b}} Q' \left|\Phi_{a,\boldsymbol{b}}\right\rangle \left\langle\Phi_{a,\boldsymbol{b}}\right| \text{ if } P_2 = Q'_2 \\
&= V'V'^{\dagger} P'^{(n')}
\end{aligned}
$$

where and Q'_2 and Q' indicate Q restricted to the first $k-1$ and remaining $n-k-1$ qudits respectively ($Q = Q'_2 \otimes Q'$).

Therefore, if Q acts as P_2 on the first $k-1$ qudits, then $P_1 \otimes P_2$ maps to a Pauli under V'. The operator Q is not unique, and from Lemma 97 we know that its action on $\left\lfloor \frac{t}{2} \right\rfloor - 1$ qudits can be chosen to be any element of $\mathcal{G}_{\lfloor \frac{t}{2} \rfloor - 1, p}$. So we can choose that Q acts as P_2 on the first $k-1$ qudits, for $k \leq \left\lfloor \frac{t}{2} \right\rfloor$. □

C.5 Existence of (pseudo-)perfect stabilizer tensors

C.5.1 Classical coding theory

A classical linear $[n,k]_d$ code, C_{cl}, encodes k d-dimensional dits of information in n dits. It can be described by a generator matrix $G^T : \mathbb{Z}_p^k \to \mathbb{Z}_d^n$, where information is encoded as $\boldsymbol{x} \to G^T\boldsymbol{x}$ for $\boldsymbol{x} \in \mathbb{Z}_d^k$. Equivalently, C_{cl} admits a description as the kernel of a parity check matrix $H : \mathbb{Z}_d^n \to \mathbb{Z}_d^{n-k}$. Consistency of the two descriptions implies $HG^T\boldsymbol{x} = 0$, $\forall \boldsymbol{x} \in \mathbb{Z}_d^n$, and hence the rows of H are orthogonal to the rows of G.

The minimum distance δ of a classical code is defined as the minimum Hamming distance between any two code words. It is bounded by the classical Singleton bound, $\delta \leq n - k + 1$. Codes which saturate the classical Singleton bound are referred to as classical MDS codes.

Reed-Solomon codes are a class of classical MDS codes [156].[6]

Definition 99. *Let p be a prime, and let k, n be integers such that $k < n \leq p$. For a set $S = \{\alpha_1, \alpha_2, ..., \alpha_n\} \in \mathbb{Z}_p$, the Reed-Solomon code over $\mathbb{Z}_p$ is defined as:*

$$C_{RS}[n,k] = \{(P(\alpha_1), P(\alpha_2), ..., P(\alpha_n)) \in \mathbb{Z}_p^n \mid P(X) \in \mathbb{Z}_p[X], \deg(P) \leq k-1\} \tag{C.26}$$

where $\mathbb{Z}_p[X]$ is the polynomial ring in X over $\mathbb{Z}_p$.[7]

To encode a message $\boldsymbol{a} = (a_0, a_1, ..., a_{k-1}) \in \mathbb{Z}_p^k$ in the Reed-Solomon code define the polynomial:

$$P_{\boldsymbol{a}}(X) = a_0 + a_1 X + a_2 X^2 + ... + a_{k-1} X^{k-1} \tag{C.27}$$

and construct the codeword $(P_{\boldsymbol{a}}(\alpha_1), P_{\boldsymbol{a}}(\alpha_2), ..., P_{\boldsymbol{a}}(\alpha_n)) \in C_{RS}[n,k]$.

Reed-Solomon codes are linear codes, with generating matrix:

$$G = \begin{pmatrix} 1 & 1 & 1 & .... & 1 \\ \alpha_1 & \alpha_2 & \alpha_3 & ... & \alpha_n \\ \alpha_1^2 & \alpha_2^2 & \alpha_3^2 & ... & \alpha_n^2 \\ \vdots & \vdots & \vdots & \ddots & \vdots \\ \alpha_1^{k-1} & \alpha_2^{k-1} & \alpha_3^{k-1} & ... & \alpha_n^{k-1} \end{pmatrix} \tag{C.28}$$

The generator matrix can be put into standard form $G = [I_k|P]$ (where P is a $k \times (n-k)$ matrix) using Gauss-Jordan elimination over the field $\mathbb{Z}_p$. The parity check matrix is then given by $H = [P^T|I_{n-k}]$.

C.5.2 Constructing AME stabilizer states

An AME(t,p) stabilizer state $|\Phi\rangle$ can be constructed from a classical $[t, \lfloor \frac{t}{2} \rfloor]_p$ MDS code with $\delta = \lceil \frac{t}{2} \rceil + 1$. The state is given by [127]:

$$|\Phi\rangle = \frac{1}{d^{\frac{l}{2}}} \sum_{\boldsymbol{x} \in \mathbb{Z}_p^l} |G\boldsymbol{x}\rangle \tag{C.29}$$

[6] Reed Solomon codes can be defined over any finite field, but we only require the definition of Reed Solomon codes over $\mathbb{Z}_p$ for our construction.

[7] The polynomial ring in X over $\mathbb{Z}_p$, $\mathbb{Z}_p[X]$, is the set of polynomials $P(X) = a_0 + a_1 X + a_2 X^2 + ... + a_m X^m$ where $a_i \in \mathbb{Z}_p$.

and has stabilizers $X^{G\boldsymbol{y}}$ for all $\boldsymbol{y} \in \mathbb{Z}_p^l$, and $Z^{\boldsymbol{y}}$ where $\boldsymbol{y}^T = \boldsymbol{z}^T H$ for all $\boldsymbol{z} \in \mathbb{Z}_p^m$. The full set of stabilizers is given by the generator matrix [127]:

$$M = \left(\begin{array}{c|c} G & 0 \\ 0 & H \end{array}\right) \tag{C.30}$$

where $(\boldsymbol{\alpha} \mid \boldsymbol{\beta}) \equiv X^{\boldsymbol{\alpha}} \cdot Z^{\boldsymbol{\beta}}$ for $\boldsymbol{\alpha}, \boldsymbol{\beta} \in \mathbb{Z}_p^t$.

Reed-Solomon codes can be constructed for any k, n satisfying $k < n \leq p$ [156], so by increasing p this construction can provide AME(t, p) stabilizer states for arbitrarily large t. By Theorem 95 the tensor which describes the AME(t, p) stabilizer states will be a stabilizer (pseudo-)perfect tensor.

This construction is not optimised to minimise p for a given t. It is possible to construct generalised Reed-Solomon codes which exist for $n = p + 1$ [157], which if used in this construction will give (pseudo-)perfect stabilizer tensors acting on lower dimensional qudits for certain values of t. There are also methods for constructing stabilizer perfect tensors for which $p \propto \sqrt{t}$ using cyclic and constacyclic classical MDS codes [158], but this method is significantly more involved than the one presented here, and does not work for pseudo-perfect tensors. In our construction there is no benefit to minimising p, so we have selected the simplest, most universal method for constructing (pseudo-)perfect stabilizer tensors.

Appendix D

Appendices for Chapter 7

D.1 Perturbative simulations

In this appendix we collect some results regarding perturbative techniques, and introduce the new qudit perturbation gadgets which are used in this paper. All the perturbation gadgets we introduce are qudit generalisations of the qubit gadgets from [28].

Let $\mathcal{H}$ be a Hilbert space decomposed as $\mathcal{H} = \mathcal{H}_- \oplus \mathcal{H}_+$. Let $\Pi_\pm$ be the projectors onto $\mathcal{H}_\pm$. For arbitrary operator M define $M_{++} = \Pi_+ M \Pi_+$, $M_{--} = \Pi_- M \Pi_-$, $M_{+-} = \Pi_+ M \Pi_-$, and $M_{-+} = \Pi_- M \Pi_+$.

Consider an unperturbed Hamiltonian $H = \Delta H_0$, where H_0 is block-diagonal with respect to the split $\mathcal{H} = \mathcal{H}_- \oplus \mathcal{H}_+$, $(H_0)_{--} = 0$, $\lambda_{\min}((H_0)_{++}) \geq 1$.

We will use Lemmas 19 and 20 from subsection 7.3.2 to construct qudit perturbation gadgets, which generalise qubit gadgets from [28]. In our analysis we assume without loss of generality that every interaction is a Pauli-rank 2 interaction of the form $P_a + P_a^\dagger$.

Qudit subdivision gadget

The subdivision gadget is used to simulate a k-local interaction by interactions which are at most $\lceil \frac{k}{2} \rceil + 1$-local. We want to simulate the Hamiltonian:

$$H_{\text{target}} = H_{\text{else}} + (P_A \otimes P_B + P_A^\dagger \otimes P_B^\dagger) \tag{D.1}$$

Let $\tilde{H} = H + V$ where:

$$H = \Delta \Pi_+ \tag{D.2}$$

$$V = H_1 + \Delta^{\frac{1}{2}} H_2 \tag{D.3}$$

where:

$$\Pi_+ = |1\rangle\langle 1|_w + |2\rangle\langle 2|_w + \ldots + |p-1\rangle\langle p-1|_w \tag{D.4}$$

$$H_1 = H_{\text{else}} + 2\mathbb{1} \tag{D.5}$$

$$H_2 = -P_A \otimes X_w - P_A^\dagger \otimes X_w^\dagger + P_B \otimes X_w^\dagger + P_B^\dagger \otimes X_w \tag{D.6}$$

The degenerate ground space of H has the mediator qubit w in the state $|0\rangle\langle 0|$ so $\Pi_- = |0\rangle\langle 0|_w$. This gives:

$$(H_1)_{--} = (H_{\text{else}} + 2\mathbb{1}) \otimes |0\rangle\langle 0|_w \tag{D.7}$$

and:

$$(H_2)_{-+} = -P_A \otimes |0\rangle\langle p-1|_w - P_A^\dagger \otimes |0\rangle\langle 1|_w + P_B \otimes |0\rangle\langle 1|_w + P_B^\dagger \otimes |0\rangle\langle p-1|_w \tag{D.8}$$

Therefore:

$$(H_2)_{-+} H_0^{-1} (H_2)_{+-} = \left(P_A \otimes P_B + P_A^\dagger \otimes P_B^\dagger - 2\mathbb{1}\right) \otimes |0\rangle\langle 0|_w \tag{D.9}$$

If we define an isometry W by $W|\psi\rangle_A = |\psi\rangle_A |0\rangle_w$ then:

$$||W H_{\text{target}} W^\dagger - (H_1)_{--} + (H_2)_{-+} H_0^{-1} (H_2)_{+-}|| = 0 \tag{D.10}$$

Therefore eq. (1.8) is satisfied for all $\epsilon \geq 0$. So, provided a Δ is picked which satisfies the conditions of Lemma 19, $\tilde{H}$ is a $(\frac{\Delta}{2}, \eta, \epsilon)$-simulation of H_{target}.

Qudit 3-2 gadget

The Hamiltonian we want to simulate is:

$$H_{\text{target}} = H_{\text{else}} + P_A \otimes P_B \otimes P_C + P_A^\dagger \otimes P_B^\dagger \otimes P_C^\dagger \tag{D.11}$$

Let $\tilde{H} = H + V$ where:

$$H = \Delta \Pi_+ \tag{D.12}$$

$$V = H_1 + \Delta^{\frac{1}{3}} H_1' + \Delta^{\frac{2}{3}} H_2 \tag{D.13}$$

where:

$$\Pi_+ = |1\rangle\langle 1|_w + \ldots + |p-1\rangle\langle p-1|_w \tag{D.14}$$

$$H_1 = H_{\text{else}} + \frac{1}{2}\left(P_A^2 \otimes P_C + (P_A^\dagger)^2 \otimes P_C^\dagger + P_B^2 \otimes P_C + (P_B^\dagger)^2 \otimes P_C^\dagger\right) + \frac{1}{2\sqrt{2}}\left[(-P_A + P_B)^2\left(-P_A^\dagger + P_B^\dagger\right) + \left(-P_A^\dagger + P_B^\dagger\right)^2(-P_A + P_B)\right] \tag{D.15}$$

$$H_1' = -P_A \otimes P_B^\dagger - P_A^\dagger \otimes P_B \tag{D.16}$$

$$H_2 = \left(P_C \otimes |p-1\rangle\langle 1|_w + P_C^\dagger \otimes |1\rangle\langle p-1|_w\right) + \frac{1}{\sqrt{2}}\left((-P_A + P_B) \otimes X_w + (-P_A^\dagger + P_B^\dagger) \otimes X_w^\dagger\right) \tag{D.17}$$

This gives:

$$(H_1)_{--} = H_1 \otimes |0\rangle\langle 0|_w \tag{D.18}$$

$$(H_1')_{--} = H_1' \otimes |0\rangle\langle 0|_w \tag{D.19}$$

$$(H_2)_{++} = -\left(P_C \otimes |p-1\rangle\langle 1|_w + P_C^\dagger \otimes |1\rangle\langle p-1|_w\right) + \frac{1}{\sqrt{2}}\left[(-P_A + P_B) \otimes Q_w + \left(-P_A^\dagger + P_B^\dagger\right) \otimes R_w\right] \tag{D.20}$$

where $Q = |2\rangle\langle 2| + \ldots + |p-1\rangle\langle p-1|$ and $R = |1\rangle\langle 1| + \ldots + |p-2\rangle\langle p-2|$.

$$(H_2)_{-+} = \frac{1}{\sqrt{2}}\left[(-P_A + P_B) \otimes |0\rangle\langle p-1|_w + \left(-P_A^\dagger + P_B^\dagger\right) \otimes |0\rangle\langle 1|_w\right] \tag{D.21}$$

If we define an isometry W by $W|\psi\rangle_A = |\psi\rangle_A |0\rangle_w$ then:

$$||WH_{\text{target}}W^\dagger - (H_1)_{--} + (H_2)_{-+}H_0^{-1}(H_2)_{++}H_0^{-1}(H_2)_{+-}|| = 0 \tag{D.22}$$

Therefore eq. (1.9) is satisfied for all $\epsilon \geq 0$.

We also have:

$$(H_2)_{-+}H_0^{-1}(H_2)_{+-} = -P_A \otimes P_B^\dagger - P_A^\dagger \otimes P_B = (H_1')_{--} \tag{D.23}$$

As required by eq. (1.10). So, provided a Δ is picked which satisfies the conditions of Lemma 20, $\tilde{H}$ is a $(\frac{\Delta}{2}, \eta, \epsilon)$-simulation of H_{target}.

Qudit crossing gadget

We want to generate the Hamiltonian:

$$H_{\text{target}} = H_{\text{else}} + \alpha_{ad}\left(P_A \otimes P_D + P_A^\dagger \otimes P_D^\dagger\right) + \alpha_{bc}\left(P_B \otimes P_C + P_B^\dagger \otimes P_C^\dagger\right) \tag{D.24}$$

Set $\tilde{H} = H + V$ where:

$$H = \Delta\Pi_+ \tag{D.25}$$

$$V = H_1 + \Delta^{\frac{1}{2}} H_2 \tag{D.26}$$

where:

$$\Pi_+ = |1\rangle\langle 1|_w + ... + |p-1\rangle\langle p-1|_w \tag{D.27}$$

$$\begin{aligned} H_1 = H_{\text{else}} + [&\alpha_{ad}\alpha_{bc}(P_A \otimes P_B^\dagger + P_A^\dagger \otimes P_B) - \alpha_{ad}(P_A \otimes P_C^\dagger + P_A^\dagger \otimes P_C) \\ &-\alpha_{bc}(P_B \otimes P_D^\dagger + P_B^\dagger \otimes P_D) + (P_C \otimes P_D^\dagger + P_C^\dagger \otimes P_D) \\ &+\mathbb{1}(\alpha_{ad}^2 + \alpha_{bc}^2 + 2)] \end{aligned} \tag{D.28}$$

$$\begin{aligned} H_2 = \frac{1}{\sqrt{2}}[&-\alpha_{ad}(P_A \otimes X_w + P_A^\dagger \otimes X_w^\dagger) - \alpha_{bc}(P_B \otimes X_w + P_B^\dagger \otimes X_w^\dagger) \\ &+(P_C \otimes X_w^\dagger + P_C^\dagger \otimes X) + (P_D \otimes X_w^\dagger + P_D^\dagger \otimes X_w)] \end{aligned} \tag{D.29}$$

Then:

$$(H_1)_{--} = H_1 \otimes |0\rangle\langle 0|_w \tag{D.30}$$

$$\begin{aligned} (H_2)_{-+} = \sqrt{\frac{1}{2}}[&-\alpha_{ad}(P_A \otimes |0\rangle\langle p-1|_w + P_A^\dagger |0\rangle\langle 1|_w) - \alpha_{bc}(P_B \otimes |0\rangle\langle p-1|_w + P_B^\dagger |0\rangle\langle 1|_w) \\ &+(P_C \otimes |0\rangle\langle 1|_w + P_C^\dagger |0\rangle\langle p-1|_w) + (P_D \otimes |0\rangle\langle 1|_w + P_D^\dagger |0\rangle\langle p-1|_w)] \end{aligned} \tag{D.31}$$

If define an isometry W by $W|\psi\rangle_A = |\psi\rangle_A |0\rangle_w$ then:

$$||WH_{\text{target}}W^\dagger - (H_1)_{--} + (H_2)_{-+}H_0^{-1}(H_2)_{+-}|| = 0 \tag{D.32}$$

Therefore $eq.$ (1.8) is satisfied for all $\epsilon \geq 0$. So, provided Δ is chosen to satisfy the conditions of Lemma 19, $\tilde{H}$ is a $(\frac{\Delta}{2}, \eta, \epsilon)$-simulation of H_{target}.

Qudit fork gadget

We want to generate the Hamiltonian:

$$H_{\text{target}} = H_{\text{else}} + \alpha_{ab}\left(P_A \otimes P_B + P_A^\dagger \otimes P_B^\dagger\right) + \alpha_{ac}\left(P_A \otimes P_C + P_A^\dagger \otimes P_C^\dagger\right) \tag{D.33}$$

Let $\tilde{H} = H + V$ where:

$$H = \Delta\Pi_+ \tag{D.34}$$

$$V = H_1 + \Delta^{\frac{1}{2}} H_2 \tag{D.35}$$

where:

$$H_1 = H_{\text{else}} + \alpha_{ab}\alpha_{ac}\left(P_B \otimes P_C^\dagger + P_B^\dagger \otimes P_C\right) + \mathbb{1}\left(1 + \alpha_{ab}^2 + \alpha_{ac} + \alpha_{ac}^2\right) \tag{D.36}$$

$$H_2 = \frac{1}{\sqrt{2}}[-(P_A \otimes X_w + P_A^\dagger \otimes X_w^\dagger) + \alpha_{ab}(P_B \otimes X_w^\dagger + P_B^\dagger \otimes X_w) + \alpha_{ac}(P_C \otimes X_w^\dagger + P_C^\dagger \otimes X_w)] \tag{D.37}$$

Then:

$$(H_1)_{--} = H_1 \otimes |0\rangle\langle 0|_w \tag{D.38}$$

$$(H_2)_{-+} = \frac{1}{\sqrt{2}}[-(P_A \otimes |0\rangle\langle p-1|_w + P_A^\dagger \otimes |0\rangle\langle 1|_w) + \alpha_{ab}(P_B \otimes |0\rangle\langle 1|_w + P_B^\dagger \otimes |0\rangle\langle p-1|_w) + \alpha_{ac}(P_C \otimes |0\rangle\langle 1|_w + P_C^\dagger \otimes |0\rangle\langle p-1|_w)] \tag{D.39}$$

If define an isometry W by $W|\psi\rangle_A = |\psi\rangle_A |0\rangle_w$ then:

$$||WH_{\text{target}}W^\dagger - (H_1)_{--} + (H_2)_{-+}H_0^{-1}(H_2)_{+-}|| = 0 \tag{D.40}$$

Therefore $eq.$ (1.8) is satisfied for all $\epsilon \geq 0$. So, provided Δ is chosen to satisfy the conditions of Lemma 19, $\tilde{H}$ is a $(\frac{\Delta}{2}, \eta, \epsilon)$-simulation of H_{target}.

D.2 Translational invariance in the boundary model of the 3D/2D construction

In general the boundary model which results from pushing a translationally invariant bulk Hamiltonian through the 3D/2D HQECC will not be translationally invariant, but for particular choices of tessellation and (pseudo-)perfect tensor the boundary model will exhibit block translational invariance.

To see how this comes about consider the example discussed in subsection 7.4.3. First consider the symmetry of the honeycombing of $\mathbb{H}^3$. The tessellation is the order-4 dodecahedral honeycomb. The symmetry group of the dodecahedron is the icosahedral symmetry group, which is the Coxeter group H_3 with Coxeter diagram given in Fig. D.1. The rotation subgroup of this group is the alternating group A_5, and contains rotations by $\frac{2\pi}{5}$ about centres of pairs of opposite faces, rotations by π about centres of pairs of opposite edges, and rotations by $\frac{2\pi}{3}$ about pairs of opposite vertices. The symmetry group of the entire tessellation is the Coxeter group $\overline{BH}_3$, which has Coxeter diagram given in Fig. D.2.[1] Clearly $H_3 < \overline{BH}_3$. Therefore the

[1]This is not the Coxeter diagram given for the tessellation in subsection 7.4.3. In general a Coxeter group can have many different Coxeter diagrams depending on which presentation is used. In

Figure D.1: Coxeter diagram for the icosahedral symmetry group H_3.

Figure D.2: Coxeter diagram for the group $\overline{BH}_3$.

symmetry group of the tessellation contains all of the rotational symmetries of the dodecahedron itself.

Cutting off the tessellation at some finite radius will not break the rotational symmetry. Therefore, so long as we can align the perfect tensors within the dodecahedral cells of the tessellations in such a way that the tensors don't break the symmetry, the HQECC will have the same rotational symmetry as the dodecahedron.

Ignoring the central tensor for now, it is clear that for the remaining tensors in the network it is possible to align them in such a way that rotational symmetry about at least one axis is preserved. To see this consider starting with an empty tessellation (of finite radius). Pick an arbitrary cell in the tessellation, $P^{(w)}$, and place the pseudo-perfect tensor in that cell in an arbitrary orientation. Now pick an axis of rotation, and consider rotating the tessellation by the minimum rotation about that axis which is in H_3. This sends $P^{(w)}$ to $P^{(w')}$, and the resulting tensor in $P^{(w')}$ will have some particular orientation. Place a tensor with this orientation in $P^{(w')}$. We can now repeat this process, placing tensors in every cell which is equivalent to $P^{(w)}$ under rotation about this axis. Then pick another empty cell in the tessellation, and repeat the process, keeping the axis of rotation the same. We are guaranteed to be able to complete the process consistently as rotations about the same axis commute, and there are no conditions on how tensors in neighbouring cells have to be connected.

Now consider the central tensor. Rotating the HQECC doesn't send the central tensor to another tensor in the network, it permutes 12 of the indices of the bulk tensor (leaving the final index, the bulk logical index, unchanged). The stabilizer generators of the pseudo-perfect tensor used in the HQECC are given in eq. (7.29). Viewed as a isometry from any one index to the other twelve indices the pseudo-perfect tensor is the encoding isometry of a $[12,1,6]_{13}$ QECC. Reed-Solomon codes are cyclic

subsection 7.4.3 we used the presentation corresponding to reflections in the faces of the dodecahedron. Here we are using the Coxeter diagram which makes the link between H_3 and $\overline{BH}_3$ explicit.

codes, so the pseudo-perfect tensor is symmetric under cyclic permutations of the 13 indices. Which index we chose as the logical index is therefore not important.

Reading off from eq. (7.22) one of the stabilizer generators of the AME(13,13) state is $X^{\otimes 13}$. Therefore using the process described in [155] for generating new stabilizer codes from old stabilizer codes we can construct a logical X operator for the $[12,1,6]_{13}$ code as:

$$\bar{X} = X^{\otimes 12} \tag{D.41}$$

In order to construct a logical Z operator we need to find an operator which commutes with every element of the stabilizer such that $\bar{X}\bar{Z} = \omega\bar{Z}\bar{X}$. One such operator is:

$$\bar{Z} = \left(Z^{12}\right)^{\otimes 12} \tag{D.42}$$

Both the encoded X and Z operators on the central bulk index can be realised using operators which are symmetric under any permutation of the contracted tensor indices. Therefore so can any operator we push through the central bulk tensor, so the central tensor does not break the rotational symmetry of the HQECC.

Since the HQECC (including the tensors) can be constructed to preserve rotational symmetry about at least one axis, a rotation about that axis will send the entire HQECC, including the boundary, to itself. Therefore the boundary exhibits a form of 'block translational invariance' - the Hamiltonian is a repeating pattern.

It is known that 2D translationally invariant universal quantum Hamiltonians exist [33], however these are not efficient for general Hamiltonians. So simulating H_{boundary} using the 2D translationally invariant construction could incur an exponential overhead in terms of number of spins on the boundary manifold. The construction in [33] is efficient for simulating target Hamiltonians which are themselves translationally invariant - checking the overhead incurred when simulating a 'block translationally-invariant' Hamiltonian such as the one outlined in this section may be a way to construct a 3D/2D HQECC with translationally invariant boundary.

Appendix E

Appendices for Chapter 8

E.1 Generalisation of the Ising mapping

Section 4 of [110] introduces a generalisation of the Ising mapping where the Rényi entropy considered is a function of a state with different support. We now take the full tensor network state, written as a pure state defined by the tensor network isometry, V, in an orthonormal basis of the bulk, $\{|\alpha\rangle\}$, and boundary, $\{|a\rangle\}$:

$$|\Psi_V\rangle = \frac{1}{p^{v/2}} \sum_{\alpha,a} \langle \alpha|V|a|\alpha|V|a\rangle \, |\alpha\rangle \otimes |a\rangle \,, \tag{E.1}$$

and trace out subregions of either the bulk or the boundary or both. v here is the number of vertices in the tensor network graph.

Similarly to the mapping described for boundary states, they find that a function related to the Rényi-2 entropy of $\rho = |\Psi_V\rangle \langle \Psi_V|$ can be equated to an Ising model partition function:

$$\langle \mathrm{tr} \left[(\rho \otimes \rho) \mathcal{F}_Y \right] \rangle = \sum_{\{s_x\}} e^{-\mathcal{A}[\{s_x\}]}, \tag{E.2}$$

where Y can be any subregion of the full tensor network state i.e. include part of the boundary and/or the bulk. The Ising action is given by

$$\mathcal{A}\left[\{s_x\}\right] = -\frac{1}{2} \log D \left[\sum_{\langle xy \rangle} (s_x s_y - 1) + \sum_{x \in \mathcal{B}} (h_x s_x - 1) \right] - \frac{1}{2} \log D_b \sum_{x \in b} (b_x s_x - 1), \tag{E.3}$$

where we have introduced a bulk pinning field b_x,

$$\text{Boundary pinning field, } h_x = \begin{cases} +1 & x \in Y \\ -1 & x \in \bar{Y} \end{cases} \tag{E.4}$$

$$\text{Bulk pinning field, } b_x = \begin{cases} +1 & x \in Y \\ -1 & x \in \bar{Y} \end{cases} \tag{E.5}$$

We have also introduced D, the dimension of the bond connecting two tensors in the network and D_b, the dimension of the bulk dangling index. We use this notation for our construction elsewhere although we chose every leg in our tensors will have dimension p and achieve different dimensions by grouping legs together.

As before, this convenient function is not directly the Rényi-2 entropy,

$$S_2(\rho_Y) = -\frac{1}{2}\ln \mathrm{tr}\left[\rho_Y\right] = \frac{1}{2}\ln \mathrm{tr}\left[(\rho \otimes \rho)\,\mathcal{F}_Y\right] \tag{E.6}$$

where $\rho_Y = \mathrm{tr}_{\bar{Y}}(\rho)$. However, the method of appendix F of [110] follows through when considering a full tensor network state rather than a boundary state so we can again bound the average Rényi-2 entropy in terms of the free energy of the ground state Ising model described by the action in equation denoted $F_{\mathcal{A}}(\rho_Y)$:

$$F_{\mathcal{A}}(\rho_Y) - \langle S(\rho_Y)\rangle \leq \ln k + o(1). \tag{E.7}$$

Since $|\Psi_M\rangle$ is a stabilizer state and hence has quantised entropy, following the proof of Lemma 87 we can conclude that the von Neumann entropies of subregions of this state can be made equal to $F_{\mathcal{A}}(\rho_Y)$ with probability greater than $\left(1 - \frac{1}{\delta}\right)$ which can be made arbitrarily close to 1 by choosing a sufficiently high bond dimension p.

Bibliography

[1] Richard Feynman. Simulating physics with computers. *International Journal of Theoretical Physics*, 1982.

[2] J. Ignacio Cirac and Peter Zoller. Goals and opportunities in quantum simulation. *Nature Physics*, 2012.

[3] Immanuel Bloch, Jean Dalibard, and Sylvain Nascimbene. Quantum simulations with ultracold quantum gases. *Nature Physics*, 2012.

[4] R. Blatt and C. Roos. Quantum simulations with trapped ions. *Nature Physics*, 2012.

[5] Andrew Houck, Hakan Tureci, and Jens Koch. On-chip quantum simulation with superconducting circuits. *Nature Physics*, 2012.

[6] Toby Cubitt, Ashley Montanaro, and Stephen Piddock. Universal Quantum Hamiltonians. *Proceedings of the National Academy of Sciences*, 115(38):9497–9502, Aug 2018.

[7] https://gitlab.com/TamaraKohler/non-markovianity.

[8] Tamara Kohler, Stephen Piddock, Johannes Bausch, and Toby Cubitt. Translationally invariant universal quantum Hamiltonians in 1D. *Annales Henri Poincaré*, 23(1):223–254, Oct 2021.

[9] Tamara Kohler, Stephen Piddock, Johannes Bausch, and Toby Cubitt. General conditions for universality of quantum Hamiltonians. *PRX Quantum*, 3:010308, Jan 2022.

[10] Tamara Kohler and Toby Cubitt. Toy models of holographic duality between local Hamiltonians. *Journal of High Energy Physics*, 2019(8), Aug 2019.

[11] Emilio Onorati, Tamara Kohler, and Toby Cubitt. Fitting quantum noise models to tomography data. *arXiv:2103.17243*, 2021.

[12] Harriet Apel, Tamara Kohler, and Toby Cubitt. Holographic duality between local Hamiltonians from random tensor networks. *Journal of High Energy Physics*, 2022(3):52, 2022.

[13] M. O. Rabin. Degree of difficulty of computing a function and a partial ordering of recursive sets. Technical Report 2, Hebrew University, 1960.

[14] A. Cobham. The intrinsic computational difficulty of functions. In *Proceedings of the 1964 Congress on Logic, Mathematics and the Methodology of Science*, pages 24–30, 1964.

[15] Elizabeth Crosson and John Bowen. Quantum ground state isoperimetric inequalities for the energy spectrum of local Hamiltonians. *arXiv:1703.10133*, 2017.

[16] Alexei Yu. Kitaev, Alexander Shen, and Mikhail N. Vyalyi. Classical and quantum computing. In *Quantum Information*, pages 203–217. Springer New York, New York, NY, 2002.

[17] Bill Fefferman and Cedric Yen-Yu Lin. A Complete Characterization of Unitary Quantum Space. In *Leibniz International Proceedings in Informatics (LIPIcs)*. 9th Innovations in Theoretical Computer Science Conference, Apr 2016.

[18] Daniel Gottesman and Sandy Irani. The Quantum and Classical Complexity of Translationally Invariant Tiling and Hamiltonian Problems. *Theory of Computing*, 9(1):31–116, May 2009.

[19] J. Kempe and O. Regev. 3-local Hamiltonian is QMA-complete. *Quantum information and computation*, page 0302079, 2003.

[20] J. Kempe, A Kitaev, and O. Regev. The complexity of the local Hamiltonian problem. *SIAM Journal on Computing*, 2006.

[21] Johannes Bausch, Toby Cubitt, and Maris Ozols. The Complexity of Translationally Invariant Spin Chains with Low Local Dimension. *Annales Henri Poincaré*, 18(11):3449–3513, Nov 2017.

[22] Johannes Bausch and Stephen Piddock. The complexity of translationally invariant low-dimensional spin lattices in 3D. *Journal of Mathematical Physics*, 58(11):111901, Nov 2017.

[23] Richard P. Feynman. Quantum Mechanical Computers. *Optics News*, 11(2):11, Feb 1985.

[24] Carlos E. González-Guillén and Toby S. Cubitt. History-state Hamiltonians are critical. *arXiv:1810.06528*, 2018.

[25] Naïri Usher, Matty J. Hoban, and Dan E. Browne. Nonunitary quantum computation in the ground space of local Hamiltonians. *Physical Review A*, 96(3):032321, Sep 2017.

[26] Keneth G. Wilson. Renormalization group and critical phenomena. I. renormalization group and the Kadanoff scaling pictre. *Phys. Rev. B*, 4, 1971.

[27] Keneth G. Wilson. The renormalization group and critical phenomena II: Phase space cell analysis of critical behavior. *Phys. Rev. B*, 4, 1971.

[28] Roberto I. Oliveira and Barbara M. Terhal. The complexity of quantum spin systems on a two-dimensional square lattice. *Quantum Information and Computation*, 8(10):1–23, Apr 2005.

[29] Toby S. Cubitt and Ashley Montanaro. Complexity Classification of Local Hamiltonian Problems. In *2014 IEEE 55th Annual Symposium on Foundations of Computer Science*, pages 120–129. IEEE, Oct 2014.

[30] Stephen Piddock and Ashley Montanaro. The complexity of antiferromagnetic interactions and 2D lattices. *Quantum Information and Computation*, 2017.

[31] Sergey Bravyi and Matthew Hastings. On complexity of the quantum Ising model. *Communications in Mathematical Physics*, 349(1):1–45, 2017.

[32] Stephen Piddock and Ashley Montanaro. Universal qudit Hamiltonians. *Communications in Mathematical Physics*, 382(2):721–771, 2021.

[33] Stephen Piddock and Johannes Bausch. Universal translationally-invariant Hamiltonians. *arXiv:2001.08050*, 2020.

[34] Dorit Aharonov et al. Adiabatic quantum computation is equivalent to standard quantum computation. *SIAM Journal of Computing*, 37(1):166–194, 2007.

[35] Dorit Aharonov and Leo Zhou. Hamiltonian sparsification and gap-simulation. *arXiv:1804.11084*, 2018.

[36] Chinmay Nirkhe, Umesh Vazirani, and Henry Yuen. Approximate low-weight check codes and circuit lower bounds for noisy ground states. *arXiv:1802.07419*, Feb 2018.

[37] Dorit Aharonov et al. Local tests of global entanglement and a counterexample to the generalized area law. *2014 IEEE 55th Annual Symposium on Foundations of Computer Science*, Oct 2014.

[38] Gemma De las Cuevas and Toby S. Cubitt. Simple universal models capture all classical spin physics. *Science*, 351(6278):1180–1183, Mar 2016.

[39] Toby S. Cubitt, David Perez-Garcia, and Michael M. Wolf. Undecidability of the spectral gap. *Nature*, 528(7581):207–211, Dec 2015.

[40] Peter Fenwick. Universal codes. In Khalid Sayood, editor, *Lossless Data Compression Handbook*. Academic Press, 2003.

[41] Tamara Kohler and Toby Cubitt. Translationally invariant universal classical Hamiltonians. *Journal of Statistical Physics*, 176(1):228–261, Apr 2019.

[42] Michael Fox. 84.57 Solving General Linear Diophantine Equations. *The Mathematical Gazette*, 84(501):505, Nov 2000.

[43] Toby Cubitt, David Perez-Garcia, and Michael M. Wolf. Undecidability of the spectral gap (full version). *arXiv:1502.04573*, Feb 2015.

[44] Johannes Bausch and Elizabeth Crosson. Analysis and limitations of modified circuit-to-Hamiltonian constructions. *Quantum*, 2:94, Sep 2018.

[45] James D. Watson. Detailed analysis of circuit-to-Hamiltonian mappings. *arXiv:1910.01481*, 2019.

[46] S. Lloyd. Universal Quantum Simulators. *Science*, 273(5278):1073–1078, Aug 1996.

[47] Dominic W. Berry, Graeme Ahokas, Richard Cleve, and Barry C. Sanders. Efficient quantum algorithms for simulating sparse hamiltonians. *Communications in Mathematical Physics*, 270(2):359–371, 2007.

[48] Dominic W. Berry, Andrew M. Childs, and Robin Kothari. Hamiltonian simulation with nearly optimal dependence on all parameters. *2015 IEEE 56th Annual Symposium on Foundations of Computer Science*, Oct 2015.

[49] Johannes Bausch, Toby S. Cubitt, Angelo Lucia, and David Perez-Garcia. Undecidability of the spectral gap in one dimension. *Phys. Rev. X*, 10:031038, Aug 2020.

[50] C. Marriott and J. Watrous. Quantum arthur-merlin games. In *Proceedings. 19th IEEE Annual Conference on Computational Complexity, 2004.*, pages 275–285, 2004.

[51] Dorit Aharonov, Michael Ben-Or, Fernando G.S.L. Brandão, and Or Sattath. The Pursuit of Uniqueness: Extending Valiant-Vazirani Theorem to the Probabilistic and Quantum Settings. *Quantum*, 6:668, Mar 2022.

[52] Abhinav Deshpande, Alexey V. Gorshkov, and Bill Fefferman. The importance of the spectral gap in estimating ground-state energies. *arXiv:2007.11582*, 2020.

[53] Chandler Davis and W. M. Kahan. Some new bounds on perturbation of subspaces. *Bull. Amer. Math. Soc.*, 75(4):863–868, Jul 1969.

[54] Leo Zhou and Dorit Aharonov. Strongly universal Hamiltonian simulators. *arXiv:2102.02991*, 2021.

[55] M. Morgado and S. Whitlock. Quantum simulation and computing with Rydberg-interacting qubits. *AVS Quantum Science*, 3(2):023501, Jun 2021.

[56] Pascal Scholl et al. Quantum simulation of 2D antiferromagnets with hundreds of Rydberg atoms. *Nature*, 595(7866):233–238, Jul 2021.

[57] Xiaoling Wu et al. A concise review of Rydberg atom based quantum computation and quantum simulation*. *Chinese Physics B*, 30(2):020305, Feb 2021.

[58] Alexander W. Glaetzle et al. Designing frustrated quantum magnets with laser-dressed Rydberg atoms. *Physical Review Letters*, 114(17), Apr 2015.

[59] John Preskill. Quantum Computing in the NISQ era and beyond. *Quantum*, 2:79, Aug 2018.

[60] Jens Eisert et al. Quantum certification and benchmarking. *Nature Reviews Physics*, 2:382–390, 2020.

[61] G. Lindblad. On the generators of quantum dynamical semigroups. *Comm. Math. Phys.*, 48(2):119–130, 1976.

[62] Vittorio Gorini, Andrzej Kossakowski, and E. C. G. Sudarshan. Completely positive dynamical semigroups of N-level systems. *Journal of Mathematical Physics*, 17(5):821–825, 1976.

[63] M. M. Wolf, J. Eisert, T. S. Cubitt, and J. I. Cirac. Assessing non-markovian quantum dynamics. *Phys. Rev. Lett.*, 101:150402, Oct 2008.

[64] Toby Cubitt, Jens Eisert, and Michael Wolf. The complexity of relating quantum channels to master equations. *Communications in Mathematical Physics*, 310:383–418, 08 2009.

[65] G. W. Stewart and Ji-guang Sun. *Matrix Perturbation Theory*. Academic Press, 1990.

[66] `https://github.com/quantumlib/Cirq`.

[67] Timothy Proctor et al. Detecting and tracking drift in quantum information processors. *Nature Communications*, 11(1), Oct 2020.

[68] Ángel Rivas, Susana F Huelga, and Martin B Plenio. Quantum non-markovianity: characterization, quantification and detection. *Reports on Progress in Physics*, 77(9):094001, Aug 2014.

[69] Carole Addis, Bogna Bylicka, Dariusz Chruscinski, and Sabrina Maniscalco. Comparative study of non-markovianity measures in exactly solvable one- and two-qubit models. *Phys. Rev. A*, 90:052103, Nov 2014.

[70] Li Li, Michael J.W. Hall, and Howard M. Wiseman. Concepts of quantum non-markovianity: A hierarchy. *Physics Reports*, 759:1 – 51, 2018.

[71] Dariusz Chruscinski and Sabrina Maniscalco. Degree of non-markovianity of quantum evolution. *Phys. Rev. Lett.*, 112:120404, Mar 2014.

[72] Michael M. Wolf and J. Ignacio Cirac. Dividing quantum channels. *Communications in Mathematical Physics*, 279:147–168, 2008.

[73] S. C. Hou, X. X. Yi, S. X. Yu, and C. H. Oh. Alternative non-markovianity measure by divisibility of dynamical maps. *Phys. Rev. A*, 83:062115, Jun 2011.

[74] Johannes Bausch and Toby Cubitt. The complexity of divisibility. *Linear Algebra and its Applications*, 504:64–107, 2016.

[75] Ángel Rivas, Susana F. Huelga, and Martin B. Plenio. Entanglement and non-Markovianity of quantum evolutions. *Physical Review Letters*, 105(5), Jul 2010.

[76] Kang-Da Wu et al. Detecting non-markovianity via quantified coherence: theory and experiments. *NPJ Quantum Information*, 6:55, 2020.

[77] A. R. Usha Devi, A. K. Rajagopal, and Sudha. Open-system quantum dynamics with correlated initial states, not completely positive maps, and non-markovianity. *Phys. Rev. A*, 83:022109, Feb 2011.

[78] Shunlong Luo, Shuangshuang Fu, and Hongting Song. Quantifying non-markovianity via correlations. *Phys. Rev. A*, 86:044101, Oct 2012.

[79] Elsi-Mari Laine, Jyrki Piilo, and Heinz-Peter Breuer. Measure for the non-markovianity of quantum processes. *Physical Review A*, 81(6), Jun 2010.

[80] Xiao-Ming Lu, Xiaoguang Wang, and C. P. Sun. Quantum fisher information flow and non-markovian processes of open systems. *Phys. Rev. A*, 82:042103, Oct 2010.

[81] Heinz-Peter Breuer, Elsi-Mari Laine, and Jyrki Piilo. Measure for the degree of non-markovian behavior of quantum processes in open systems. *Physical Review Letters*, 103(21), Nov 2009.

[82] Bogna Bylicka, Dariusz Chruscinski, and Sabrina Maniscalco. Non-Markovianity as a resource for quantum technologies. *arXiv:1301.2585*, 2013.

[83] Salvatore Lorenzo, Francesco Plastina, and Mauro Paternostro. Geometrical characterization of non-markovianity. *Phys. Rev. A*, 88:020102, Aug 2013.

[84] Kade Head-Marsden, Stefan Krastanov, David A. Mazziotti, and Prineha Narang. Capturing non-Markovian dynamics on near-term quantum computers. *Phys. Rev. Research*, 3:013182, Feb 2021.

[85] Murphy Yuezhen Niu et al. Learning non-Markovian quantum noise from Moiré-enhanced swap spectroscopy with deep evolutionary algorithm. *arXiv:1912.04368*, 2019.

[86] I. A. Luchnikov, S. V. Vintskevich, D. A. Grigoriev, and S. N. Filippov. Machine learning non-markovian quantum dynamics. *Physical Review Letters*, 124(14), Apr 2020.

[87] I. A. Luchnikov et al. Probing non-markovian quantum dynamics with data-driven analysis: Beyond 'black-box' machine learning models. *arXiv:2103.14490*, 2021.

[88] Roger A. Horn and Charles R. Johnson. *Matrix Analysis*. Cambridge University Press, second edition edition, 2012.

[89] Stephen Boyd and Lieven Vandenberghe. *Convex Optimization*. Cambridge University Press, 2004.

[90] Steven Diamond and Stephen Boyd. CVXPY: A Python-embedded modeling language for convex optimization. *Journal of Machine Learning Research*, 17(83):1–5, 2016.

[91] Akshay Agrawal, Robin Verschueren, Steven Diamond, and Stephen Boyd. A rewriting system for convex optimization problems. *Journal of Control and Decision*, 5(1):42–60, 2018.

[92] E. Davies. Embeddable markov matrices. *Electron. J. Probab.*, 15:1474–1486, 2010.

[93] Kamil Korzekwa and Matteo Lostaglio. Quantum advantage in simulating stochastic processes. *Phys. Rev. X*, 11:021019, Apr 2021.

[94] David E. Evans. Conditionally completely positive maps on operator algebras. *The Quarterly Journal of Mathematics*, 28(3):271–283, 09 1977.

[95] V. I. Danilov and V. V. Shokurov. *Algebraic Geometry I*, volume 23. Springer-Verlag Berlin Heidelberg, 1994.

[96] S. H. Weintraub. *Jordan Canonical Form: Theory and Practice*. Synthesis Lectures on Mathematics and Statistics. Morgan and Claypool Publishers, 2009.

[97] Leonid Khachiyan and Lorant Porkolab. Computing integral points in convex semi-algebraic sets. In *Proceedings 38th Annual Symposium on Foundations of Computer Science*, pages 162–171. IEEE, 1997.

[98] John E. Mitchell. *Integer programming: branch and cut algorithmsInteger Programming: Branch and Cut Algorithms*, pages 1643–1650. Springer US, Boston, MA, 2009.

[99] Tosio Kato. *Perturbation theory for linear operators*, volume 132. Springer-Verlag Berlin Heidelberg, 1995.

[100] Erika Andersson, James D. Cresser, and Michael J. W. Hall. Finding the Kraus decomposition from a master equation and vice versa. *Journal of Modern Optics*, 54(12):1695–1716, Aug 2007.

[101] Gerard 't Hooft. Dimensional reduction in quantum gravity. *Salamfest 93*, pages 284–296, 1993.

[102] Leonard Susskind. The world as a hologram. *Journal of Mathematical Physics*, 36(11):6377–6396, 11 1995.

[103] J. M. Maldacena. Eternal black holes in anti-de Sitter. *Journal of High Energy Physics*, 2003.

[104] S. Ryu and T. Takayanagi. Holographic derivation of entanglement entropy from AdS/CFT. *Physical Review Letters*, 2006.

[105] Xi Dong Ahmed Almheiri and Daniel Harlow. Bulk locality and quantum error correction in Ads/CFT. *Journal of High Energy Physics*, 2015.

[106] Fernando Pastawski, Beni Yoshida, Daniel Harlow, and John Preskill. Holographic quantum error-correcting codes: toy models for the bulk/boundary correspondence. *Journal of High Energy Physics*, 2015(6), Jun 2015.

[107] B. Swingle. Entanglement renormalization and holography. *Physical Review D*, 2012.

[108] Brian Swingle. Constructing holographic spacetimes using entanglement renormalization. *arXiv:1209.3304*, 2012.

[109] Zhao Yang, Patrick Hayden, and Xiao-Liang Qi. Bidirectional holographic codes and sub-AdS locality. *Journal of High Energy Physics*, 2016.

[110] Patrick Hayden et al. Holographic duality from random tensor networks. *Journal of High Energy Physics*, 2016(11), Nov 2016.

[111] Arpah Bhattacharyya, Zhe-Shen Gao, Ling-Yan Hung, and Si-Nong liu. Exploring the tensor networks / AdS correspondence. *Journal of High Energy Physics*, 2016.

[112] Tobias J. Osborne and Deniz E. Stiegemann. Dynamics for holographic codes. *Journal of High Energy Physics*, 2020(4):154, 2020.

[113] Thomas Faulkner, Aitor Lewkowycz, and Juan Maldacena. Quantum corrections to holographic entanglement entropy. *Journal of High Energy Physics*, 2013(11), 11 2013.

[114] Aron C Wall. Maximin surfaces, and the strong subadditivity of the covariant holographic entanglement entropy. *Classical and Quantum Gravity*, 31(22):225007, 11 2014.

[115] Thomas Hartman. Lectures on quantum gravity and black holes. http://www.hartmanhep.net/topics2015/gravity-lectures.pdf.

[116] Edward Witten. Anti de sitter space and holography. 1998.

[117] Patrick Hayden, Debbie W. Leung, and Andreas Winter. Aspects of generic entanglement. *Communications in Mathematical Physics*, 265(1), 3 2006.

[118] Christoph Dankert, Richard Cleve, Joseph Emerson, and Etera Livine. Exact and approximate unitary 2-designs and their application to fidelity estimation. *Physical Review A*, 80(1), 7 2009.

[119] W. Dür, M. Hein, J. I. Cirac, and H.-J. Briegel. Standard forms of noisy quantum operations via depolarization. *Physical Review A*, 72(5), 11 2005.

[120] H.F. Chau. Unconditionally secure key distribution in higher dimensions by depolarization. *IEEE Transactions on Information Theory*, 51(4):1451–1468, 4 2005.

[121] Mischa Woods and Alvaro Alhambra. Continous groups of transversal gates for quantum error correcting codes from finite clock reference frames. *arXiv:1902.07725*, 2019.

[122] Philippe Faist et al. Continuous symmetries and approximate quantum error correction. *arXiv:1902.07714*, 2019.

[123] Matthew Headrick, Veronika E. Hubeny, Albion Lawrence, and Mukund Rangamani. Causality and holographic entanglement entropy. *Journal of High Energy Physics*, 2014(12), Dec 2014.

[124] G. Gour and N. R. Wallach. All maximally entangled four-qubit states. *Journal of Mathematical Physics*, 2010.

[125] E. M. Rains. Quantum codes of minimum distance two. *IEEE Transactions on Information Theory*, 1999.

[126] Felix Huber, Otfried Guene, and Jens Siewert. Absolutely maximally entanged states of seven qubits do not exist. *Physical Review Letters*, 2017.

[127] Wolfram Helwig. Absolutely maximally entangled qudit graph states. *arXiv:1306.2879*, 2013.

[128] Anna Felikson and Pavel Tumarkin. Hyperbolic Coxeter polytopes.

[129] J. Tits. Groupes et geometries de Coxeter. Unpublished manuscript, 1961.

[130] Michael W. Davis. *The geometry and topology of Coxeter groups*. Princeton University Press, 2007.

[131] E. B. Vinberg. Hyperbolic reflection groups. *Russian Math. Surveys*, 1985.

[132] Peter Abramenko and Kenneth Brown. *Buildings Theory and Applications*. Graduate Texts in Mathematics. Springer, 2008.

[133] Arjeh M. Cohen. Finite Coxeter groups. http://www.win.tue.nl/ amc/buek/B13.ps.

[134] Jeff Weeks. Kaleidotile. http://geometrygames.org/KaleidoTile/index.html.

[135] Rafael Guglielmetti. CoxiterWeb. https://coxiterweb.rafaelguglielmetti.ch.

[136] J.D. Beckenstein. Black holes and entropy. *Physical Review D*, 1973.

[137] S. W. Hawking. Particle creation by black holes. *Communications in Mathematical Physics*, 1975.

[138] Patrick Hayden and Geoffrey Penington. Learning the alpha-bits of black holes. *arXiv:1807.06041*, 2018.

[139] Michel Ledoux. *The Concentration of Measure Phenomenon*, volume 89 of *Mathematical Surveys and Monographs*. American Mathematical Society, Providence, Rhode Island, 2001.

[140] Richard A. Low. Large deviation bounds for k -designs. *Proceedings of the Royal Society A: Mathematical, Physical and Engineering Sciences*, 465(2111):3289–3308, Aug 2009.

[141] M. Fréchet. Généralisation du théorème des probabilités totales. *Fundamenta Mathematicae*, 25:379–387, 1935.

[142] M. Fréchet. Sur les tableaux de correlation dont les marges sont donnees. In *Annales del'Université de Lyon. Section A: Sciences mathématiques et astronomie*, volume 9, pages 53–77, 1951.

[143] S. W. Hawking and Don N. Page. Thermodynamics of black holes in anti-de sitter space. *Communications in Mathematical Physics*, 87(4):577–588, 1983.

[144] Idse Heemskerk, Joao Penedones, Joseph Polchinski, and James Sully. Holography from conformal field theory. *Journal of High Energy Physics*, 2009(10):079–079, 10 2009.

[145] Sheer El-Showk and Kyriakos Papadodimas. Emergent spacetime and holographic CFTs. *Journal of High Energy Physics*, 2012(10), 10 2012.

[146] Daniel Harlow. The Ryu-Takayanagi formula from quantum error correction. *arXiv:1607.03901v2 [hep-th]*, 2016.

[147] S. Ryu and T. Takayanagi. Aspects of holographic entanglement entropy. *Journal of High Energy Physics*, 2006.

[148] Sergey Bravyi, David P. DiVincenzo, and Daniel Loss. Schrieffer–wolff transformation for quantum many-body systems. *Annals of Physics*, 326(10):2793–2826, Oct 2011.

[149] Wofram Helwig and Wei Cui. Absolutely maximally entangled states: Existence and applications. *arXiv:1306.2536*, 2013.

[150] Dardo Goyeneche, Daniel Alsina, José I. Latorre, Arnau Riera, and Karol Życzkowski. Absolutely maximally entangled states, combinatorial design and multi-unitary matrices. *Physical Review A*, 2015.

[151] Wofram Helwig, Wei Cui, Arnau Riera, José I. Latorre, and Hoi-Kwong Lo. Absolute maximal entanglement and quantum secret sharing. *Physical Review A*, 2012.

[152] Richard Cleve, Daniel Gottesman, and Hoi-Kwong Lo. How to share a quantum secret. *Physical Review Letters*, 1999.

[153] Vlad Gheorghiu. Standard form of qudit stabilizer groups. *Physics Letters A*, 2014.

[154] Hans Kurzweil and Bernd Stellmacher. *The theory of finite groups: an introduction*. Springer, 2004.

[155] Daniel Gottesman. *Stabilizer Codes and Quantum Error Correction*. PhD thesis, Caltech, 1997.

[156] I. Reed and G. Solomon. Polynomial codes over certain finite fields. *Journal of the Society for Industrial and Applied Mathematics*, 1960.

[157] G. Seroussi and R. Roth. On MDS extensions of generalized Reed-Solomon codes. *Information Theory, IEEE Transactions on*, 32, 1986.

[158] M. Grassl and M. Roetteler. Quantum MDS codes over small fields. In *IEEE International Symposium on Information Theory*, 2015.